PROTEASE ASSAYS FOR CANCER DIAGNOSTICS

by

DINUSHA NISHANI UDUKALA

B.S., University of Colombo, Sri Lanka, 2007

AN ABSTRACT OF A DISSERTATION

submitted in partial fulfillment of the requirements for the degree

DOCTOR OF PHILOSOPHY

Department of Chemistry
College of Arts and Sciences

KANSAS STATE UNIVERSITY
Manhattan, Kansas

2014

Abstract

Numerous proteases are known to be necessary for cancer development and progression including Matrix Metalloproteinases (MMPs), Tissue Serine Proteases, and Cathepsins. The goal of this research is to develop a Fe/Fe_3O_4 nanoparticle-based system for clinical diagnostics, which has the potential to measure the activity of cancer-associated proteases in biospecimens. Our nanoparticle-based "light switches" for measuring protease activity, consist of fluorescent cyanine dyes which are directly attached to Fe/Fe_3O_4 nanoparticles and porphyrins that are attached to Fe/Fe_3O_4 nanoparticles via consensus sequences.

The consensus (cleavage) sequences can be cleaved in the presence of the correct protease, thus releasing a fluorescent dye from the Fe/Fe_3O_4 nanoparticle resulting in highly sensitive (down to 1×10^{-16} mol L^{-1} for 12 proteases), selective, and fast nanoplatforms (required time: 60 min.). Upon escape, the emission intensity of the organic dye will significantly increase, which can be detected using fluorescence spectroscopy.

In order to demonstrate the potential of this new technology of early recognition of various cancers several analysis types have been used. Blood and urine samples from human cancer patients and healthy volunteers, tissue and blood serum samples from human cancer patients, and canine urine and blood serum samples are some of those types.

Blood samples from human cancer patients and healthy volunteers were used to demonstrate the potential of this new technology for the early recognition of breast and lung cancers. We were able to establish several proteases with diagnostic potential for breast cancer and non-small cell lung cancer. It is very likely that different cancers will feature different "protease signatures", meaning that different proteases will be activated, depending on the origin of cancer. This permits the diagnosis of various solid tumors at different stages.

Tissue samples were collected from normal tissues, from the boundary of the tumor and from the tumor of the same person. Performed fluorescence experiments clearly indicate that tissue samples from the tumor show the highest fluorescence indicating the highest concentration of the protease. Results can be used excellently in a diagnostic system for breast cancer. Based on our results measuring protease signatures offers an inexpensive and fast approach towards early cancer diagnostics.

PROTEASE ASSAYS FOR CANCER DIAGNOSTICS

by

DINUSHA NISHANI UDUKALA

B.S., University of Colombo, Sri Lanka, 2007

A DISSERTATION

submitted in partial fulfillment of the requirements for the degree

DOCTOR OF PHILOSOPHY

Department of Chemistry
College of Arts and Sciences

KANSAS STATE UNIVERSITY
Manhattan, Kansas

2014

Approved by:

Major Professor
Dr. Stefan H. Bossmann

Abstract

Numerous proteases are known to be necessary for cancer development and progression including Matrix Metalloproteinases (MMPs), Tissue Serine Proteases, and Cathepsins. The goal of this research is to develop a Fe/Fe_3O_4 nanoparticle-based system for clinical diagnostics, which has the potential to measure the activity of cancer-associated proteases in biospecimens. Our nanoparticle-based "light switches" for measuring protease activity, consist of fluorescent cyanine dyes which are directly attached to Fe/Fe_3O_4 nanoparticles and porphyrins that are attached to Fe/Fe_3O_4 nanoparticles via consensus sequences.

The consensus (cleavage) sequences can be cleaved in the presence of the correct protease, thus releasing a fluorescent dye from the Fe/Fe_3O_4 nanoparticle resulting in highly sensitive (down to 1×10^{-16} mol L^{-1} for 12 proteases), selective, and fast nanoplatforms (required time: 60 min.). Upon escape, the emission intensity of the organic dye will significantly increase, which can be detected using fluorescence spectroscopy.

In order to demonstrate the potential of this new technology of early recognition of various cancers several analysis types have been used. Blood and urine samples from human cancer patients and healthy volunteers, tissue and blood serum samples from human cancer patients, and canine urine and blood serum samples are some of those types.

Blood samples from human cancer patients and healthy volunteers were used to demonstrate the potential of this new technology for the early recognition of breast and lung cancers. We were able to establish several proteases with diagnostic potential for breast cancer and non-small cell lung cancer. It is very likely that different cancers will feature different "protease signatures", meaning that different proteases will be activated, depending on the origin of cancer. This permits the diagnosis of various solid tumors at different stages.

Tissue samples were collected from normal tissues, from the boundary of the tumor and from the tumor of the same person. Performed fluorescence experiments clearly indicate that tissue samples from the tumor show the highest fluorescence indicating the highest concentration of the protease. Results can be used excellently in a diagnostic system for breast cancer. Based on our results measuring protease signatures offers an inexpensive and fast approach towards early cancer diagnostics.

Table of Contents

List of Figures

List of Tables

Acknowledgements

Foremost, I would like to express my sincere gratitude to my research advisor and mentor Professor Stefan H. Bossmann, at Kansas State University, for the encouragement, patient guidance and mentorship rendered to me throughout my PhD. I am very grateful to that extraordinary mentor, for the continuous support and the freedom he provided to me from the day I first decided applying for the PhD in Department of Chemistry, Kansas State University to the completion of my PhD. His advices were priceless on both science and life for which I am extremely grateful. I believe it is a great honor to work with such an exceptional scientist.

Besides my advisor, I would like to especially acknowledge the rest of my PhD committee: Professor. Eric Maatta, Professor. Daniel Higgins, Professor. Deryl Troyer and outside chair person Professor. Revathi Govind for their valuable time and support.

A special thanks to Katharine Bossmann for being a kind, supportive and wonderful friend throughout the years.

I will fondly remember good times with my past and present colleagues of the Bossmann group. Special thanks goes out to Dr. Hongwang Wang and the members of the Troyer group for their support.

I also extend my acknowledgements to Professor. Daniel Higgins, Professor. Kent Klabunde for allowing me to use their resources and Professor. Gary Gadbury for the contribution on statistical analysis. Also my sincere thanks goes to the graduate faculty, non-graduate faculty, staff and all the colleagues in Department of Chemistry. It was a pleasure to work there with such talented people.

My sincere thanks goes to two special families. Dr. Thilani Samarakoon and Dhanushka Samarakoon, Dr. Manindu Weerasinghe and Dulan Weerasinghe for the continuous friendship and for everything they have done for me over the last four years.

I would also like to thank my dearest friend Dhanushi and all my friends for being there for me whenever needed. I feel very lucky to have such wonderful friends in my life.

I am grateful to all the Sri Lankan friends in Manhattan, for making my life much easier by making K-State a home.

Last but not least, my deepest gratitude goes to my mother for all of the sacrifices that she has made on my behalf and the unconditional support. Also I am grateful to all other family and friends for their love and support.

Dedication

My dissertation is dedicated to my loving Amma.

Chapter 1 - Introduction

1.1 Cancer

Diseases in which abnormal cells divide without control and are able to invade other tissues are known as cancer. Blood and lymph systems are the chief vectors in spreading cancer.[1] The causes for cancer can be divided into two major divisions: external factors and internal factors. Tobacco, infectious organisms, chemicals, and radiation are so-called external factors. Inherited mutations, hormones, immune conditions, and spontaneous mutations that occur from metabolism are so-called internal factors.[2] Cancer is a major cause of death in the world, especially in USA, where it is the second major cause of death. In 2013, about 1,660,290 new cancer cases were diagnosed and about 580,350 Americans have died of cancer.[2]

There is a variety of treatment methods available in order to treat cancer. Most common methods are surgery, radiation, chemotherapy, hormone therapy and biological therapy. Before any treatment of cancer can be attempted, a correct diagnosis has to be performed. Therefore, developing robust methods for diagnosing cancer in the earliest disease stages is the key to overcoming this often fatal disease. The early cancer detection methods are so important, because the cancer survival rates can be significantly increased if it is detected at an early stage. The process of checking people for cancer, who do not have any symptoms of cancer, is commonly referred to as "screening".[3] Screening and detection methods differ from one type of cancer to the other, because there are significant biochemical differences between the types of cancer (e.g. brain, breast, lung, pancreas, prostate etc.). Most of these differences arise, because different types of cancer develop from different types of cells.

This research is mainly focused on considers two main types of cancer, namely breast cancer and lung cancer. Consequently, the diagnostics of breast and lung cancer will be discussed.

1.1.1 Breast Cancer

Other than skin cancer, breast cancer is the most widespread cancer type in women.[2] In the USA breast cancer shows the highest incidence rate. The lifetime probability of developing cancer for women is also high with breast cancer comparative to other cancer types. These facts warrant the importance of breast cancer detection: The 5-year relative survival decreases to 24

percent at the distant stage, from 84 percent at the regional stage and 98 percent at the localized stage.[1]

There are several stages of breast cancer. The pathological classification of tumors that exist today is mainly based on changes in cell morphology. Early stage or stage 0 breast cancer is when the disease is localized to the breast with no evidence of spreading to the lymph nodes (carcinoma in situ).[1] Stage 1 breast cancers are two centimeters or less in size and it has not spread any further. Stage 2 again can be divided into two categories.[1] Stage 2A breast cancer is a tumor less than two centimeters across with lymph node involvement, or a tumor that is larger than two (but less than five) centimeters across without underarm lymph node involvement.[1] Stage 2B is a tumor that is greater than five centimeters across without lymph node involvement, or a tumor that is larger than two but less than five centimeters across with lymph node involvement.[1] Locally advanced breast cancer (metastatic) results after cancer cells spread to the lymph nodes. Stage 3 can be divided in to three key parts. Stage 3A breast cancer is also called locally advanced breast cancer.[1] The tumor is larger than five centimeters and has spread to the lymph nodes under the arm, or a tumor that is any size with involvement of 4-9 axillary lymph nodes.[1] Stage 3B breast cancer is a tumor of any size that has spread to the skin, chest wall, or internal mammary lymph nodes (located beneath the breast and inside the chest). Inflammatory breast cancer falls into this category.[1] Stage 3C breast cancer is a tumor of any size that has spread to more than 10 axillary lymph nodes. The Final stage is Stage 4 breast cancer. It is defined as a tumor, regardless of size, that has spread to places far away from the breast, such as bones, lungs, liver, brain, or distant lymph nodes.[1]

There is another approach to define the types of breast cancer, depending on the expression of receptors in the cell walls of the cancer cells. Endocrine receptors (estrogen or progesterone receptor) target hormones. ER+ means, the tumor expresses receptors for estrogen. PR+ means, it has receptors for progesterone. ER- and PR- mean that the tumor does not express receptors for either hormone. In general, hormone receptors promote tumor growth if they bind their targets. Roughly, two out of three of all breast cancer tests are positive for hormone receptors.

HER2/neu (human epidermal growth factor receptor 2), also called ErbB2, is a protein that appears on the surface of some breast cancer cells. HER2 positive cancers express receptors for human epidermal growth factor.

All remaining tumors are grouped together and classified as "Triple Negative breast cancers". That means, these cancers are not positive for estrogen, progesterone, or HER2 receptors. It is noteworthy that the group of Triple Negative breast cancers is by no means homogeneous.

On the other hand, the fourth group, "Triple Positive breast cancer", is positive for estrogen receptors, progesterone and HER2 receptors.

Depending on this classification, physicians obtain important information with regard to cancer treatment. For instance, the various sub-groups of breast cancers are known to react differently to combinations of anticancer drugs. The exception of this rule is again the group of Triple Negative breast cancers, which is very heterogeneous.[4]

To date, there are several breast cancer detection methods available. The most important are mammography, ultrasound detection, magnetic resonance imaging and molecular breast imaging.[5] Regarding the early detection of breast cancer, the American cancer society suggests following several screening guidelines.[1] Firstly, starting at age 40, yearly mammograms are recommended. Secondly, as a part of the periodic health examination, a clinical breast exam should be included. Thirdly, women at the beginning in their early 20s should be told about the benefits and limitations of breast self exams.

Figure 1.1 shows survival of breast cancer patients vs. stage of detection. According to Figure 1.1 breast cancer mortality can be substantially reduced if we can detect breast cancer at the localized stage, before it has metastasized.
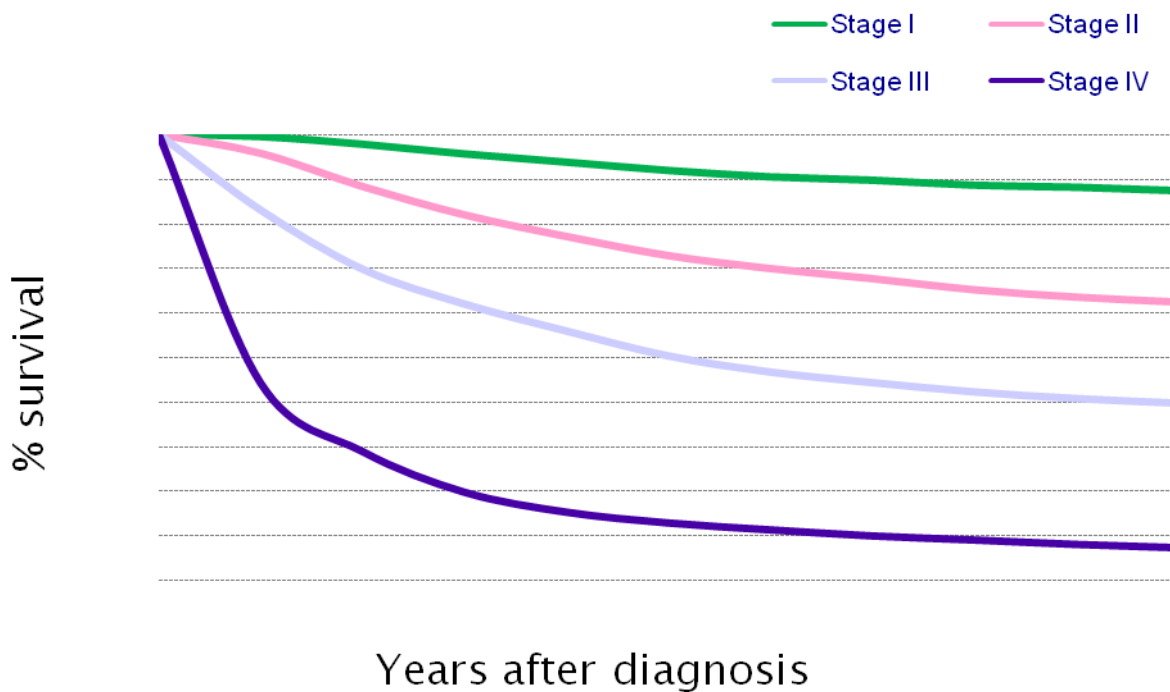
Figure 1.1 : Survival of Breast Cancer Patients vs. Stage of Detection (Taken from : West Midlands Cancer Intelligence Unit, UK, 2009) (British Cancer Society, 2011). [6]

1.1.2 Lung Cancer

In both men and women, lung cancer causes more deaths than any other cancer. The 5-year relative survival decreases to 4 percent at the distant stage, from 25 percent at the regional stage and 52 percent at the localized stage.[1]

There are three main factors, which decide the stage of the lung cancer. They are the size, how deep the tumor has invaded nearby tissue, and whether the cancer cells have spread to lymph nodes.[1] Two major types of lung cancer are non-small cell lung cancer (NSCLC) and small cell lung cancer (SCLC).[1]

There are five stages of non-small cell lung cancer. Stage 0, abnormal cells are found only in the innermost lining of the lung.[1] Stage 1, the tumor has grown through the innermost lining of the lung into deeper lung tissue and it is no more than 5 cm across.[1] Stage 2, the tumor is smaller than 7 cm across and cancer cells are found in nearby lymph nodes.[1] Stage 3, the

tumor may be any size and more than one malignant tumor may be found within the lung.[1] Stage 4, malignant tumors are found in both lungs or the cancer has spread to other parts of the body.[1]

There are two stages of small cell lung cancer. The first stage is limited stage. Cancer is found only on one side of the chest.[1] The second stage is called the extensive stage. Cancer is found in the lung and also in tissues on both sides of the chest or found in distant organs.[1]

There are several screening methods available for lung cancer. Some of them are tests of sputum (mucus brought up from the lungs by coughing), chest X-rays and spiral (helical) CT (Computerized Tomography) scans.[3]

1.2 Proteases

Proteases are a class of enzymes that catalyze the cleavage of a specific peptide bond in other proteins. They are also called proteolytic enzymes or proteinases.[7] There are six different catalytic classes of proteases named as aspartic, metallo-, cysteine, serine, threonine and glutamic. This classification is based on the group performing the nucleophilic attack at the carbonyl group. The nucleophile differs from one group to the other. Aspartic, metallo- and glutamic proteases have a polarized water molecule as the nucleophile within their active center. Serine and threonine proteases have the hydroxyl group and cysteine proteases have the sulfhydryl group as the nucleophile at the active center.[8]

Cancer-related proteases have the potential to become reliable biomarkers for the detection of solid tumors in early stages.[9,10,11] Quite a few proteases are known to be necessary for cancer development and progression including Matrix Metallo-proteinases (MMPs), urokinase plasminogen activator (uPA) and Cathepsins (CTSs).[9,10,11] They are critical cofactors during cancer progression. There are several remodeling processes that take place with the stroma, the ECM (Extra Cellular Matrix) and cell surfaces. Those processes are the requirements of the tumorigenic processes for the neoplastic, vascular or inflammatory cells invasion. These proteases are expressed with tumor progression and metastasis. Also they cooperate with ECM and cell surface substrates. They do activate inactive zymogens, which are initially secreted as well. Figure 1.2 shows how these proteases act with cancer development.[12],[13]

These proteases don't function individually. They do act in a cascade-like manner. Figure 1.3 shows this network structure of the activity of proteases.[14,15] Also these proteases are very stable in tissue and blood serum. Therefore, they are suitable biomarkers.[16]

1.2.1 Serine Proteases

"Serine proteases are members of the protease family. These enzymes are named after the reactive serine residue located in the active site that is essential for the function of the enzyme."[17] Among those serine proteases, urokinase plasminogen activator (uPA) is playing a major role in association with cancer. It is involved in the processes of ECMdegradation and basement membrane dissolution, which will be linked to the invasiveness and metastasis of various cancers.[18]

There are four main components of the uPA/uPAR system such as serine protease uPA, its cell membrane associated receptor (uPAR), a substrate (plasminogen) and plasminogen activator inhibitors (PAI-1 and PAI-2).[19]
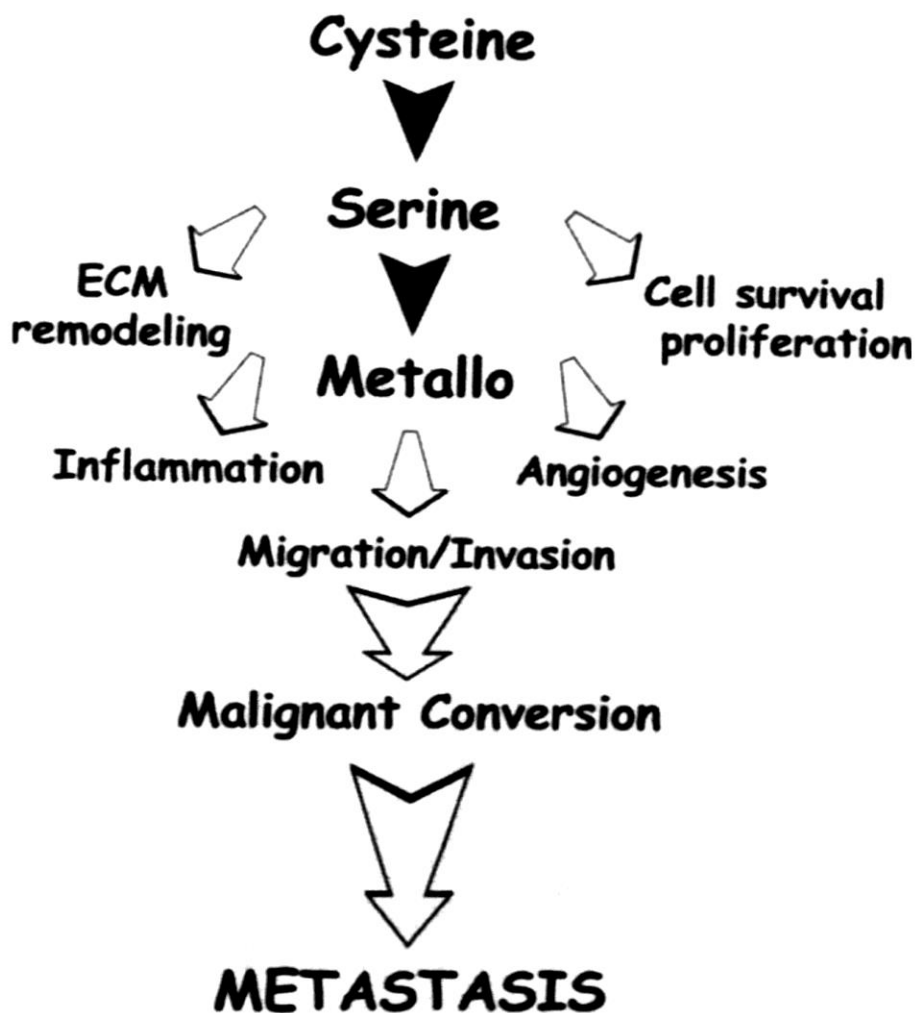
Figure 1.2: Involvement of Proteases with Cancer Development, With Permission of Reference 13
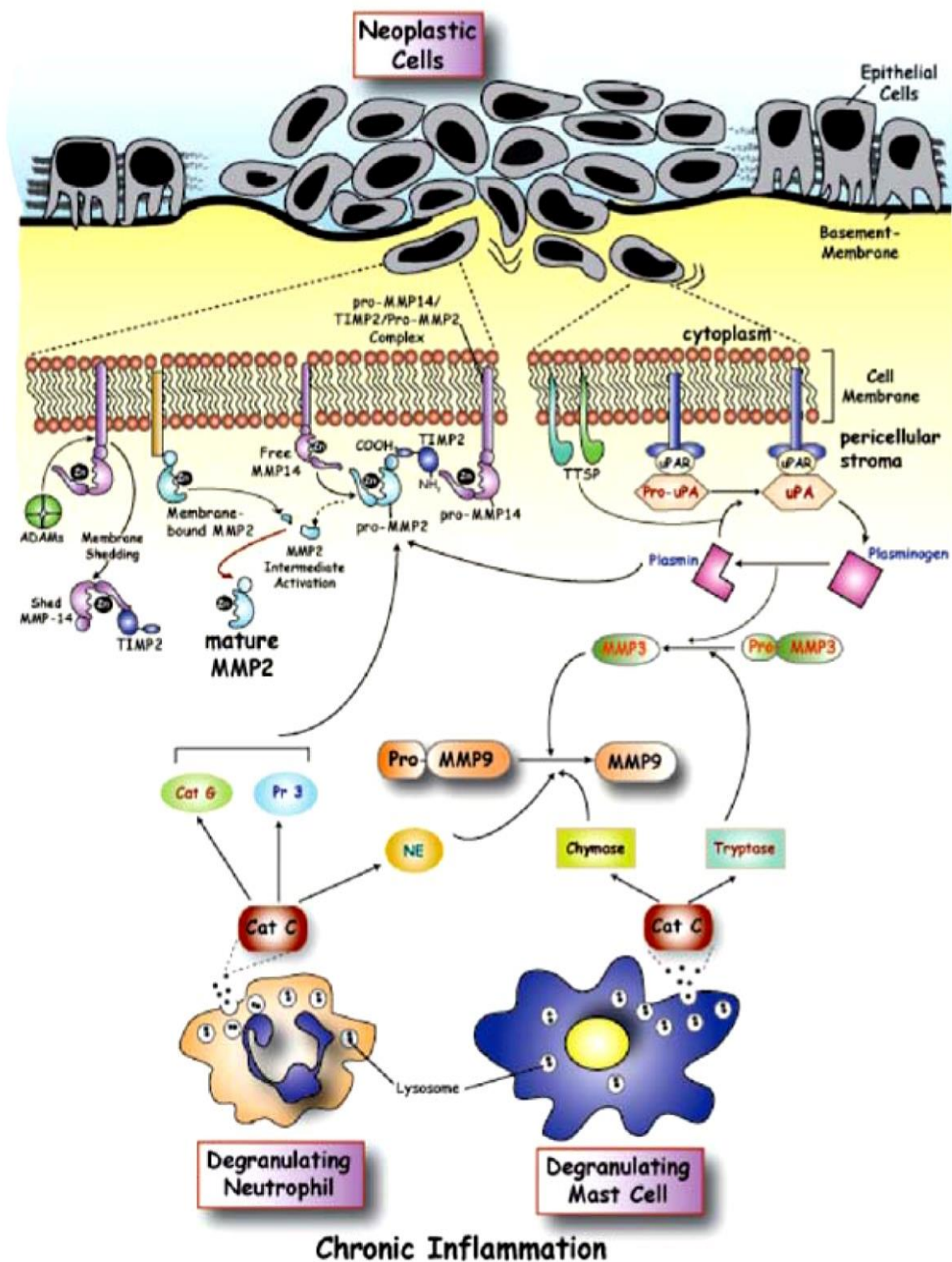
Figure 1.3: Intersecting Protease Pathways during Neoplastic Progression, With Permission of Reference 13

In order to get the uPA enzyme active, several processes should be followed. The zymogen plasminogen can be transferred to the active serine protease plasmin by the active uPA enzyme. This active serine protease plasmin engages in supporting tumor migration by means of direct proteolytic digestion or activation of other zymogen proteases. The active uPA enzyme is an active two-chain uPA molecule. It is formed upon the cleavage of bound pro-uPA and uPAR system by various proteases. Pro-uPA is a zymogen, which is deficient in plasminogen activating activity. So uPA is produced and secreted as single chain polypeptide, pro-uPA.[20]

1.2.2 Matrix Metalloproteinases
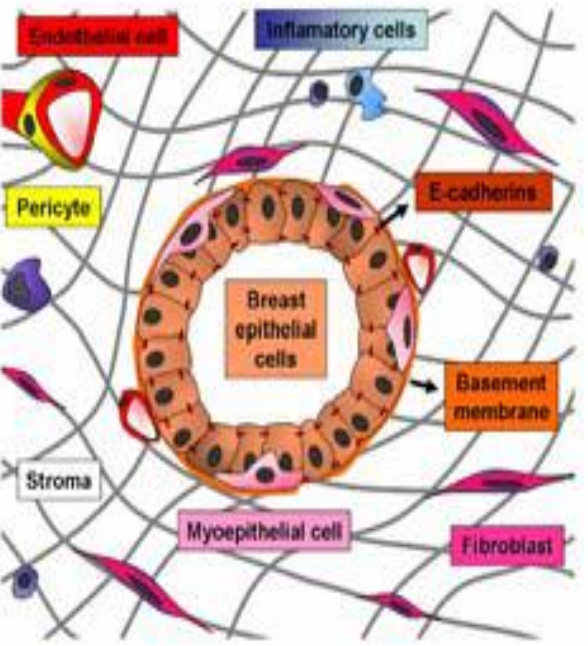
"Matrix metalloproteinases (MMPs) constitute a family of extracellular matrix (ECM) remodeling proteinases implicated in physiological and pathological processes that include morphogenesis, wound healing, tissue repair and the progression of diseases such as arthritis, cancer and cardiovascular disease."[8] They can be sub classified according to substrate specificity (e.g. collagenases, gelatinases, stromelysins). They need a zinc (II) cation at the active site. This family consists of about 20 enzymes.[21] There are at least three conserved regions with these MMPs. Proteolytic activity is performed by the zinc binding motif (HEXXHXXGXXH), interaction with the zinc ion in the zymogen form is achieved by the cysteine residue of the propeptide cysteine site (PRCGXPD) and maintenance of the zinc binding site integrity is done by the methionine turn (XXMXP).[22] Tumor angiogenesis is the key step in which MMPs are involved, especially MMP2 and MT1-MMP that are expressed by endothelial cells.[21] Hormones, growth factors, cytokines and tissue inhibitors of metalloproteinases (TIMPs) are the regulatory factors of the expression of most MMPs. Table 1.1[23] shows the categorization of the MMP family and Table 1.2[22] shows implication of MMPs in cancer progression. Figure 1.4 shows how these proteases behave with the progression of cancer[24].

Table 1.1 : Categorization of the Matrix Metalloproteinases Family

MMP Designation	Structural Class	Common Name(s)
MMP-1	Simple hemopexin domain	Collagenase-1, interstitial collagenase, fibroblast collagenase, tissue collagenase
MMP-2	Gelatin-binding	Gelatinase A, 72-kDa gelatinase, 72-kDa type IV collagenase, neutrophil gelatinase
MMP-3	Simple hemopexin domain	Stromelysin-1, transin-1, proteoglycanase, procollagenaseactivatin protein
MMP-7	Minimal domain	Matrilysin, matrin, PUMP1, small uterine metalloproteinase
MMP-8	Simple hemopexin domain	Collagenase-2, neutrophil collagenase, PMN collagenase, granulocyte collagenase
MMP-9	Gelatin-binding	Gelatinase B, 92-kDa gelatinase, 92-kDa type IV collagenase
MMP-10	Simple hemopexin domain	Stromelysin-2, transin-2
MMP-11	Furin-activated and secreted	Stromelysin-3
MMP-12	Simple hemopexin domain	Metalloelastase, macrophage elastase, macrophage metalloelastase
MMP-13	Simple hemopexin domain	Collagenase-3
MMP-14	Transmembrane	MT1-MMP, MT-MMP1
MMP-15	Transmembrane	MT2-MMP, MT-MMP2

MMP-16	Transmembrane	MT3-MMP, MT-MMP3
MMP-17	GPI-linked	MT4-MMP, MT-MMP4
MMP-18	Simple hemopexin domain	Collagenase-4 (*Xenopus;* no human homologue known)
MMP-19	Simple hemopexin domain	RASI-1, MMP-18
MMP-20	Simple hemopexin domain	Enamelysin
MMP-21	Vitronectin-like insert	Homologue of *Xenopus* XMMP
MMP-22	Simple hemopexin domain	CMMP (chicken; no human homologue known)
MMP-23	Type II transmembrane	Cysteine array MMP (CA-MMP), femalysin, MIFR,

Table 1.2 : Implication of MMPs in Cancer Progression, Taken from Reference 22

Sources of MMPs

- Tumor cells
- Myoepithelial cells
- Endothelial cells
- Perivascular cells (pericytes, smooth muscle cells)
- Inflammatory cells (neutrophils, macrophages, mast cells)
- Fibroblasts (myofibroblasts)

1 - Epithelial to mesenchymal transition
- Loss of cell-cell adhesion:
  E-cadherin cleavage
- Release of β-catenin and transcriptional regulation of gene expression

2 - Proliferation, apoptosis
- Activation of growth factors
- Release of growth factors from bound protein or ECM
- Shedding of cell surface receptor (FGF-R1)
- Shedding of FasL, TNFa

3 - Angiogenesis
- Activation of angiogenic factors
- Release of angiogenic factors from bound protein or ECM
- Activation of integrin subunits
- Generation of angiogenic inhibitors (angiostatin, tumstatin, endostatin)
- Recruitment of perivascular cells
- Endothelial cell tubulogenesis
4 - Migration, invasion, metastases
- ECM degradation
- Exposition of cryptic site by proteolysis
- Shedding of cell surface molecules (CD44, tTG)
- Activation of integrin subunits

| Initial Mutations | → | Cell Survival & Tumor Progression Mutations | → | Angiogenesis | → | Invasion |

| None implicated | MMP 1 - Collagenase 1
MMP 3 – Stromolysin 1
MMP 7 – Matrilysin
MMP 11 – Stromolysin 3
MMP 13 – Collagenase | Urokinase (uPA)
Seprase
MMP 3 – Stromolysin 1
MMP 7 – Matrilysin | MMP 1 - Collagenase 1
MMP 2 – Gelatinase 1
MMP 3 – Stromolysin 1
MMP 7 – Matrilysin
MMP 8 - Collagenase 2
MMP 9 - Gelatinase 2
MMP 11 – Stromolysin 3
MMP 13 – Collagenase 3 |

Figure 1.4 : General Paradigm for the Expression of Proteases during Cancer Progression, Angiogenesis and Invasion. (Reproduced with Permission from Reference 24)

1.2.3 Cathepsins

Cathepsins are a group of lysosomal cysteine proteases belong to the papain family. Cathepsins B, C, H, F, K, L, O, S, V, W and X (sometimes called cathepsin Z) are the 11 members of human Cathepsins and there are 18 members found in mice. The active site of these cathepsins consists of cysteine, histidine and asparagine residues. Table 1.3 shows the nomenclature and expression patterns of cysteine cathepsins.[25]

Table 1.3 : Nomenclature and Expression Patterns of Cysteine Cathepsins in Human and Mouse (Taken from Reference 25)

Protease (Alternative names)	Human (11)	Mouse (18)	Expression Pattern
Cathepsin B	CTSB	CtsB	Ubiquitous
Cathepsin C (J, Dipeptidyl peptidase I)	CTSC	CtsC	Ubiquitous
Cathepsin F	CTSF	CtsF	Ubiquitous
Cathepsin H	CTSH	CtsH	Ubiquitous
Cathepsin K (O, O2)	CTSK	CtsK	Osteoclasts, lung-epithelium, thyroid gland
Cathepsin L	CTSL	-	Ubiquitous
Cathepsin L2 (V)	CTSL2	CtsL	Thymus, testis, cornea, epidermis, macrophages
Cathepsin O	CTSO	CtsO	Ubiquitous
Cathepsin S	CTSS	CtsS	Lymphatic tissues, antigen -presenting cells (APC), muscle
Cathepsin W (Lymphopain)	CTSW	CtsW	Natural killer (NK) cells, cytotoxic T lymphocytes

Cathepsin X (Z, P, Y)	CTSZ	CtsZ	Ubiquitous
Cathepsin J	-	CtsJ	Placenta
Cathepsin M	-	CtsM	Placenta
Cathepsin Q	-	CtsQ	Placenta
Cathepsin R	-	CtsR	Placenta
Cathepsin 1	-	Cts1	Placenta
Cathepsin 2	-	Cts2	Placenta
Cathepsin 3	-	Cts3	Placenta
Cathepsin 6	-	Cts6	Placenta

Figure 1.5: Overexpression and Secretion of Cathepsins Induce the Invasion and Metastasis of Tumor Cells, From Reference 26

"Cathepsins B, L and D are lysosomal cysteine and aspartic proteinases, distributed in almost all mammalian cells."[26] Basically all cathepsins are involved in cancer progression. Degradation of the extracellular matrix is the major activity of cathepsin L.[26] Cathepsin B promotes cancer cell in invasion via matrix degradation. Reduction of the primary immune response is the important activity of cathepsin D.[26]

Figure 1.5 shows the imbalance between cathepsins and CPIs, cathepsin protease inhibitors in tumor cells.[26]

1.3 Proteases and Breast Cancer

Several proteases from the above three families are specifically involved in the progression of breast cancer.

First, from the MMPs family, Iwata et al. have shown MMP 1, MMP 2 and MMP 9 are highly expressed in human breast carcinoma cells.[27] Kossakowska et al. and other researchers have shown that in addition to MMPs 1, 2 and 9, MMPs 3, 11, 13 and 16 also have a high frequency of expression in breast cancers.[27]

Second, from the family of serine proteases, urokinase plasminogen activator (uPA) is the key member, which is involved in the progression of breast cancer. [28,29]

Third, we have to consider the cathepsin family. Estrogen has an effect on breast cancer growth and invasion. That effect can be mediated by cathepsin D, because it can work as an autocrine mitogen that can be activated at acidic pH, which will lead to the degradation of the extracelluar matrix.[30] Also cathepsin B can degrade type IV collagen, which will lead to the invasion by inflammatory breast cancer cells.[31]

1.4 Proteases and Lung cancer

There are several proteases engaged in lung cancer. Most of them belong to any of the three protease families discussed in 1.2.

Starting with the MMP family, Muller et al. reported the overexpression of some MMPs with the NSCLC. They showed overexpression of stromelysin-2 (MMP 10), collagenase-1 (MMP 1), and pump-1 (matrilysin, or MMP 7) messenger RNA in human non-small cell lung cancer (NSCLC) tissues.[32] The levels are high compared to normal bronchial mucosa. Also Compared to normal tissue stromelysin-3 (MMP 11), collagenase-1 (MMP 1), gelatinase B (MMP 9), and matrilysin (MMP 7) are significantly higher in lung tumors.[31]

Urokinase - type plasminogen activator (uPA) and its receptor (uPAR) also play a major role in lung cancer metastasis.[33]

With regard to the cathepsin family, tumor progression is accelerated by overexpression of cathepsin B.[34] Cathepsin L is another enzyme from the cathepsins family, which is elevated in lung tumor tissue. Cathepsin S is elevated in non-infiltrated and infiltrated lymph nodes.[35] Also increased levels of cathepsin H, L and K provide a greater chance to the development of lung cancer.[36]

Acknowledgement

At this point, I would like to acknowledge all the collaborators, who contributed their knowledge and expertise towards the success of the projects on protease assays.

These material described in section 1.5 and 1.6 has led to the following publication.

1.5 Nanoparticle based "Light Switches"

1.5.1 Motivation for the Development of a "Light Switch"

Most of the studies in cancer diagnostics have been performed using ELISA (enzyme linked immunosorbent assays).[37] It is impossible to determine the activity of the proteases when the concentration of them is measured using ELISA. The reason behind that is, these proteases occur as inactive precursors (zymogens), active enzymes or enzyme inhibitor complexes. They are activated through an activation network. The activation network for MMPs is shown in Figure 1.6.
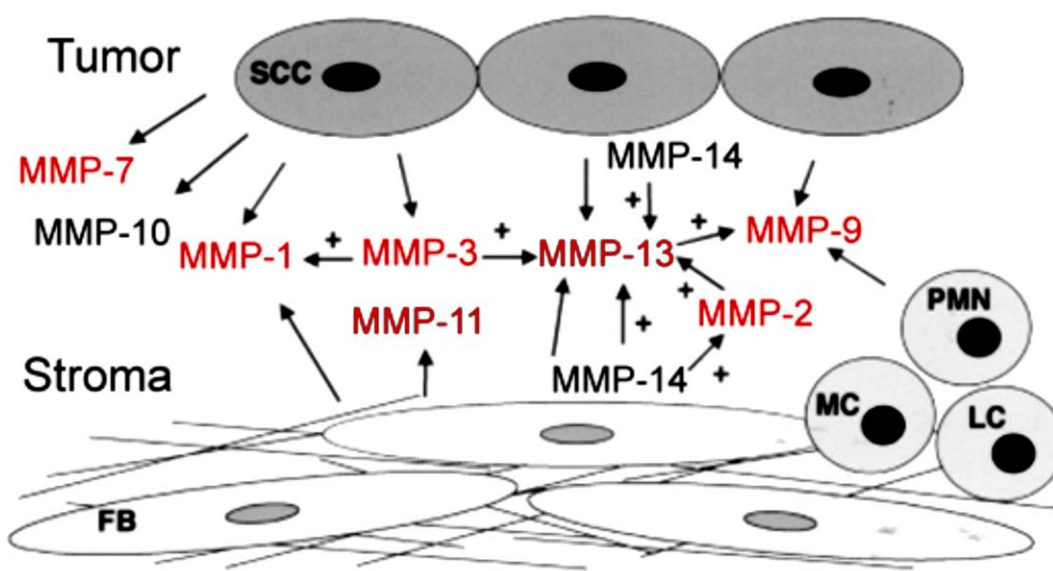
Figure 1.6 : Expression of Distinct Matrix Metalloproteinases (MMP's) by Tumor Cells, Stromal Fibroblasts (FB), and Inflammatory Cells (PMN, polymorphonuclear leukocyte; MC, monocyte; LC, lymphocyte, scc: squamous cell carcinoma, (Taken from Reference 38)

In Figure 1.6, the emphasis is on "carcinoma". Activation of latent MMPs is indicated by "+". MMP's that have been measured in the research are marked in red.

Other than ELISA, there are several approaches towards cancer diagnostics. Some of them are electrochemical analysis methods[39], immunohistochemical staining methods[40] and fluorescence in situ hybridization (FISH).[41]

Unfortunately, cancer does not show significant symptoms in early stages. Consequently, the detection of cancer at stages where treatment is feasible with established technologies, is very challenging. If we can identify cancer by performing a blood test of a person, that would be a significantly early cancer detection method. This should be done during the annual checkup of a person. My thesis research is based on the paradigm that monitoring the protease signature of the patient provides the basic concept for early cancer detection and detecting cancer recurrence. This is, principally, the motivation behind developing nanoplatforms for cancer detection based on the "nanoparticle based light switch" technology.

I have used fluorescence detection for the quantitative monitoring of active proteases (not zymogens!) using highly protease-selective nanoplatforms. Fluorescence detection methods have the advantage of being more sensitive than ELISA measurements, electrochemical methods and UV/Vis absorption methods.[42]

Based on the literature quote above, I have tested 12 proteases using this nanoparticle - based system (Light switch). Table 1.4 shows the proteases that were used and the consensus sequences for them.

Table 1.4: Consensus Sequences of the Proteases[43,44]

Protease	Consensus Sequence (Cleavage Sequence)
MMP-1	VPMS-MRGG
MMP-2	IPVS-LRSG
MMP-3	RPFS-MIMG
MMP-7	VPLS-LTMG
MMP-9	VPLS-LYSG
MMP-11	GGAAN-LVRGG
MMP-13	GPQGLA-GQRGIV
uPA	SGR-SA

Cathepsin B	SLLKSR-MVPNFN
Cathepsin D	SLLIFR-SWANFN
Cathepsin K	GPR-AG
Cathepsin L	SGVVIA-TVIVIT

The development of fluorescence-based molecular[45], macro-molecular[46] and nanoparticle-based protease sensors[47] that feature consensus sequences (cleavage sequences) between a fluorescent dye and a quencher has been sparked by the pioneering research of R. Weissleder and collaborators.[48] Consensus sequences are oligopeptides that are optimized to facilitate fast proteolytic cleavage by their respective protease, but not by every other protease. Therefore, they are characterized by a very high selectivity (by a factor of 40 to 1,000) towards the protease they are designed to detect.[44] Influenced by N. J. Turro, who introduced the concept of a "molecular light switch" in 1990[49], the research on *in-vitro* protease activity sensors during the last decade has been geared towards ever higher fluorescence signal enhancement upon cleavage of the consensus sequence between fluorophore and quencher.[50] For *in-vitro* applications, near-infrared (NIR) dyes have been developed, which were optimized for maximal light penetration depth.[51] Protease sensor based on fluorescence quenching by tethered nanoparticles[52] or fluorescent quantum dots to which quenchers are tethered via consensus sequences[53], were explored during the last decade. The established limit of detection of fluorescent protease sensors is in the low picomolar to sub-picomolar range.[54]

1.5.2 Consensus-Sequence Based Fluorescence Detection of Protease Activity

In this work we have combined fluorescence resonance energy transfer quenching (FRET)[55] and plasmon-resonance quenching[56] to push the limits of detection (LOD) to as low as 10^{-16} mol L^{-1} for a series of 12 cancer-related proteases. The resulting nanoplatforms are based on a central Fe/Fe_3O_4 core/shell nanoparticle that can be synthesized with very low polydispersity.[57,58] Tetrakis(4-carboxyphenyl)porphyrin (TCPP)[59] is tethered via consensus sequence to dopamine, which is bound to the Fe_3O_4 layer at the Fe/Fe_3O_4 surface. The dye cyanine 5.5[60], which possesses overlapping absorption/fluorescence spectra with the

fluorescence spectrum of TCPP, was permanently attached via dopamine-anchors to the nanoparticle's surface.

The logic behind this light switch technology is that it can be switched "on" in the presence and activity of the enzyme. This process is as follows: A specific consensus sequence can be cleaved by its specific enzyme, which will lead to fluorescence of the attached fluorophore. Before we introduce the specific protease that is able to cleave the consensus sequence to the system, the fluorescence of the fluorophore is quenched. Quenching of TCPP-fluorescence occurs via two pathways. The first is plasmonic quenching by the nanoparticle. [61,62] The second is singlet to singlet energy transfer from TCPP to cyanine 5.5, also known as fluorescence resonance energy transfer (FRET).[61] Both pathways are necessary to ensure significant quenching of TCPP as long as it is tethered to the Fe/Fe_3O_4-nanoparticle. After the introduction of the protease, it will cleave the consensus sequence and then the fluorophore is free to move away from the nanoplatform. Consequently, both quenching mechanisms become inefficient with increasing distance.

1.5.3 Technical Requirements for a Successful Nanoplatform for Early Cancer Diagnostics by Means of Fluorescence Detection

Many state-of-the-art analytical methods, such as immunoassays[16] or electrochemical detection methods[63,64] can quantify the protease concentrations occurring in cancer tissue, but they are not (yet) sensitive enough to measure protease activities that are observed during early stages of cancer development. These tests have to be performed in blood (serum) to have any value in early diagnostics. This requirement leads to significant dilution effects. The development of nanoplatforms for the diagnostics of solid tumors, such as breast cancer or lung cancer, in early stages, is based on the paradigm that the concentration of each proteolytically active cancer-related protease is typically below 10^{-13} mol L^{-1} in the blood serum of healthy human subjects.[42] It is anticipated that one or several proteases are overexpressed in early cancers and that, therefore, their concentrations in blood serum increase to 10^{-12} mol L^{-1} to 10^{-10} mol L^{-1}. The concentration of selected proteases will then further increase in late stage cancer patients.[42] It is noteworthy that virtually all proteases are biosynthesized as zymogens (inactive precursor enzymes), which require enzymatic activation.[65] Zymogens are usually not indicative of tumor progression.[65] Therefore, it is of great importance to measure the activity, and not the

concentration, of cancer-related proteases.[42] In stark contrast, immunoassays rely on the presence of epitopes, which are present in active and inactive proteases alike.[16]
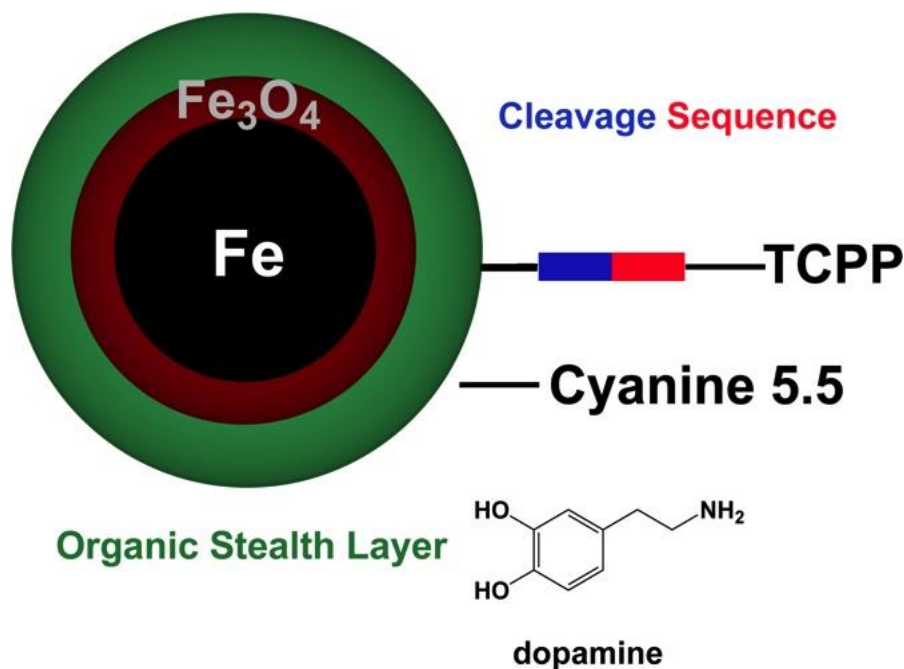
Figure 1.7 : Nanoplatform for Protease Detection.

With this nanoplatfrom, which is shown in figure 1.7, one Fe/Fe_3O_4-nanoparticle is linked in average to 35+/-3 TCPP-molecules via consensus sequence (one type of sequence per nanoplatform) and 50+/-4 cyanine 5.5 molecules via amide linkages.

1.6 Fluorescence Detection

Steady state fluorescence detection is the technique used during the analysis. This technique was selected due to its high sensitivity in detecting variations in the concentration of fluorophores.[66] "Fluorescence is the property of some atoms and molecules to absorb light of a particular wavelength and after a brief interval, termed the fluorescence lifetime, to emit light at a longer wavelength."[67] That means the luminescence occurs from one excited electronic singlet state to another singlet (usually the ground state). With fluorescence $\Delta s=0$ processes are allowed and $\Delta s= 1$ processes are forbidden. That means singlet-to-singlet energy transfer is spin allowed and singlet to triplet energy transfer is spin forbidden. Generally fluorescence life-time is around 10 ns.[68]
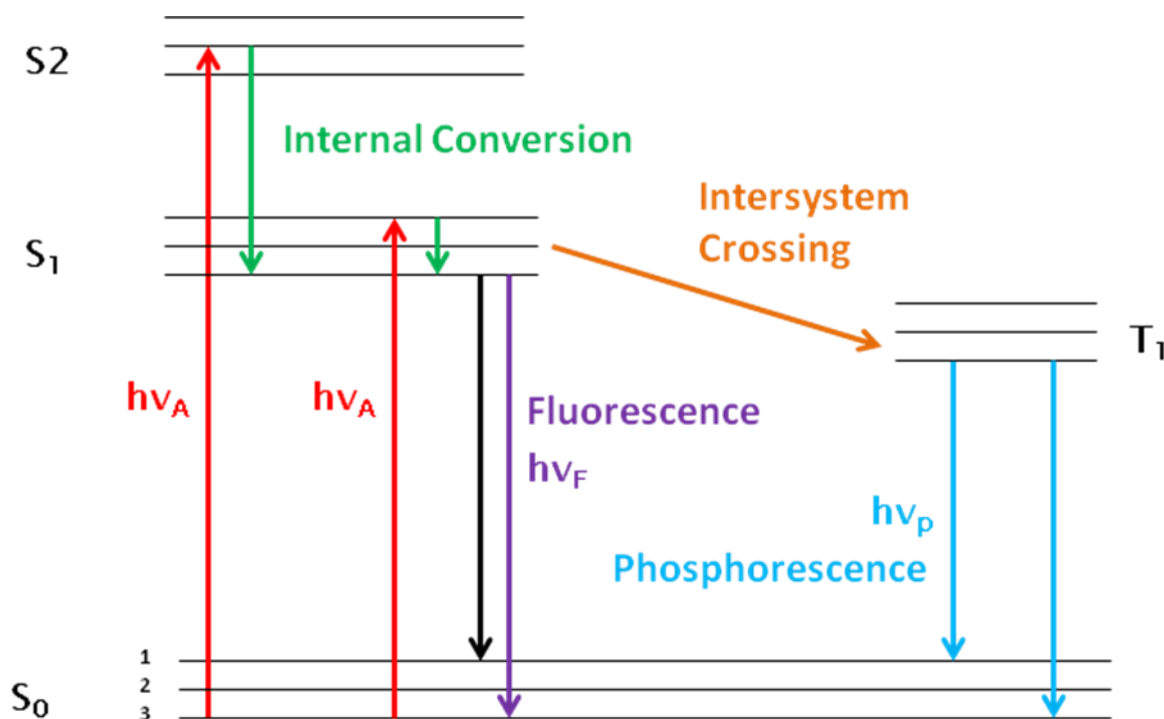
Figure 1.8: Simplified Version of Jablonski Diagram (According to Reference 68)

Figure 1.8 shows the resulting energy diagram.[68] Electronic energy states are denoted as S. The Singlet ground state is S_0, singlet first state is S_1 and singlet second state is S_2 etc. In each electronic energy state, there are several vibrational energy levels denoted as 0,1,2, etc. Upon light absorption a fluorophore is excited to a higher energy electronic state such as S_1 or S_2. Then the internal conversion occurs which means the fluorophore is relaxed back to the lowest vibrational level of S_1. Then the emission from S_1 to S_0 is known as fluorescence.

Figure 1.9 shows the schematic diagram of the spectrofluorometer.[68] The quality of the parts of the spectrofluorometer is important for the accomplishment of accurate fluorescence measurements.
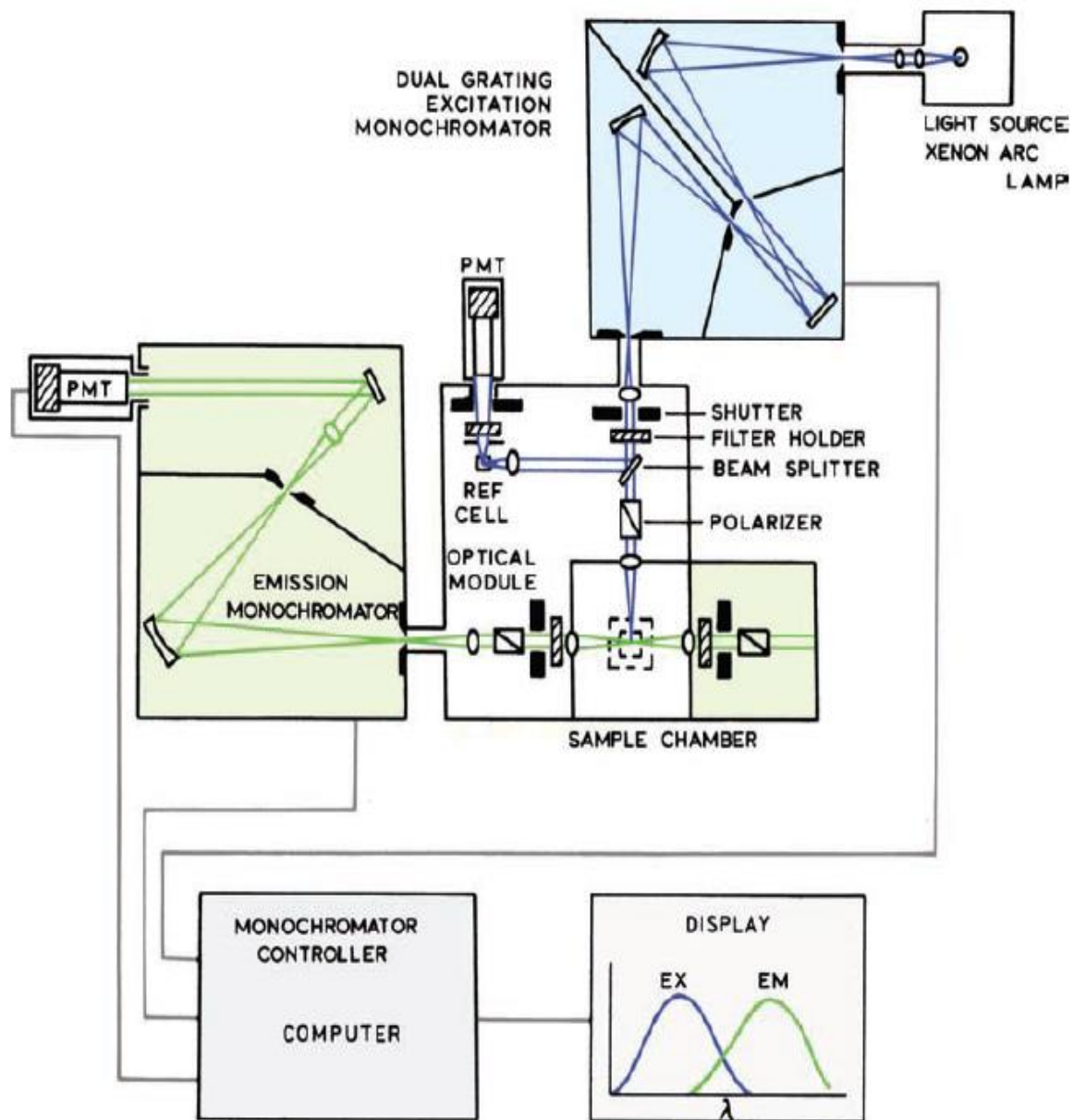
Figure 1.9: Schematic Diagram of the Spectrofluorometer, with permission from Reference 68 (PMT: Photomultiplier Tube)

The two main types of fluorescence measurements are steady-state and time resolved fluorescence.[68] Steady state measurements are the widespread type. Throughout my research, steady state fluorescence measurements are used. The fluorescence intensity is recorded upon illuminating the sample with a continuous light beam.

1.6.1 Fluorophores

A fluorescent molecule (usually a aromatic molecule), which can emit light upon excitation is a fluorophore. There are two major classes: Intrinsic and extrinsic fluorophores. Naturally, occurring fluorpohores are known as intrinsic fluorophores. Well-known intrinsic fluorophores are chlorophyll, NADH and flavins. Extrinsic fluorophores are the ones, which have to be added to the sample to provide fluorescence. Well-known extrinsic fluorophores are fluorescein and rhodamine. In order to be used with a given application, the optical characteristics of the particular fluorophore should be considered.[68]

1.6.1.1 Porphyrins

Porphyrins are naturally occurring organic compounds. The most important porphyrin is heme, which is the pigment in red blood cells. They are aromatic molecules. Porphyrins have a planar macrocyclic structure of four pyrrole rings connected by methine bridges.[69] There are several applications of porphyrins. Main application with this research is the capability of acting as a fluorophore. Catalysis, photosynthesis, photodynamic therapy [70]and sensors[71] are few other applications of porphyrins. Porphyrins have a strong absorption in the 400-450 nm region (Soret band) and weaker absorptions in the 500-700 nm region (Q-bands).[72] Among the porphyrins, we have selected the Tetrakis(4-carboxyphenyl)porphyrin (TCPP). Figure 1.10 shows the chemical structure of TCPP.
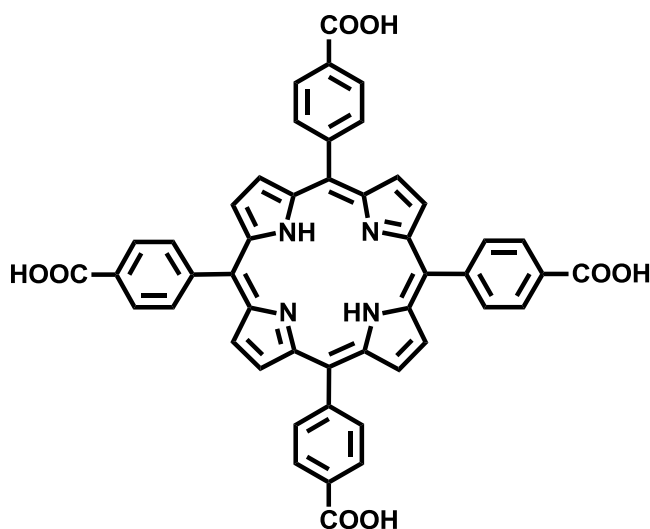
Figure 1.10: Chemical Structure of Tetrakis(4-carboxyphenyl)porphyrin (TCPP)

When excited in its Soret band at 416 nm (ϵ_{416} = 365,000 $M^{-1}cm^{-1}$ [73]), TCPP features two strong emission peaks at 650 nm and 716 nm in PBS buffer (phosphate buffered saline, pH = 7.4).[74] When tethered to Fe/Fe_3O_4-nanoparticles, the maximum of the Soret band is slightly red-shifted to 421 nm, whereas its fluorescence maxima are slightly blue-shifted (647 and 707 nm). The TCPP emission spectrum has a total range from 620 nm to 740 nm. The UV-Vis spectrum of Cy 5.5 in PBS buffer reveals a broad absorption over the range of 550 nm to 745 nm with two maxima at 630 nm and 680 nm respectively (Figure 1.11).[75] We have selected TCPP and cyanine 5.5 because of their broad overlap between the emission spectrum of TCPP and the absorption and emission spectra of cyanine 5.5. Significant fluorescence quenching of TCPP by cyanine 5.5 in PBS is observed.
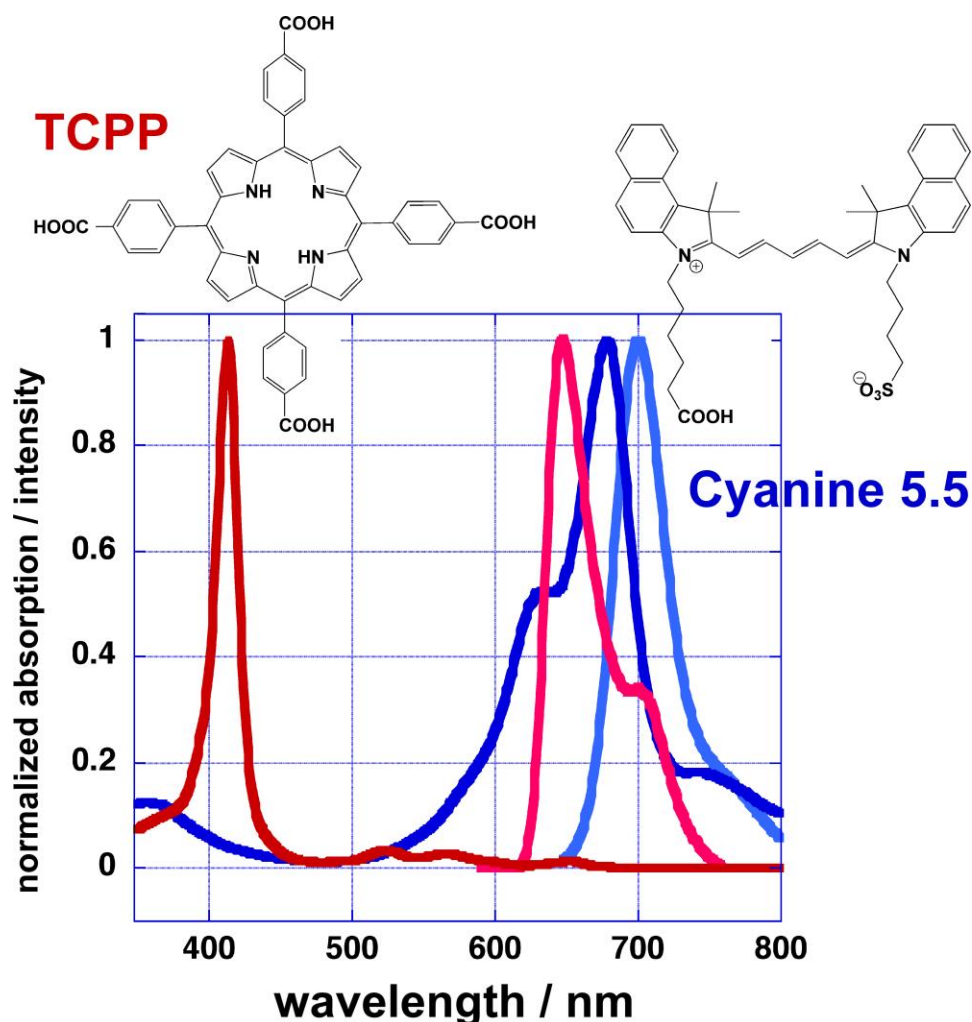
Figure 1.11: Normalized UV/Vis-Absorption and Fluorescence Spectra of TCPP and Cyanine 5.5

1.6.2 Fluorescence Quenchers

There are several substances, which can act as fluorescence quenchers. Well known ones are molecular oxygen, heavy atoms and quenchers of protein fluorescence.[68]

1.6.2.1 Quenching of Fluorescence

A process that decreases the fluorescence intensity is known as fluorescence quenching. There are several factors, which determine the extent of quenching. They are the sort of interaction between the fluorophore and the quencher, energy of the emission of the fluorophore and the characteristics of the quencher. Here with this research plasmonic quenching by the nanoparticle and Fluorescence Resonance Energy Transfer (FRET) are the two main types of quenching mechanisms that should be addressed.

1.6.2.1.1 Plasmonic Quenching by Nanoparticles

Optical properties of the nanoparticles play a main role with plasmonic quenching. "The surface plasmon resonance (SPR) is the absorption band resulting when the incident photon frequency is resonant with the collective oscillation of the conduction band electrons."[76] Excited state fluorophore acts as an oscillating dipole. When the metal nanoparticle and the fluorophore are in close proximity several modifications can occur in that environment. One modification is the change in rate of emission of radiating energy. Another modification is the change in the electric field felt by the fluorophore due to the interaction of the incident light with the close by metal surface. This modified environment, which occurred due to the above explained interactions can increase or decrease the field felt by the fluorophore also it can increase or decrease the radiative decay. Based on that, fluorescence quantum yield or the fluorescence lifetime can be either increased or decreased. Therefore the fluorescence quenching or the fluorescence enhancement of the surface plasmon of the metal nanoparticle depends on the fluorophore used.[77,78]

1.6.2.1.2 Fluorescence Resonance Energy Transfer (FRET)

This has become a widely used tool in several applications with monitoring biomolecules.[79] FRET between fluorescent proteins is a good example.[80] FRET is a nonradiative process and an electrodynamic phenomenon. In here, the energy transfer occurs between a excited dye donor and a dye acceptor in the ground state through long-range dipole dipole

interactions.[68] In FRET systems the major requirement is the spectral overlap of the donor emission and acceptor absorption. Figure 1.12 shows the schematic diagram of FRET process.[81]

$$E = R_0{}^6/(R_0{}^6 + R^6) \qquad (1)$$

FRET efficiency (E) is given by equation 1,[68] where R_0 is the forester distance at which the transfer efficiency E = 50%; R is the distance between the energy donor and acceptor.
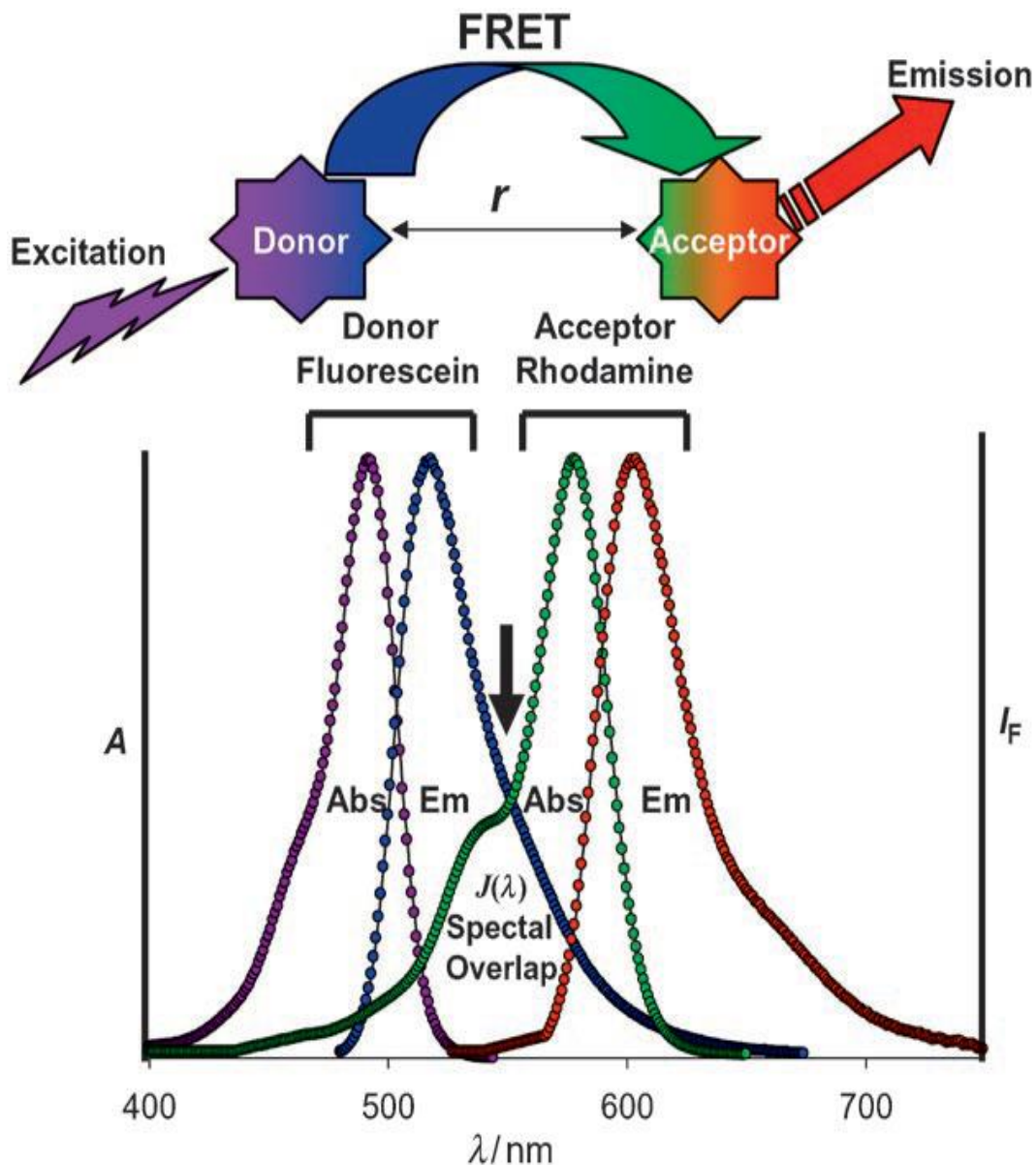
Figure 1.12: Schematic of the FRET Process between Donor and Acceptor, with permission from Reference 81

1.6.2.2. Stern - Volmer Plot

Stern - Volmer plots are based on the Stern - Volmer equation. Equation 2 shows the Stern - Volmer equation. It is used to explain collisional quenching of fluorescence. Fluorophore can be quenched by either collisions or complex formation using the same quencher.

$$\frac{F_0}{F} = 1 + k_q\tau_0[Q] = 1 + K_D[Q] \quad (2)$$

In this equation F_0 is the fluorescence in the absence of the quencher, F is the fluorescence in the presence of the quencher, k_q is the bimolecular quenching constant , τ_0 is the lifetime of the fluorophore and Q is the concentration of quencher. The Stern-Volmer quenching constant is given by $K_D = k_q\tau_0$. Stern - Volmer plots are used to analyze quenching data. The resulting plot is F_0/F versus $[Q]$. Figure 1.13 shows the standard samples of Stern - Volmer plots.[68]
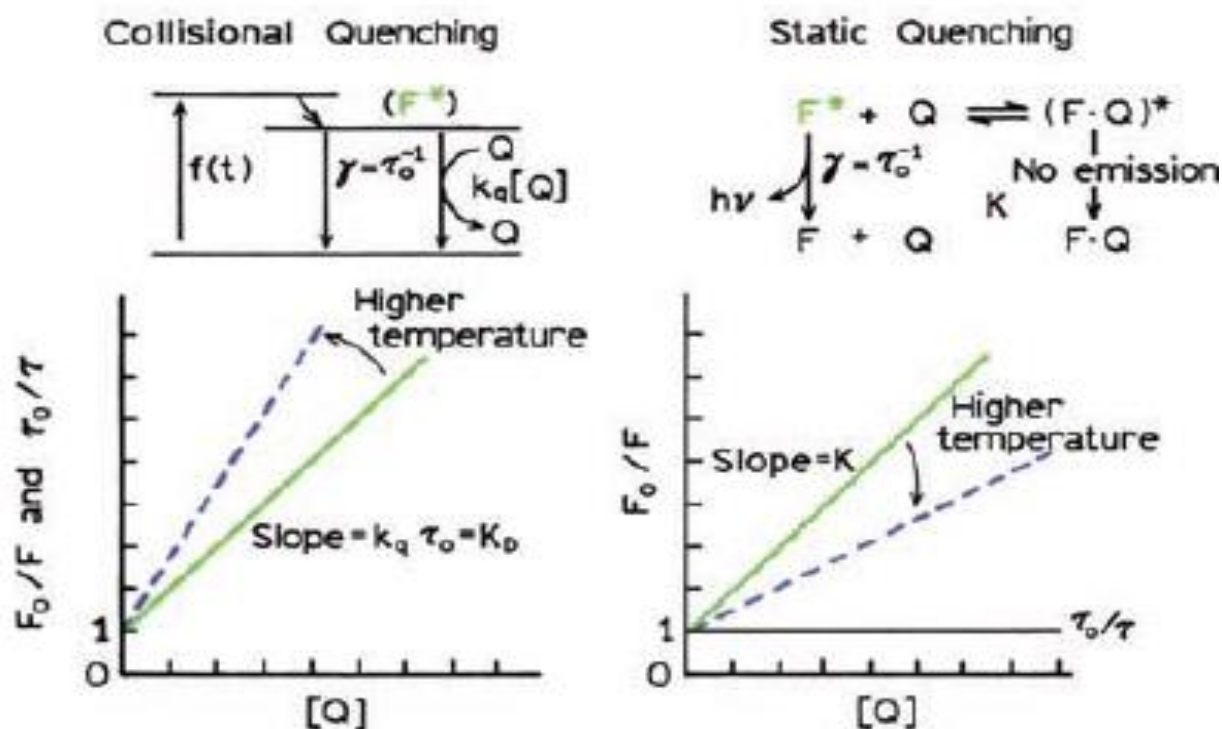
Figure 1.13: Comparison of Dynamic and Static Quenching, with permission from Reference 68

1.6.2.3. FRET of TCPP to Cyanine 5.5 at Fe/Fe$_3$O$_4$-Nanoparticles

We have analyzed the FRET of TCPP to cyanine 5.5 at the surface of the Fe/Fe$_3$O$_4$-nanoparticles by applying a mathematical model for the analysis of luminescence quenching at starburst dendrimers, which is described in detail in reference [82]. Assuming that 1) both dyes are randomly distributed at the nanoparticles' surface, and 2) that each TCPP can be quenched by more than one molecule of cyanine 5.5 and 3) that the cyanine 5.5 quenchers act independently of each other, the total intensity of TCPP can be described by equation 3.

$$I = N \sum_{n_1=0}^{\infty} \sum_{n_2=0}^{\infty} p(n_1, n_2) I_{n_1,n_2} = N v_2 I_{0,1} e^{v_1(\alpha-1)} \quad (3)$$

The variables used here are defined as follows: p, Poisson distribution, N, number of nanoparticles, n_1, number of TCPP molecules, n_2, number of cyanine 5.5 molecules, v_1, average number of TCPP molecules that are attached to each nanoparticle; v_2, average number of cyanine 5.5 tethered per nanoparticle, R: radius of the Fe/Fe$_3$O$_4$-nanoparticle, L, energy transfer interaction range; and I, luminescence intensity.
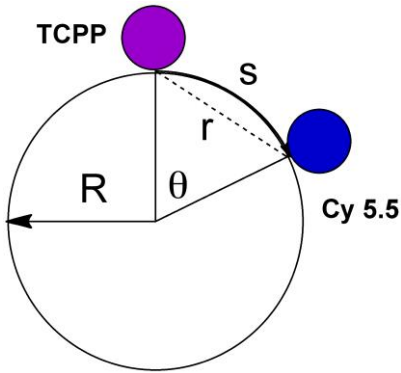
Figure 1.14: Diagram used for the Computation of the Attenuation Factor, Equation 5.

The energy transfer distance s between TCPP and cyanine 5.5 is measured on the surface of the nanoparticle (heavy line). This is not to be confused with r, the shortest distance between both dyes.

I$_0$ is obtained by substituting $v_1 = 0$:

$$(I_0/I) = e^{(1-\alpha)v_1} \quad (4)$$

The attenuating factor α represents the quenching of a single photoexcited TCPP by all cyanine 5.5, which are tethered to the surface of the nanoparticle with radius R. Quenching will depend on the distance s measured along the surface of the nanoparticle (Figure 1.14). It is approximated to $1 - e^{-s/L}$. In averaging over all possible locations of cyanine 5.5 molecules, we obtain:

$$\alpha = \frac{\int_0^{\Pi R}(1 - e^{-\frac{s}{L}})2\Pi R sin(\frac{S}{R})ds}{\int_0^{\Pi R}2\Pi R sin(\frac{S}{R})ds} = 1 - \frac{1 + e^{-\Pi(\frac{R}{L})}}{2\left[1 + \left(\frac{R}{L}\right)^2\right]} \quad (5)$$

α can be obtained experimentally according to equation 6:

$$ln(I_0/I) = (1 - \alpha)\nu_1 \quad (6)$$

For the largest consensus sequence (CTS L, R = 10.15 nm, I^0/I = 3.73), α is 0.9254 and L (Förster radius) was calculated to 4.4 nm. CTS K is the smallest consensus sequence (R = 8.7 nm, I^0/I = 1.79), α is 0.9684. For the smallest nanoplatform, L is 2.3 nm. Both, the upper and lower bound for L are well within the established FRET distances (1 to 6 nm).[55] Note that the longer consensus sequences may "bend back", decreasing the effective radius of the nanoplatform. Under these conditions, FRET is enhanced while TCPP is tethered to the nanoparticles, resulting in a larger luminescence increase when TCPP is cleaved off by its respective enzyme.

1.6.3. Cyanine Dyes

Cyanine dyes are highly conjugated, fluorescent molecules. They have the absorption and emission wavelengths in the near red and infra-red region (600–900 nm). They are known as near infra red (NIR) fluorescent dyes. Cyanine dyes have been used in many fields of science, for instance as photosensitizers, phototherapeutic agents and studies of nucleic acids. Figure 1.10 shows the general formula of the cyanine dye.[83] Some other important features of cyanine dyes are large molar extinction coefficients, and moderate fluorescence quantum yields.[84,85]
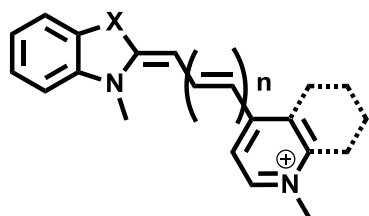
n= 0, 1,2, etc.

X = S, O, NH, CRR'

Figure 1.15: General Formula of the Cyanine Dye

Symmetric Cyanine dyes consist of the same heteroaromatic components conjugated by a methine chain and asymmetric Cyanine dyes consist of two different heteroaromatic components conjugated by a methine chain.[86] The number of the cyanine denotes the number of methine groups in the structure. There are several cyanine dyes having different absorption and emission bands; e.g.: (Cy-3.0 (λ_{ex}=538, λ_{em}=560), Cy-5.0 (λ_{ex}=639, λ_{em}=660), Cy-7.0 (λ_{ex}=740, λ_{em}=760) and Cy-7.5 (λ_{ex}=808, λ_{em}=830))

There are also some draw-backs of cyanine dyes, such as hydrophobicity and a strong tendency towards aggregation.

Through out this research, biological samples such as urine, blood serum and tissue samples are analyzed. In order to increase the sensitivity of these dyes, they should comprise of hydrophilic character. Since cyanine dyes have a highly conjugated Π system, they are hydrophobic in nature. So the dye should be structurally modified to introduce hydrophilic groups. Linking polar groups such as sulfonate (SO_3^-) is the best strategy to achieve this. It gives negative charge to the dye structure, making it more hydrophilic.[84,85]

Aggregation of these dyes can result in low fluorescence intensities and blue-shifted absorption peak. In our assay model Cyanine 5.5 dye is attached to the iron/iron oxide nanoparticle. So it prevents their aggregation.[84,85]
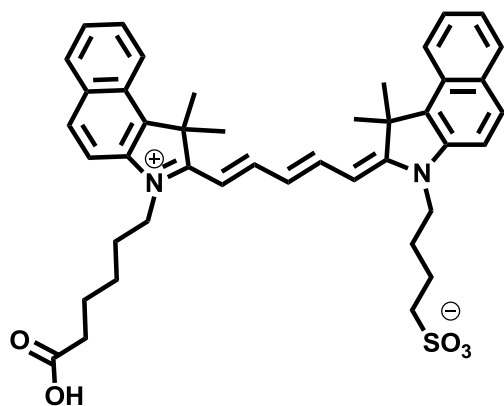
Figure 1.16: Chemical Structure of Cyanine 5.5

Key features of Cyanine 5.5 are long wavelength absorption in the NIR region, large extinction coefficient, good solubility and minor tendency to self-aggregate, which make it one of the major contributors to the nanoplatform[87] The reason behind choosing cyanine 5.5 as the fluorescence quencher is explained in section 1.6.2.1.

1.7 Iron/ Iron oxide Nanoparticles

Nanoparticles are particles with sizes in the range of 1–100 nm, dispersed in gaseous, liquid or solid media. Nanoparticles are thermodynamically unstable. The major difference between nanoparticles and larger colloids or bulk materials is their very high surface area. Due to the small size of nanoparticles, they have unique optical, magnetic and chemical properties. Iron nanoparticles are attractive to work with because of their chemical and physical properties, among them their very soft magnetic nature, the second highest room temperature value for the saturation magnetization, σ_s, and low magnetocrystalline anisotropy.[88]

The earliest method of producing iron nanoparticles is dispersing them in mercury. Lately organic solvent-based methodologies have been used in preparation. The reasons behind this change are the toxicity of mercury vapors and the relative ease of removing organic solvents.[89]

There are several methods that are currently used in the synthesis of iron nanoparticles. One is thermal decomposition of iron pentacarbonyl. The major requirements of this method are iron pentacarbonyl, energy in the form of heat (or sonication), an appropriate surfactant/solvent system, and a means to remove the only by-product, carbon monoxide. Sonochemical

decomposition of iron pentacarbonyl is the second method.[90] Iron carbonyl is decomposed due to the localized heat provided by the acoustic activation. The third method is the reduction of iron salts and oxides. The vapor phase method is the forth type for the synthesis of iron nanoparticles. When a metal is evaporated on to a non-wetting surface, deposition begins with the formation of islands forming nanoparticles.[88]

There is a vast array of applications with iron nanoparticles. They can be used in magnetic and electrical applications. Also they can be used in catalytic applications. Biomedical applications, such as Magnetic Resonance Imaging (MRI) or magnetic hyperthermia are another very important application of iron nanoparticles.[91] The key reason in using iron/iron oxide nanoparticles in this research is that they provide additional surface plasmonic quenching to the fluorophore. Also it serves as a platform to link the fluorophore via peptide sequence and the fluorescence quencher independently of each other.

1.8 References

[1] http://www.cancer.gov/cancertopics/

[2] American Cancer Society. Cancer Facts & Figures 2013. Atlanta: American Cancer Society; **2013**.

[3] http://www.cancer.gov/cancertopics/screening

[4] http://www.breastcancer.org/symptoms/diagnosis/hormone_status

[5] http://www.dilon.com/pages/current_methods_for_detecting_breast_cancer/

[6] Taylor, P. Modelling the impact of changes in sensitivity on the outcomes of the UK breast screening programme, *J. Med. Screen,* **2010**, *17*, 31-36.

[7] Duffy, M. J. Proteases as Prognostic Markers in Cancer, *Clin. Cancer Res.* **1996**, *2*, 613-618.

[8] Ugalde, A. P.; Ordonez, G. R.; Quiros, P. M.; Puente, X. S.; Lopez-Otin, C. Metalloproteases and the degradome, *Methods Mol. Biol.* **2010**, *622*, 3-29.

[9] Mandhare, M. N.; Patil, P. H.; Jagdale, D. M.; Kadam, V. J. Targeting matrix metalloproteinases: an important strategy in cancer therapeutics, *Int. J. Pharm. Sci. Rev. Res.* **2012**, *12*, 27-39.

[10] Rabbani, S. A.; Xing, R. H. Role of urokinase (uPA) and its receptor (uPAR) in invasion and metastasis of hormone-dependent malignancies, *Int. J. Oncol.* **1998**, *12*, 911-920.

[11] Vasiljeva, O.; Turk, B. Dual contrasting roles of cysteine cathepsins in cancer progression: Apoptosis versus tumor invasion, *Biochimie*, **2008**, *90*, 380-386.

[12] Lopez-Otin, C.; Matrisian, L.M. Tumour microenvironment: Emerging roles of proteases in tumour suppression, *Nat. Rev. Cancer*, **2007**, *7*, 800-808.

[13] Antalis, T. M.; Bugge, T. H. *Proteases and cancer methods and protocols*, Springer: New York, USA, 2009; 1-32.

[14] Carroll, M. C.; The complement system in regulation of adaptive immunity*, nature immunology*, **2004**, *5*, 981-986.

[15] Hoffman, M.; Monroe, D. M. Rethinking the coagulation cascade, *Curr. Hematol. Rep.* **2005**, *4,* 391-396.

[16] Szarvas, T.; Dorp, F. V.; Ergun, S.; Rubben, H. Matrix metalloproteinases and their clinical relevance in urinary bladder cancer, *Nat. Rev. Urol.* **2011**, *8*, 241-254.

[17] Serine proteases, Center for Biomolecular Imaging, **2008.**

[18] Tang, C. H.; Wei, Y. The urokinase receptor and integrins in cancer progression, *Cell. Mol. Life Sci.* **2008**, *65*, 1916 – 1932.

[19] Huai, Q.; Mazar, A. P.; Kuo, A.; Parry, G. C.; Shaw, D. E.; Callahan, J.; Li, Y.; Yuan, C.; Bian, C.; Chen, L.; Furie, B.; Furie, B. C.; Cines, D. B.; Huang, M. Structure of Human Urokinase Plasminogen Activator in Complex with Its Receptor, *Science,* **2006***, 311*, 656-659.

[20] Mazzieri, R.; Furlan, F.; Alessio, S. D.; Zonari, E.; Talotta, F.; Verde, P.; Blasi, F. A direct link between expression of urokinase plasminogen activator receptor, growth rate and oncogenic transformation in mouse embryonic fibroblasts, *Oncogene,* **2007***, 26*, 725-732.

[21] Foda, H. D.; Zucker, S. Matrix metalloproteinases in cancer invasion, metastasis and angiogenesis, *Drug Discovery Today*, **2001**, *6*, 478-482.

[22] Chabottaux, V.; Noel, A. Breast cancer progression: insights into multifaceted matrix metalloproteinases, *Clin. Exp. Metastasis,* **2007**, *24*, 647–656.

[23] Egeblad, M.; Werb, Z., New functions for the matrix metalloproteinases in cancer progression, *Nat. Rev. Cancer*, **2002**, *2*, 161-174.

[24] Bogenrieder, T.; Herlyn, M. Axis of evil: molecular mechanisms of cancer metastasis, *Oncogene,* **2003**, *22,* 6524-6536.

[25] Lecaille, F.; Kaleta, J.; Bromme, D. Human and Parasitic Papain-Like Cysteine Proteases: Their Role in Physiology and Pathology and Recent Developments in Inhibitor Design, *Chem. Rev.* **2002***, 102*, 4459-4488.

[26] Nomura, T.; Katunuma, N. Involvement of cathepsins in the invasion, metathesis, and proliferation of cancer cells, *The Journal of Medical Investigation,* **2005**, *52*, 1-9.

[27] Bartsch, J. E.; Staren, E. D.; Appert, H. E. Matrix Metalloproteinase Expression in Breast Cancer, *Journal of Surgical Research,* **2003**, *110***,** 383–392.

[28] Tetu, B.; Brisson, J.; Lapointe, H.; Bernard, P. Prognostic significance of stromelysin 3, Gelatinase A, urokinase expression in breast cancer, *Human Pathology,* **1998**, *29*, 979-985.

[29] Kantelhardt, E. J.; Vetter, M.; Schmidt, M.; Veyret, C.; Augustin, D.; Hanf, V.; Meisner, C.; Paepke, D.; Schmitt, M.; Sweep, F.; Minckwitz, G.V.; Martin, P.; Jaenicke, F.; Thomssen, C.; Harveck, N. Prospective evaluation of prognostic factors uPA/PAI-1 in node-negative breast cancer: Phase III NNBC3-Europe trial (AGO, GBG, EORTC-PBG) comparing 6 × FEC versus 3 × FEC/3 × Docetaxel*, BMC Cancer,* **2011**, *11*, 1-10.

[30] Riley, L. B.; Lange, M. K.; Browne, R. J.; Cochrane, P. J.; Choi, I.-J.; Davis, B.; Arcona, S.; Alhadeff, J. A. Analysis of cathepsin D in human breast cancer: usefulness of the processed

31kDa active form of the enzyme as a prognostic indicator in node-negative and node-positive patients, *Breast Cancer Research and Treatment,* **2000**, *60,* 173-179.

[31] Foekens, J. A.; Kos, J.; Peters, H. A.; Krasovec, M.; Look, M. P.; Cimerman, N.; Meijer-Van Gelder, M. E.; Henzen-Logmans, S. C.; Van Putten, W. L. J.; Klijn, J. G. M. Prognostic significance of cathepsins B and L in primary human breast cancer, *Journal of Clinical Oncology,* **1998**, *16,* 1013-1021.

32 Muller, D.; Breathnach, R.; Engelmann, A.; Millon, R.; Bronner, G.; Flesch, H.; Dumont, P.; Eber, M.; Abecassis, J. Expression of collagenase-related metalloproteinase genes in human lung or head and neck tumours, *Int. J. Cancer*, **1991**, *48*, 550–556.

[33] Lakka, S. S.; Rajagopal, R.; Rajan, M. K.; Mohan, P. M.; Adachi, Y.; Dinh, D. H.; Olivero, W. C.; Gujrati, M.; Ali-Osman, F.; Roth, J. A.; Yung, W. K. A.; Kyritsis, A. P.; Rao, J. S. Adenovirus-mediated Antisense Urokinase-Type Plasminogen Activator Receptor Gene Transfer Reduces Tumor Cell Invasion and Metastasis in Non-Small Cell Lung Cancer Cell Lines, *Clinical Cancer Research,* **2001**, *7*, 1087-1093.

[34] Werle, B.; Kotzsch, M.; Lah, T. T.; Kos, J.; Gabrijelcic-Geiger, D.; Spiess, E.; Schirren, J.; Ebert, W.; Fiehn, W.; Luther, T.; Magdolen, V.; Schmitt, M.; Harbeck, N. Cathepsin B, Plasminogenactivator-inhibitor (PAI-1) and Plasminogenactivator-receptor (uPAR) are Prognostic Factors for Patients with Non-small Cell Lung Cancer, *Anticancer Research,* **2004**, *24*, 4147-4162.

[35] Kos J.; Sekirnik, A.; Kopitar G.; Cimerman, N.; Kayser, K.; Stremmer, A.; Fiehn, W.; Werle, B. Cathepsin S in tumors, regional lymph nodes and sera of patients with lung cancer: Relation to prognosis, *British Journal of Cancer* , **2001**, *85*, 1193-1200.

[36] Bühling, F.; Waldburg, N.; Krüger, S.; Röcken, C.; Wiesner, O.; Weber, E.; Welte, T. Expression of cathepsins B, H, K, L, and S during human fetal lung development, *Developmental Dynamics,* **2002**, *225*, 14-21.

[37] Schmitt, M.; Sturmheit, A. S.; Welk, A.; Schnelldorfer, C.; Harbeck, N. Procedures for the quantitative protein determination of urokinase and its inhibitor, PAI-1, in human breast cancer tissue extracts by ELISA, *Methods in Molecular Medicine*, Brooks, S. A.; Harris, A. L.; Humana Press Inc., Totowa, New Jersey, 2006, pp 245-265.

[38] Johansson, N.; Ahonen, M.; Kähäri, V. -M. Matrix metalloproteinases in tumor invasion, *Cellular and Molecular Life Sciences,* **2000**, *57,* 5-15.

[39] Chikkaveeraiah, B. V.; Bhirde, A. A.; Morgan, N. Y.; Eden, H. S.; Chen, X. Electrochemical immunosensors for detection of cancer protein biomarkers, *ACS Nano,* **2012,** *6*, 6546–6561.

[40] Idikio, H. A. Immunohistochemistry in diagnostic surgical pathology: contributions of protein life-cycle, use of evidence based methods and data normalization on interpretation of immunohistochemical stains. *Int. J. Clin. Exp. Pathol.* **2010**, *3*, 169–176.

[41] Bishop, R. Applications of fluorescence in situ hybridization (FISH) in detecting genetic aberrations of medical significance, *Bioscience Horizons,* **2010**, *3*, 85–95.

[42] Bossmann, S. H.; Troyer, D. L. Point-of-care routine rapid screening: the future of cancer diagnosis, *Expert Rev. Mol. Diagn.* **2013**, *13*, 107-109.

[43] Khasigov, P. Z.; Podobed, O. V.; Gracheva, T. S.; Salbiev, K. D.; Grachev, S. V.; Berezov, T. T. Role of matrix metalloproteinases and their inhibitors in tumor invasion and metastasis. *Biochemistry*, **2003**, *68*, 711-717.

[44] Turk, B. E.; Huang, L. L.; Piro, E. T.; Cantley, L. C. Determination of protease cleavage site motifs using mixture-based oriented peptide libraries, *Nature Biotechnology,* **2001**, *19*, 661-667.

[45] Pham, W.; Weissleder, R.; Tung, C. -H. An azulene dimer as a near-infrared quencher, *Angew. Chem. Int. Ed*. **2002**, *41*, 3659-3662.

[46] Pham, W.; Choi, Y.; Weissleder, R.; Tung, C. -H. Developing a peptide-based near-infrared molecular probe for protease sensing, *Bioconjugate Chem.* **2004**, *15*, 1403-1407.

[47] Zhao, M.; Josephson, L.; Tang, Y.; Weissleder, R. Magnetic sensors for protease assays, *Angew. Chem. Int. Ed*. **2003**, *42*, 1375-1378.

[48] Funovics, M.; Weissleder, R.; Tung, C.-H. Protease sensors for bioimaging, *Anal. Bioanal. Chem.* **2003**, 377, 956-963.

[49] Friedman, A. E.; Chambron, J. -C.; Sauvage, J. -P.; Turro N. J.; Barton, J. K. Molecular light switch for DNA: Ru(bpy)$_2$(dppz)$^{2+}$, *J. Am. Chem. Soc*. **1990**, *112*, 4960-4962.

[50] Simard, B.; Tomanek, B.; van Veggel F. C. J. M.; Abulrob, A. Optimal dye-quencher pairs for the design of an "activatable" nanoprobe for optical imaging, *Photochemical & Photobiological Sciences*, **2013**, *12*, 1824-1829.

[51] Quillard, T.; Croce, K.; Jaffer, F. A.; Weissleder R.; Libby, P. Molecular imaging of macrophage protease activity in cardiovascular inflammation in vivo, *Thromb. Haemos.* **2011**, *105*, 828-836.

[52] Welser, K.; Adsley, R.; Moore, B. M.; Chan, W. C.; Aylott, J. W. Protease sensing with nanoparticle based platforms, *Analyst*, **2011**, *136*, 29-41.

[53] Kim, G. B.; Kim, Y.-P. Analysis of protease activity using quantum dots and resonance energy transfer, *Theranostics*, **2012**, *2*, 127-138.

[54] Pavan, S.; Berti, F. Short peptides as biosensor transducers, *Anal. Bioanal. Chem*. **2012**, *402*, 3055-3070.

[55] Kobayashi, H.; Choyke, P. L. Target-Cancer-Cell-Specific Activatable Fluorescence Imaging Probes: Rational Design and in Vivo Applications, *Acc. Chem. Res*. **2011**, *44*, 83-90.

[56] Huang, X.; El-Sayed I. H.; El-Sayed, M. A. Fluorescent quenching gold nanoparticles: potential biomedical applications, *Metal enhanced fluorescence*; Geddes, C. D. John Wiley & Sons, Inc., 2010, pp 573-599.

[57] Lacroix, L.-M.; Huls, N. F.; Ho, D.; Sun, X.; Cheng, K.; Sun, S. Stable Single-Crystalline Body Centered Cubic Fe Nanoparticles, *Nano Lett*. **2011**, *11*, 1641-1645.

[58] Wang, H.; Shrestha, T. B.; Basel, M. T.; Dani, R. K.; Seo, G. -M.; Balivada, S.; Pyle, M. M.; Prock, H.; Koper, O. B.; Thapa, P. S.; Moore, D.; Li, P.; Chikan, V.; Troyer D. L.; Bossmann, S. H. Magnetic-Fe/Fe_3O_4-nanoparticle-bound SN38 as carboxylesterase-cleavable prodrug for the delivery to tumors within monocytes/macrophages, *Beilstein J. Nanotechnol*. **2012**, *3*, 444-455.

[59] Sobczynski, J.; Toennesen, H. H.; Kristensen, S. Influence of aqueous media properties on aggregation and solubility of four structurally related meso-porphyrin photosensitizers evaluated by spectrophotometric measurements, *Pharmazie*. **2013**, *68*, 100-109.

[60] Patsenker, L.; Tatarets, A.; Kolosova, O.; Obukhova, O.; Povrozin, Y.; Fedyunyayeva, I.; Yermolenko, I.; Terpetschnig, E. Fluorescent probes and labels for biomedical applications, *Ann. N. Y. Acad. Sci*. **2008**, *1130*, 179-187.

[61] Kalita, M.; Basel, M. T.; Janik, K.; Bossmann, S. H. Optical and Electronic Properties of Metals and Semiconductors in Nanoscale Materials in Chemistry, *Nanoscale Materials in Chemistry*, Klabunde, K. J. Wiley & Sons: New York, USA, 2009; pp 539-578.

[62] Tam, F.; Goodrich, G. P.; Johnson, B. R.; Halas, N. J. Plasmonic Enhancement of Molecular Fluorescence, *Nano Lett.* **2007**, *7*, 496-501.

[63] Song, E.; Cheng, D.; Song, Y.; Jiang, M.; Yu J.; Wang, Y. A graphene oxide-based FRET sensor for rapid and sensitive detection of matrix metalloproteinase 2 in human serum sample, *Biosens. Bioelectron.* **2013**, *47*, 445-450.

[64] Swisher, L. Z.; Syed, L. U.; Prior, A. M.; Madiyar, F. R.; Carlson, K. R.; Nguyen, T. A.; Hua, D. H.; Li, J. Electrochemical Protease Biosensor Based on Enhanced AC Voltammetry Using Carbon Nanofiber Nanoelectrode Arrays, *J. Phys. Chem. C*, **2013**, *117*, 4268-4277.

[65] Swedberg, J. E.; Harris, J. M. Natural and Engineered Plasmin Inhibitors: Applications and Design Strategies, *ChemBioChem.* **2012**, *13*, 336-348.

[66] Perinchery, S. M.; Kuzhiumparambil, U.; Vemulpad, S.; Goldys, E. M. The potential of autofluorescence spectroscopy to detect human urinary tract infection, *Talanta,* **2010**, *82*, 912–917.

[67] Herman, B. Fluorescence microscopy : State of the art, *Fluorescence Microscopy and Fluorescent Probes*, Slavik, J. Plenum Press, New York, 1996, pp 1-12.

[68] Lakowicz, J. *Principles of Fluorescence Spectroscopy*, 3rd ed., Plenum, Springer: Singapore, 2006**.**

[69] Jeong, E.-Y.; Burri, A.; Lee, S. -Y.; Park, S. Synthesis and catalytic behavior of tetrakis(4-carboxyphenyl) porphyrin-periodic mesoporous organosilica. *J. Mater. Chem.* **2010**, *20*, 10869-10875.

[70]Scalise, I.; Durantini, E. N. Photodynamic effect of metallo 5-(4-carboxyphenyl)-10,15,20-tris(4-methylphenyl) porphyrins in biomimetic AOT reverse micelles containing urease, *Journal of Photochemistry and Photobiology A:Chemistry,* **2004***, 162*, 105-113.

[71] Johnson-White, B.; Zeinali, M.; Shaffer, K. M.; Patterson Jr. C. H.; Charles, P. T.; Markowitz, M. A. Detection of organics using porphyrin embedded nanoporous organosilicas. *Biosensors and Bioelectronics,* **2007***, 22*, 1154-1162.

[72] Cherian, S.; Wamser, C. C. Adsorption and Photoactivity of Tetra(4-carboxyphenyl)porphyrin (TCPP) on Nanoparticulate TiO_2, *J. Phys. Chem. B,* **2000***, 104*, 3624-3629.

[73] Besschetnova, I. A.; Chudinov, A. V.; Kaluzhny, D. N.; Shchyolkina, A. K.; Borisova, O. F.; Tokalov, S. V.; Kuznetsova, V. E.; Lobanov, A. V.; Rumyantseva, V. D.; Barsky, V. E.; Mirzabekov, A. D. Fluorescence of meso-tetrakis[4-(carboxy)phenyl]porphine covalently bound to oligonucleotides $d(CG)_5$ and $d(TA)_5$, *Biofizika*, **2002**, *47*, 259-267.

[74] Lambert, C. R.; Reddi, E.; Spikes, J. D.; Rodgers, M. A. J.; Jori, G. The effects of porphyrin structure and aggregation state on photosensitized processes in aqueous and micellar media, *Photochem. Photobiol.*, **1986**, *44*, 595-601.

[75] Buschmann, V.; Weston, K. D.; Sauer, M. Spectroscopic study and evaluation of red-absorbing fluorescent dyes, *Bioconjugate Chem.* **2003**, *14*, 195-204.

[76] Raikar, U. S.; Tangod, V. B.; Mastiholi, B. M.; Fulari, V. J. Fluorescence quenching using plasmonic gold nanoparticles. *Optics Communications,* **2011***, 284*, 4761-4765.

[77] Mayilo, S.; Kloster, M. A.; Wunderlich, M.; Lutich, A.; Klar, T. A.; Nichtl, A.; Kurzinger, K.; Stefani, F. D.; Feldmann, J. Long-Range Fluorescence Quenching by Gold Nanoparticles in a Sandwich Immunoassay for Cardiac Troponin T. *Nano Lett.* **2009***, 9*, 4558-4563.

[78] Ancukiewicz, D. Enhanced Light Emission Using Plasmonic Gold Nanoparticles, *Optics & Opto-electronics*, **2008**, 100-101.

[79] Yuan, L.; Lin, W.; Zheng, K.; Zhu, S. FRET-Based Small-Molecule Fluorescent Probes: Rational Design and Bioimaging Applications, *Acc. Chem. Res.* **2013**, *46*, 1462-1473.

[80] Lam, A. J.; St-Pierre, F.; Gong, Y.; Marshall, J. D.; Cranfill, P. J.; Baird, M. A.; McKeown, M. R.; Wiedenmann, J.; Davidson, M. W.; Schnitzer, M. J.; Tsien, R. Y.; Lin, M. Z. Improving FRET dynamic range with bright green and red fluorescent proteins, *Nature Methods,* **2012**, *9,* 1-7.

[81] Sapsford, K. E.; Berti, L.; Medintz, I. L. Materials for fluorescence resonance energy transferanalysis: Beyond traditional donor_acceptor combinations. *Angew. Chem., Int. Ed.* **2006**, *45*, 4562–4588.

[82] Ben-Avraham, D.; Schulman, L. S.; Bossmann, S. H.; Turro, C.; Turro, N. J. Luminescence Quenching of Ruthenium(II)-Tris(phenanthroline) by Cobalt(III)-Tris(phenanthroline) Bound to the Surface of Starburst Dendrimers, *J. Phys. Chem. B*, **1998**, *102*, 5088-5093.

[83] Isacsson, J.; Westman, G. Solid-phase synthesis of asymmetric cyanine dyes. *Tetrahedron Lett.* **2001**, *42*, 3207-3210.

[84] Fayed, T. A.; Extension of fluorescence response to the near -IR region, *Reviews in Fluorescence*, Geddes, C. D.; Lakowicz, J. R.; Springer: New York, 2011, pp 75-111.

[85] Nolting, D. D.; Gore, J. C.; Pham, W., Near-Infrared Dyes: Probe Development and Applications in Optical Molecular Imaging, *Curr. Org. Synth.* **2011**, *8*, 521-534.

[86] Xu, D. -Q.; Yang, W. -L.; Luo, S. -P.; Wang, B. -T.; Wu, J.; Xu, Z. -Y. Fischer Indole Synthesis in Brønsted Acidic Ionic Liquids: A Green, Mild, and Regiospecific Reaction System, *Eur. J. Org. Chem.* **2007**, 1007–1012.

[87] Pandey, R. K.; James, N.; Chen, Y.; Dobhal, M. P. Cyanine Dye-Based Compounds for Tumor Imaging With and Without Photodynamic Therapy, *Top Heterocycl. Chem.* **2008**, *14*, 41-74.

[88] Huber, D. L. Synthesis, properties, and applications of iron nanoparticles. *Small,* **2005,** 1, 482-501.

[89] http://www.epa.gov/hg/exposure.htm

[90] Suslick, K. S.; Fang, M.; Hyeon, T. Sonochemical Synthesis of Iron Colloids *J. Am. Chem. Soc.* **1996**, *118*, 11960–11961.

[91] Li, J.; Wu, N. *Biosensors based on nanomaterials and nanodevices*, CRC Press: New York, USA, 2014.

Chapter 2 - Synthesis of Magnetic-Nanoparticle (Fe/Fe_3O_4) - based Nanoplatforms for Highly Sensitive Fluorescence Detection of Cancer-Related Proteases

Acknowledgement

2.1 Design of the Nanoplatform

Fe/Fe_3O_4 nanoparticles were synthesized by thermal decomposition of $Fe(CO)_5$ in the presence of oleylamine and hexadecylammonium chloride (HADxHCl) using 1-octadecene (ODE) as solvent.[1] Figure 2.1 shows the transmission electron microscopy (TEM) images (1a, 1b) and high-resolution transmission electron microscopy (HRTEM) image (1c) of the obtained nanoparticles. The nanoparticles have a well-defined core/shell structure, with the average Fe(0) core diameter of 13 ± 0.5 nm and the Fe_3O_4 shell thickness of 2.0 ± 0.5 nm, respectively. The HRTEM image reveals polycrystalline nature of the nanoparticles. Dopamine forms robust organic coatings with binding constants of the order of 10^{15} L mol^{-1}.[2] It also increases the water-solubility of the resulting nanoplatforms to > 5 gL^{-1}.[2]
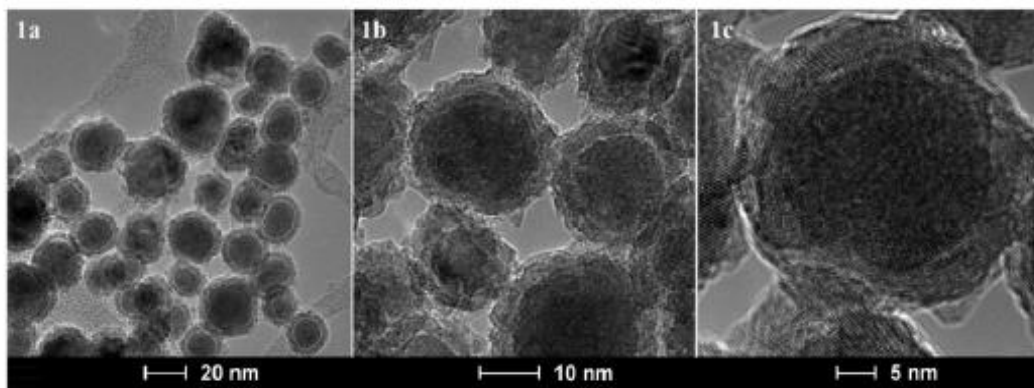
Figure 2.1: TEM (1a,1b) and HRTEM (1c) Images of Fe/Fe₃O₄ - Core/Shell Nanoparticles that are Forming the Inorganic Core of the Nanoplatforms for Protease Detection

In Table 2.1, the consensus sequences that have been employed for detecting 12 proteases, as well as the resulting lengths of the enzyme-cleavable tethers between nanoparticle and TCCP are summarized. Cyanine 5.5 was permanently linked to dopamine without using an enzyme-cleavable tether. Consequently, Cy 5.5 remains permanently bonded to the nanoparticle during the protease detection process.

Table 2.1: Consensus Sequences in Single-Letter Code for 12 Proteases and Distance (Tether Length) between the Surface of the Dopamine-coated Fe/Fe₃O₄ Nanoplatforms and TCPP[a]

Protease	Consensus Sequence	Tether Length /nm
MMP 1	VPMS-MRGG	2.46
MMP 2	IPVS-LRSG	2.10
MMP 3	RPFS-MIMG	2.57
MMP 7	VPLS-LTMG	2.49

MMP 9	VPLS-LYSG	2.41
MMP 11	GGAAN-LVRGG	3.44
MMP 13	GPQGLA-GQRGIV	3.66
uPA	SGR-SA	1.79
CTS B	SLLKSR-MVPNFN	3.53
CTS D	SLLIFR-SWANFN	1.74
CTS K	GPR-AG	1.37
CTS L	SGVVIA-TVIVIT	4.29

[a)] Molecular Modeling has been performed using an MM3 force field

The Bossmann/Troyer group has explored the synthesis and application of Fe/Fe$_3$O$_4$-nanoparticles in numerous fields of application, such as cell-delivered hyperthermia[3] and chemical catalysis.[4] The synthesis Fe/Fe$_3$O$_4$-nanoparticles was achieved by following a synthetic procedure[5] based on the work of S. Sun et al.[1] Porphyrins have been used as effective photosensitizers in photodynamic therapy (PDT). Their photophysical properties are excellently characterized.[6] Cyanine dyes have been widely used in DNA sequencing, genetic analysis, and *in-vivo* imaging due to their superior photochemical properties such as large molar extinction coefficients, moderate-to-high fluorescence quantum yields, and broad wavelength tunability.[7] Figure 2.2 shows the structure of the nanoplatform comprised of dopamine-coated Fe/Fe$_3$O$_4$ nanoparticle, consensus sequence, TCPP, and Cy 5.5.
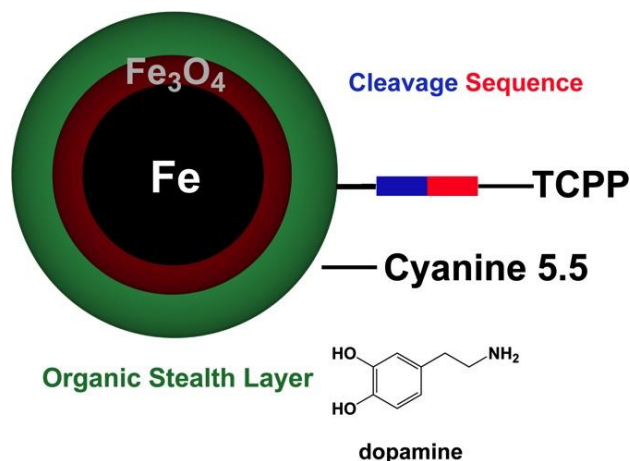
Figure 2.2: Nanoplatform for Protease Detection

One Fe/Fe$_3$O$_4$-nanoparticle is linked in average to 35+/-3 TCPP-molecules via consensus sequence (one type of sequence per nanoplatform) and 50+/-4 cyanine 5.5 molecules via amide linkages.

2.1.1 Synthesis of Iron/Iron oxide - Fe/Fe$_3$O$_4$ Nanoparticles

Iron nanoparticles were prepared with slight modification of a literature procedure described by Lacroix et al.[1] A 250 mL, three-necked, round-bottom flask equipped with a magnetic stir bar, one cold water cooled jacket condenser on the middle neck, one septum and one temperature probe on each of the outer necks was charged with 60 mL 1-octadecene (ODE), 0.9 mL oleylamine and 0.831 g hexadecylammonium chloride (HADxHCl). The reaction system was connected to a Schlenk line through the top of the jacket condenser. The reaction mixture was degassed at 120 ^{o}C for 30 min with vigorous stirring. After being refilled with argon, the reaction mixture was heated to 180° C. Three portions of 0.7 mL Fe(CO)$_5$ were injected into the reaction mixture via syringe, every 20 min. The reaction mixture was kept at 180 ^{o}C for another 20 min after the last injection, and then cooled to room temperature naturally. The supernatant was decanted, and the iron nanoparticles accumulated on the magnetic stir bar were washed with hexane and ethanol. The product was dried in vacuum and stored at room temperature under argon for further use. Based on the iron content of the nanoparticles, which was determined spectrophotometrially after dissolving the nanoparticles in aqueous HCl (1.0 M) and subsequent complexation with ferrozine (sodium 4,4'-(3-(pyridin-2-yl)-1,2,4-triazine-5,6-diyl)dibenzene-sulfonate)[8], the yield of the reaction is 95%.

2.1.2 Dopamine Coating of the Core/Shell Fe/Fe$_3$O$_4$ Nanoparticles

0.50 g of previously synthesized Fe/Fe$_3$O$_4$ nanoparticles was dispersed in 100 mL chloroform via sonication. With vigorous mechanical stirring, a solution of 0.50 g dopamine-hydrochloride in 50 mL chloroform was added drop-wise to the nanoparticle suspension. The reaction mixture was further stirred at room temperature for 24 h, and then the dopamine- coated nanoparticles were collected by centrifugation. After washing with chloroform 5 times, nanoparticles were dried under vacuum. 0.47 g dopamine coated Fe/Fe$_3$O$_4$ nanoparticles were collected.

2.2 Synthesis of peptides

All the peptide sequences for all twelve proteases, which were utilized in this project have been synthesized in the Bossmann Laboratory.

2.2.1 Cancer-Specific Consensus Peptide Sequence Synthesis

Cancer specific consensus peptide sequences were synthesized via standard Solid Phase Peptide Synthesis (SPPS).[9] Briefly, preloaded trityl-resin was swelled in DCM for 20 min, after washing with DMF, Fmoc-protected amino acids were added sequentially with O-Benzotriazole-N,N,N',N'-tetramethyl-uronium-hexafluoro-phosphate (HBTU) as coupling agent in a mixture of diisopropylethylamine (DIEA) and DMF. Taking advantage of the solid phase synthesis, the porphyrin TCPP was conjugated to the N-terminal of peptide sequence under standard coupling conditions. Finally, the TCPP-labeled cancer specific consensus peptide sequence was cleaved from the solid phase using 95/2.5/2.5 TFA (Trifluoroacetic acid) /TIPS (triisopropylsilane) /H$_2$O solution. The purity of the consensus sequences was examined by using HPLC (RP18 column using CF$_3$COOH/H$_2$O/CH$_3$CN gradients, using a Waters 1525 binary pump HPLC station).[10] For all 12 TCPP-labeled consensus sequences, the analytical purity exceeded 95 percent. They were then used for the synthesis of the nanoplatforms without further purification.

Loading of the resin

Removal of the temporary protecting group

Coupling of the next activated amino acid

n cycles

47
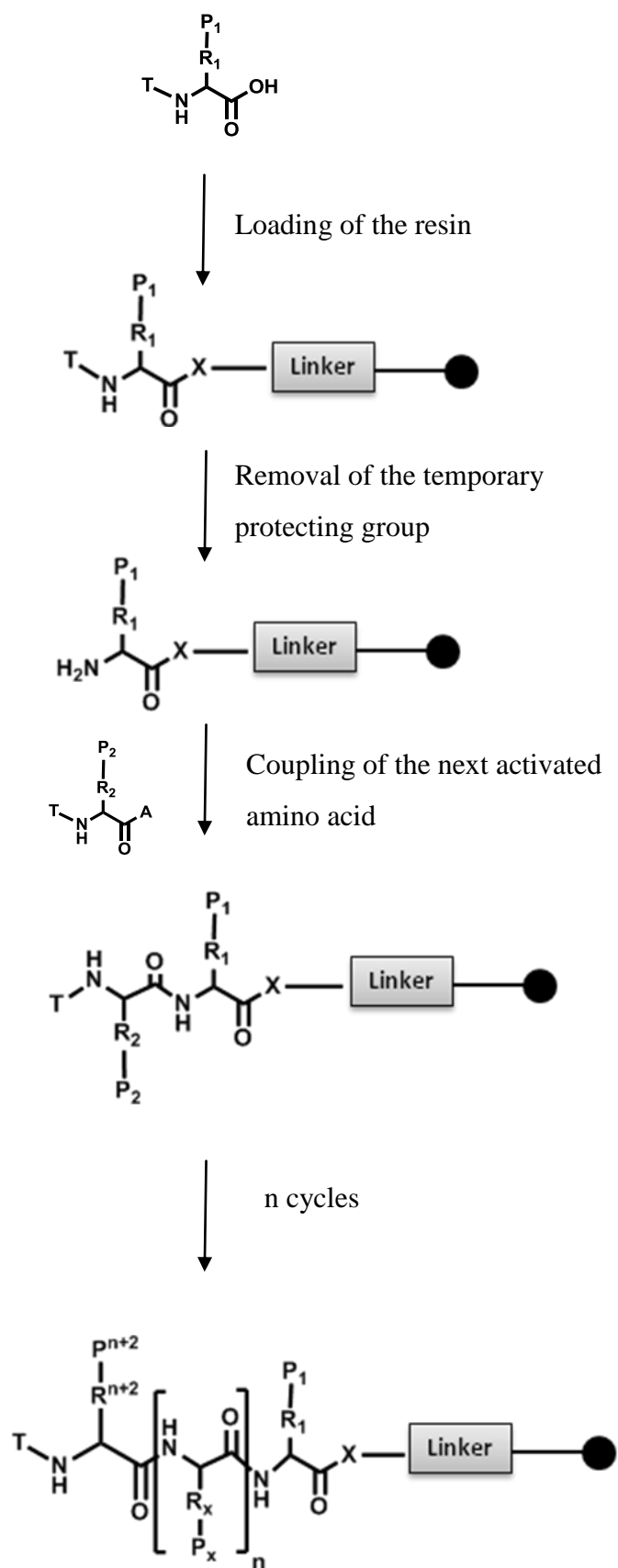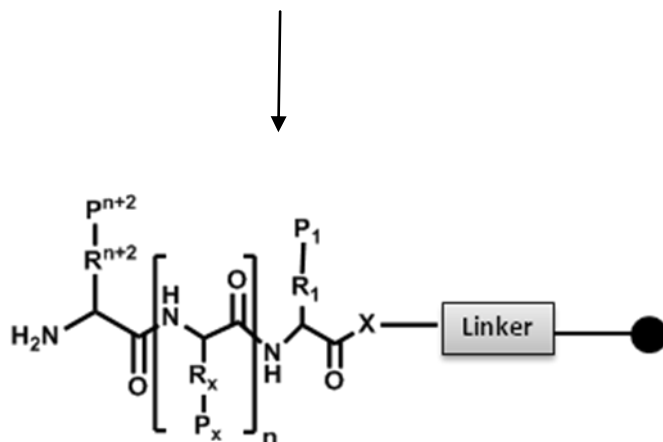
Figure 2.3: Principles of SPPS, Taken from Reference 11

Figure 2.3 shows the principle of solid phase peptide synthesis.[11] Here P, permanent side chain protecting group, T, temporary protecting group, ●, solid support, A, activating group, and X, NH or O.

2.3 Synthesis of Cyanine dyes

This cyanine synthesis is following environmentally friendly and cost-efficient methods. The starting point is the synthesis of indoles. For the n.0 series of the cyanine dyes, 2,3,3-trimethyl-3*H*-indole and for the n.5 series 1,1,2-trimethyl-1*H*-benzo[*e*]indole should be used. To add the hydrophilic character to these cyanine dyes, we have selected hexanoic acid and 1,4-butanesultone as alkyl substituents of the indole nitrogens.

2.3.1 Cyanine 5.5 Synthesis

In order to synthesize the cyanine dye first the two ring components (indolium salts) should be synthesized. Then the two components can be linked through the appropriate linker.

2.3.1.1 Synthesis of 4-(1,1,2-trimethyl-1H-benzo[e]indol-3-ium-3-yl)butane-1-sulfonate (3)

The synthetic procedure was a modification of reference [12]. A 50 mL two necked round bottom flask fitted with a magnetic stirrer and a condenser was flame dried. 1,1,2-trimethyl-1H-benzo[e]indole (1) (1.0 g, 4.78 mmol) was dissolved in dry o-dichlorobenzene (10 mL). 1,4-butanesultone (2) (0.58 mL, 5.73 mmol) was added drop-wise under a continuous flow of argon. The reaction mixture was, then, allowed to heat up to 130° C for 24 h. The reaction mixture was allowed to cool down to room temperature to obtain a blue colored precipitate. The precipitate

was triturated with ice-cold diethyl ether (40 mL) for 15 min. The precipitate was filtered through frit glass, washed with cold diethyl ether (3 x 5 mL), dried in vacuum yielding 0.70 g of compound 3. Percentage yield: 42%. ^{1}H NMR (DMSO-d6, 400 MHz) δ (ppm): 8.36 (d, 1H), 8.27 (d, 1H), 8.22 (s, 1H), 8.20(d, 1H), 7.76(dt, 2H), 4.60(t, 2H), 3.31(t, 2H), 2.0(qi, 2H), 1.77(m, 2H), 1.75(s, 6H)
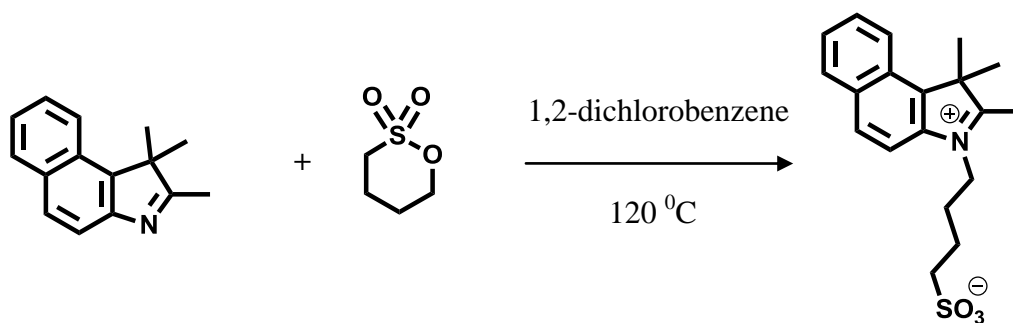
Figure 2.4: Synthesis of Indolium Salt 4-(1,1,2-trimethyl-1H-benzo[e]indol-3-ium-3-yl)butane-1-sulfonate (3)

2.3.1.2 Synthesis of 3-(5-carboxypentyl)-1,1,2-trimethyl-1H-benzo[e]indol-3-ium (5)

The synthetic procedure was a modification of reference [12]. A two-necked 50 mL round bottom flask fitted with reflux condenser and stirring bar was charged with 1,1,2-trimethyl-1H-benzo[e]indole, (1) (1.0 g, 4.78 mmol) which was flushed with argon three times. After dissolving in dry o-dichlorobenzene (15 mL), (0.93 g, 4.78 mmol) of 6-bromohexanoic acid (4) was added. The reaction mixture was stirred for 36 h at 120 ^{o}C by using an oil bath. This resulted in a dark blue solution. The reaction mixture was allowed to cool down to room temperature. This cooled solution was triturated with 1:1 diethyl ether and hexane mixture (total volume 90 mL) for an hour. The blue precipitate was filtered off, washed with diethyl ether (3 x 20 mL) and dried in vacuum yielding 1.1 g of the compound 5. Percentage yield: 56%. ^{1}H NMR (DMSO-d6, 400 MHz) δ (ppm): 12 (br, s, 1H), 8.37 (d, J=8.4Hz, 1H), 8.29 (d, J=9Hz, 1H), 8.21 (d, J=7.8Hz, 1H), 8.14 (d, J=8.8Hz, 1H), 7.79 (t, J=7.0Hz, 7.2Hz, 1H), 7.73 (t, J=7.2Hz, 1H), 4.57 (t, J=7.6Hz, 2H), 2.93 (s, 3H), 2.23 (t, J=7.0Hz, 2H), 1.9 (qi, 2H), 1.76 (s, 6H), 1.56 (m, 2H), 1.45 (m, 2H)
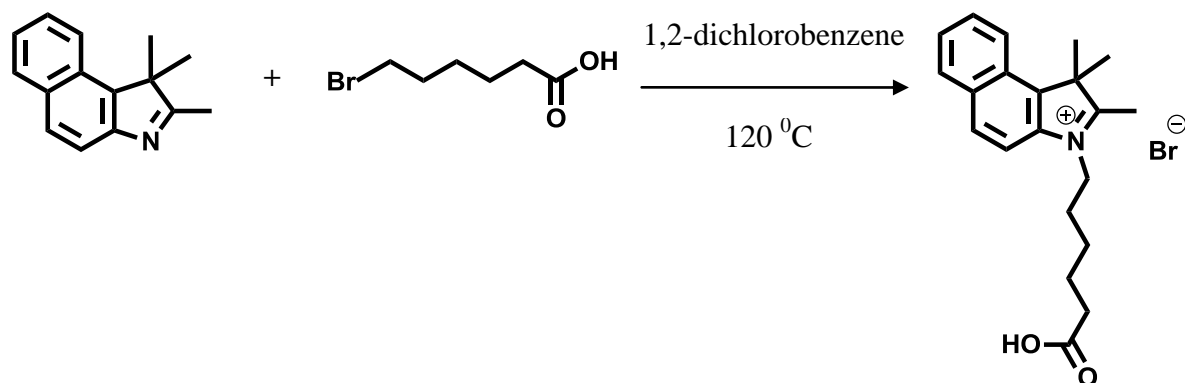
Figure 2.5: Synthesis of Indolium Salt 3-(5-carboxypentyl)-1,1,2-trimethyl-1H-benzo[e]indol-3-ium (5)

2.3.1.3 Synthesis of Cyanine 5.5 (8)

(4-(2-((1E,3E,5E)-5-(3-(5-carboxypentyl)-1,1-dimethyl-1H-benzo[e]indol-2(3H)-ylidene)penta-1,3-dien-1-yl)-1,1-dimethyl-1H-benzo[e]indol-3-ium-3-yl)   butane-1-sulfonate, bromide salt)
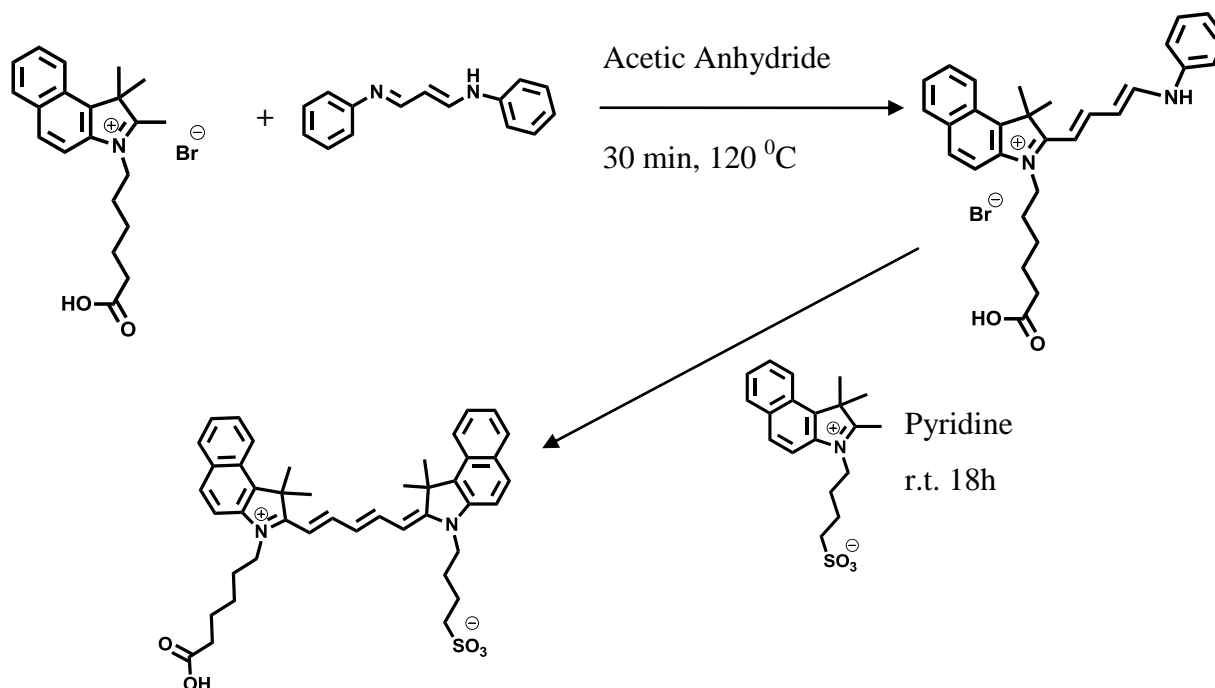
Figure 2.6: Synthesis of Cyanine 5.5

The synthetic procedure was a modification of reference [12]. A 50 mL two-necked oven dry round bottom flask fitted with a magnetic stir bar was flushed with argon. Indolium salt, (3) (0.1 g, 0.9 mmol) and malondialdehyde bis(phenylimine) monohydrochloride (6) (0.09 g, 0.35 mmol) were charged into the 50 mL round bottom flask. Acetic anhydride (10 mL) was added to this mixture and slowly heated to 120 ^{o}C in an oil bath and the reaction was monitored through TLC. The reaction was allowed to remain at 120 ^{o}C for half an hour. The reaction was then cooled to room temperature. An indolium salt, (5) (0.175 g, 0.433 mmol) in dry pyridine (5 mL) was added to the above reaction dropwise. The reaction was allowed to stir at room temperature for 16 h. The mixture was, then, concentrated in rotavap and the residue was dissolved in CH_2Cl_2 (3 mL) and loaded on silica column chromatography with CH_2Cl_2:MeOH solvent system (total volume = 2 L). A gradient of 100% to 25% of solvent CH_2Cl_2 was used to obtain 0.21 g of a deep blue colored dye. Percentage yield of cyanine 5.5: 92%. ^{1}H NMR (DMSO-d6, 400 MHz) δ (ppm): 8.48 (t, J=12Hz, 2H), 8.24(d, J=8.2Hz, 2H), 8.06(m, 2H), 7.78(m, 1H), 7.67(m, 1H), 7.51(m, 2H), 6.65(dd, J=8Hz, 1H), 6.44(d, J=12Hz, 1H), 6.33(d, J=12Hz, 1H), 4.23(m, 4H), 3.0(m, 2H), 2.08(m, 2H), 1.96(m, 2H), 1.78(s, 16H), 1.57(m, 2H), 1.42(m, 2H)

2.4 Synthesis of (4-carboxyphenyl)porphyrin (TCPP) (11)

The synthetic procedure was a variation of reference [13]. 1.50 g 4-carboxybenzaldehyde (9) was dissolved in 80 mL acetic acid. The solution was warmed to 100 ^{o}C and a solution of 0.67 g pyrrole (10) in 10 mL acetic acid was added dropwise over 20 min. Upon completion of addition, the solution was warmed to 120 ^{o}C slowly and was kept at 120 ^{o}C for 1 h. The mixture was cooled to 80 ^{o}C and 100 mL 95% ethanol was added and then lowered to room temperature, while stirring in 3 h. Then the mixture was kept in at -15 ^{o}C for 24 h. Purple solid was collected by vacuum filtration. The filter cake was washed with cold 50/50 ethanol/acetic acid (3×5 mL) and dried under high vacuum (oil pump) overnight. 0.51 g of pure product was obtained (25.5% yield). ^{1}H NMR (DMSO-d6) δ: -2.94 (s, 2H); 8.35 (d, 8H); 8.39 (d, 8H); 8.86 (s, 8H); 13.31 (s, 4H). ^{13}C NMR (DMSO-d6) δ: 119.31; 127.90; 130.51; 134.44; 145.42; 167.46. MS-ESI+: m/z 791.2. Molecular weight calculated as 790.2.
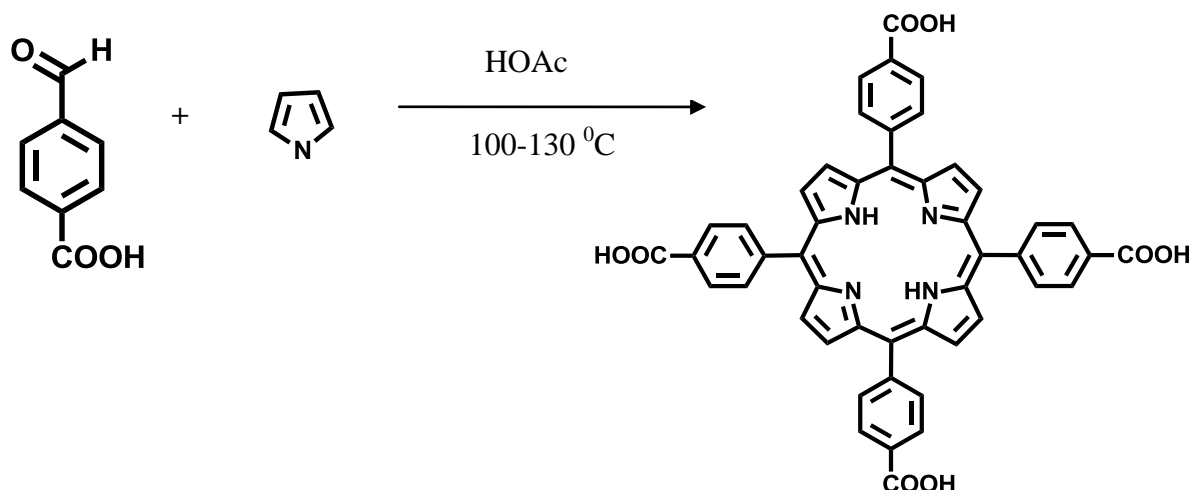
Figure 2.7: Synthesis of (4-carboxyphenyl)porphyrin (TCPP)

2.5 Final Assembly of the Nanoplatforms for Protease Detection

200 mg of dopamine coated Fe/Fe_3O_4 nanoparticles were dispersed in 5 mL of DMF. A solution of 3 mmol of Cy5.5, 3.3 mmol of EDC (1-Ethyl-3-(3-dimethylaminopropyl)carbodiimide), 1 mmol of DMAP (4-Dimethylaminopyridine) in 1 mL of DMF was added to this dispersion. After sonicating for 1 h, the nanoparticles were precipitated by a magnet, and thoroughly washed with DMF (1 mL $\times$ 10). The recovered nanoparticles were redispersed in 5 mL of DMF, and to this dispersion, 2 mmol of TCPP linked peptide sequence, 2.2 mmol of EDC, 1 mmol of DMAP in 2 mL of DMF were added. After sonicating for 1 h, the nanoparticles were precipitated by a magnet (0.55T), and thoroughly washed with DMF (1 mL $\times$ 10). After drying in high vacuum, 170-185 mg of nanoplatform can be obtained. The composition of the nanoplatform was analyzed by means of UV-Vis spectroscopy (Agilent HP 8543A). After combining all washing fractions and subsequent solvent removal in high vacuum, TCPP (log ε (420 nm) = 5.65) and cyanine 5.5 (lg ε (682 nm) = 5.17) were taken up in 1.0 ml methanol and quantitatively measured taking advantage of their high absorption coefficients. The nanoplatforms were dispersed in PBS, and TCPP and cyanine 5.5 were measured UV/Vis-spectroscopically as well, using dopamine coated Fe/Fe_3O_4-nanoparticles in PBS as reference. The iron-content of the nanoplatforms was independently determined using the ferrozine assay.[8]

This resulting data, together with the size of the Fe/Fe$_3$O$_4$-nanoparticles, enables the calculation of the average ratio of TCPP and cyanine 5.5 per nanoparticle.

2.6 Control Experiments and Additional Photophysical Information

2.6.1 UV/Vis-absorption of the Nanoplatforms

As shown in Figure 2.1, one Fe/Fe$_3$O$_4$-nanoparticle is linked in average to 35+/-3 TCPP-molecules via consensus sequence (one type of sequence per nanoplatform) and 50+/-4 cyanine 5.5 molecules via amide linkages. Assuming that all nanoplatforms feature an iron core of 13 nm in diameter, a Fe$_3$O$_4$ shell of 2 nm, and an outer dopamine layer of 1 nm, and that the weight of Fe is 7873 kg/m^3,[14] of Fe$_3$O$_4$ is 5100 kg/m^3, [15] and of dopamine is 1000 kg/m^3 (estimated surface coverage 80 percent), the weight of one Fe/Fe$_3$O$_4$/dopamine nanoparticle is approx. 1.26×10^{-20} kg = 1.26×10^{-14} mg. Furthermore, the weight of the attached dyes and consensus sequences does not exceed 1.5 percent of the total weight of the nanoplatform. Therefore, one mg contains approx. 7.9×10^{13} nanoplatforms. Since 50 cyanine 5.5 and 35 TCPP molecules are attached per nanoplatform, their concentrations are 3.96×10^{-8} moles and 2.77×10^{-8} moles per mg, respectively. 0.075 mg of each nanoplatform is added to 3.0 mL of PBS solution. The resulting TCPP concentration is 6.09×10^{-7} M. Based on this estimate, the observable TCPP absorption band at 421 nm should have an absorption of E = 0.23.
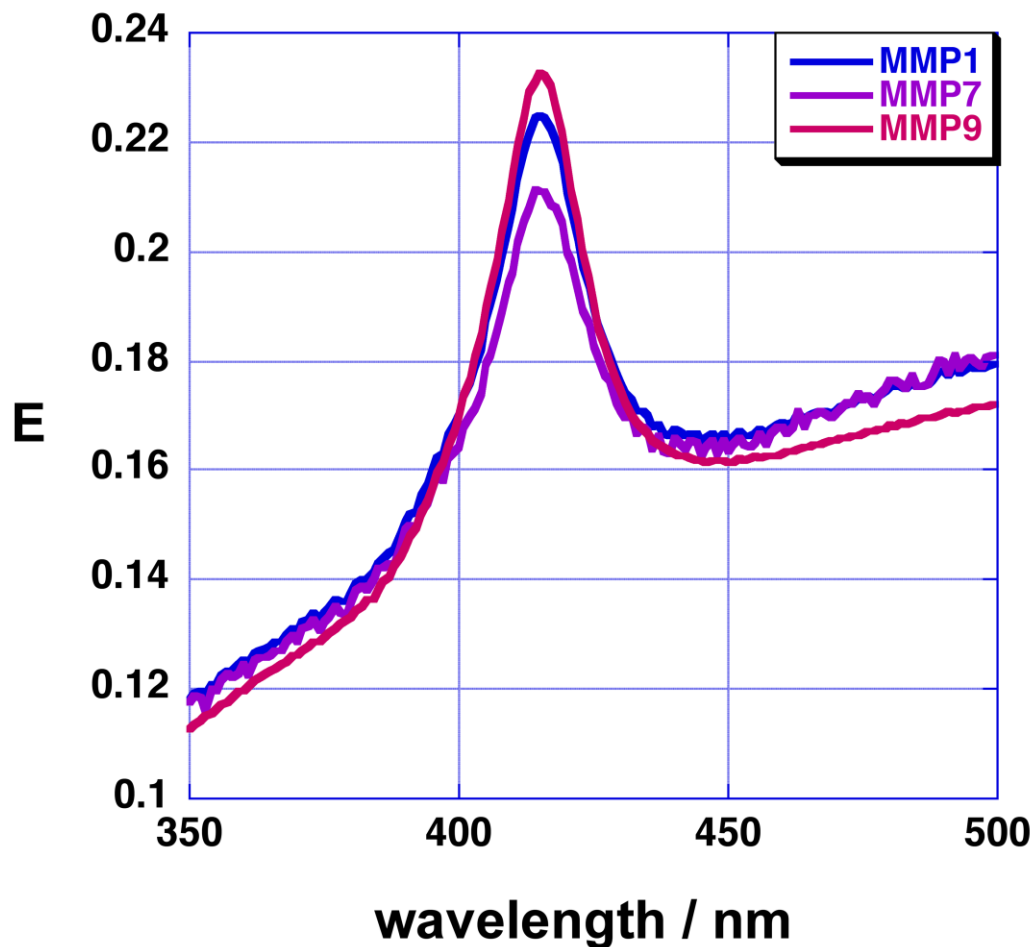
Figure 2.8: UV/Vis-Absorption of the Nanoplatforms for Determining the Activities of MMP 1, MMP 7, and MMP 9 in PBS.

The observed TCPP absorption peaks of the nanoplatforms (Figure 2.8) are significantly smaller (ΔE = 0.1 to 0.07) and slightly broadened, indicating plasmonic coupling between the Fe/Fe_3O_4-nanoparticles and the tethered dyes. It is noteworthy that the cyanine 5.5 absorption band of the nanoplatforms is strongly broadened, and that its fluorescence is almost completely quenched. This behavior has been found for various dyes featuring small stokes shifts when immobilized in a magnetic nanoparticle.[16]

2.6.2. Plasmon Resonance Quenching

Plasmon-resonance quenching[17] between consensus-sequence bound TCPP and the dopamine-coated Fe/Fe_3O_4 nanoparticles was observed in the absence of co-tethered cyanine 5.5. The quenching of TCPP by Fe/Fe_3O_4 was static. The fluorescence intensity of TCPP in PBS at

298 K decreased from 72 to 47 percent, when tethered to Fe/Fe$_3$O$_4$, dependent on the length dynamics of the consensus sequence.[18]

2.6.2.1. TCPP Quenching in Dopamine-coated Fe/Fe$_3$O$_4$ Nanoparticles in the Absence of Cyanine 5.5

A typical comparison of TCPP fluorescence spectra in the presence and absence of Fe/Fe$_3$O$_4$ is shown in the figure 2.9. Figure 2.9 shows the maximal fluorescence increase observed after incubating a nanoplatform consisting of dopamine-protected Fe/Fe$_3$O$_4$ nanoparticles bound to TCPP, by means of the consensus sequence for MMP 2 (IPVS-LRSG) in PBS at 25 ^{o}C for 24 h. The observed increase in fluorescence intensity is 65%.
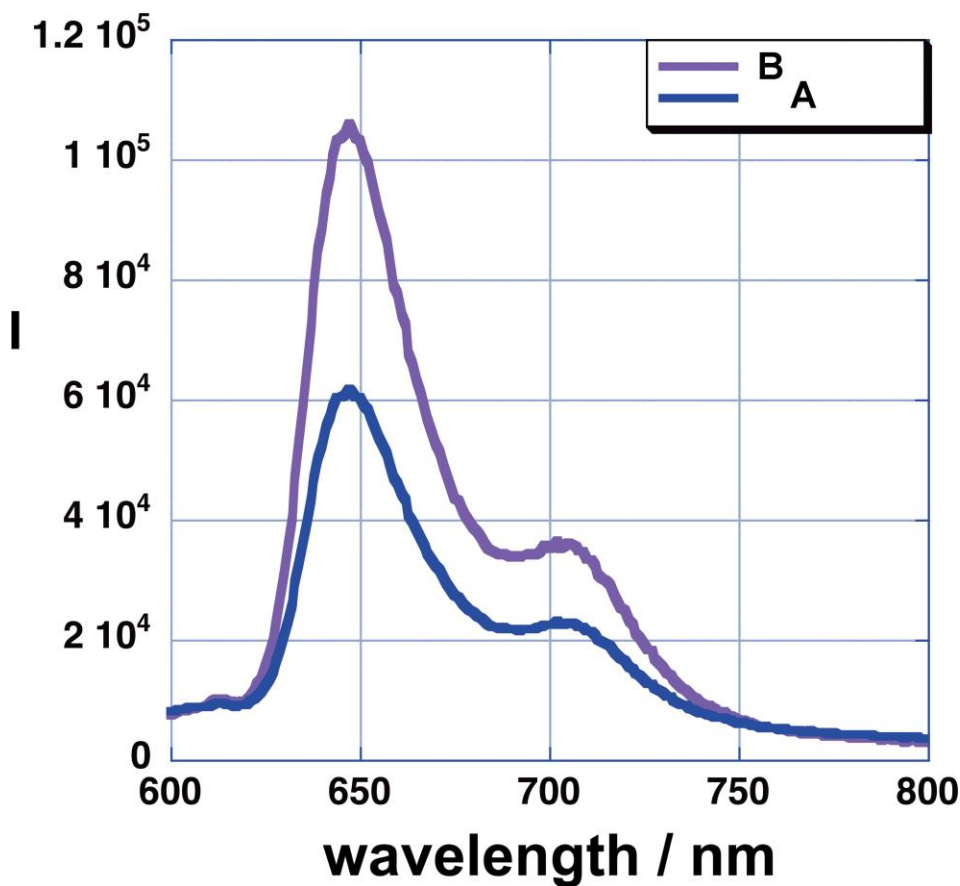
Figure 2.9: Fluorescence Spectra of TCPP when bound to Fe/Fe$_3$O$_4$ Nanoparticles (32+/-4 TCCP Molecules per Nanoplatform) (A) and after 24 h of Incubation with 1 x 10^{-10} mol l^{-1} MMP 2 in PBS at 25 ^{o}C (B).

2.6.2.2 Fluorescence Intensity Quenching of TCPP by Dopamine-coated Fe/Fe$_3$O$_4$-Nanoparticles

Figure 2.10 shows a Stern-Volmer plot of the integrated emission intensity of TCPP as a function of added dopamine-coated Fe/Fe$_3$O$_4$-nanoparticles. Two regions are clearly discernible: at very low nanoparticle concentrations, strong plasmonic resonance quenching is observed (k_{SET}= 8 x 10^{18} Lmol(nanoparticle)$^{-1}$s^{-1}), whereas at increased concentrations light scattering by the nanoparticles leads to an enhancement in fluorescence from TCPP.[19] This effect levels off at higher nanoparticle concentrations.
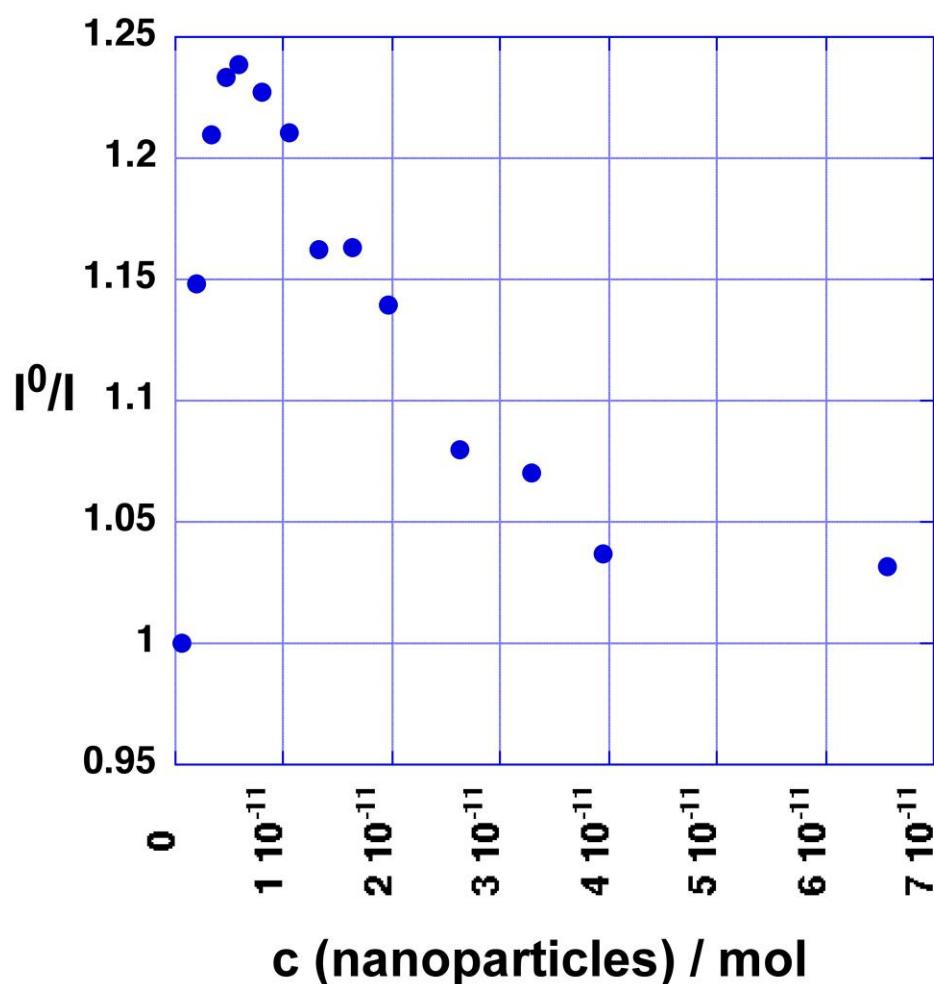
Figure 2.10: Stern-Volmer Plot of the Fluorescence Intensity Quenching of TCPP (Integrated Intensities from 640 to 720 nm) by Dopamine-coated Fe/Fe$_3$O$_4$-Nanoparticles in PBS.

2.6.3 Fluorescence Intensity Quenching of TCPP by Cyanine 5.5

The Stern-Volmer plot of the data (Figure 2.11) leads to the quenching constant $k_q = 3.36+/-0.05 \times 10^{10}$ Lmol^{-1}s^{-1}, which exceeds the limit of diffusion[20] by one order of magnitude. These findings strongly support the assumption of Fluorescence Resonance Energy Transfer (FRET) between TCPP and Cy 5.5, although a linear Stern-Volmer plot is not necessarily in agreement with a classic dipole-dipole coupling mechanism and its inverse 6th power dependence in energy transfer efficiency.[20]
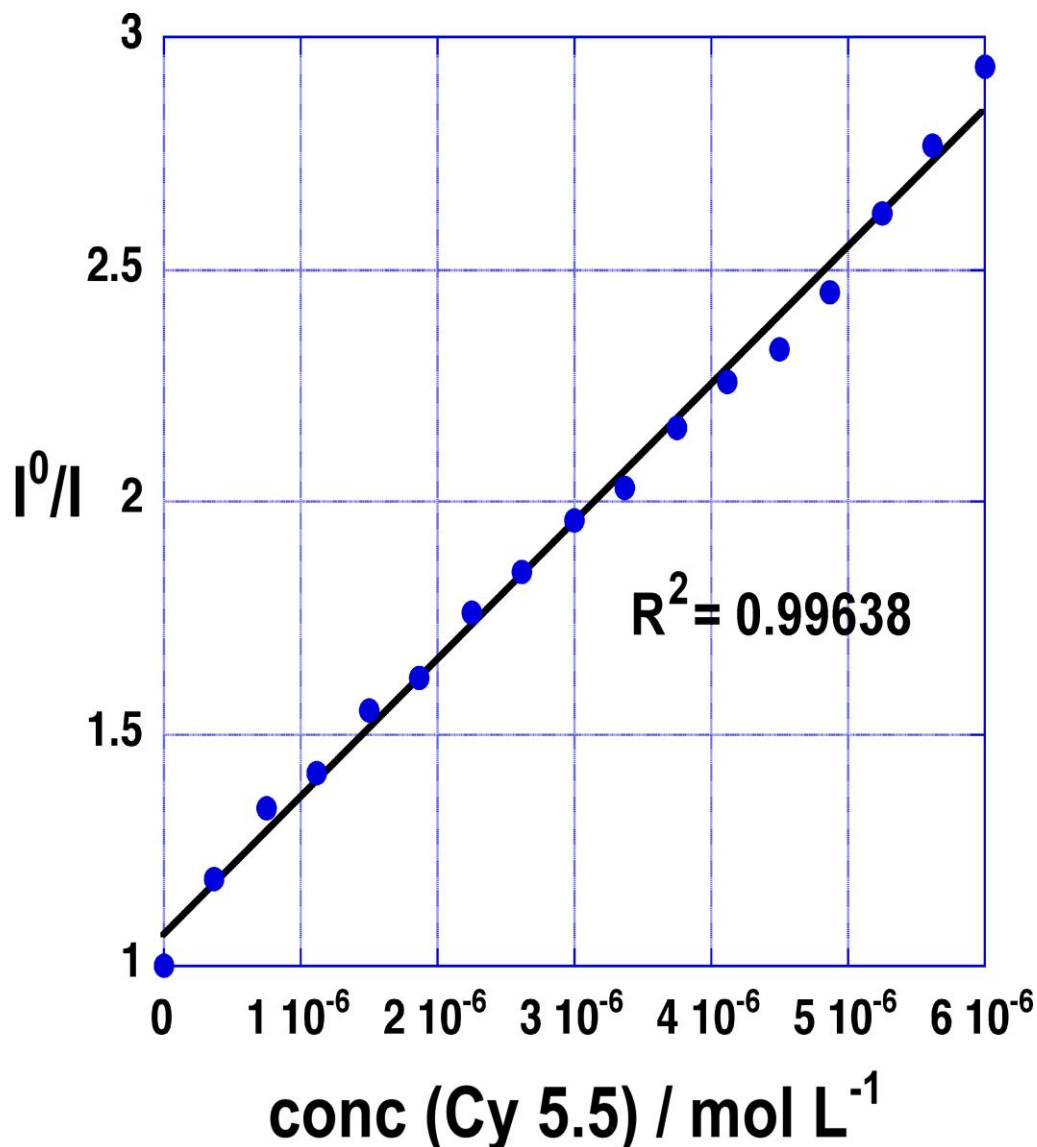
Figure 2.11: Stern-Volmer Plot of the Fluorescence Intensity Quenching of TCPP (Integrated Intensities from 640 to 720 nm) by Cyanine 5.5 in PBS.

2.6.4. UV/Vis-Absorption and Fluorescence Spectra of TCPP in the Presence of Dopamine-Coated Fe/Fe$_3$O$_4$ Nanoparticles

It is noteworthy that the absorption and emission spectra of TCPP do not indicate clustering, when dissolved in PBS at pH=7.4, mixed with dopamine-coated Fe/Fe$_3$O$_4$-nanoparticles, or tethered to the Fe/Fe$_3$O$_4$-nanoparticles. Bathochromic shifts in TCPP absorption (Figure 2.12) and emission (Figure 2.13) spectra, which would indicate aggregation[21], are not discernible.
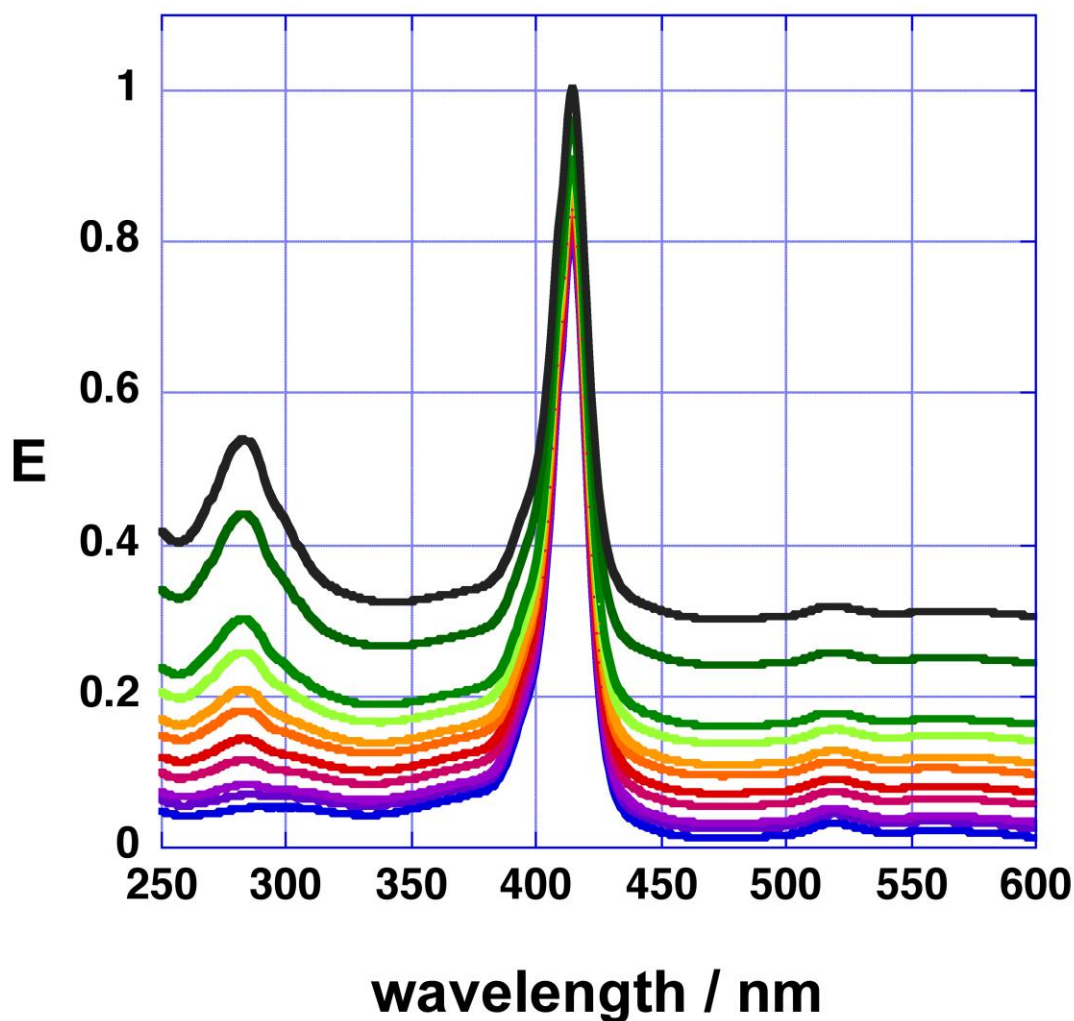
Figure 2.12: UV/Vis-Absorption Spectra of TCPP in PBS in the Presence of Increasing Concentrations of Dopamine-Coated Fe/Fe$_3$O$_4$ Nanoparticles.

These nanoparticles are virtually identical with these employed in the nanoplatforms for protease detection. Nanoparticle concentrations: 0.00167 mg mL^{-1}, 0.005 mg mL^{-1}, 0.0083 mg

mL^{-1}, 0.0117 mg mL^{-1}, 0.015 mg mL^{-1}, 0.02 mg mL^{-1}, 0.0267 mg mL^{-1}, 0.033 mg mL^{-1}, 0.067 mg mL^{-1}, 0.10 mg mL^{-1}, 0.167 mg mL^{-1}
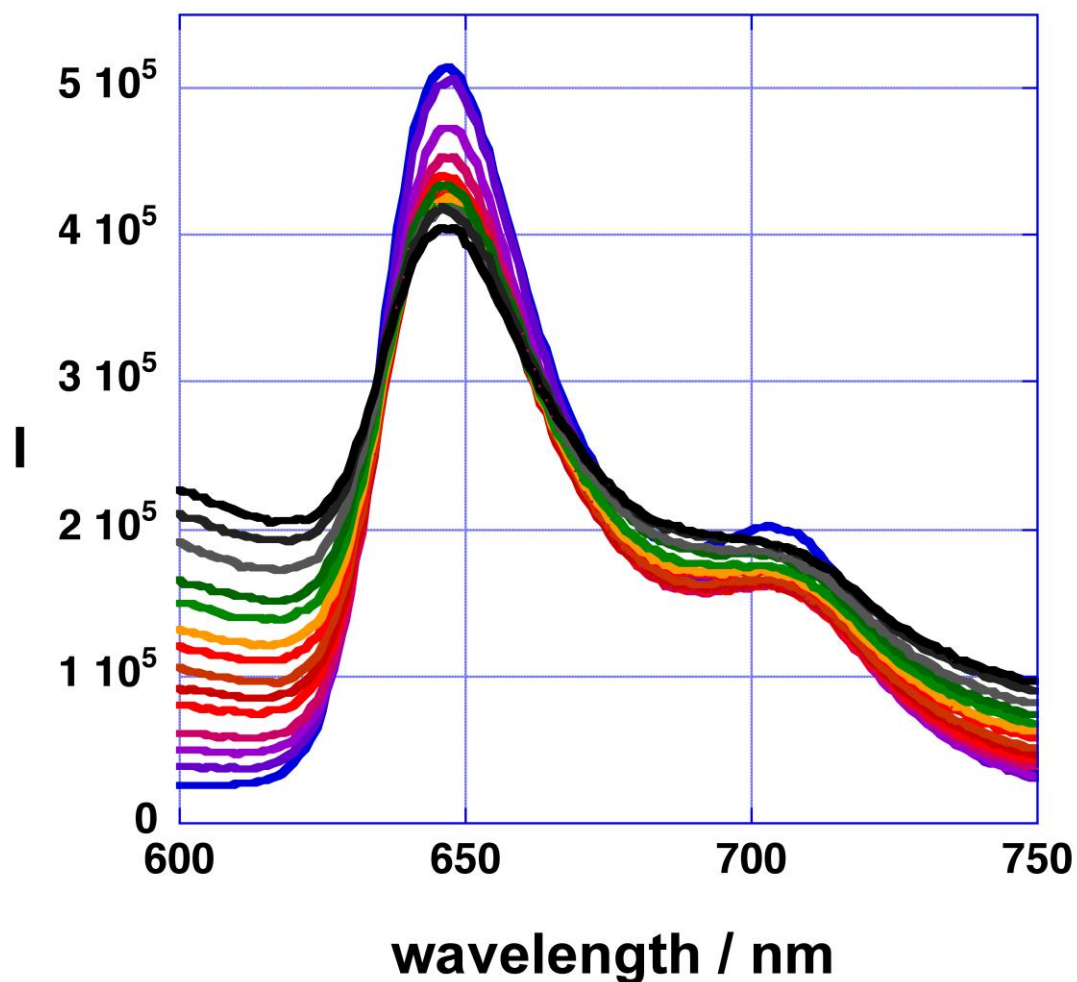
Figure 2.13: Fluorescence Spectra of TCPP in PBS in the presence of Increasing Concentrations of Dopamine-Coated Fe/Fe$_3$O$_4$ nanoparticles

These nanoparticles are virtually identical with these employed in the nanoplatforms for protease detection. Nanoparticle concentrations: 0.00167 mg mL^{-1}, 0.005 mg mL^{-1}, 0.0083 mg mL^{-1}, 0.0117 mg mL^{-1}, 0.015 mg mL^{-1}, 0.02 mg mL^{-1}, 0.0267 mg mL^{-1}, 0.033 mg mL^{-1}, 0.067 mg mL^{-1}, 0.10 mg mL^{-1}, 0.167 mg mL^{-1}.

2.6.5 Nonaggregation of TCPP

This is in agreement with the literature: the aggregation constant of TCPP in aqueous solution at pH=7.5 (ethylene glycol added) was determined to 4.55 x 10^4 M^{-1}.[22] The TCPP concentrations employed in this study are three orders of magnitude lower.
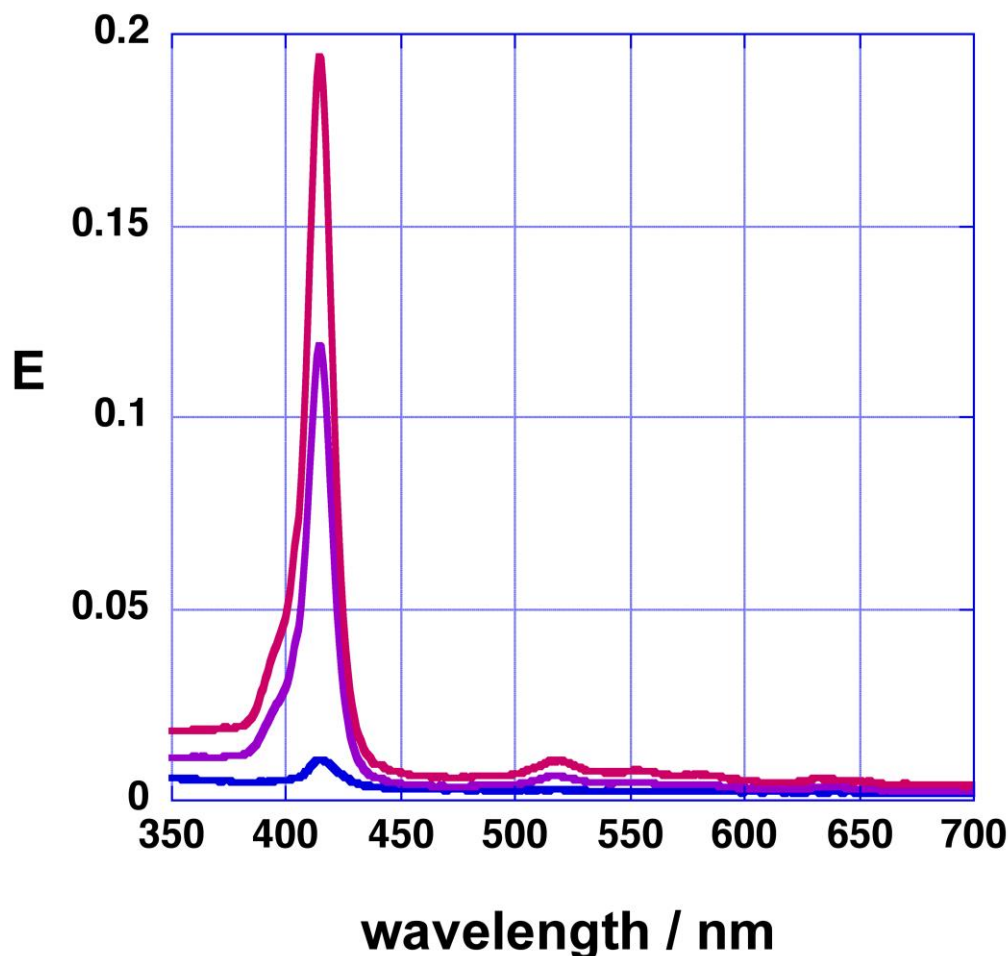
Figure 2.14*: UV/Vis-Absorption Spectra of TCPP in PBS (5.05 x 10^{-8} M, 3.25 x 10^{-7} M, 5.05 x 10^{-7} M).**

The maxima of the Soret bands are at 416 +/- 1 nm, indicating that TCPP does not aggregate at pH = 7.4 at the chosen concentrations.

At the same time, TCPP will remain linked to half of the consensus sequence, making the porphyrin distinctly more water-soluble. The octanol/water partitioning coefficients (log P)[23] of TCPP and TCPP-peptide adducts are summarized in Table 2.2.

Table 2.2: Octanol/Water Partitioning Coefficients, Calculated by Using Chemdraw Ultra (version 12.0.3.1216)

Protease	Consensus Sequence	Log P when tethered to TCPP at pH 7.4
H$_2$TCPP (pH=2)		9.6
H$_2$TCPP (pH=7)		7.6
MMP 1	VPMS-	4.1
MMP 2	IPVS-	4.6
MMP 3	RPFS-	3.7
MMP 7	VPLS-	4.5
MMP 9	VPLS-	4.5
MMP 11	GGAAN-	3.2
MMP 13	GPQGLA-	2.9
uPA	SGR-	4.7
CTS B	SLLKSR-	1.7
CTS D	SLLIFR-	3.4
CTS K	GPR-	4.5
CTS L	SGVVIA-	3.5

2.7 References

[1] Lacroix, L.-M.; Huls, N. F.; Ho, D.; Sun, X.; Cheng, K.; Sun, S. Stable Single-Crystalline Body Centered Cubic Fe Nanoparticles, *Nano Lett*. **2011**, *11*, 1641-1645.

[2] Xu, C.; Xu, K.; Gu, H.; Zheng, R.; Liu, H.; Zhang, X.; Guo, Z.; Xu, B. Dopamine as a robust anchor to immobilize functional molecules on the iron oxide shell of magnetic nanoparticles, *J. Am. Chem. Soc.* **2004**, *126*, 9938-9939.

[3] Basel, M. T.; Balivada, S.; Wang, H.; Shrestha, T. B.; Seo, G. M.; Pyle, M.; Abayaweera, G.; Dani, R.; Koper, O. B.; Tamura, M.; Chikan, V.; Bossmann S. H.; Troyer, D. L. Cell-delivered magnetic nanoparticles caused hyperthermia-mediated increased survival in a murine pancreatic cancer model, *Int. J. Nanomed*. **2012**, *7*, 297-306.

[4] Ahn, B. K.; Wang, H.; Robinson, S.; Shrestha, T. B.; Troyer, D. L.; Bossmann S. H.; Sun, X. S. Ring opening of epoxidized methyl oleate using a novel acid-functionalized iron nanoparticle catalyst, *Green Chem*. **2012**, *14,* 136-142.

[5] Wang, H.; Shrestha, T. B.; Basel, M. T.; Dani, R. K.; Seo, G.-M.; Balivada, S.; Pyle, M. M.; Prock, H.; Koper, O. B.; Thapa, P. S.; Moore, D.; Li, P.; Chikan, V.; Troyer D. L.; Bossmann, S. H. Magnetic-Fe/Fe3O4-nanoparticle-bound SN38 as carboxylesterase-cleavable prodrug for the delivery to tumors within monocytes/macrophages, *Beilstein J. Nanotechnol*. **2012**, *3*, 444-455.

[6] Sobczynski, J.; Toennesen, H. H.; Kristensen, S. Influence of aqueous media properties on aggregation and solubility of four structurally related meso-porphyrin photosensitizers evaluated by spectrophotometric measurements, *Pharmazie.* **2013**, *68*, 100-109.

[7] Patsenker, L.; Tatarets, A.; Kolosova, O.; Obukhova, O.; Povrozin, Y.; Fedyunyayeva, I.; Yermolenko I.; Terpetschnig, E. Fluorescent probes and labels for biomedical applications, *Ann. N. Y. Acad. Sci*. **2008**, *1130*, 179-187.

[8] Berker, K. I.; Guclu, K.; Demirata, B.; Apak, R. A novel antioxidant assay of ferric reducing capacity measurement using ferrozine as the colour forming complexation reagent, *Anal. Methods*, **2010**, *2*, 1770-1778.

[9] El-Faham, A.; Albericio, F. Peptide Coupling Reagents, More than a Letter Soup, *Chem. Rev*. **2011**, *111*, 6557-6602.

[10] Mant, C. T.; Chen, Y.; Yan, Z.; Popa, T. V.; Kovacs, J. M.; Mills, J. B.; Tripet B. P.; Hodges, R. S. HPLC analysis and purification of peptides, *Methods Mol. Biol*. **2007**, *386*, 3-55.

[11] Amblard, M.; Fehrentz, J. -A.; Martinez, J.; Subra, G. Methods and protocols of modern solid phase peptide synthesis, *Molecular Biotechnology*, **2006**, *33*, 239-254.

[12] Carreon, J. R.; Stewart, K. M.; Mahon, K. P.; Shin, S.; Kelley, S. O. Cyanine dye conjugates as probes for live cell imaging, *Bioorg. Med. Chem. Lett.* **2007**, *17*, 5182-5185.

[13] Pereira, M. M.; Monteiro C. J. P.; Peixoto, A. F. Meso-substituted porphyrin synthesis from monopyrrole: an overview, *Targets in Heterocyclic Systems chemistry and properties*, Attanasi, O. A.; Spinelli, D. Springer: New York, USA, 2008; pp.258-278.

[14] http://www.rsc.org/periodic-table/element/26/iron

[15] Kalambur, V. S.; Longmire E. K.; Bischof, J. C. Cellular Level Loading and Heating of Superparamagnetic Iron Oxide Nanoparticles, *Langmuir*, **2007**, *23*, 12329-12336.

[16] Kell, A. J.; Barnes, M. L.; Jakubek Z. J.; Simard, B. Toward Brighter Hybrid Magnetic-Luminescent Nanoparticles: Luminosity Dependence on the Excited State Properties of Embedded Dyes, *J. Phys. Chem. C*, **2011**, *115*, 18412-18421.

[17] Huang, X.; El-Sayed I. H.; El-Sayed, M. A. Fluorescent quenching gold nanoparticles: potential biomedical applications, *Metal Enhanced Fluorescence,* Geddes, C. D. John Wiley & Sons, Inc.: Hoboken, NJ, USA, 2010; pp.573-599.

[18] Samarakoon, T. N. PhD. Dissertation, Kansas State University, 2010.

[19] Yun, C.S.; Javier, A.; Jennings, T.; Fisher, M.; Hira, S.; Peterson, S.; Hopkins, B.; Reich N.O.; Strouse, G.F. Nano-metal surface energy transfer in optical rulers, breaking the FRET barrier, *J. Am. Chem. Soc.* **2005**, *127*, 3115-3119.

[20] Turro, N. J.; Ramamurthy V.; Scaiano, J. C. *Modern Molecular Photochemistry of Organic Molecules*, 1st ed.; University Science Books: California, USA, 2010.

[21] Lambert, C. R.; Reddi, E.; Spikes, J. D.; Rodgers M. A. J.; Jori, G. The effects of porphyrin structure and aggregation state on photosensitized processes in aqueous and micellar media, *Photochem. Photobiol*. **1986**, *44,* 595-601.

[22] Pasternack, R. F.; Huber, P. R.; Boyd, P.; Engasser, G.; Francesconi, L.; Gibbs, E.; Fasella, P.; Venturo. G. C.; Hinds, L. de C. On the aggregation of meso-substituted water-soluble porphyrins, *J. Am. Chem. Soc.* **1972**, *94*, 4511-4517.

[23] Testa, B.; Kramer, S. D.; Wunderli-Allenspach, H.; Folkers, G. Calculation of lipophilicity: a classification of methods, *Pharmacokinetic Profiling in Drug Research: Biological, Physicochemical, and Computational Strategies*, Mannhold, R. Wiley-VCH: Weinheim, Germany, 2006; pp. 333-352.

Chapter 3 - Calibration of Magnetic-Nanoparticle (Fe/Fe₃O₄) - based Nanoplatforms for Highly Sensitive Fluorescence Detection of Cancer-Related Proteases

3.1 Validation of the Nanoplatform Designed for Measuring MMP 13

The nanoplatform for detecting the activity of MMP 13 was incubated with three different concentrations of the enzyme (commercially available from Enzo Lifesciences) under sstandard cconditions at 298 K as a function of time. In short, 3.0 mL of PBS/dextran (10 mg dextran in 1.0 ml of PBS) were mixed with 75 µL of the nanoplatform dispersion (1.0 mg in 1.0 ml of PBS) and 30 µl of the protease at each concentration level in PBS. In Figure 3.1, the results for 1.0×10^{-12} mol L^{-1} of MMP 13 are shown. The nanoplatform shows the typical "Light Switch Effect": TCPP (partially) escapes the quenching influence of Fe/Fe₃O₄ and the co-tethered cyanine 5.5. Consequently, its fluorescence quantum efficiency increases. Fluorescence increase as a function of reaction time under standard conditions at 298 K after addition of 1.0×10^{-12} mol l^{-1} of MMP 13 is shown in Figure 3.1.
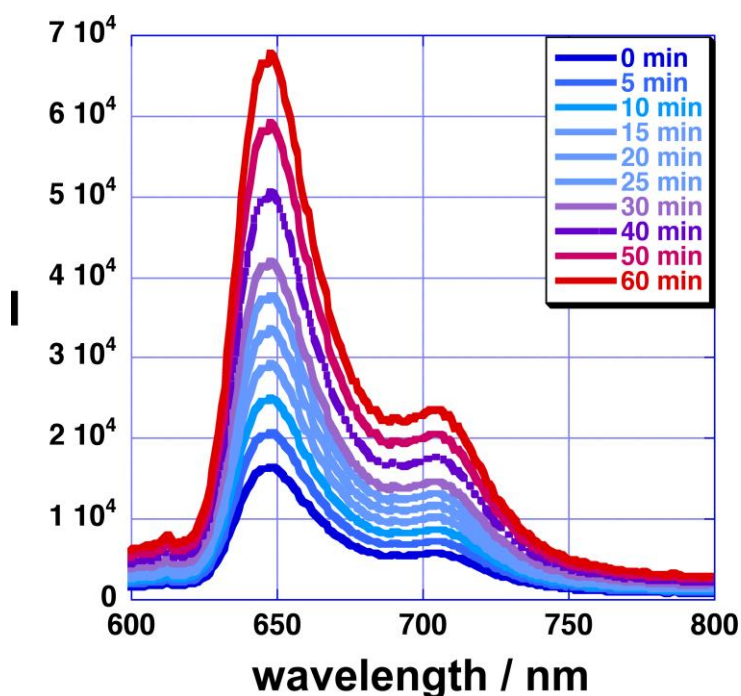
Figure 3.1: Light Switch Effect of the Fe/Fe₃O₄ Nanoplatform Capable of Detecting MMP 13

64

In Figure 3.2, the fluorescence increase of the nanoplatform capable of detecting MMP 13 during 60 min of incubation at 298 K under standard conditions in the presence of 1.0×10^{-8} mol L^{-1}, 1.0×10^{-10} mol L^{-1} and 1.0×10^{-12} mol L^{-1} of MMP 13 is shown. As anticipated for a matrix metalloproteinases, Michaelis-Menton kinetics is, principally, observed: the increase in reaction rate is limited with increasing substrate concentration.[1]
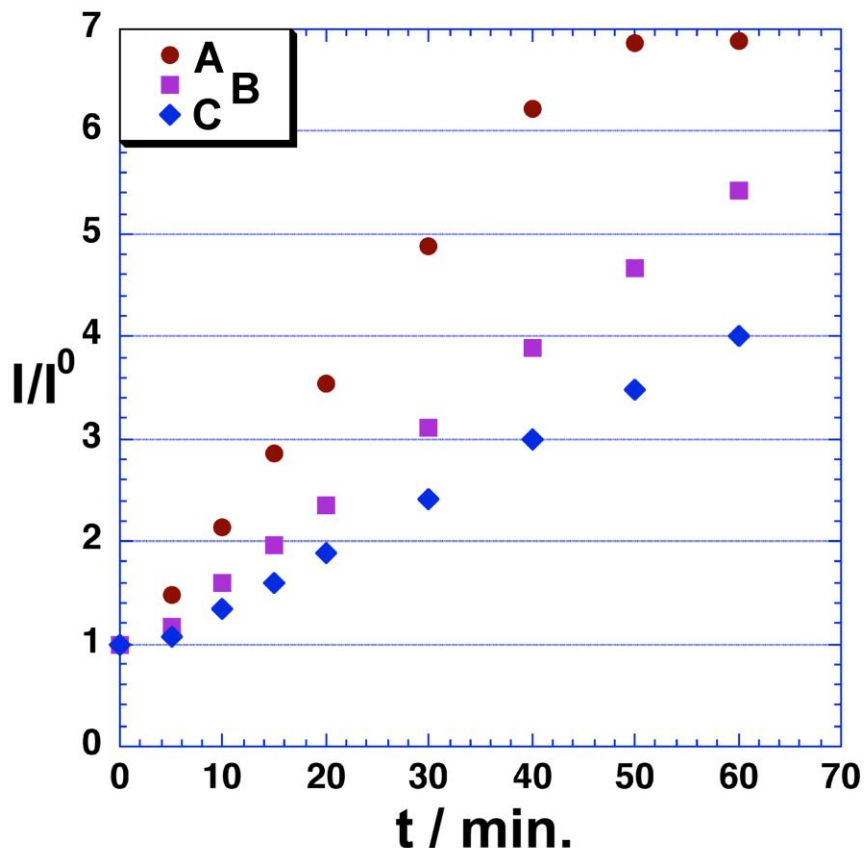
Figure 3.2: Fluorescence Increase when Incubating the Fe/Fe$_3$O$_4$-Nanoplaform Capable of Detecting MMP 13 as a Function of Reaction Time

The experiment which has done to obtain the results shown in Figure 3.2 is carried out under Standard Conditions at 298 K: A: 1.0×10^{-8} mol L^{-1}; B: 1.0×10^{-10} mol L^{-1}; C: 1.0×10^{-12} mol L^{-1}. The TCPP fluorescence is integrated from $\lambda = 620$ nm to 680 nm. At the highest protease concentration, virtually all cleavable substrate is processed after 50 min and a plateau is reached. Since 10^{-8} mol L^{-1} is the upper bound of the concentration range of clinical interest, we have not adjusted the concentration of the nanoplatform to measure higher protease activities.

3.2 The Nanoplatform Designed for MMP 13 is Not Activated by MMP 9 or When Using a Scrambled Peptide Sequence Instead of the Consensus Sequence

The next step of the nanoplatform validation process consisted in testing a scrambled version of the consensus sequence for MMP 13: GRPGAGQVQLGI as a component of a nanoplatform. After adding 1.0×10^{-12} mol L^{-1} of MMP 13 and incubating at 298 K for 60 min, the fluorescence increased to $I/I^0 = 1.06$, indicating that the reaction of MMP 13 with the scrambled sequence is 51 times slower. (I: TCPP fluorescence intensity after 60 min. of incubation, I^0: TCPP fluorescence intensity before incubation). This is shown in Figure 3.3.

It should be noted that a fraction of the observed increase in fluorescence could also occur from desorption of peptide-sequence attached TCPP that has been physisorbed at the dopamine coated Fe/Fe_3O_4 surface during the synthesis procedure because of competitive absorption of the enzyme. The nanoplatform did not show a measurable increase in fluorescence when dispersed in PBS, due to thorough washing procedures during synthesis.
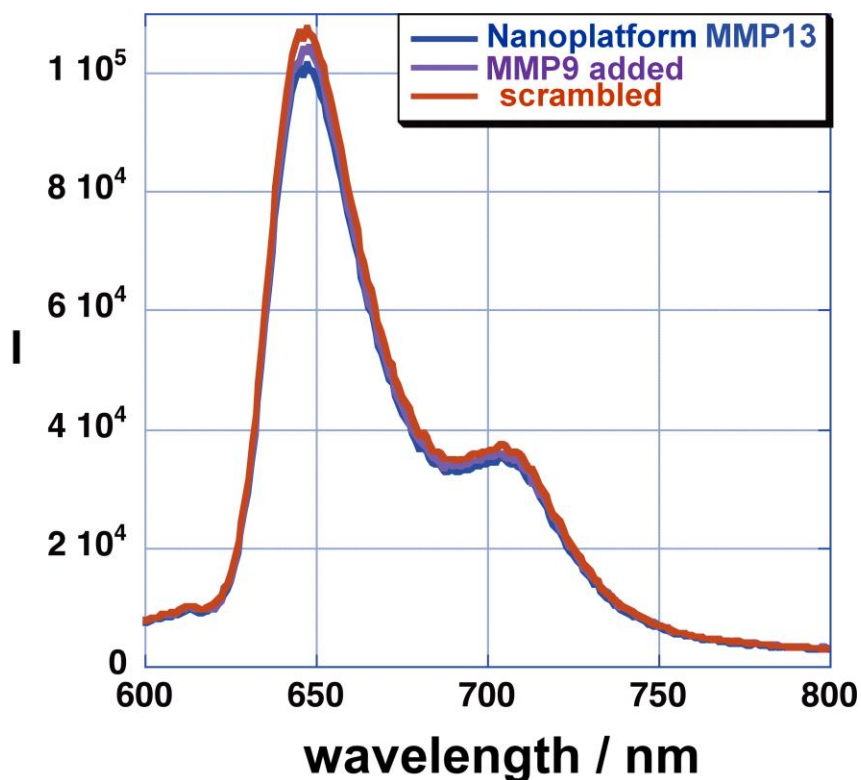
Figure 3.3: **Fluorescence Spectra of the Nanoplatform for MMP 13 in the Absence of the Protease, as well as in the Presence of 1×10^{-12} mol L^{-1} of MMP 9**

The third validation procedure entailed incubation of the nanoplatform designed for detecting MMP 13 with MMP 9. After adding 1.0 x 10^{-12} mol L^{-1} of MMP 9 and incubating at 298 K for 60 min, the fluorescence increased to I/I^0 = 1.027, which is 114 times slower. This is also shown in Figure 3.3. This experiment added further confidence in the selection of previously established consensus sequences from the literature, as described above. According to Figure 3.3, the "wrong" protease failed to activate the nanoplatform. Also it shows the fluorescence occurring from a nanoplatform using a scrambled version of the consensus sequence (GRPGAGQVQLGI instead of GPQGLAGQRGIV) in the presence of 1 x 10^{-12} mol L^{-1} of MMP 13. Both nanoplatforms were incubated under standard conditions.

3.3 Calibration of 12 Nanoplatforms Designed for Measuring the Activities of 12 Cancer-Related Proteases

After establishing the initial validation experiments using the nanoplatform designed for MMP 13, we have performed successful calibration procedures for all 12 nanoplatforms in the concentration range of 10^{-8} mol L^{-1} to 10^{-16} mol L^{-1}. Each nanoplatform comprised a dopamine-coated Fe/Fe$_3$O$_4$-nanoparticle, and, in average, 50+/-4 permanently tethered cyanine 5.5 molecules and 35+/-3 consensus-sequence-bound TCCP fluorophores. To avoid possible misunderstandings, we would like to emphasize again that each nanoplatform is capable of measuring one protease, multitasking was not attempted in the work described here. In following the outcome of the preliminary experiments described above, all nanoplatforms have been incubated in PBS in the presence of the anti-coagulation agent dextran at 298 K for exactly 60 min. The fluorescence was measured at t = 0 min. and t = 60 min. The fluorescence signal was integrated from 620 nm to 680 nm.

A control sample, to which no protease was added, was incubated for 60 min. and then measured also to detect systematic errors occurring from nanoplatforms releasing TCPP for reasons other than enzymatic activity. For all investigated nanoplatforms (see Table 1.4), there was virtually no detectable increase in fluorescence after 60 min. of incubation in the absence of added protease (I/I^0 < 1.05). The I/I^0 response as a function of protease concentration was recorded by dividing the integrated fluorescence signal after 60 min. in the presence of the protease at respective concentration, I, by the reference signal obtained under (otherwise) identical conditions in the absence of the protease, I$^0_{ref}$. For the majority of proteases, three

repetitions of the calibration procedure established a relative error under 2 percent, which is sufficient for clinical applications.[2] The calibration of uPA needed seven repetitive calibration procedures to achieve the required precision, MMP9 and cathepsin L required five. Based on our calibration results, we have found three principal groups:

3.3.1 The Highly Reactive Proteases

The group of proteases that causes the fastest increase of fluorescence intensity upon enzyme activation of their respective nanoplatforms is comprised of MMP 7, MMP 11, MMP 13, and cathepsin L, MMP 13 being the most reactive (Figure 3.4). For these three MMPs, the plots of I/I^0_{ref} vs. log c are fairly linear, indicating that the Michaelis-Menton plateau was approached, but not reached, within the region of clinical interest. Both I and I^0_{ref} were obtained after 60 min. of incubation at 298 K under standard conditions.
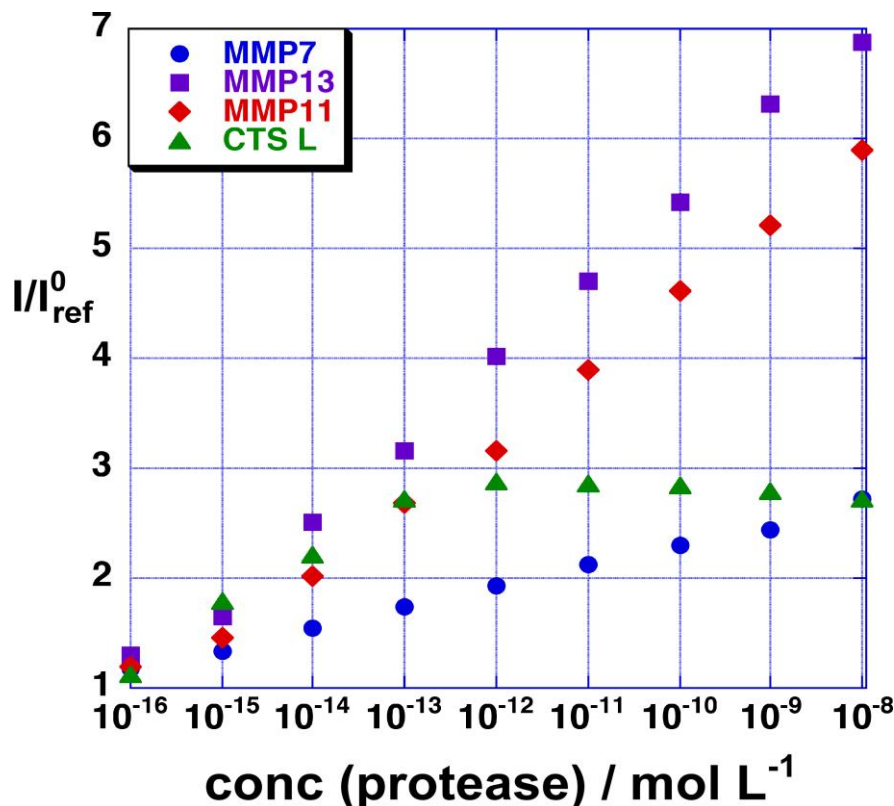
Figure 3.4: Calibration Results for MMP 7, MMP 11, MMP 13, and Cathepsin L after 60 min. of Incubation at 298 K Under Standard Conditions

For cathepsin L, this limit was reached when approaching 10^{-12} mol L^{-1}. In order to avoid systematic errors, these measurements have to be precisely timed.

3.3.2 The Moderately Reactive Proteases

The nanoplatforms for measuring MMP 1, MMP 2, MMP 3, cathepsin B and cathepsin D show less pronounced fluorescence increases after 60 min. of incubation, compared to the nanoplatforms for the first group of proteases (Figure 3.5). The Michaelis-Menton plateau was not reached for any of these proteases.
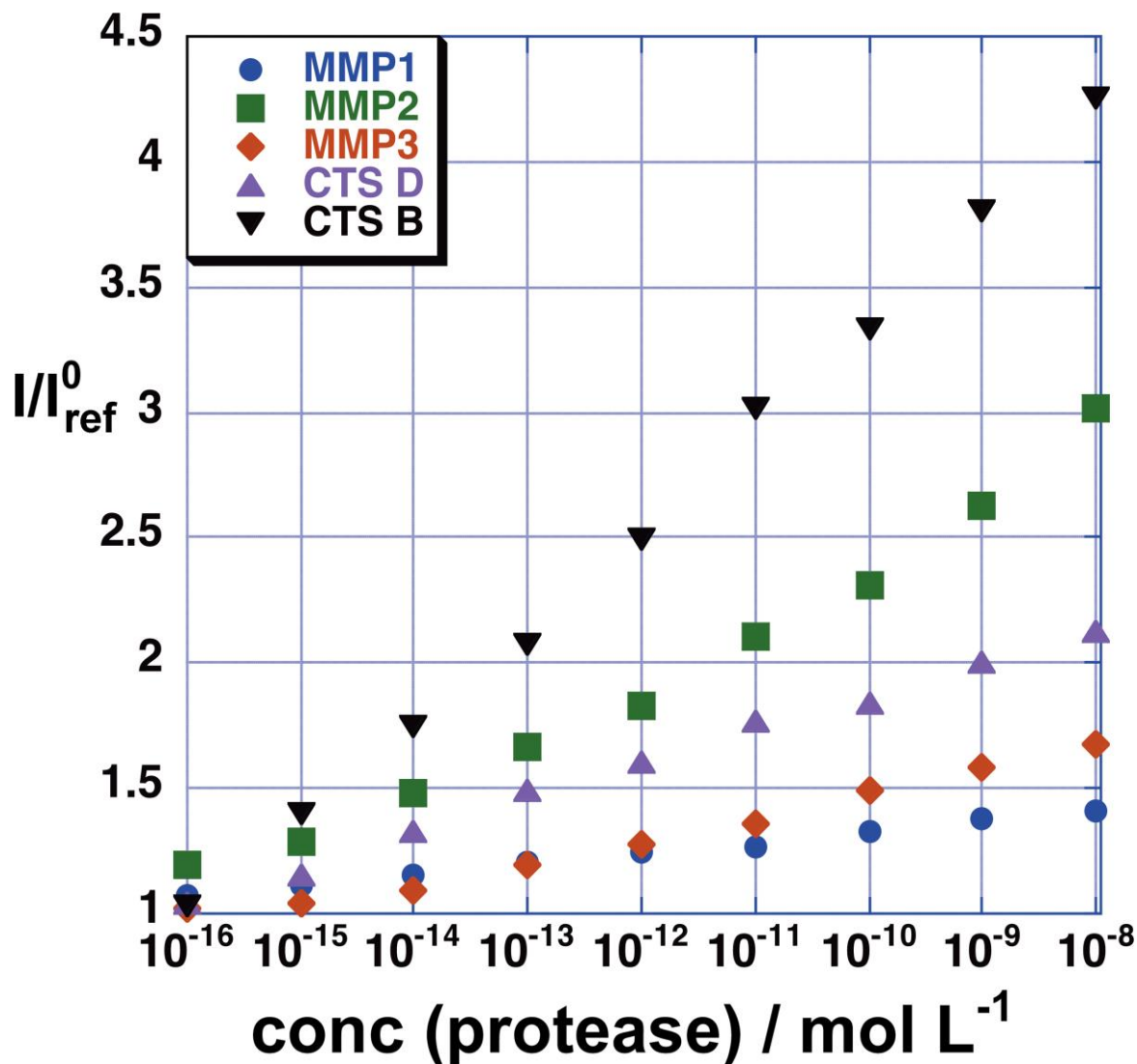
Figure 3.5: Calibration Results for MMP 1, MMP 2, MMP 3, Cathepsin B and Cathepsin D after 60 min of Incubation at 298 K under Standard Conditions

With respect to future clinical diagnostics, it is of importance that the somewhat lower increases in fluorescence intensities upon incubation that were observed for the nanoplatforms designed for the second group of proteases do not impede any future applications of the nanoplatforms, because the experimental error from independent calibration procedures is less than 2 percent. This considerably low error permits the identification of the correct order of magnitude for every protease that was investigated.

3.3.3 The Group of Proteases Defying the "Light Switch" Paradigm

From a mechanistical standpoint, the group comprising the nanoplatforms designed for measuring uPA, MMP 9 and cathepsin K is most interesting, because they show a decrease and not an increase of I/I^0_{ref} after incubation with their respective proteases. Again, we were able to reach an experimental error from three or more independent calibration procedures of less than 2 percent, demonstrating that also the third group of nanoplatforms is potentially clinically viable.

But why does their fluorescence decrease, in spite of fluorescence resonance energy transfer quenching (FRET)[3] and plasmon-resonance quenching[4] that are equally viable deactivation pathways in all of the nanoplatforms? According to Table 2.1 (see page 56), we have employed consensus sequences of different lengths. uPA and cathepsin K are among the shortest sequences used, and one may expect that the shorter distance between TCPP and the nanoparticle may result in an increase of TCPP fluorescence when bound. Although the plasmon absorption of the Fe-core in Fe/Fe_3O_4-nanoparticles is distinctly weaker than of a gold nanoparticle, there is a discernible plasmon-dye interaction.[5]

Furthermore, Fe/Fe_3O_4-nanoparticles scatter the incident light efficiently, which also may enhance the light absorption by TCPP when tethered.[6] In both cases, cutting TCPP loose will result in a decrease of fluorescence intensity. For MMP 9, this case is harder to make, because the lengths of the consensus sequences for MMP 1, MMP 3, MMP 7, and MMP 9 are of comparable length. However, the reactivity that is observed with MMP 9 can be better understood when looking at the observed activities of all nanoplatforms for protease measurements.
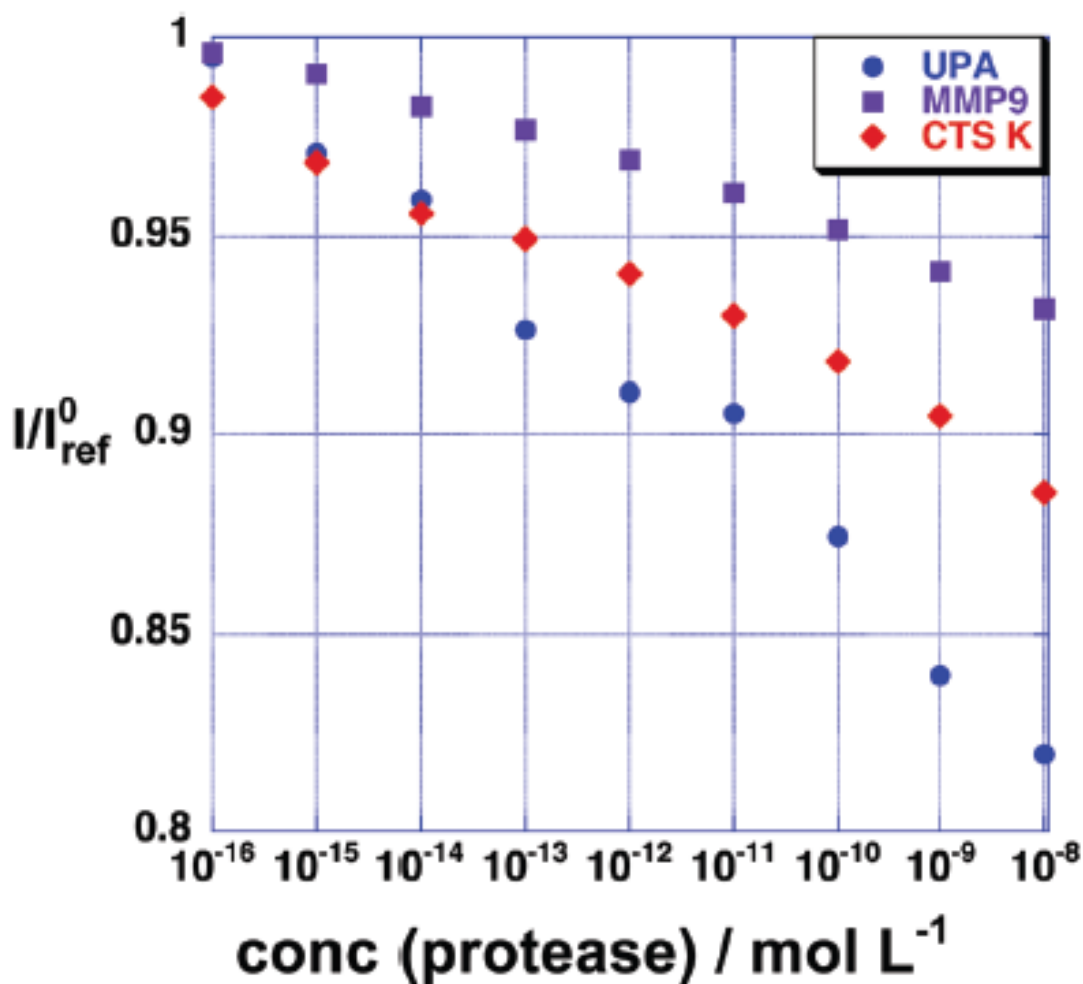
Figure 3.6: Calibration Results for uPA, MMP 11, MMP 9, and Cathepsin K after 60 min. of Incubation at 298 K under Standard Conditions

3.4 Dependence of Fluorescence Activation Upon the Length of the Consensus Sequence

The plots of I/I^0_{ref} vs. log c are sufficiently linear ($R^2 > 0.95$ for all proteases except cathepsin L, for which only the concentration range from 10^{-16} mol L^{-1} to 10^{-12} mol L^{-1} was analyzed) to permit their analysis according to: $I/I^0_{ref} = k_{max} + k \log [c \text{ (protease)}]$. MMP 2 was identified as an outlier among the group of MMPs. In this study, uPA does not belong to a group of proteases. The resulting k-values for each protease were then plotted vs. the length of the

71

consensus sequence that was used to tether TCPP and the Fe/Fe_3O_4-nanoplatform, as determined by using MM3.[7]

Although MM3 is a simple force field and cannot account for the dynamics of the oligopeptides, this simple analysis offers an interesting mechanistic insight into the reactivity of the nanoplatforms designed for analysing MMPs and cathepsins with their respective enzymes. Most interestingly, the "Light Switch" Effect intensifies with increasing distance between Fe/Fe_3O_4-nanoparticle and TCPP. This is counter-intuitive, because both, FRET[3] and plasmon-resonance quenching[4] increase with decreasing distance. According to the literature, plasmon-resonance quenching, also known as dipole-surface energy transfer (SET), shows inverse 4th power dependence in energy transfer efficiency.[8] As already mentioned, FRET has often an inverse 6th power dependence[3], although this assumption is not necessarily in agreement with the linear Stern-Volmer plot reported in Figure 2.11 (see page 70).
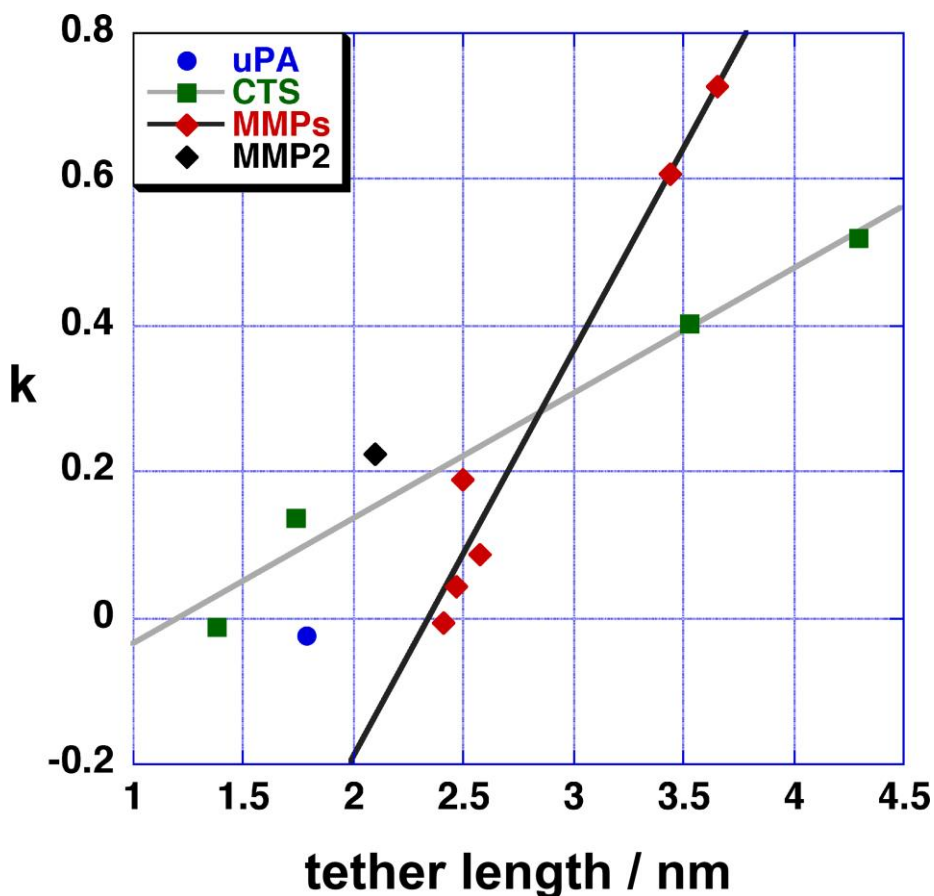
Figure 3.7: Plot of the kinetic Constant k

72

In figure 3.7, The K has been obtained from the concentration dependence of the observed fluorescence increase/decrease for each enzyme, vs. the length of the consensus sequence that was used to tether TCPP and the Fe/Fe_3O_4-nanoplatform.

It is apparent that the groups of nanoplatforms for measuring MMPs and cathepsins have different linear responses to the increase in tether length. The fluorescence increase of the group of nanoplatforms for MMP detection ($R^2 = 0.968$) proceeds 3.2 times faster with increasing tether lengths than for the group of nanoplatforms for cathepsin detection ($R^2 = 0.979$). MMP9 is among the sub-group of MMP's with the least activity.

There is a possible explanation for the observed behavior (or combinations thereof): longer consensus sequences allow the proteases better access and, therefore, faster hydrolytic cleavage is observed. TCPP, which is tethered to the "tip" of the oligopeptides causes significant sterical hindrance. In agreement with our mathematical analysis of FRET occurring at the surface of the nanoplatforms, the longer consensus sequences may "bend back", leading to a better contact between TCPP and the cyanine-5.5 tethered Fe/Fe_3O_4-nanoparticle.

3.5 Experimental Procedures

3.5.1 UV/Vis-Absorbance and Fluorescence Measurement

Both experiments were carried out in 4.0 mL quartz-cuvettes (Helma) using a spectrofluoro-meter (Fluoromax2) with dual monochromators and a diode array UV-vis absorption spectrometer (HP 8453). PBS buffer (phosphate buffered saline (8 g NaCl, 0.2 g KCl, 1.44 g Na_2PO_4, 0.24 g KH_2PO_4, dissolved in 1 l of bidest H_2O), pH=7.2) was used as solvent.

3.5.2 Standard Procedure of Preparing Protease Assays:

3.0 mg of nanoplatform are dissolved in 3 mL of PBS. The dispersion is sonicated for 10 min. The resulting dispersion is chemically stable for 14 d at 277 K. 900 mg of dextran are dissolved in 90 mL of PBS.

Stock solutions of all 12 enzymes were prepared by consecutive dilution of commercially available proteases (Enzo Lifesciences).

3 ml of PBS/dextran (10 mg dextran in 1.0 mL of PBS) are mixed with 75 μL of the nanoplatform dispersion (3.0 mg in 3.0 mL of PBS) and 30 μL of the protease at each concentration level in PBS.

3.6 References

[1] Palmier, M. O.; Doren, S. R. V. Rapid determination of enzyme kinetics from fluorescence: Overcoming the inner filter effect, *Anal. Biochem.* **2007**, *371*, 43-51.

[2] Bossmann, S. H.; Troyer, D. L. Point-of-care routine rapid screening: the future of cancer diagnosis? *Expert Rev. Mol. Diagn.* **2013**, *13*, 107-109.

[3] Kobayashi, H.; Choyke, P. L. Target-Cancer-Cell-Specific Activatable Fluorescence Imaging Probes: Rational Design and in Vivo Applications, *Acc. Chem. Res.* **2011**, *44*, 83-90.

[4] Huang, X.; El-Sayed I. H.; El-Sayed, M. A. Fluorescent quenching gold nanoparticles: potential biomedical applications, *Metal enhanced fluorescence*; Geddes, C. D. John Wiley & Sons, Inc., 2010, pp 573-599.

[5] Bossmann, S. H.; Troyer, D. L.; Basel, M. T. Diagnostic protease assay using a nanoparticle-linked oligopeptide substrate, and use for cancer detection and prognosis, Kansas State University Research Foundation, USA, WO2009-US35875, **2009**.

[6] Menichetti, L.; Manzoni, L.; Paduano, L.; Flori, A.; Kusmic, C.; Marchi. D. D.; Casciaro, S.; Conversano, F.; Lombardi, M.; Positano, V.; Arosio, D. Iron oxide-gold core-shell nanoparticles as multimodal imaging contrast agent, *IEEE Sensors Journal,* **2013**, *13*, 2341-2347.

[7] Todebush, P. M.; Bowen, J. P. Molecular mechanics force field development and applications, Kluwer Academic/Plenum Publishers, **2001**, pp. 37-59.

[8] Yun, C. S.; Javier, A.; Jennings, T.; Fisher, M.; Hira, S.; Peterson, S.; Hopkins, B.; Reich, N. O.; Strouse, G. F. Nanometal surface energy transfer in optical rulers, breaking the FRET barrier, *J. Am. Chem. Soc.* **2005**, *127*, 3115-3119.

Chapter 4 - Detection of Breast And Lung Cancer Using Magnetic-Nanoparticle (Fe/Fe3O4)-based Nanoplatforms for Highly Sensitive Fluorescence Detection of Cancer-Related Proteases

4.1 Background

The validated protease assays (as described in chapter 2) were used for the analysis of biospecimens, instead of commercially available enzymes. The analysis work of this dissertation started with canine urine samples. A series of urine samples was analyzed using the protease assay for MMP 9 and urokinase. Urine samples from lymphoma dogs and healthy dogs were analyzed, which were collected by Prof. Dr. Mary Lynn Higginbotham in the Department of Anatomy & Physiology at Kansas State. Based on these results, we could basically identify two protease concentration levels for the two sets of samples. Which means, the low protease concentration range for the urine samples of healthy dogs and high protease concentration range for the urine samples of lymphoma dogs could clearly be distinguished. Since information about the stage of the cancer was unavailable, and the data were obtained only for two types of proteases, the canine urine analysis was not significant enough to approach valuable conclusions.

Our next step was to analyze human urine samples. We received 36 human urine and 36 human blood samples from Dr. Tracy Chapman, Southeastern Nebraska Cancer Center (SNCC). Among them 12 are from non small cell Lung cancer patients, 18 are from breast cancer patients (all forms of breast cancer) and 6 are from healthy human subjects. We started with MMP 9 assay for both human urine samples and human blood samples. It is noteworthy that the viscosity of the blood samples was elevated, compared with commercially available proteases in PBS, thus causing some concern.

Blood serum could be obtained from the blood samples by centrifugation. First the frozen blood vial was thawed in a water bath at 40 ^{0}C for 1 h. Then it was centrifuged for 10 min at 10,000 RPM. Subsequent to this procedure, the red and white blood cells were collected at the bottom and a clear yellowish solution remains on the top. The supernatant is the blood serum, which was used for measuring protease activities with the protease assays.[1]

4.1.1 Procedure for the Protease Assay

All the solutions were prepared as stock solutions. Since the amounts of chemical required for protease measurements can be simplified to the concentrations needed for one sample, the procedure will be given per sample. Depending on the number of samples to analyze at a time, all the calculations can be done accordingly by simple multiplication.

In a 15 mL centrifuge tube 75 µL of the assay probe was added with the concentration of 1 mg/mL. Then 30 µLof the biospecimen was added. It could be either human urine or human blood serum. Then the whole volume was increased to 3.0 mL using 1X PBS containing 10 mg/ml of dextran. Then the tubes were sonicated for 5 min. and incubated it for one hour at 25°C. At the end of the one hour of incubation, fluorescence measurements were performed. All samples were repeated in triplicates. Also assay control and biospecimen controls were performed. An assay control consisted of the assay probe only, without having any urine or blood serum added. Biospecimen control consisted only of the biospecimen in PBS/dextran, without having any assay probe. The experimental parameters of these experiments were same as described in chapter 2.

4.1.2 MMP 9 Assay for Human Blood Serum

According to Figure 4.1, expression of MMP 9 was elevated in breast cancers. Stages III and IV were prominent among them. The integrated values has been calculated by taking the integral of the fluorescence spectra within the range 620 nm to 680 nm.
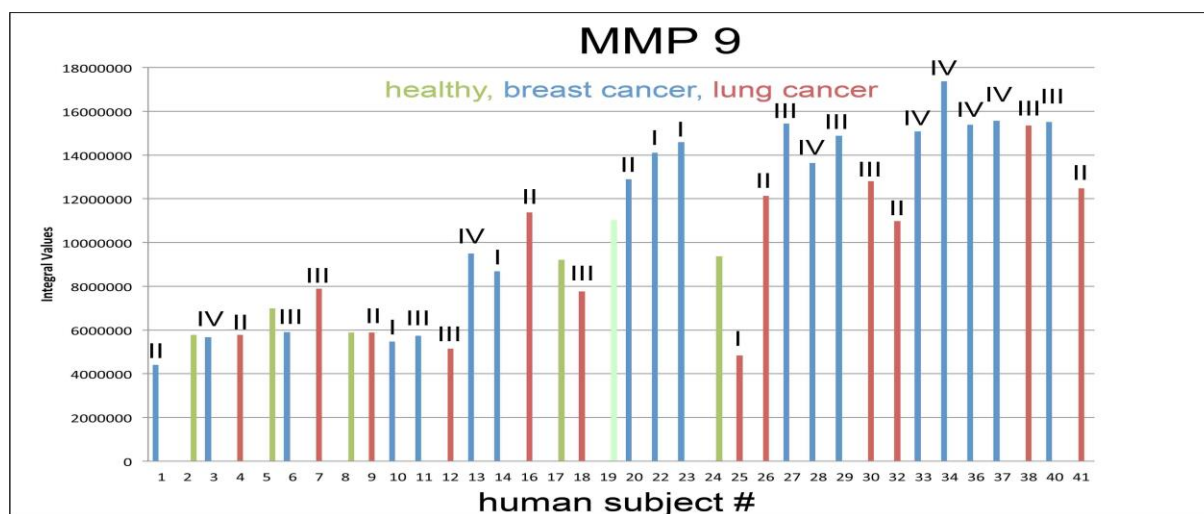
Figure 4.1: Comparison of Different Cancers and Staging using Blood Samples

4.1.3 MMP 9 Assay for Human Urine

According to Figure 4.2, the data from urine samples was not as significant as the data from blood samples (Figure 4.1) that were previously investigated.
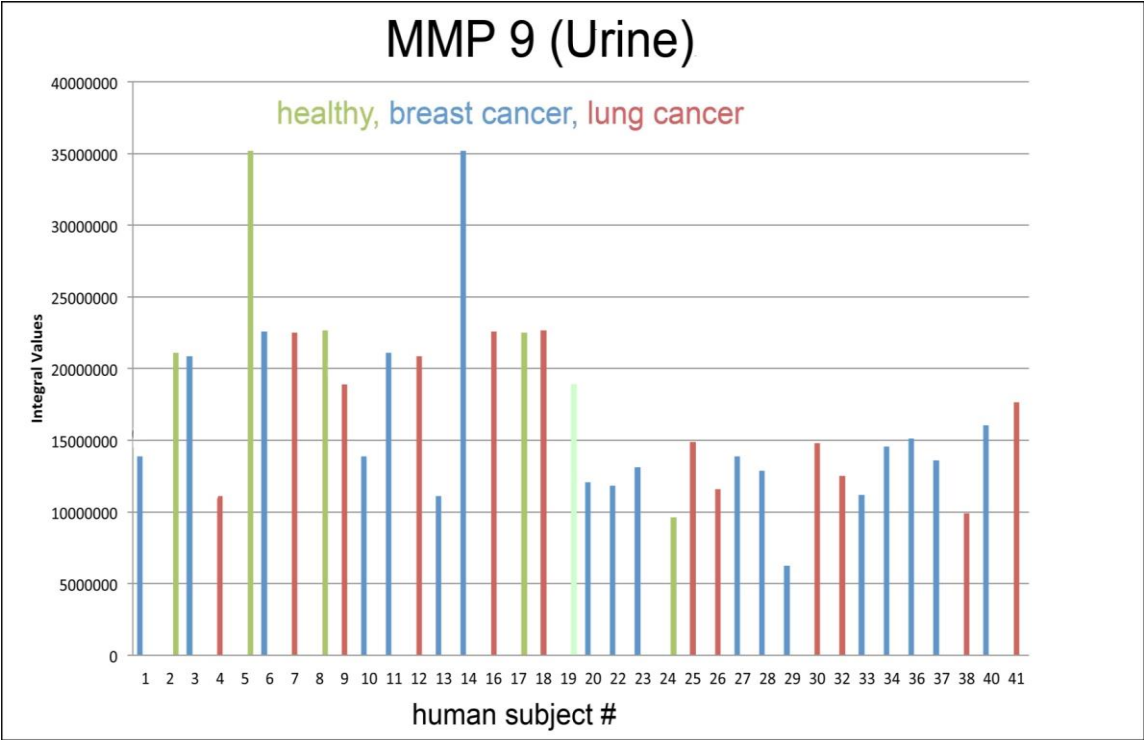
Figure 4.2: Comparison of Different Cancers using Urine Samples
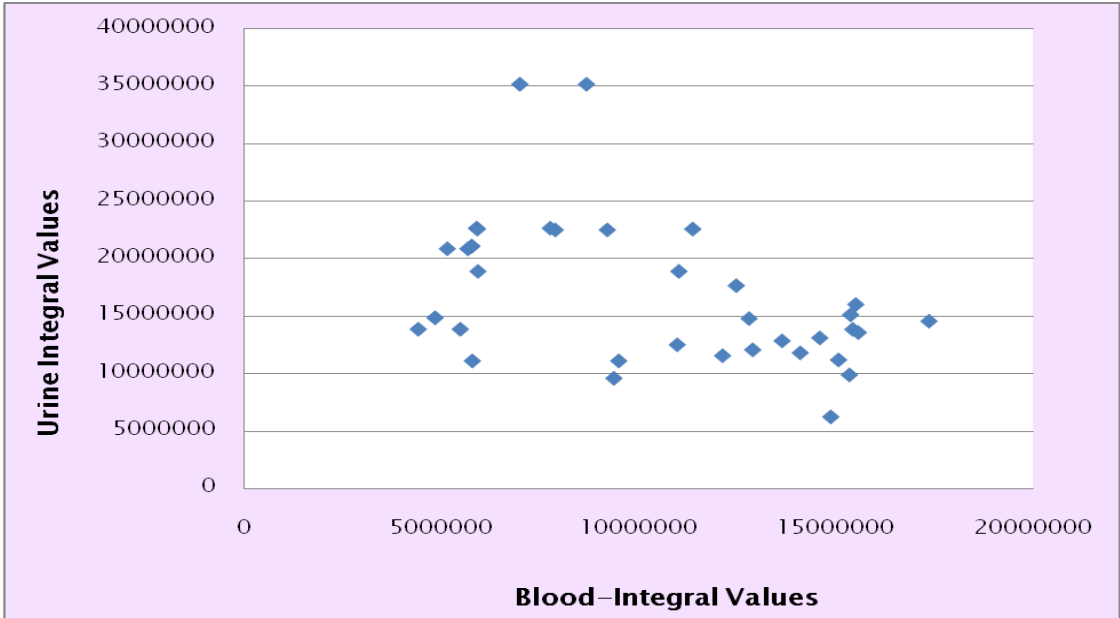
Figure 4.3: MMP 9 - Blood & Urine Comparison

As the data for the urine analysis was not significant, we thought of comparing the blood serum assay data and urine assay data with same set of samples. According to Figure 4.3, there was no correlation of the data from blood serum analysis and urine analysis. So we decided to proceed only with blood serum data analysis but to abandon the human urine analysis.

4.2 Introduction

4.2.1 Blood

Blood consists of at least 4000 different components, but the main four components are red blood cells, white blood cells, platelets, and plasma. Blood works as oxygen and nutrient transporter to cells. Also it transports metabolic waste products, such as carbon dioxide and ammonia.[2] Higher volume of the blood such as 55% is covered with plasma. Plasma consists of blood clotting factors, sugars, fats, vitamins, minerals, hormones, enzymes, antibodies and proteins.

4.2.2 Blood Serum

When the clotting elements are removed from the blood plasma, blood serum is obtained. Blood serum can be attained by allowing the blood to clot and squeezing out the yellow liquid. Most of the blood tests are carried out using blood serum, because it is long-term stable. Although we are discussing "blood tests", in most of the blood tests blood cells are actually not used. [3]

4.2.3 Urine

Urine is the liquid that consists of numerous waste products from our metabolism. Urea is the main nitrogenous waste product in urine. The urinary bladder is the storage organ for the urine. It is excreted from the urethra.[4] Approx. 95% of urine consists of water. Other components are urea, chloride, sodium, potassium, other dissolved ions, organic compounds and inorganic compounds.

4.3 Results

      Protease assays were carried out for several proteases using the blood serum samples from 12 Lung cancer patients, 18 breast cancer patients and 6 healthy humans. Codes of the samples are as follows.

Table 4.1: Codes of the Blood Samples

Breast Cancer	Lung Cancer	Healthy Humans
NS 2011 - 001B	NS 2011 - 004L	NS 2011 - 002C
NS 2011 - 003B	NS 2011 - 007L	NS 2011 - 005C
NS 2011 - 006B	NS 2011 - 009L	NS 2011 - 008C
NS 2011 - 010B	NS 2011 - 012L	NS 2011 - 017C
NS 2011 - 011B	NS 2011 - 016L	NS 2011 - 019C
NS 2011 - 013B	NS 2011 - 018L	NS 2011 - 024C
NS 2011 - 014B	NS 2011 - 025L	
NS 2011 - 020B	NS 2011 - 026L	
NS 2011 - 022B	NS 2011 - 030L	
NS 2011 - 023B	NS 2011 - 032L	
NS 2011 - 027B	NS 2011 - 038L	
NS 2011 - 028B	NS 2011 - 041L	
NS 2011 - 029B		
NS 2011 - 033B		
NS 2011 - 034B		
NS 2011 - 036B		
NS 2011 - 037B		
NS 2011 - 040B		

4.3.1 Calculations Associated with Data

First the average of the two consecutive scans for each sample was calculated. Then the average of the triplicates per each sample was calculated. From that final average data set, the integrated fluorescence value (S) was taken from 620 nm to 680 nm wavelength range of the sample. In a similar manner from the assay control (A) and blood serum control (B) samples, the integrated fluorescence value of the average data set was taken from 620 nm to 680 nm wavelength range. Then the difference between the two values S and B was calculated in order to avoid the autofluorescence occurring from the blood serum sample. Next step was to get the ratio of (S-B) and (A). This step was done to obtain information of the fluorescence increasement compared to the assay control. With the assay control there is some amount of TCPP, which is not quenched enough to avoid fluorescence. So this fluorescence should not mislead us to think that there is fluorescence occurring due to activity of the protease. This ratio is denoted as I^{S-B}/I^{A} in all the charts.

4.3.2 Study of MMP 1 Protease Assay Data
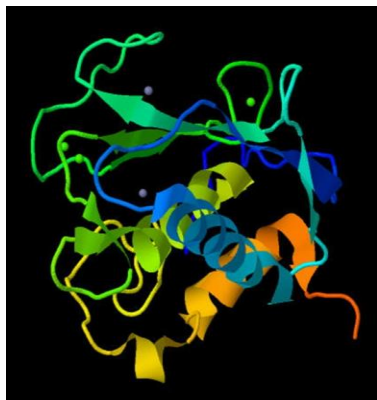
Figure 4.4: Structure of MMP 1[5]

MMP 1 is the interstitial collagenase, which is expressed abundantly within the human body. It degrades fibrillar collagens and the extracellular matrix. It is one of the highly upregulated mRNAs in ADHC (Atypical Ductal Hyperplasia Cancer). The overexpression of MMP 1 mainly associates with incidence or invasiveness of the cancer.[6] From the cell surfaces or matrix, MMP 1 releases pro-TGFα, other EGF like ligands and TGFβ. They are signaling molecule precursors which can result in autocrine or paracrine signaling with the tissue environment.[7,8] The structure of the MMP 1 is shown in Figure 4.4 and the molecular weight of MMP 1 is 52000 Da.

Figure 4.5: Integrated Fluorescence of the Blood Samples for MMP 1 Assay

In figure 4.5 the integrated fluorescence data for all the blood serum samples and in Figure 4.6 the I^{S-B}/I^A values for all the blood serum samples are shown. The majority of the breast and lung cancer blood serum samples show above 1.0 I^{S-B}/I^A value. Based on the validation shown in Chapter 3, MMP 1 is a moderately reactive protease.
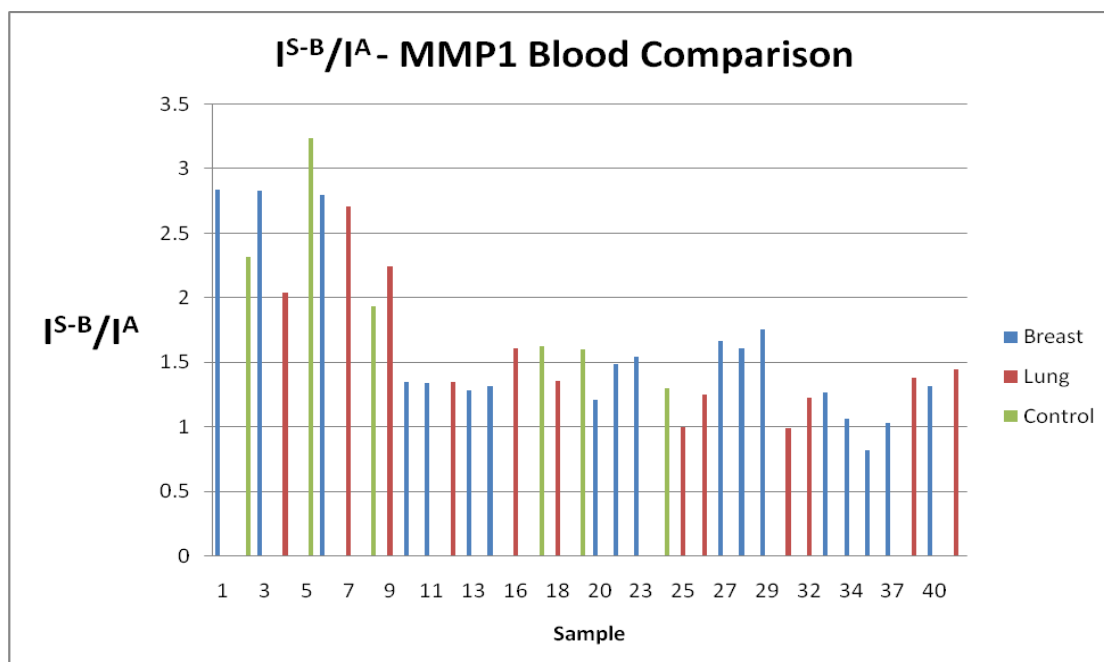
Figure 4.6: Comparison of Blood Samples for MMP 1

4.3.3 Study of MMP 2 Protease Assay Data

MMP 2 is mostly involved in tumor invasion and metastasis processes. MMP 2 can be mainly found in fibroblasts, osteoblasts, endothelial cells and macrophages. MMP 2 secretion can be performed by the tumor cells. It can degrade the basement membrane. That means MMP 2 can degrade the key components of the basement membrane such as gelatin and type IV collagen. There is a link between the tumor spread and the degradation of the basement membrane.[9,10] The structure of the MMP 2 is shown in Figure 4.7 and the molecular weight of MMP 2 is 71000 Da.
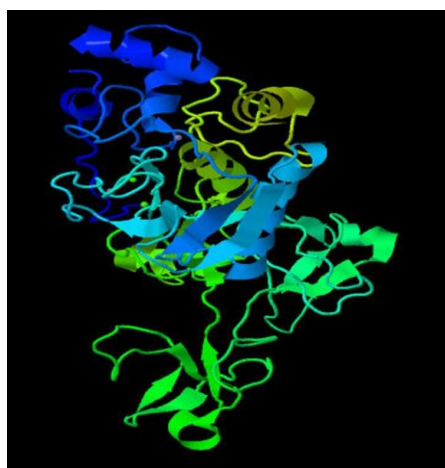
Figure 4.7: Structure of MMP 2[5]

Figure 4.8: Integrated Fluorescence of the Blood Samples for MMP 2 Assay

In Figure 4.8 the integrated fluorescence data for all the blood serum samples and in Figure 4.9 the I^{S-B}/I^A values for all the blood serum samples are shown. The majority of the breast and lung cancer blood serum samples shows I^{S-B}/I^A values above 1.0. Based on the validation shown in Chapter 3, MMP 2 is a moderately reactive protease.
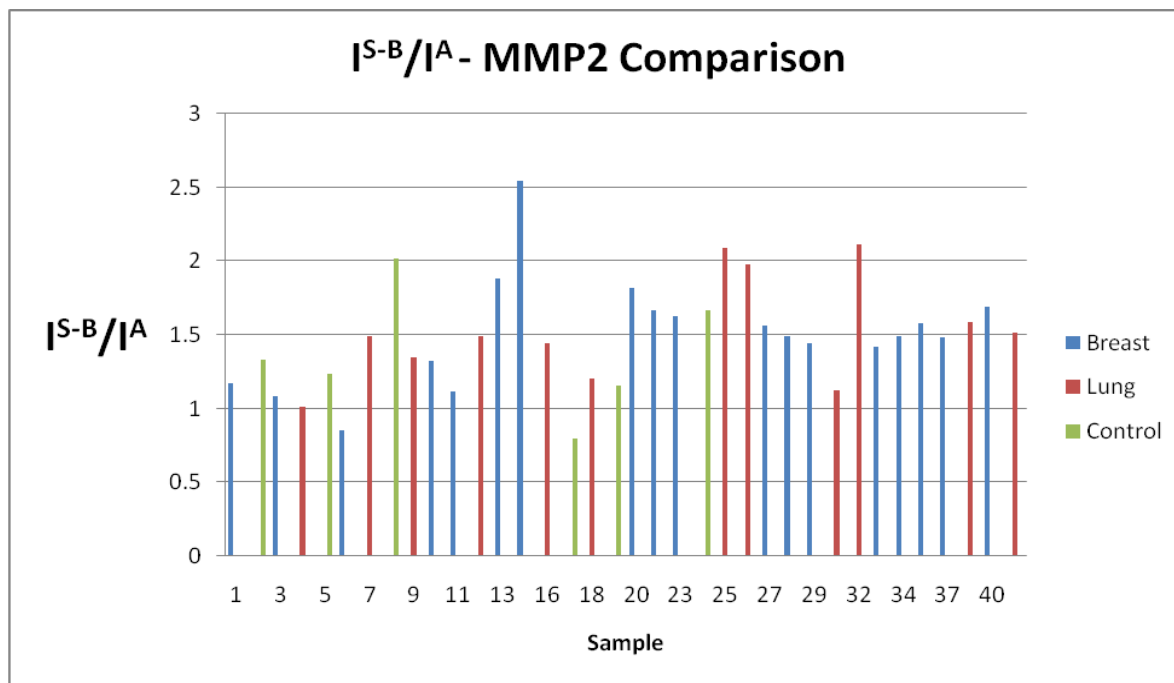
Figure 4.9: Comparison of Blood Samples for MMP 2

4.3.4 Study of MMP 7 Protease Assay Data
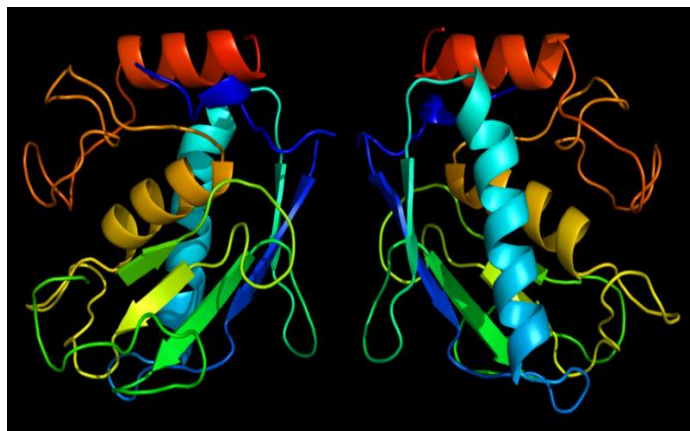
Figure 4.10: Structure of MMP 7[5]

MMP 7 is the smallest member of the MMP family. The structure of MMP 7 is shown in Figure 4.10 and the molecular weight of MMP 7 is 28000 Da. MMP 7 is also involved in tumor invasion and metastasis. MMP 7 has a wide substrate range against ECM and non ECM

components. Cellular transformation, cell survival, tumor growth, angiogenesis, and evasion of immune surveillance are some of the processes that MMP 7 is involved in. [11,12]

Figure 4.11: Integrated Fluorescence of the Blood Samples for MMP 7 Assay

In Figure 4.11 the integrated fluorescence data for all the blood samples and in Figure 4.12 the I^{S-B}/I^A values for all the blood serum samples are shown. The majority of the breast and lung cancer blood serum samples show I^{S-B}/I^A values above 1.5. Based on the validation shown in Chapter 3, MMP 7 is a highly reactive protease.
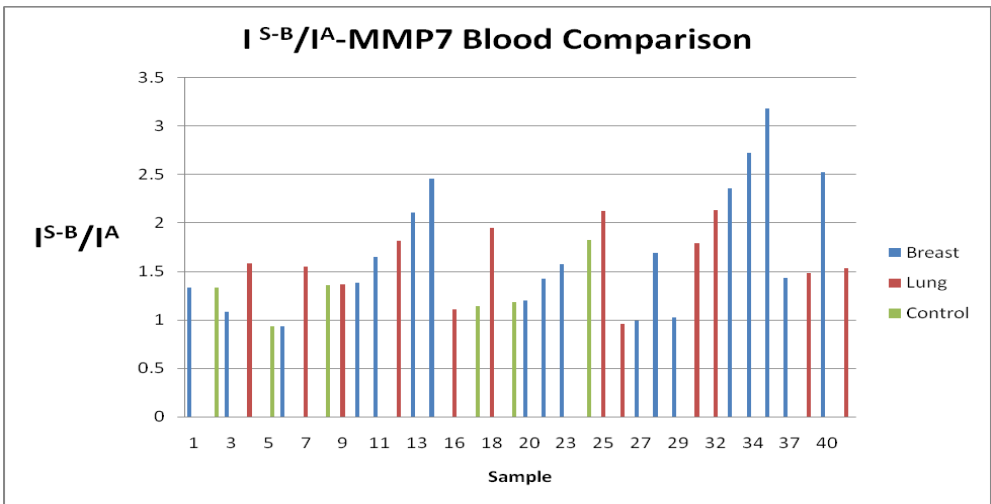
Figure 4.12: Comparison of Blood Samples for MMP 7

84

4.3.5 Study of MMP 9 Protease Assay Data
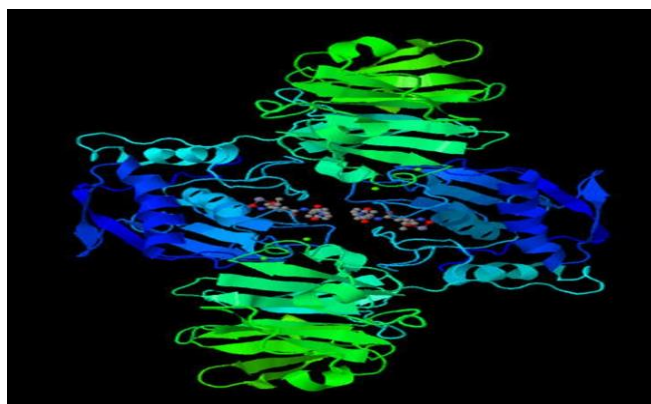
Figure 4.13: Structure of MMP 9[5]

In Figure 4.13 the structure of MMP 9 is shown. The molecular weight of MMP 9 is 92000 Da. Digestion of the subendothelial basement membrane, which is catalyzed by MMP 9, is regarded to be the first step in the intravasation and extravasation of cancer cells. Degradation of the main component of the basement membrane, which is the type IV collagen, is performed by the two structural proteins, MMP 2 and MMP 9. MMP 9 is a type IV collagenase (gelatinase B). It is produced mainly in neutrophils and macrophages. Previous studies show that with breast cancer, MMP 9 is expressed in macrophages, located adjacent to the invading tumor front.[13] MMP 9 is also expressed in NSCLC tumor cells and the surrounding stromal cells. But MMP 9 has feeble expression in tumor cells compared to MMP 2.[13,14]
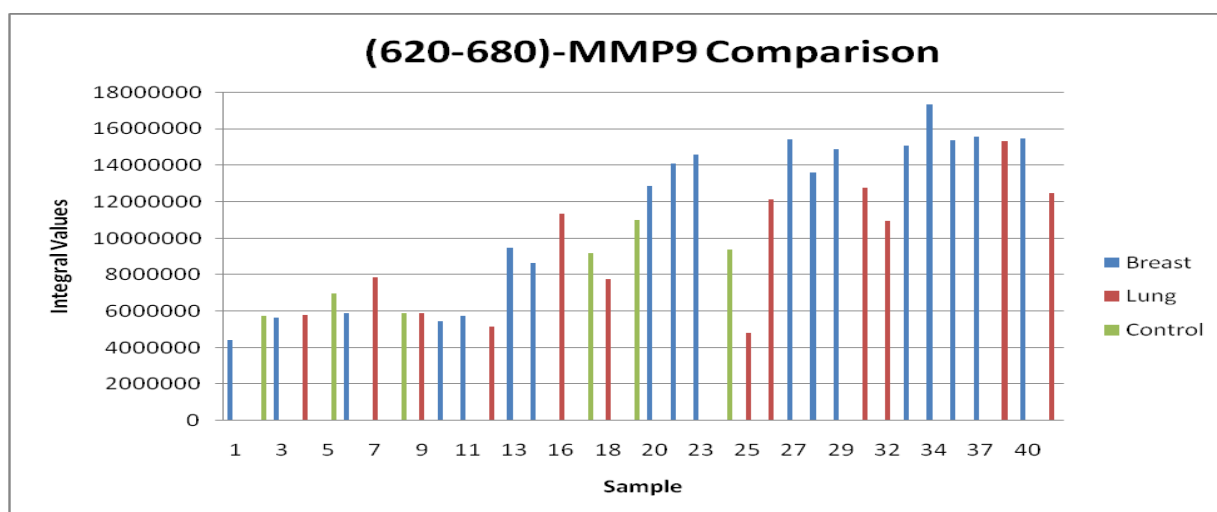
Figure 4.14: Integrated Fluorescence of the Blood Samples for MMP 9 Assay

In Figure 4.14 the integrated fluorescence data for all the blood serum samples and in Figure 4.15 the I^{S-B}/I^A values for all the blood serum samples are shown. Almost all of the blood serum samples show I^{S-B}/I^A values above 1.0. Based on the validation shown in Chapter 3, MMP 9 is a protease, which has defied the light switch paradigm. However, in blood serum, there are thousands of proteins present, which complicate the picture, because they are capable of adsorbing either at the nanoplatform or capable of adsorbing TCPP after it has been cleaved off by its respective protease. Light scattering studies of the nanoplatforms in PBS, in the presence of model proteases and blood serum, which will be presented in chapter 8, clearly indicate that the size of the formed assemblies depends on the proteins (proteases and/or proteins in blood serum) added to the mixture. Furthermore, all of these measurements are concentration dependent. Therefore, the calibration data obtained with commercially available enzymes in PBS cannot simply be applied when the protease contents of biospecimens is determined. This observation is especially important when measuring MMP 9 and urokinase plasminogen activator (uPA), which both have defied the light switch paradigm, meaning that their (TCPP) fluorescence decreased with increased protease activity.[15]
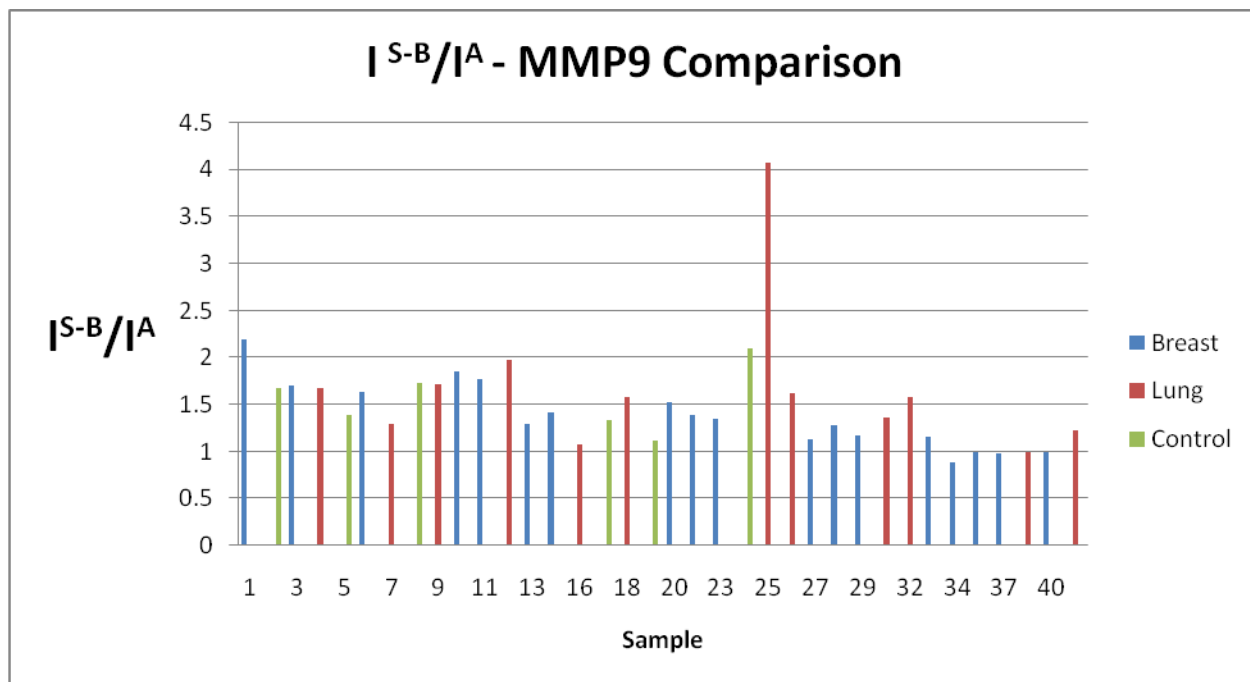
Figure 4.15: Comparison of Blood Samples for MMP 9

4.3.6 Study of MMP 13 Protease Assay Data
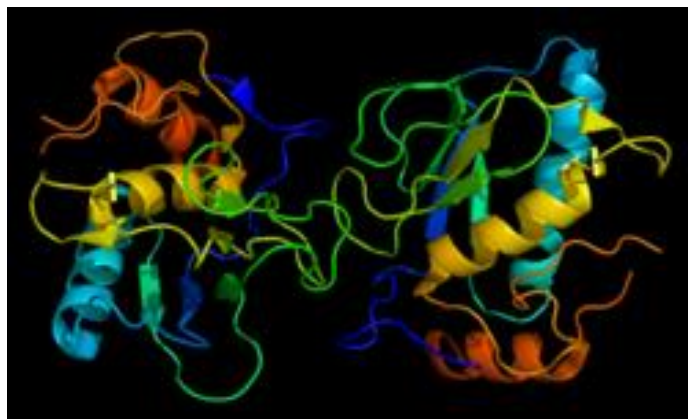
Figure 4.16: Structure of MMP 13[5]

In Figure 4.16 the structure of MMP 13 is shown. It's molecular weight is 52000 Da. MMP 13 is the main collagenase and it is known as collagenase 3. The main role of MMP 13 is the degradation of the ECM as most of the MMPs do. It is overexpressed in several types of malignant tissues. Depending on the type of the tumor, the expression distribution of MMP 13 by tumor cells and stromal cells are different. MMP 13 is actively involved in the activation of other MMPs. According to the literature the production of MMP 13 is performed either by tumor stromal fibroblast-like cells or tumor cells. [16,17]
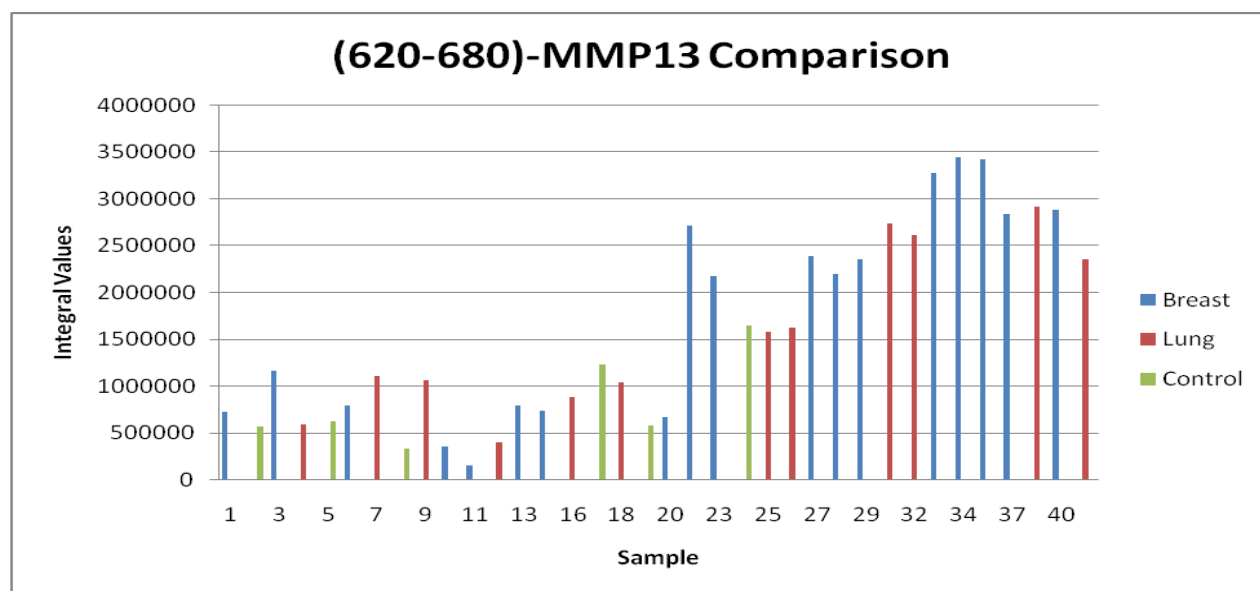
Figure 4.17: Integrated Fluorescence of the Blood Samples for MMP 13 Assay

In Figure 4.17 the integrated fluorescence data for all of the blood serum samples and in Figure 4.18 the I^{S-B}/I^A values for all the blood serum samples are shown. No significant differences between the blood samples from healthy humans and blood samples from cancer patients are discernible. Based on the validation shown in Chapter 3 MMP 13 is a highly reactive protease.
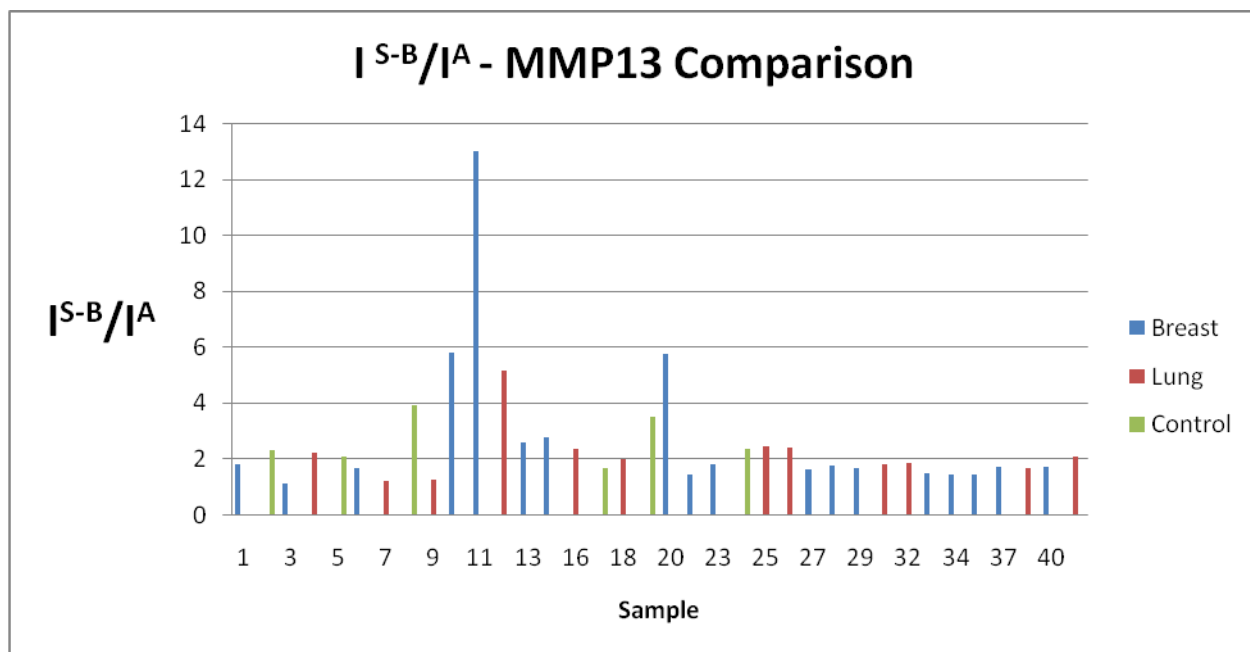
Figure 4.18: Comparison of Blood Samples for MMP 13

4.3.7 Study of uPA Protease Assay Data
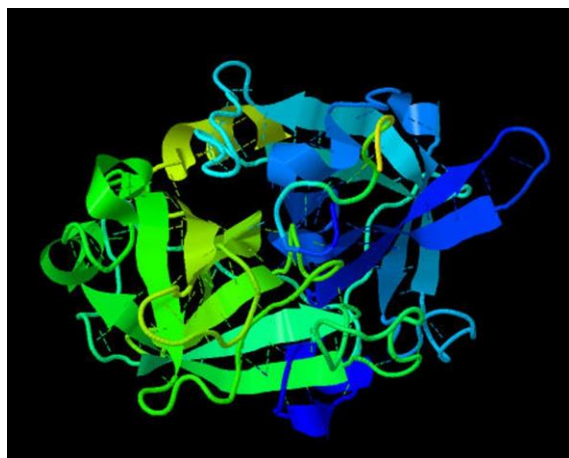
Figure 4.19: Structure of Urokinase[5]

The Urokinase plasminogen activator (uPA) structure is shown in Figure 4.19. The molecular weight of it is 58000 Da. uPA is a serine protease and it has numerous functions. Urokinase mainly involved with degradation of extracellular matrix and stimulation of cellular migration processes related to cancer progression. The receptor uPAR is a glycosylphosphatidylinositol anchor protein. This receptor can cooperate with integrins, which are membrane partners to control tumor cell adhesion, migration, invasion, protease secretion and proliferation. According to the literature uPA helps the spread of the cancer. Cell migration and signaling occurs as a result of the binding of uPA to uPAR receptor.[18,19]
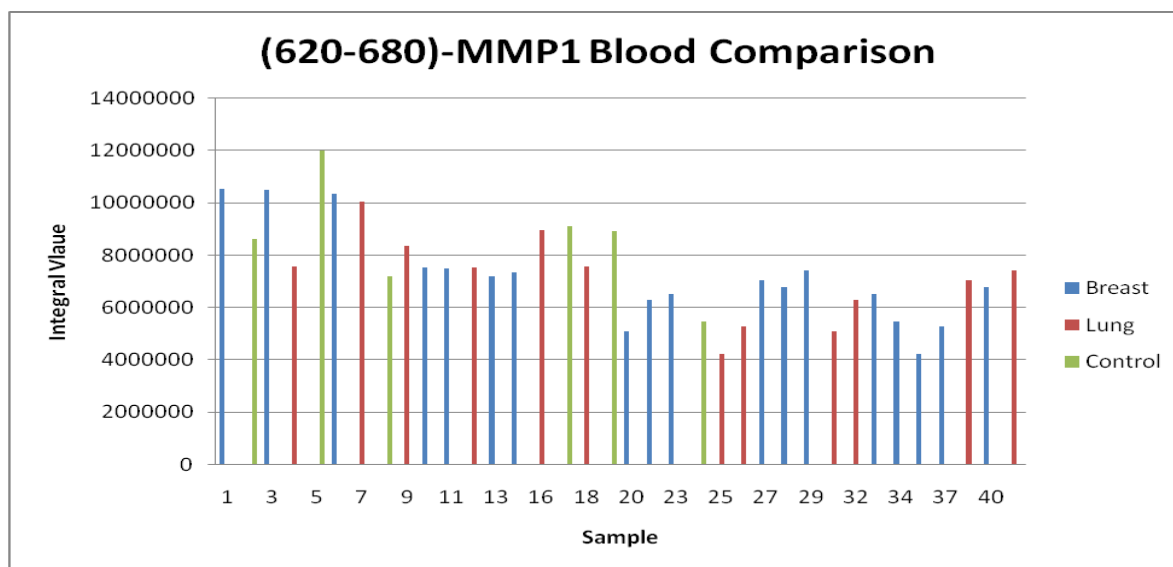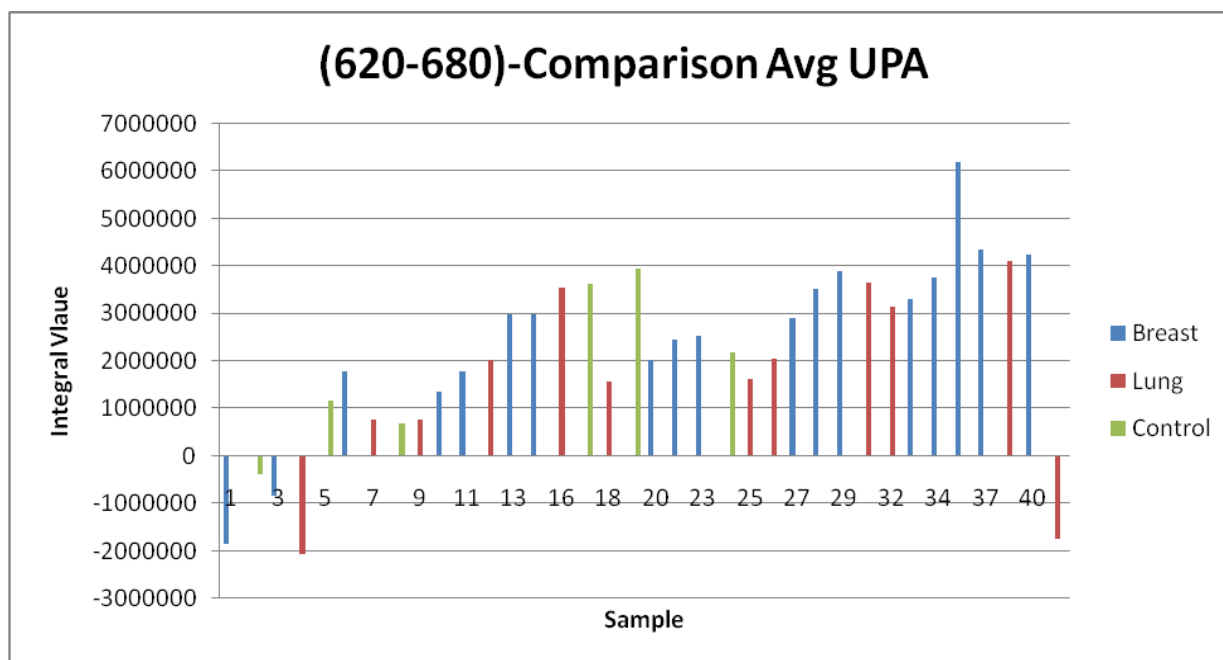

Figure 4.20: Integrated Fluorescence of the Blood Samples for Urokinase Assay

In Figure 4.20 the integrated fluorescence data for all the blood serum samples and in Figure 4.21 the I^{S-B}/I^A values for all the blood serum samples are shown. uPA shows a strange pattern of I^{S-B}/I^A values for the blood samples. Based on the validation shown in Chapter 3 urokinase is a protease, which defied the light switch paradigm. However, the presence of thousands of proteins in blood serum may complicate the situation (see chapter 8).
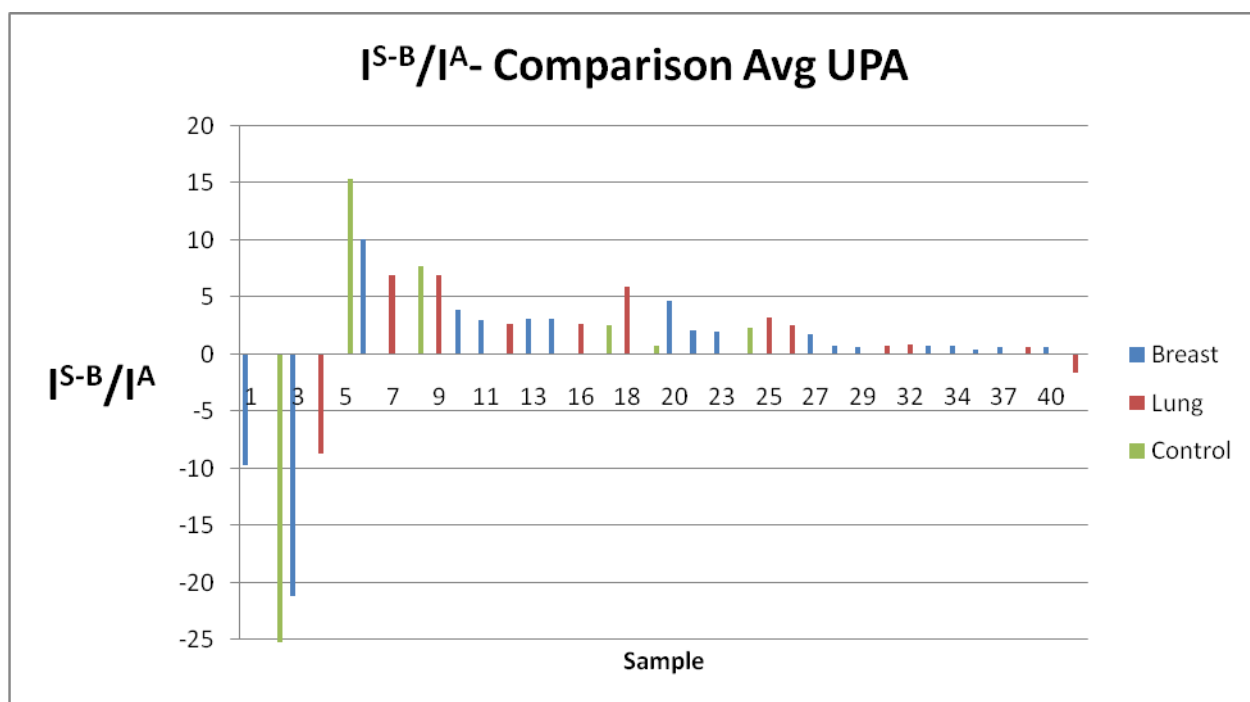
Figure 4.21: Comparison of Blood Samples for uPA

4.3.8 Study of Cathepsin B Protease Assay Data
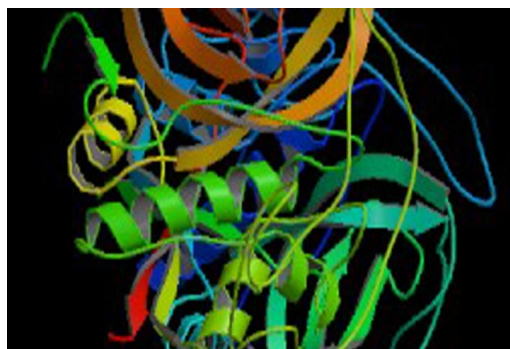
Figure 4.22: Structure of Cathepsin B[5]

The structure of Cathepsin B (CTSB) can be seen in Figure 4.22. It is a lysosomal cysteine protease, which is synthesized in the rough endoplasmic reticulum and delivered to the lysosomal compartment. The molecular weight of Cathepsin B is 37000 Da. It is mainly involved in degradation of the extracellular matrix and basement membrane, directly and indirectly. As a result, cathepsin B is playing an important role in cancer progression and invasion.[20,21]
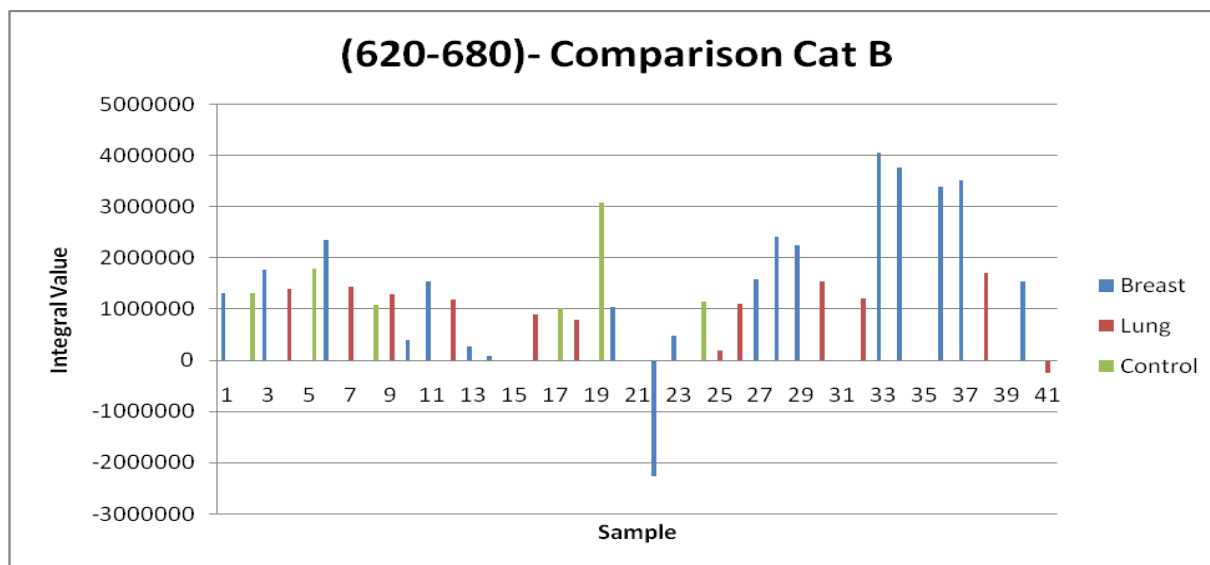
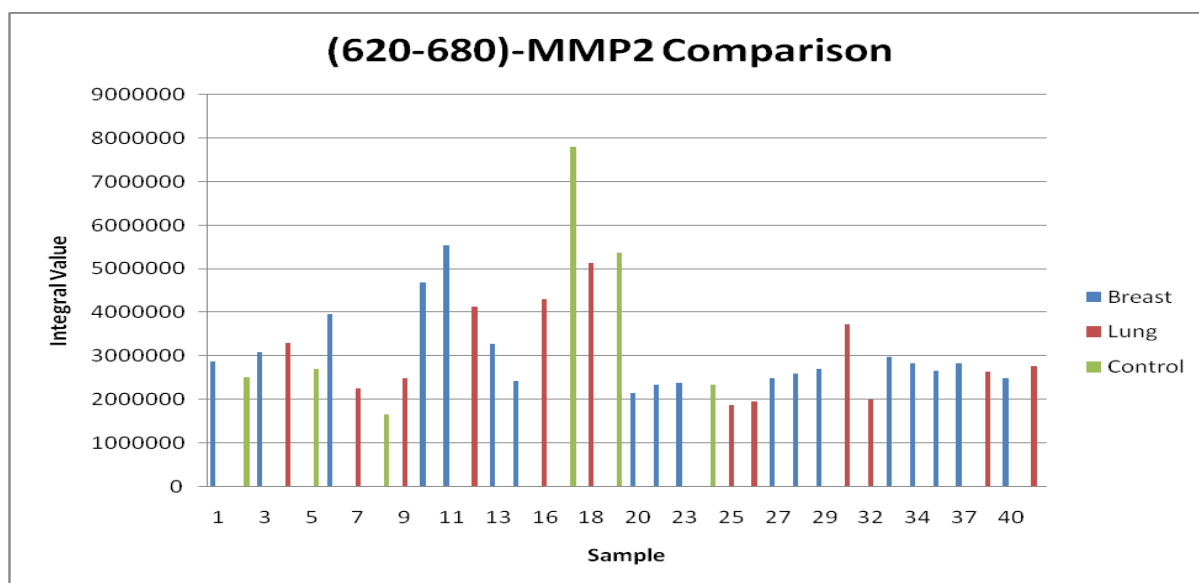**Figure 4.23: Integrated Fluorescence of the Blood Samples for Cathepsin B Assay**

In figure 4.23 the integrated fluorescence data for all the blood serum samples and in Figure 4.24 the I^{S-B}/I^A values for all the blood serum samples are shown. The I^{S-B}/I^A values for the blood samples of the cancer patients are similar with a few exceptions. Based on the validation shown in chapter 3, cathepsin B is a moderately reactive protease.
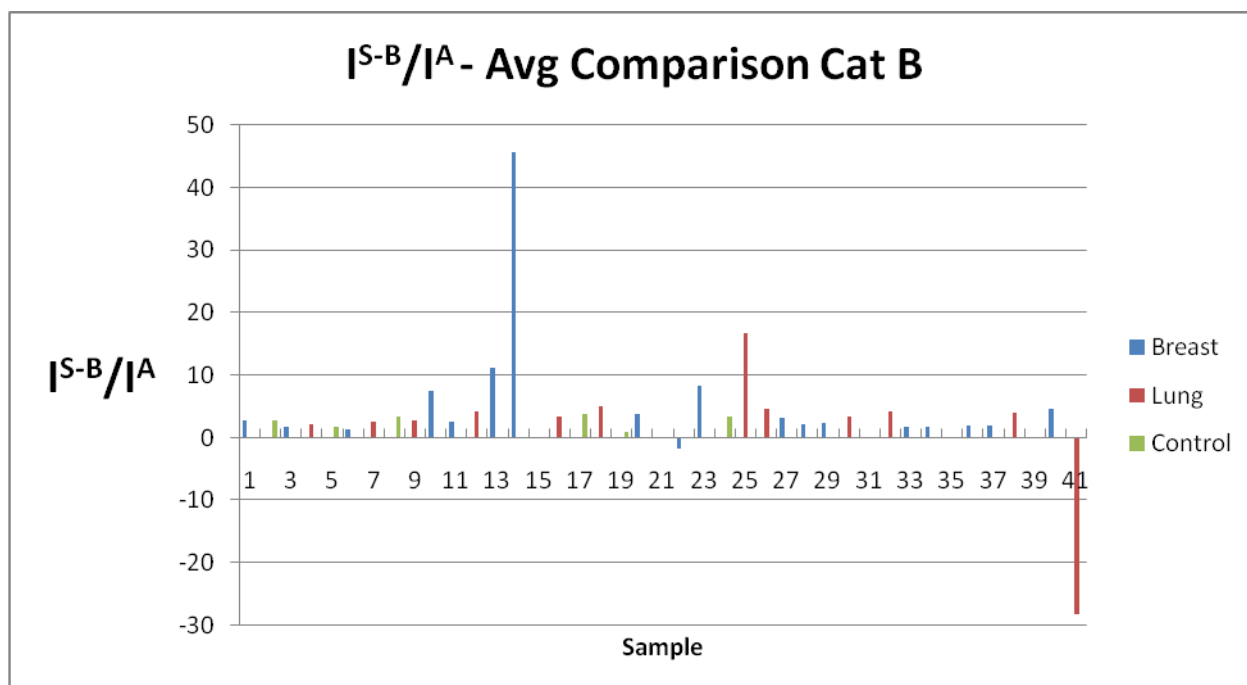
Figure 4.24: Comparison of Blood Samples for Cathepsin B

4.3.9 Study of Cathepsin L Protease Assay Data
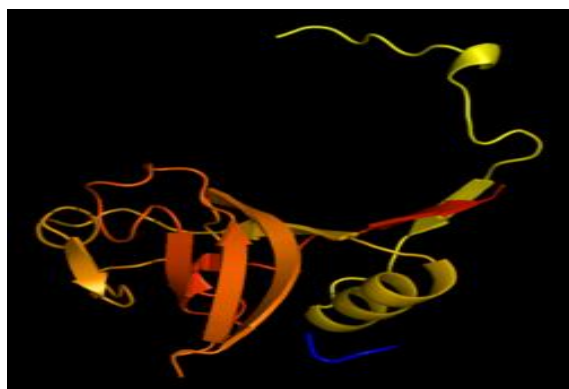
Figure 4.25: Structure of Cathepsin L[5]

Cathepsin L, a papain-like lysosomal cysteine proteinase and its structure is shown in Figure 4.25. It is synthesized as a preproenzyme. The lysosome is the location to store the mature type of the cathepsin L. There, cathepsin L functions as an endopeptidase. The molecular weight of cathepsin L is 26000 Da. It plays a key role in degradation of intracellular and extracellular proteins. At acidic pH, cathepsin L has the ability to degrade collagen, elastin, laminin and other components of the basement membrane. Therefore cathepsin L is considered as a contributor in cancer development and progression.[22,23]
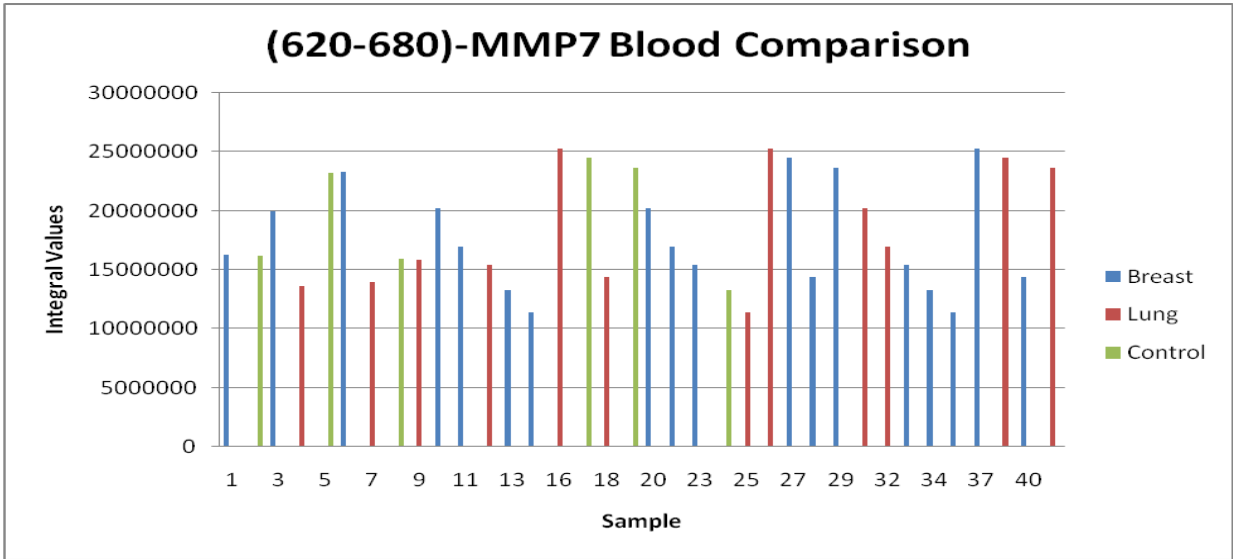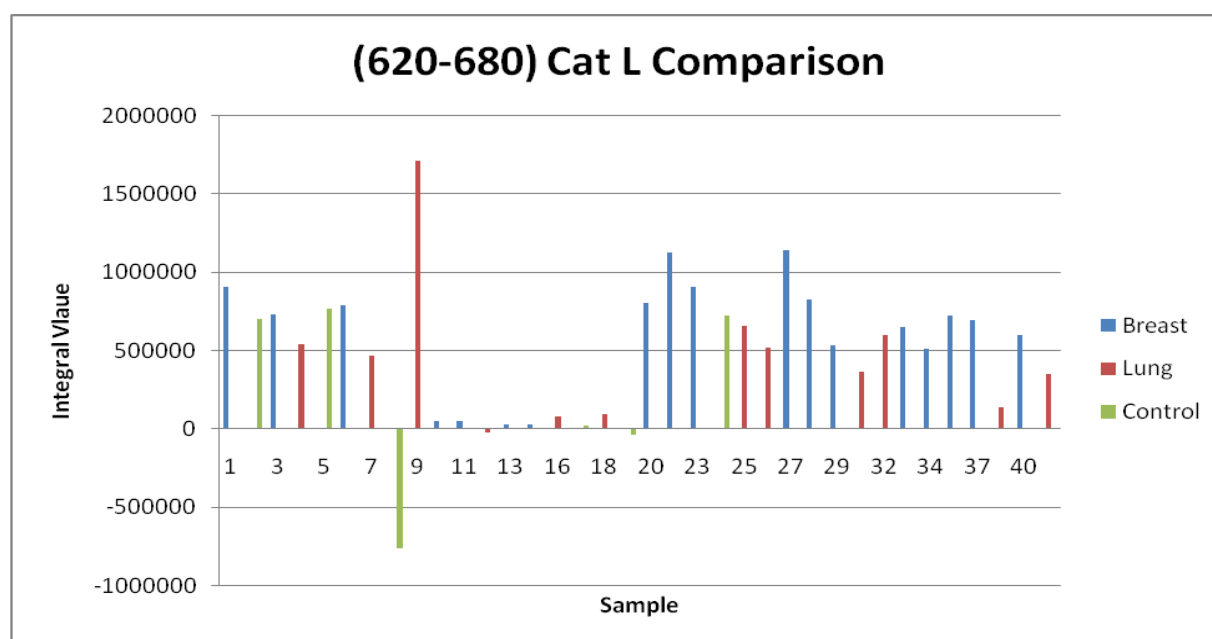

Figure 4.26: Integrated Fluorescence of the Blood Samples for Cathepsin L Assay

In Figure the 4.26 integrated fluorescence data for all blood serum samples and in Figure 4.27 the I^{S-B}/I^A values for all the blood serum samples are shown. The I^{S-B}/I^A values for the blood samples of the cancer patients are very similar, again with a few exceptions. Based on the validation shown in chapter 3, Cathepsin L is a highly reactive protease.
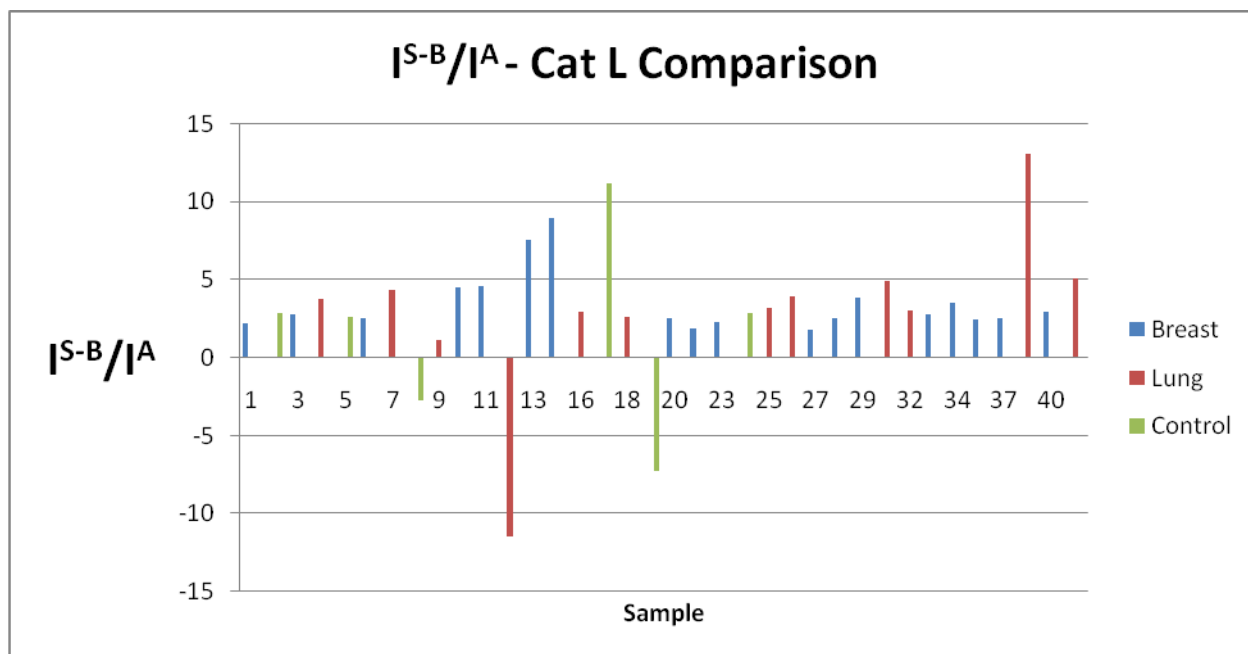
Figure 4.27: Comparison of Blood Samples for Cathepsin L

Acknowledgement

I would like to acknowledge all the collaborators, who contributed their knowledge and expertise towards the success of the projects on protease assays.

Prof. Dr. Gary Gadbury, Department Head of the Department of Statistics, Kansas State University and M. Sc. Xin Sun.

The analysis described in the section 4.4 has been performed by Dr. Gary Gadbury of the Department of Statistics, Kansas State University. The whole Analysis report will be reported in Appendix A.

4.4 Statistical Analysis

We did the statistical analysis of all the data collected for the lung and breast cancer blood samples. Statistical analyis for separate assays can be found in Appendix A. The summary of the statistical data analysis is shown here in Tables 4.2 and 4.3.

Table 4.2: Summary of Results Comparing Stage of Disease in Breast Cancer Patients with the Control Condition

Outcome	Stage 0	Stage I	Stage II	Stage III	Stage IV
Cath B	N	N	N	H	H
Cath L	N	N	N	N	H
MMP1	N	N	N	H	H
MMP2	N	N	N	N	N
MMP3	N	N	N	N	N
MMP7	N	N	H	N	N
MMP9	N	N	N	H	H
MMP13	N	N	N	N	N
uPA	N	N	L	L	L

In tables 4.2 and 4.3 "N" indicates no statistical difference, "H" indicates that the outcome was estimated to be higher in the disease stage versus control, and "L" indicates that the outcome was estimated to be lower in the disease stage versus control. There were five stages present in breast cancer patients and three stages present in lung cancer patients. Statistical differences have been determined using 95% confidence intervals with a Bonferroni adjustment within each separate analysis.

Table 4.3: Summary of Results Comparing Stage of Disease in Lung Cancer Patients with the Control Condition

Outcome	Stage I	Stage II	Stage III
Cath B	N	H	H
Cath L	N	H	H
MMP1	H	H	H
MMP2	N	N	N
MMP3	N	N	N
MMP7	H	N	H
MMP9	L	L	L
MMP13	N	N	N
uPA	N	N	N

4.5 Discussion

We carried out all the calibrations of the protease assays using commercially available enzymes in 1X PBS buffer. But when we were working with the real protease assays using blood serum samples, the behavior of the proteases in the blood samples were somewhat different compared to how they behaved in PBS buffer. For an example, as described in chapter 3, we have identified urokinase and MMP 9 as proteases which defying the light switch paradigm. But with all these blood analysis work, we achieved increasements in fluorescence of TCPP with both of these proteases. This observation led us into looking at the surface properties of the commercially available enzymes and the biospecimens.

4.6 References

[1] http://www.metromedlab.com/

[2] http://www.hematology.org/patients/blood-basics/5222.aspx

[3] http://amrita.vlab.co.in/?sub=3&brch=69&sim=196&cnt=1

[4] http://precedings.nature.com/documents/6595/version/1/files/npre20116595-1.pdf

[5] http://www.rcsb.org/pdb/

[6] Liu, H.; Kato, Y.; Erzinger, S. A.; Kiriakova, G. M.; Qian, Y.; Palmieri, D.; Steeg, P. S.; Price, J. E. The role of MMP-1 in breast cancer growth and metastasis to the brain in a xenograft model. *BMC Cancer,* **2012***, 12*, 1-11.

[7] Sauter, W.; Rosenberger, A.; Beckmann, L.; Kropp, S.; Mittelstrass, K.; Timofeeva, M.; Wölke, G.; Steinwachs, A.; Scheiner, D.; Meese, E.; Sybrecht, G.; Kronenberg, F.; Dienemann, H.; Chang-Claude, J.; Illig, T.; Wichmann, H. -E.; Bickeböller, H.; Risch, A. Matrix Metalloproteinase 1 (MMP1) Is Associated with Early-Onset Lung Cancer. *Cancer Epidemiol. Biomarkers Prev.* **2008***, 17*, 1127-1135.

[8] Poola, I.; DeWitty, R. L.; Marshalleck, J. J.; Bhatnagar, R.; Abraham, J.; Leffall, L. D. Identification of MMP-1 as a putative breast cancer predictive marker by global gene expression analysis. *Nat. Med.* **2005***, 11*, 481-483.

[9] Somiari, S. B.; Somiari, R. I.; Heckman, C. M.; Olsen, C. H.; Jordan, R. M.; Russell, S. J.; Shriver, C. D. Circulating MMP2 and MMP9 in breast cancer - Potential role in classification of patients into low risk, high risk, benign disease and breast cancer categories. *Int. J. Cancer,* **2006***, 119*, 1403-1411.

[10] Mendes, O.; Kim. H. -T.; Lungu, G.; Stoica, G. MMP2 role in breast cancer brain metastasis development and its regulation by TIMP2 and ERK1/2. *Clin. exp.metastasis,* **2007***, 24*, 341-351.

[11] Beeghly-Fadiel, A.; Long, J. -R.; Gao, Y. -T.; Li, C.; Qu, S.; Cai, Q.; Zheng, Y.; Ruan, Z. -X.; Levy, S. E.; Deming, S. L.; Snoddy, J. R.; Shu, X. -O.; Lu, W.; Zheng, W. Common MMP-7 Polymorphisms and Breast Cancer Susceptibility: A Multistage Study of Association and Functionality. *Cancer Res.* **2008***, 68*, 6453-6459.

[12] Liu, H. F.; Zhang, T.; Li, X.; Huang, J.; Wu, B.; Huang, X.; Zhou, Y.; Zhu, J.; Hou, J. Predictive value of MMP-7 expression for response to chemotherapy and survival in patients with non-small cell lung cancer. *Cancer sci.* **2008***, 99*, 2185-2192.

[13] Scorilas, A.; Karameris, A.; Arnogiannaki, N.; Ardavanis, A.; Bassilopoulos, P.; Trangas, T.; Talieri, M. Overexpression of matrix-metalloproteinase-9 in human breast cancer: a potential favourable indicator in node-negative patients, *British journal of cancer,* **2001***, 84,* 1488-1496.

[14] Iizasa, T.; Fujisawa, T.; Suzuki, M.; Motohashi, S. -I.; Yasufuku, K.; Yasukawa, T.; Baba, M.; Shiba, M. Elevated Levels of Circulating Plasma Matrix Metalloproteinase 9 in Non-Small Cell Lung Cancer Patients. *Clin. Cancer Res.* **1999***, 5*, 149-153.

[15] Wang, H.; Udukala, D. N.; Samarakoon, T. N.; Basel, M. T.; Kalita, M.; Abayaweera, G.; Manawadu, H.; Malalasekera, A.; Robinson, C.; Villanueva, D.; Maynez, P.; Bossmann, L.; Riedy, E.; Barriga, J.; Wang, N.; Li, P.; Higgins, D. A.; Zhu, G.; Troyer, D. L.; Bossmann, S. H. Nanoplatforms for highly sensitive fluorescence detection of cancer-related proteases. *Photochem. Photobiol. Sci.,* **2014***,13*, 231-240.

[16] Fukuda, H.; Mochizuki, S.; Abe, H.; Okano,,H.; Hara-Miyauchi, C.; Okano, H.; Yamaguchi, N.; Nakayama, M.; D'Armiento, J.; Okada, Y. Host-derived MMP-13 exhibits a protective role in lung metastasis of melanoma cells by local endostatin production. *British journal of cancer,* **2011**, *105*, 1415-1424.

[17] Zhang, B.; Cao, X.; Liu, Y.; Cao, W.; Zhang, F.; Zhang, S.; Li, H.; Ning, L.; Fu, L.; Niu, Y.; Niu, R.; Sun, B.; Hao, X. Tumor-derived matrix metalloproteinase-13 (MMP-13) correlates with poor prognosis of invasive breast cancer, *BMC Cancer*, **2008***, 8*, 1-10.

[18] Duffy, M. J.; Duggan, C.; Mulcahy, H. E.; McDermott, E. W.; O'Higgins, N. J. Urokinase plasminogen activator: a prognostic marker in breast cancer including patients with axillary node-negative disease. *Clinical Chemistry*, **1998***, 44*, 1177-1183.

[19] Tang, C. -H.; Hill, M. L.; Brumwell, A. N.; Chapman, H. A.; Wei, Y. Signaling through urokinase and urokinase receptor in lung cancer cells requires interactions with beta1 integrins. *Journal of cell science*, **2008**, *121*, 3747-3756.

[20] Nouh, M.; Mohamed, M. M.; El-Shinawi, M.; Shaalan, M. A.; Cavallo-Medved, D.; Khaled, H . M.; Sloane, B. F. Cathepsin B: a potential prognostic marker for inflammatory breast cancer, *Journal of Translational Medicine*, **2011***, 9*, 1-8.

[21]Erdel, M.; Trefz, G.; Spiess, E.; Habermaas, S.; Spring, H.; Lah, T.; Ebert, W. Localization of cathepsin B in two human lung cancer cell lines, *J. Histochem. Cytochem.* **1990***, 38*, 1313-1321.

[22] Abboud-Jarrous, G.; Atzmon, R.; Peretz, T.; Palermo, C.; Gadea, B. B.; Joyce, J. A.; Vlodavsky, I. Cathepsin L Is Responsible for Processing and Activation of Proheparanase through Multiple Cleavages of a Linker Segment. *J. Biol. Chem.* **2008***, 283*, 18167-18176.

[23] Hashimoto, Y.; Kondo, C.; Kojima, T.; Nagata, H.; Moriyama, A.; Hayakawa, T.; Katunuma, N. Significance of 32-kDa cathepsin L secreted from cancer cells. *Cancer biotherapy & radiopharmaceuticals*, **2006**, *21*, 217-224.

Chapter 5 - Detection of Triple Negative Breast Cancer Using Protease Assays

5.1 Triple Negative Breast Cancer

Triple Negative Breast Cancer (TNBC) is a subtype of breast cancer. As the name implies, triple negative means testing is negative for estrogen receptors (ER), progesterone receptors (PR) and HER2. Which means triple negative breast cancers do not have those biomarkers. 15-20 percent of all the breast cancer types in USA are Triple Negative. This cancer type can be mostly seen with younger women, African American women, Hispanic/Latina women, and women who have BRCA1 mutations.[1]

Triple Negative breast cancer is very aggressive, and usually hormonal therapy is not working in treating TNBC. The reason behind that is the growth of this tumor is not accelerated by hormones. Triple Negative breast cancer grows faster and it is difficult to identify it from an annual mammogram.[2]

5.2 Results of Protease Assays

We received 10 Triple Negative breast cancer blood serum samples from The University of Kansas Hospital (Prof. Dr. Priyanka Sharma, MD). The protease assay analysis was done for all 10 blood serum samples. Results were obtained for 12 types of proteases. Seven of them are from the MMP family: MMP 1, MMP 2, MMP 3, MMP 7, MMP 9, MMP 11 and MMP 13. Four of them are from the cathepsin family: Cathepsin B, cathepsin D, cathepsin K and cathepsin L. Also the analysis was performed using the urokinase assay.

The assay procedure is the same as described in section 4.1.1.

5.2.1 Study of MMPs
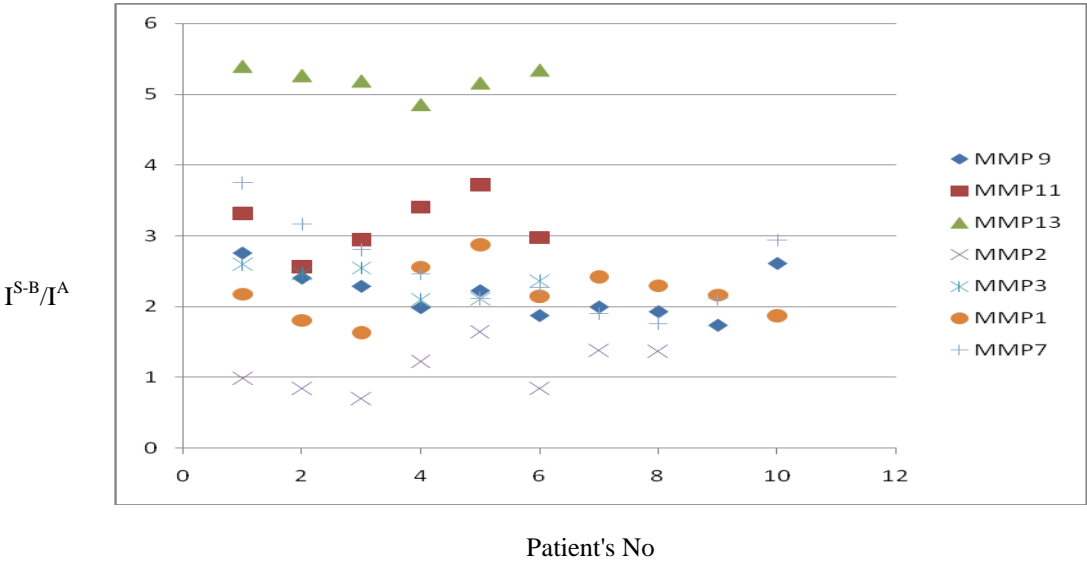
Figure 5.1: Matrix Metalloproteinases in Blood Serum of Triple-Negative Breast Cancer Patients

5.2.2 Study of Cathepsins and Urokinase
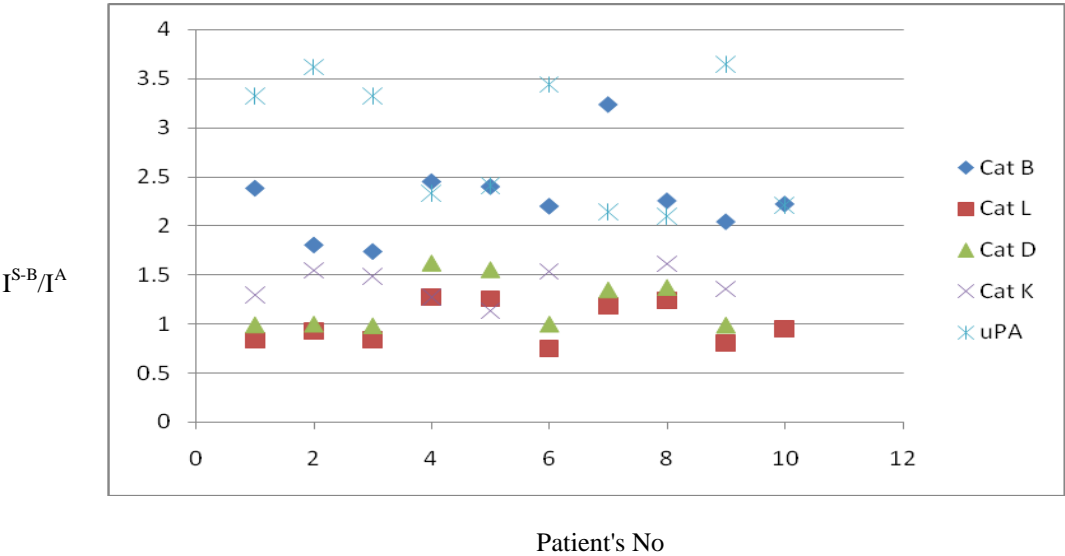
Figure 5.2: Cathepsins and Urokinase Plasminogen Activator in Blood Serum of Triple-Negative Breast Cancer Patients

5.3 Discussion

Whereas the blood samples that were obtained from the South Eastern Nebraska Cancer Center (SENCC) were comprised of all breast cancer types, the blood samples from the University of Kansas were exclusively Triple Negative Breast Cancers (TNBC). As anticipated, I found distinct differences in the expression pattern of proteases in both groups of cancer samples. It must be noted that the blood serum samples from TNBC patients did not have a control group. This limits the ability to compare protease expression patterns to a certain extent. It is of interest that these samples have originated in the year 2008. I did not have any problems to obtain meaningful results utilizing the protease assays that were developed in this thesis. Therefore, it is safe to assume that blood serum samples can be stored either at -80°C or in liquid nitrogen for years prior to measuring protease signatures. Considering the infrastructure requirements necessary for early blood tests for cancer in millions of patients, this finding must be regarded as very good news, because it permits the design of central testing facilities with very high throughput.

MMP 11 was not analyzed in the samples obtained from SENCC. However, MMP 11 is potentially of high diagnostic value for detecting triple negative breast cancers. Gli1 is an established oncogene that is expressed in TNBC. It enhances migration and invasion via upregulation of MMP 11.[3] It is noteworthy that we did not discern a significant overexpression of MMP 13 in the blood serum samples obtained from SENCC, but in the group of TNBC patients from KUMED. There is an emerging paradigm in the recent literature that some of the same factors that drive epithelial–mesenchymal transition (EMT) upregulate MMP13 expression (e.g., TGFβ, IL1b, TNFα), indicating an association of MMP13 with invasion and metastasis.[4]

It was our original strategy to compare the MMP-activities with the complete histology of the TNBCs that will be performed by Dr. Sharma. Unfortunately, these studies have been delayed due to legal complications, which have arisen from the bankruptcy of NanoScale Corporation (a spin-off of Kansas State University). NanoScale Corporation was involved in the cancer endeavors of the Bossmann group from 2008 to 2012. The goal of this study is to verify/falsify these two pathways in patient-specific TNBC pathology, with the goal of developing better predictors for cancer treatment and survival. This analysis will be continued, but the work will have to be performed in continuation of my thesis research.

MMP 9, which is a typical inflammation marker, was overexpressed in the blood serum of late stage breast cancer patients (states 3 and 4) from SENCC. It is of interest that MMP 9 overexpression is apparently a hallmark of all breast cancers. Urokinase plasminogen activator (uPA) is mainly involved in the degradation of extracellular matrix and stimulation of cellular migration processes related to cancer progression. uPA is apparently involved in the progression of all breast cancers, disregarding of the cancer type. That also means that MMP 9 and uPA are suitable proteases to detect all types of breast cancers in a simple blood serum test. However, both proteases are highly overexpressed only in late stage breast cancers, which limits their usefulness.

The expression of MMP 1, MMP 3, and MMP 7 varies from sample to sample. In the samples obtained from SENCC, MMP 7 activity was significantly elevated in stage 2 breast cancers, whereas MMP 1 was significantly elevated in later stages (3 and 4). It is of importance that triple negative breast cancers are not a homogeneous group, as discussed in the introduction. Therefore, it is possible that several sub-groups of TNBC's feature different protease signatures. My findings with MMP 1, MMP 3, and MMP 7 may be a first indication for this behavior. However, larger sample numbers are required to verify this assumption. These studies will be continued in collaboration with Prof. Dr. Sharma.

It should also be noted that MMP 2 expression was insignificant for all blood samples investigated.

Among the group of the cathepsins, cathepsin B was elevated in all blood serum samples from TNBC patients, whereas cathepsins D, L, and K were not significant. In the group of samples obtained from SENCC, cathepsin B was a significant late stage breast cancer marker (stages 3 and 4). We will require a higher number of blood serum samples from TNBC patients to arrive at a statistically significant conclusion, whether cathepsin B is also elevated in some breast cancers types in early stages. To date, we have established that cathepsin B, together with MMP1 and MMP9 is a reliable late-stage marker for breast cancer.

5.4 References

[1] http://ww5.komen.org/uploadedFiles/Content_Binaries/KOMEED079100.pdf

[2] http://www.breastcancer.org/symptoms/diagnosis/trip_neg

[3] Kwon, Y.-J.; Hurst, D. R.; Steg, A. D.; Yuan, K.; Vaidya, K. S.; Welch, D. R.; Frost, A. R. Gli1 enhances migration and invasion via up-regulation of MMP-11 and promotes metastasis in ERα negative breast cancer cell lines. *Clin. Exp. Metastasis*, **2011**, *28*, 437-449.

[4] Asiedu, M. K.; Ingle, J. N.; Behrens, M. D.; Radisky, D. C.; Knutson, K. L. TGFβ/TNFα-Mediated Epithelial-Mesenchymal Transition Generates Breast Cancer Stem Cells with a Claudin-Low Phenotype, *Cancer Res.* **2011**, *71*, 4707-4719.

Chapter 6 - Detection of the Breast Cancer Boundary Using Magnetic-Nanoparticle (Fe/Fe₃O₄)-based Nanoplatforms for Highly Sensitive Fluorescence Detection of Cancer-Related Proteases

6.1 Introduction

On the path of the development of the protease assay, we wanted to look into the activity of proteases in tumor tissue. The underlying paradigm of this research is that protease activity in the tumor core, boundary region, and adjacent "healthy tissue" may be significantly different to permit an exact elucidation of the tumor boundary. In order to perform this research, we received tissue samples from 12 breast cancer patients from the University of Kansas Medical Center. This work is performed in collaboration with Dr. Fang Fan, MD, Director, Cytopathology Fellowship Program. From each patient three types of tissue samples were obtained. The samples are described in Tables 6.1 and 6.2.

Table 6.1: Tissue Samples

No	Code	Type
1	A	Inside the tumor core
2	B	Boundary of the tumor
3	C	Control healthy tissue next to the tumor

Table 6.2: Codes of the Tissue Samples

	Code	Tumor Type	Resection Margins	ER	PR	HER-2/neu	Histo Grade	Nuclear Grade	T	N	M
1	3267	Ductal	Negative	positive	positive	negative	I	2	1c	0	
2	3275	Ductal	Negative	positive	positive	negative	2	2	1c	0	
3	3315	Ductal	Negative	positive	positive	negative	1	2	1c	0	X
4	3662	Ductal	Negative	positive	positive	negative	II/III	3	2	2	

5	3681	Other	Negative	positive	positive	negative	1	2	2	0	
6	3768	Ductal	Negative	positive	positive	negative	1	1	2	1a	X
7	3773	Ductal	Negative	positive	positive	negative	2	2	2	2	
8	3780	Ductal	Negative	positive	positive	negative	II	3	1c	0	
9	3890	Ductal	Negative	positive	negative	negative	2	2	1c	1a	X
10	3922	Ductal	Negative	positive	negative	negative	2	2	2	0	X
11	3988	Ductal	Negative	positive	positive	negative	2	3	1c	1	
12	4533	Ductal	Positive	positive	negative	negative	II/III	3	1c	0	

In Table 6.2 the information about the tumors is summarized.

6.1.1 Preparation of the Samples

All the tissue samples were prepared in a manner that is compatible with using the protease assay. First the tissue was cut in to very small pieces (<1 mm^3). Then 1-5 mg of tissue was homogenized (mini homogenizer) for 5 min. in 600 µLof (PBS+dextran) solution (concentration: 10 mg of dextran in 1 mL of 1x PBS). At the end of the 5 min almost all of the solid was homogenized. After quick centrifugation, the homogenous supernatant was used in the assays.

6.1.2 Procedure for the Protease Assay

The protease assay procedure that was developed in chapter 4 was further modified for measuring the protease activity of biospecimens.

In a 15 mL centrifuge tube 75 µL of a dispersion of nanoplatform in 1X PBS (concentration: 1.0 mg/mL) was given. Then 30 µLof the homogenized tissue sample (see above) was added. Then the total volume was increased to 3.0 mL using 1X PBS/dextran. This solution is a dextran solution with the concentration of 10 mg/mL. Then sonicated the tube for 5 min. and incubated it for 1 h at 25 ^{o}C. At the end of the 1 h incubation period, fluorescence measurements were performed. Per each sample two scans were performed. Each sample was recorded in

triplicates. Furthermore, assay control and tissue control were performed. The assay control consisted of measuring the fluorescence of the nanoplatform only without having any biospecimen present after the incubation period. The tissue control consisted only of the tissue (after the one hour incubation period) without having any nanoplatform present. Photophysical parameters of the experiment are excitation wavelength (λ =421 nm) and the wavelength range of detection (λ = 590 nm to 760 nm).

Basically two peaks could be discerned in the fluorescence spectrum at 620 nm – 680 nm range and at 690 nm – 730 nm range. The intensity was highest at with the peak of 620 nm - 680 nm range. As a result, only the peak occurring at 620 nm - 680 nm was considered in the calculations reported in this chapter.

6.2 Results

All 36 tissue samples were analyzed using all 12 protease assays. By analyzing the data, basically, we could identify three types of tumor patients. They are as follows: First, some patients have high protease concentrations inside the tumor core. Second, some patients have high protease concentrations within the boundary of the tumor. Third, some patients have high protease concentrations within the (presumably) healthy tissue next to the tumor.

6.2.1 Type 1 (High Protease Concentrations Inside the Tumor Core)

Figure 6.1 shows an example of type 1. Here the fluorescence intensity, which corresponds to the tissue A, is high compared to tissue B and tissue C. In Figure 6.1 "Tissue A, B and C" means the (respective) tissue controls.
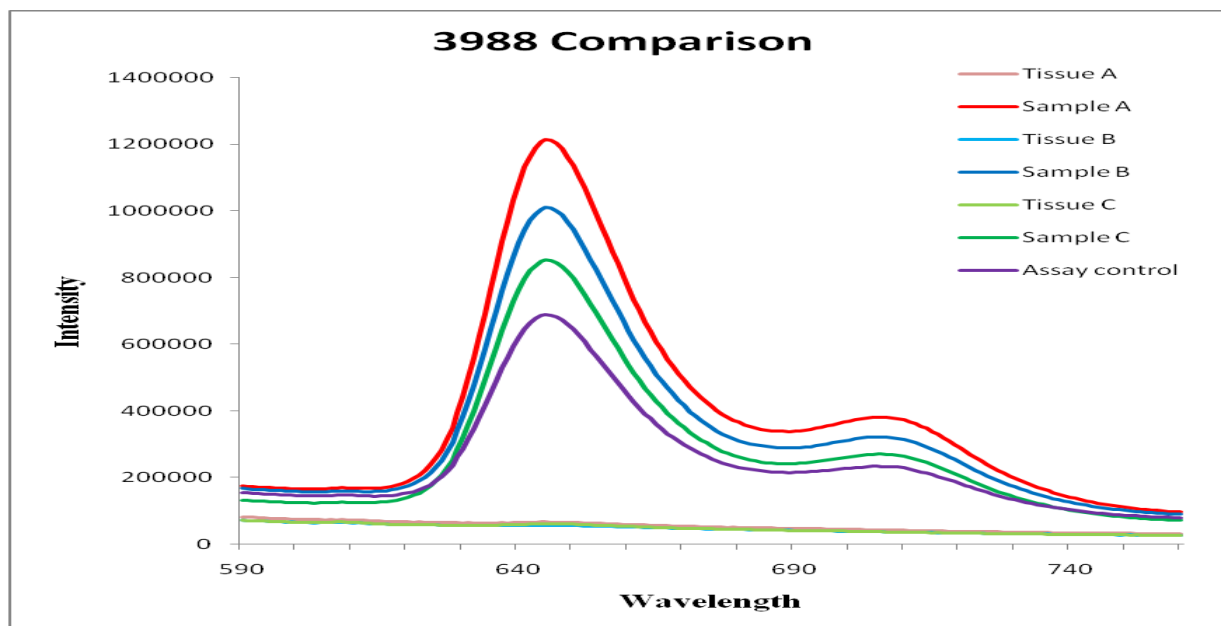
Figure 6.1: Fluorescence Graph of Patient's no: 3988, MMP 13 Assay

6.2.2 Type 2 (High Protease Concentration within the Boundary of the Tumor)

Figure 6.2 shows an example of type 2. Here the fluorescence intensity, which corresponds to tissue B is high compared to tissue A and tissue C. Also in Figure 6.2 "tissue A, B and C" means the tissue controls.
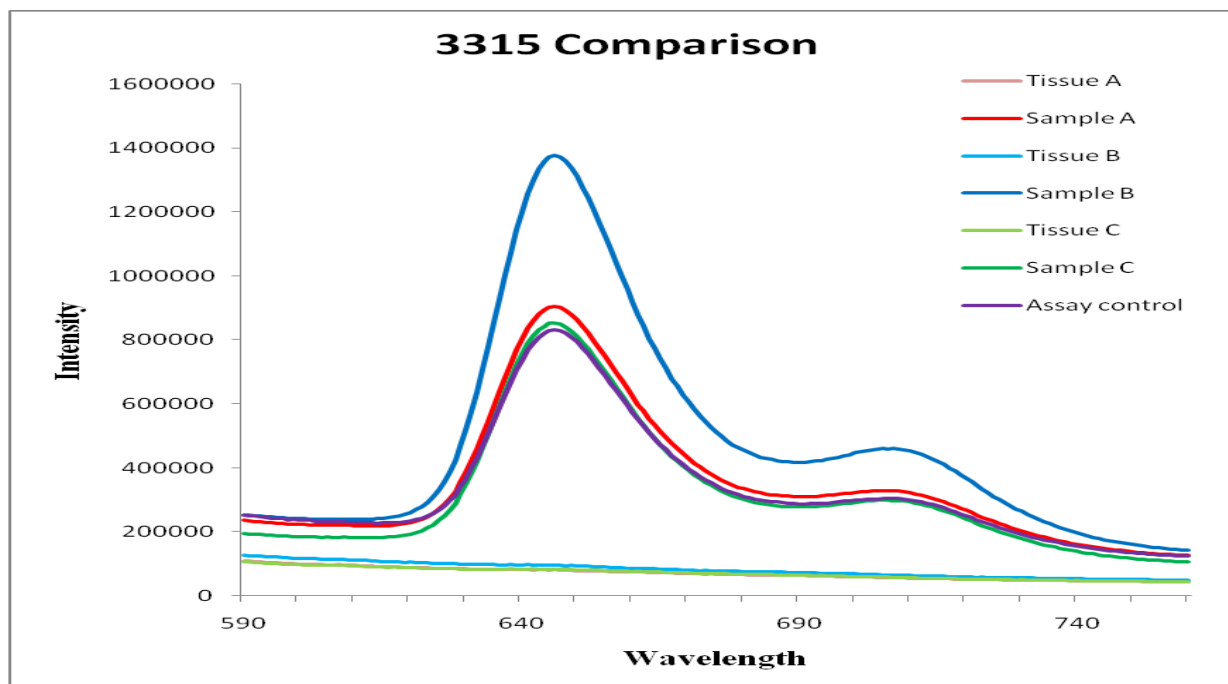
Figure 6.2: Fluorescence Graph of Patient's no: 3315, MMP 13 Assay

6.2.3 Type 3 (High Protease Concentrations within the (Presumably) Healthy Tissue next to the Tumor)

Figure 6.3 shows an example of type 3. Here the fluorescence intensity, which corresponds to tissue C is high compared to tissue A and tissue B. In Figure 6.3 "tissue A, B and C" means the (respective) tissue controls.
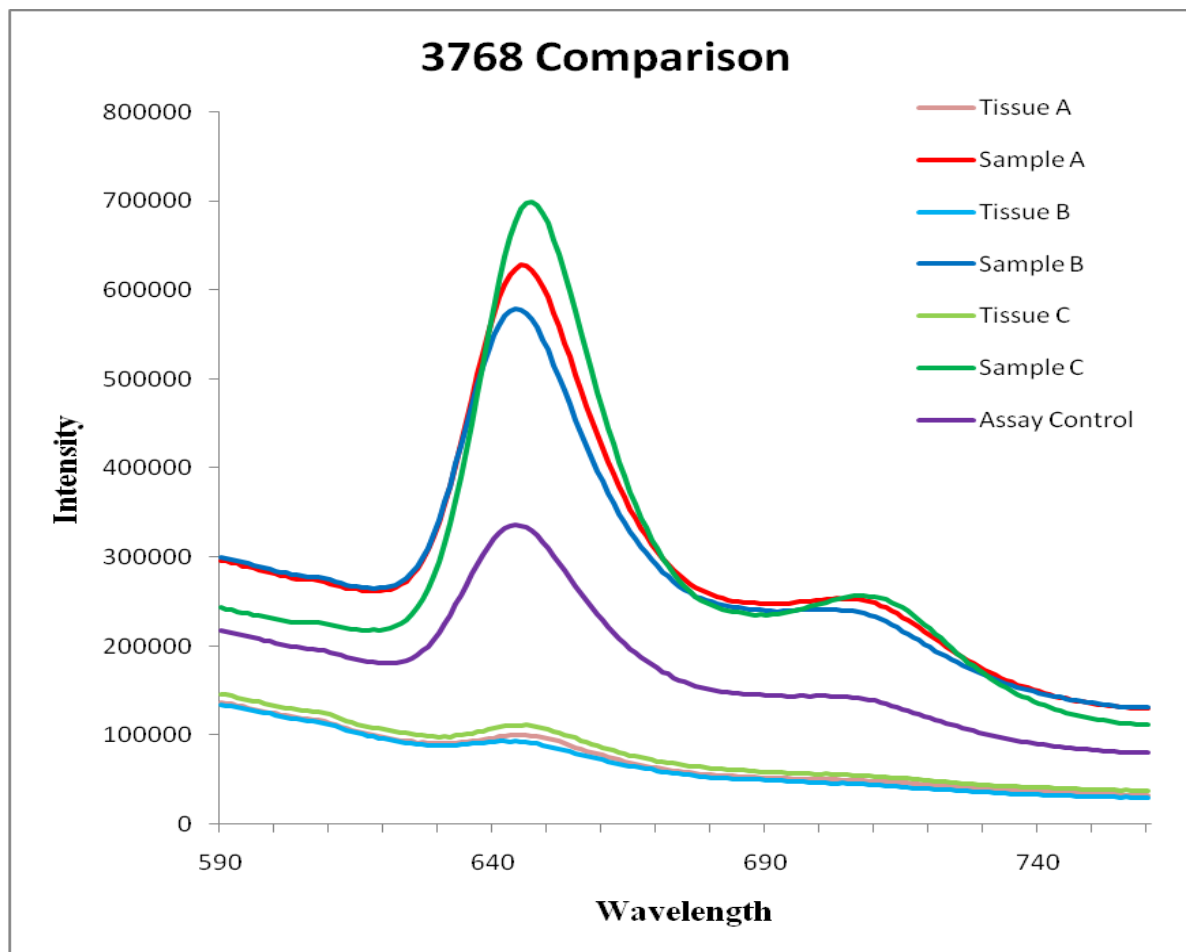
Figure 6.3: Fluorescence Graph of Patient's no: 3768, MMP 11 Assay

6.2.4 Matrix of 12 Patients and 12 Cancer-Related Proteases

As described above, different patients belong in different categories, based on the data. However, this behavior is not uniform for every protease investigated, as this becomes clear from Table 6.3. Then I compared all the data for 12 patients with all 12 proteases. The data has been tabulated in Table 6.3. In Table 6.3, A max denotes type 1 samples, the samples, which have the highest fluorescence increase when measuring tissue A, compared to tissue B and tissue C. B

max denotes type 2 samples, the samples, which have the highest fluorescence increase when measuring tissue B, compared to tissue A and tissue C. C max denotes type 3 samples, the samples, which have the highest fluorescence increase when measuring tissue C compared to tissues A and B.

Table 6.3: Matrix of 12 Patients and 12 Cancer-Related Proteases

	Code	MMP 1	MMP 2	MMP 3	MMP 7	MMP 9	MMP 11	MMP 13	uPA	Cat B	Cat D	Cat K	Cat L
1	3267	B max	B max	B max	B max	A max	C max	B Max	B max			B max	A max
2	3275	B max	B max	A max	B max	B max	A max	B max	A max	B max	B max	B max	B max
3	3315	B max	B max	B max	A max	A max	B max	B max	B max	B max	B max	A max	B max
4	3662	A max	B max	B max	A max	A max	B max	A max	A max	A max	A max	A max	A max
5	3681	A max	A max	B max	A max	C max	A max	B max	A max	B max	A max	A max	B max
6	3768	B max	A max	A max	A max	C max	C max	A max	A max	B max	B max	B max	A max
7	3773	A max	B max	B max	B max	B max	A max	B Max	B max	A max	A max	A max	B max
8	3780	A max	B max	B max	A max	C max	A max	A Max	B max	A max	A max	A max	A max
9	3890	B max	B max	B max	B max	B max	B max	B max	B max	B max	B max	B max	B max
10	3922	A max	B max	B max	B max	B max	B max	B max	B max	B max	A max	A max	A max
11	3988	B max	B max	A max	A max	B max	A max	A max	A max	A max	B max	B max	A max
12	4533	A max	A max	A max	A max	B max	B max	B max	A max	B max	A max	A max	B max

Just by analysing the data in the Table 6.3 it is hard to come to definite conclusions. So I looked into the relative protease concentrations in detail.

6.2.5 Calculations Associated with Data

First the average of the two scans was taken. The integrated fluorescence values of the average data set were collected from 620 nm to 680 nm. Then the average of the triplicates per each sample was taken. From that final averaged data set, the integrated fluorescence value (S) was taken from 620 nm to 680 nm. The integrated fluorescence values of the average data sets from 620 nm to 680 nm of the assay control (A) and tissue control (T) samples were recorded for comparison purposes. Then the difference between the two values S and T was calculated in order to eliminate the autofluorescence that occurs form the blood serum sample. The next step was to obtain the difference between (S-T) and (A). This step was performed to obtain the actual fluorescence increment due to the protease activity, because in the assay control there is some amount of TCPP that was not quenched enough to avoid a minimum of fluorescence. This fluorescence should not mislead us to think that it occurs due to activity of the protease.

6.3 Discussion

It is noteworthy that the 36 tissue samples from 12 female patients, who underwent mastectomies, have been identified by Dr. Fang Fan as stage 2 or lower. Unfortunately, the survival data for these patients are not yet available from the University of Kansas Medical Center. It would have been very interesting to discern, whether the overexpression of any protease or group of protease is indicative for enhanced or decreased survival. These studies will be completed by my colleagues in the Bossmann group as soon as these data are available.

Generally, the more positive the readings in Figures 6.4 to 6.15 are, the higher are the levels or protease expression. Levels close to zero are essentially not distinguishable from the controls, levels that are negative are significantly lower than their respective controls. It is our general paradigm that high levels of protease expression are a hallmark for aggressive cancers, whereas low levels are typical for benign tumors. However, we have to look at each enzyme individually, because it is possible that only a few proteases are significantly enhanced during angiogenesis and invasion.

6.3.1 Study of MMP 1 Protease Assay Data

The statistical analysis of the results obtained using blood serum from breast and non-small lung cancer patients that we had obtained from the Southeastern Nebraska Cancer Center (SNCC see chapter 4) clearly indicate that MMP 1 is a later stage cancer marker, because it was statistically significantly overexpressed in stage 3 and 4 cancers. In contrast, the breast cancer tissue samples investigated here are mainly stage 2 and lower. It is striking that the results from each individual patient are different. In most of the patients, the highest level of MMP 1 expression is found in the tumor core, followed by the tumor boundary. It is noteworthy that the MMP 1 levels in the adjacent tissue are only elevated in three patients. These findings are consistent with the staging of the breast tissue samples. From these data, MMP 1 does not seem to be implicated in aggressive tissue invasion. However, I am aware of the fact that we have only investigated biospecimens from 12 patients.

Figure 6.4: Integrated Fluorescence of the Tissue Samples for MMP 1 Assay

In Figure 6.4 the integrated fluorescence data for all the tissue samples is shown.

111

6.3.2 Study of MMP 2 Protease Assay Data

Figure 6.5: Integrated Fluorescence of the Tissue Samples for MMP 2 Assay

In Figure 6.5 the integrated fluorescence data of all the tissue samples is shown. In our earlier studies, MMP 2 was not identified as a significant cancer marker for stage 2 breast cancers in blood serum samples. Our studies here are in agreement with our earlier findings. Only in 6 patients MMP 2 overexpression in the tumor core and boundary region is discernible.

6.3.3 Study of MMP 3 Protease Assay Data

Figure 6.6: Integrated Fluorescence of the Tissue Samples for MMP 3 Assay

In Figure 6.6 the integrated fluorescence data for all the tissue samples is shown. Basically, the same general behavior is found as for MMP 2. MMP 3 is overexpressed only in the tumor cores of four patients, and in the tumor boundaries of four patients. Note that one patient had only an elevated tumor core, whereas another has only increased MMP 3 in the boundary region.

6.3.4 Study of MMP 7 Protease Assay Data

Figure 6.7: Integrated Fluorescence of the Tissue Samples for MMP 7 Assay

In Figure 6.7 the integrated fluorescence data for all the tissue samples is shown. The "picture" with MMP 7 is clearly different from MMP 1, 2, and 3. MMP 7 had been identified in our earlier studies (chapter 4) as marker for stage 2 breast cancers when analyzing blood serum samples. MMP 7 is overexpressed in the tumor cores and boundary regions of all 12 investigated patients. Furthermore, MMP 7 expression is highest in the boundary region of 4 cancer patients. Overall, the levels of MMP 7 expression found here are in excellent agreement with the results described in chapter 4. MMP 7 overexpression in tumor cores and boundaries seems to be universal in all types of breast cancer at stage 2. It is noteworthy that the expression levels of MMP 7 in the adjacent tissue regions are close to zero or smaller than the controls, indicating that MMP 7 is not majorly involved in invasion and/or angiogenesis.

6.3.5 Study of MMP 9 Protease Assay Data
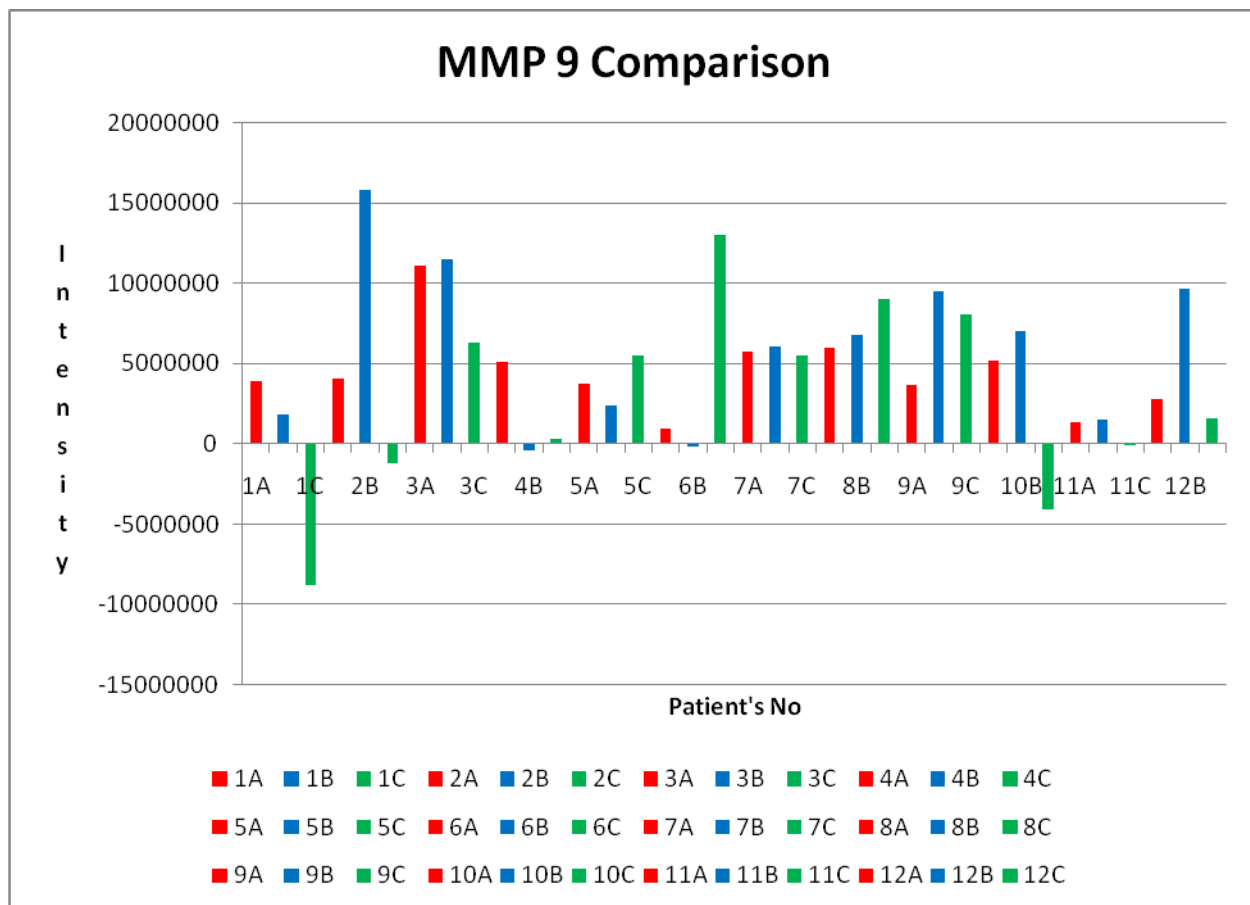
Figure 6.8: Integrated Fluorescence of the Tissue Samples for MMP 9 Assay

In Figure 6.8 the integrated fluorescence data for all the tissue samples is shown. Contrary to MMP 1, 2, 3, and 7, MMP 9 is a typical inflammation marker.[1] Neutrophils, which are attracted by tumor[1], are a major source of MMP 9. Therefore, it was predicted prior to my experiments reported here that substantial levels of MMP 9 should be found in the tissue that is adjacent to the tumor boundary. [1] The experiments summarized in Figure 6.8 provide experimental support for this theory: MMP 9 levels are elevated in 10 tumor cores, nine tumor boundaries and six adjacent tissue regions. MMP 9 production is highest in the tumor boundary of six patients, and in the adjacent tissue of three patients. Since it is known that inflammation promotes invasion in breast cancers[1], it is my prediction that high MMP 9 levels in the boundary region and adjacent tissue will be a prognosticator of low survival probability.

115

6.3.6 Study of MMP 11 Protease Assay Data
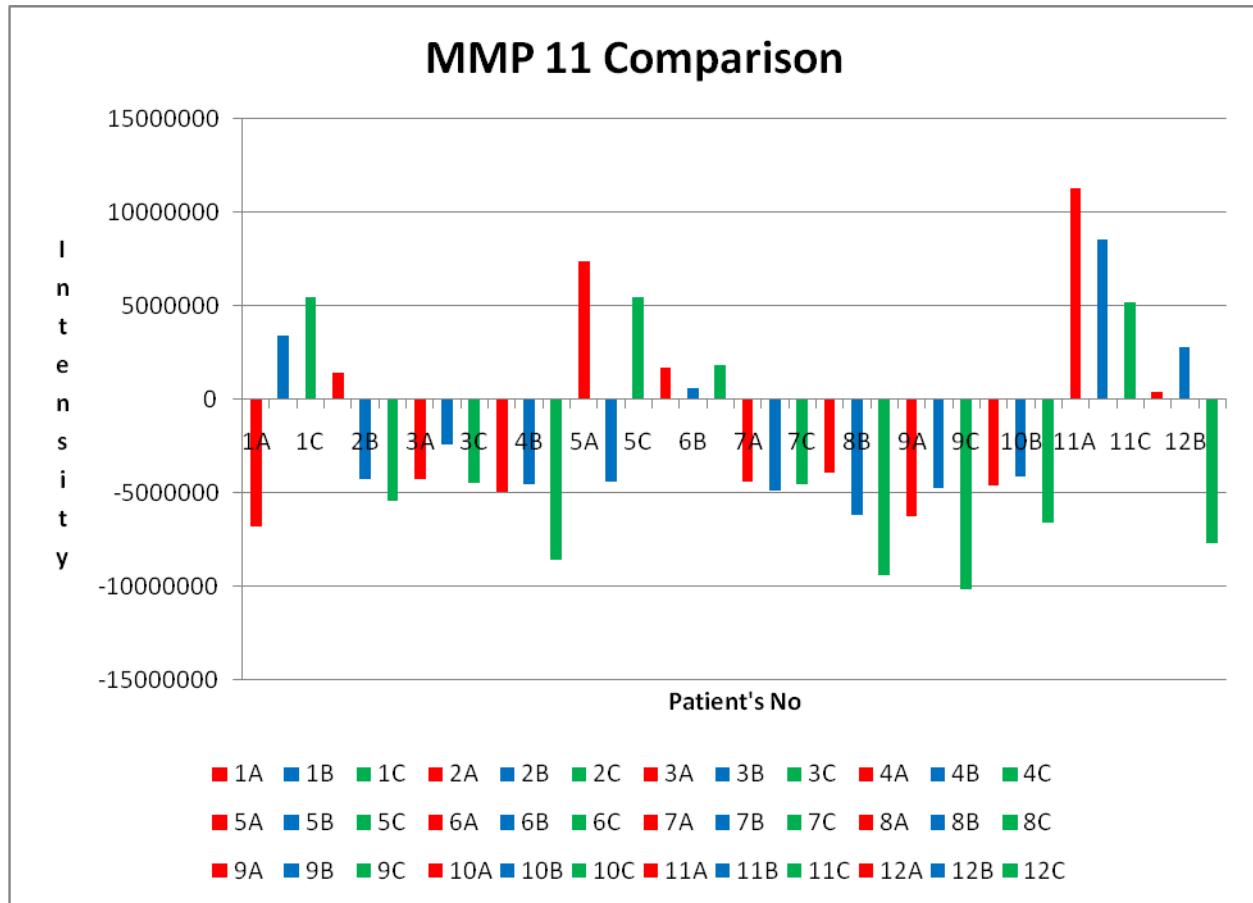
Figure 6.9: Integrated Fluorescence of the Tissue Samples for MMP 11 Assay

In Figure 6.9 the integrated fluorescence data for all the tissue samples is shown. As discussed in chapter 5, MMP 11 is potentially of high diagnostic value. Although most of the tumors that were investigated here don't overexpress MMP 11, it is noteworthy that it is found in the adjacent tissue of four patients. The correlation of the patient survival data and MMP 11 expression will show, whether this enzyme is indeed of diagnostic value.

6.3.7 Study of MMP 13 Protease Assay Data
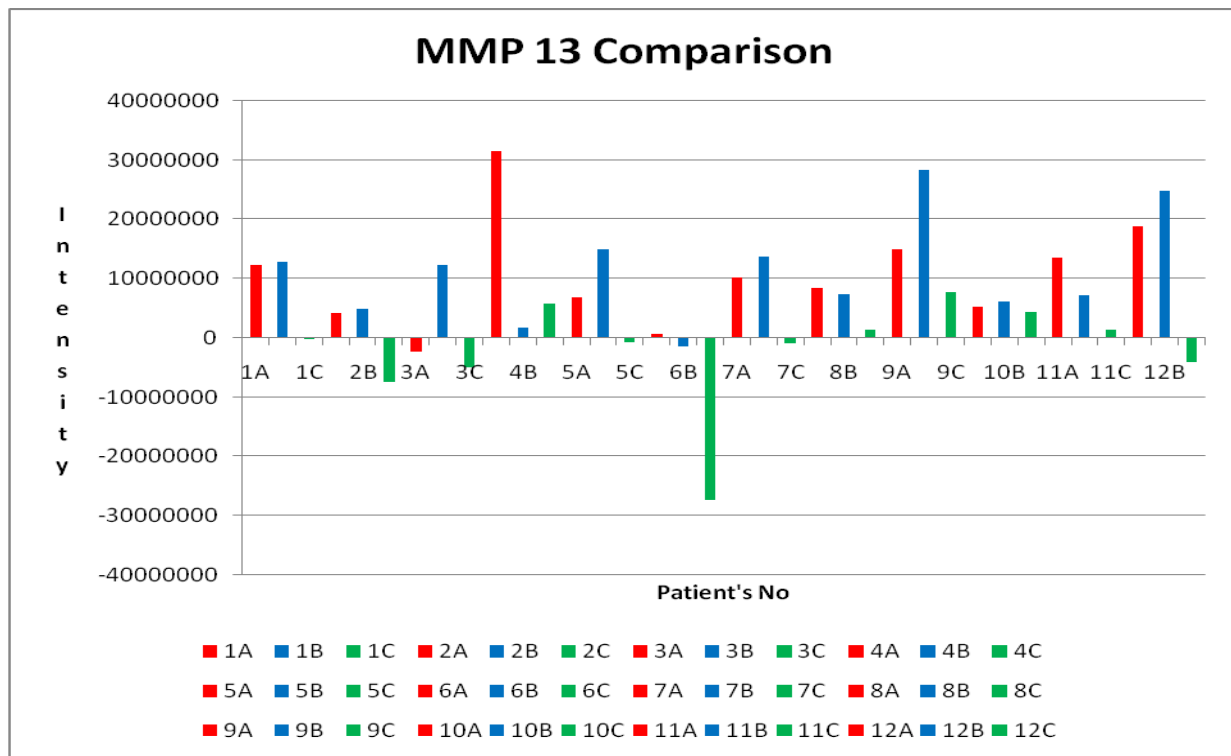
Figure 6.10: Integrated Fluorescence of the Tissue Samples for MMP 13 Assay

In Figure 6.10 the integrated fluorescence data for all the tissue samples is shown. I have also discussed in chapter 5 that there is an emerging paradigm in the recent literature that some of the same factors that drive epithelial–mesenchymal transition (EMT) upregulate MMP13 expression (e.g., TGFβ, IL1b, TNFα), indicating an association of MMP13 with invasion and metastasis. Therefore, it is most interesting that 11 or 12 patients show upegulated MMP 13 levels. Seven of these 11 patients show highest MMP 13 expression in the boundary region. As discussed above, all patients were diagnosed with stage 2 (or lower). Therefore, it is most interesting that MMP 13 is almost abundantly expressed in tumor cores and tumor boundaries. Furthermore, MMP 13 is also found in the adjacent tissue of three patients. Based on these findings, MMP 13 may be a good biomarker for mapping early breast tumors and to observe the transition between benign and cancerous lesions.

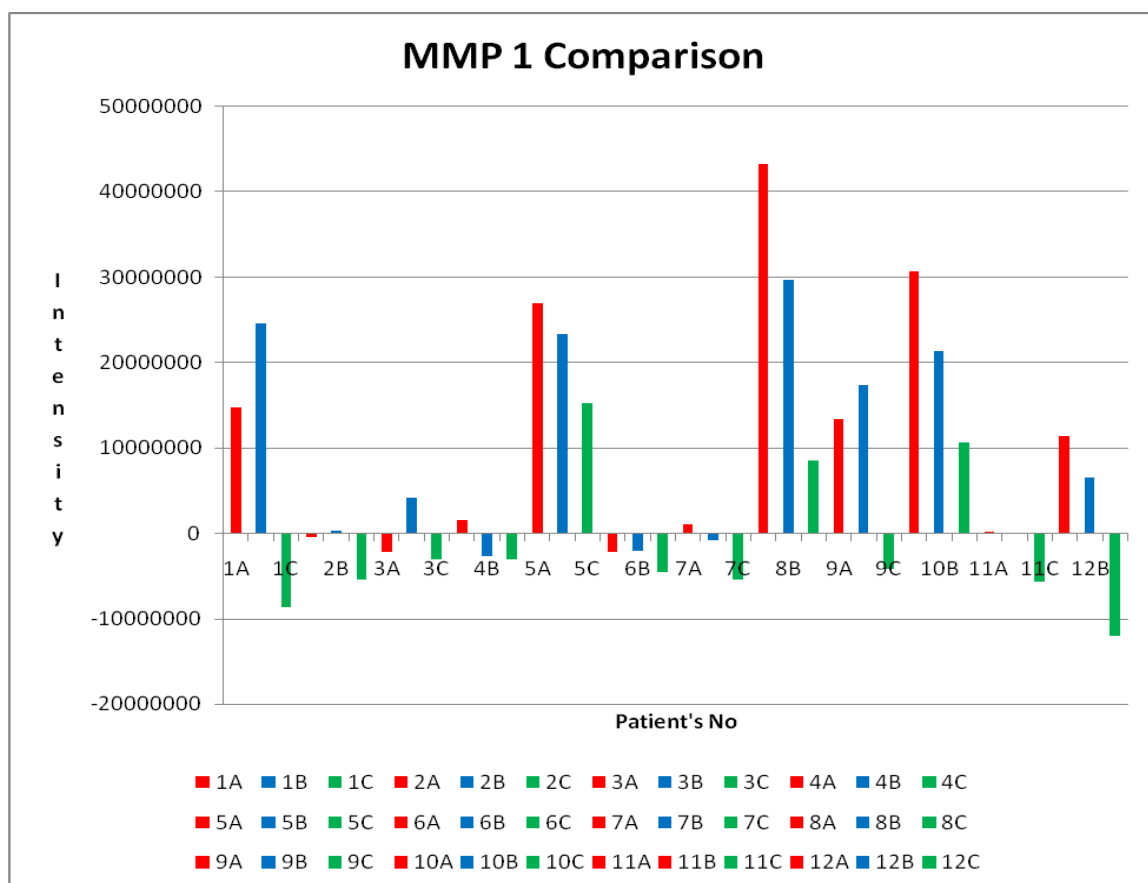## 6.3.8 Study of Cathepsin B Protease Assay Data
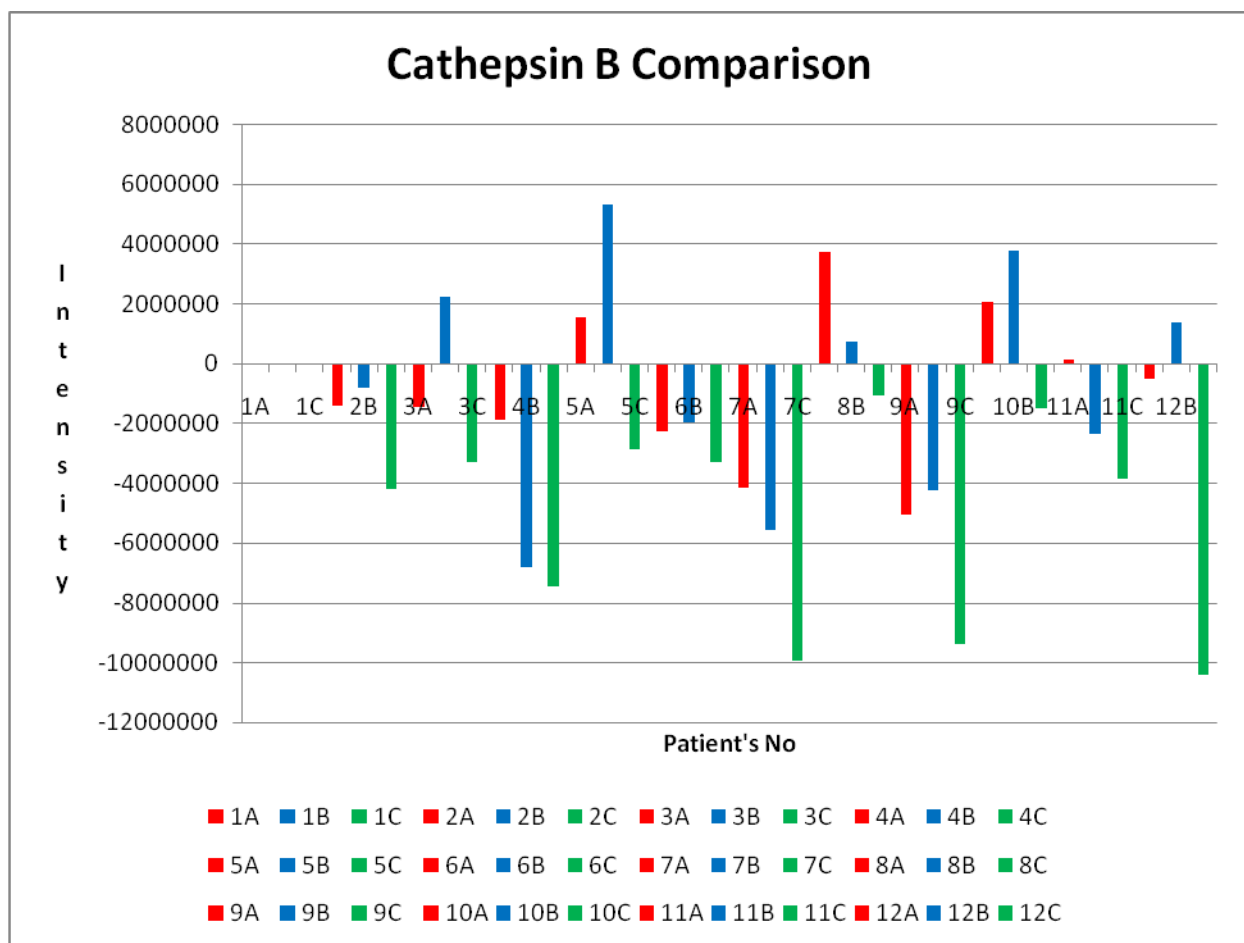
Figure 6.11: Integrated Fluorescence of the Tissue Samples for Cathepsin B Assay

In Figure 6.11 the integrated fluorescence data for all the tissue samples is shown. Cathepsin B has been identified as "late stage breast cancer marker" in our studies that are described in chapter 4. These findings are in agreement with this assessment. Cathepsin B is overexpressed only in five patients, in four of these five patients it is highest in the boundary regions. I anticipate that cathepsin B expression may significantly increase in stage 3 and 4 cancer patients, but only very limited conclusions can be drawn from the data shown in Figure 6.11.

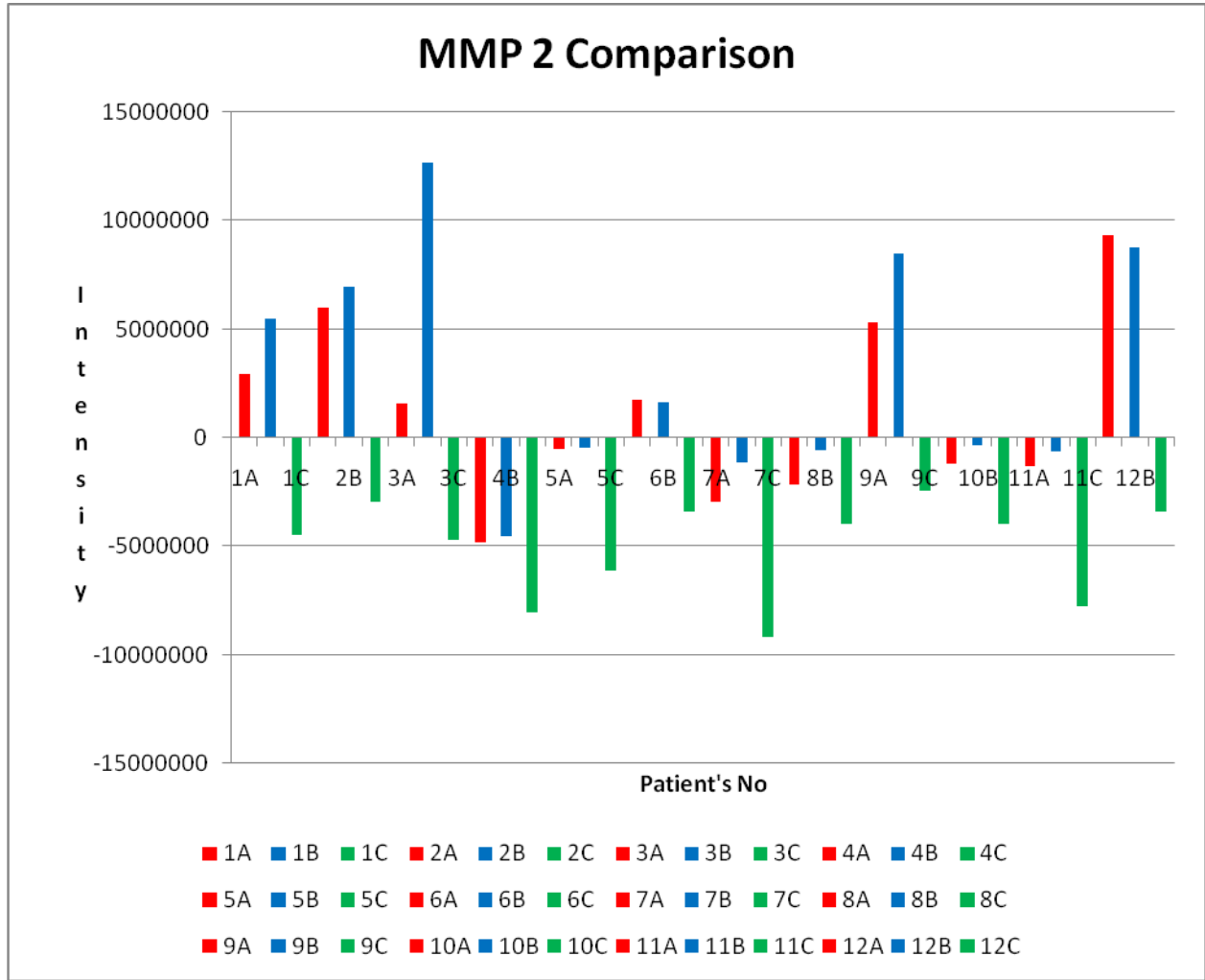## 6.3.9 Study of Cathepsin D Assay Data
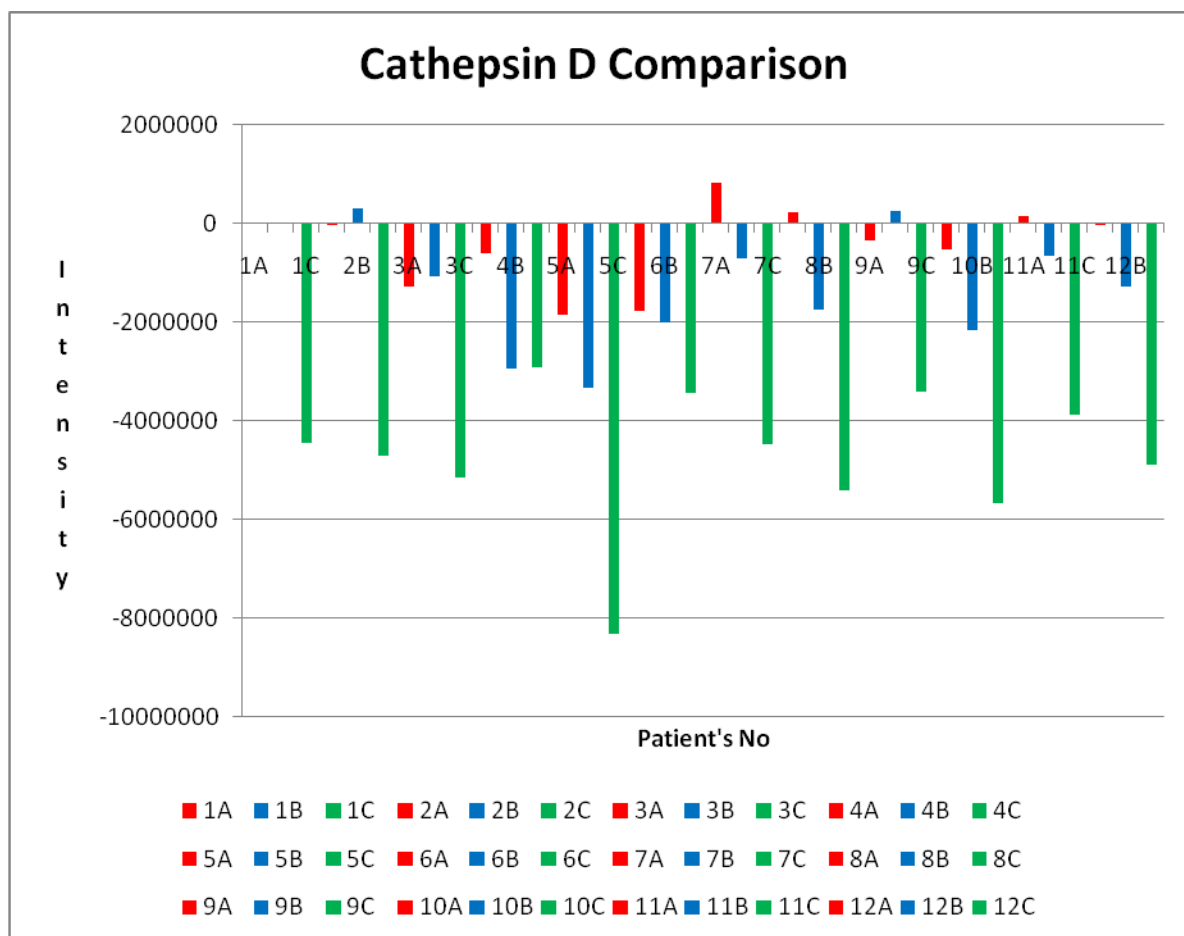
Figure 6.12: Integrated Fluorescence of the Tissue Samples for Cathepsin D Assay

In Figure 6.12 the integrated fluorescence data for all the tissue samples is shown. With one exception, it is not significantly expressed in the investigated tissue samples.
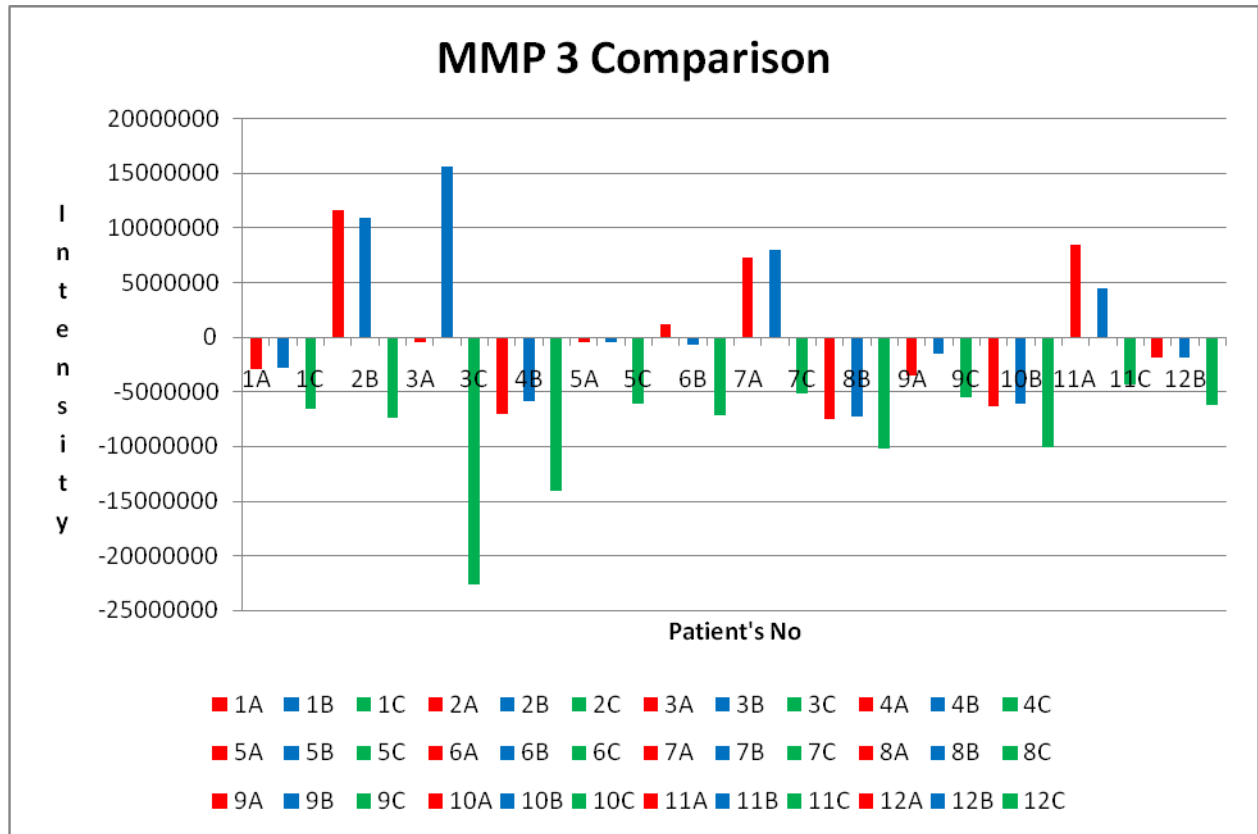
6.3.10 Study of Cathepsin K Assay Data
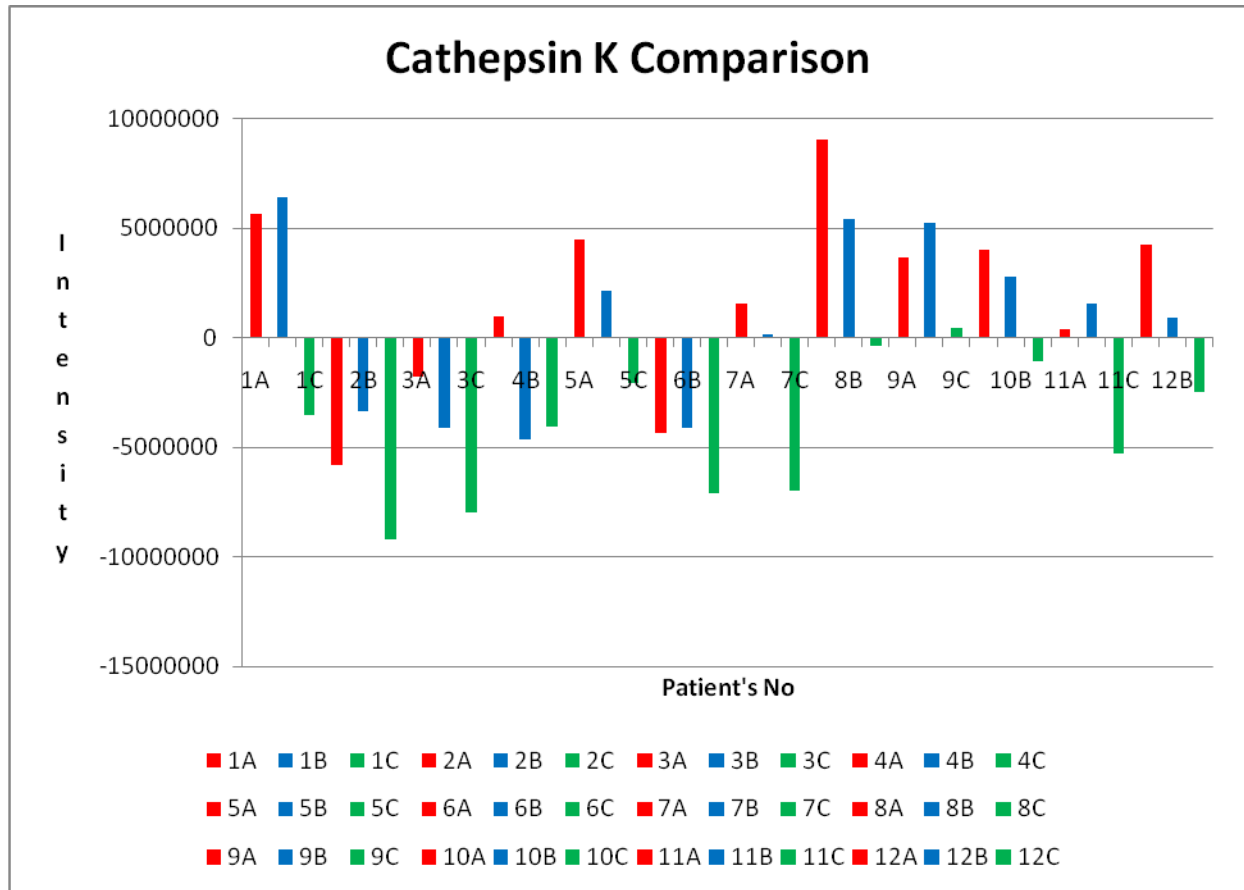
Figure 6.13: Integrated Fluorescence of the Tissue Samples for Cathepsin K Assay

In Figure 6.13 the integrated fluorescence data for all the tissue samples is shown. Cathepsin K is significantly expressed in nine patients. In only two of these samples, the expression level in the boundary region was higher than in the core of the tumors. Cathepsin K has been established in the literature as a biomarker for bone invasion[2]. Because of this reason, cathepsin K may be also linked to patient survival probability.

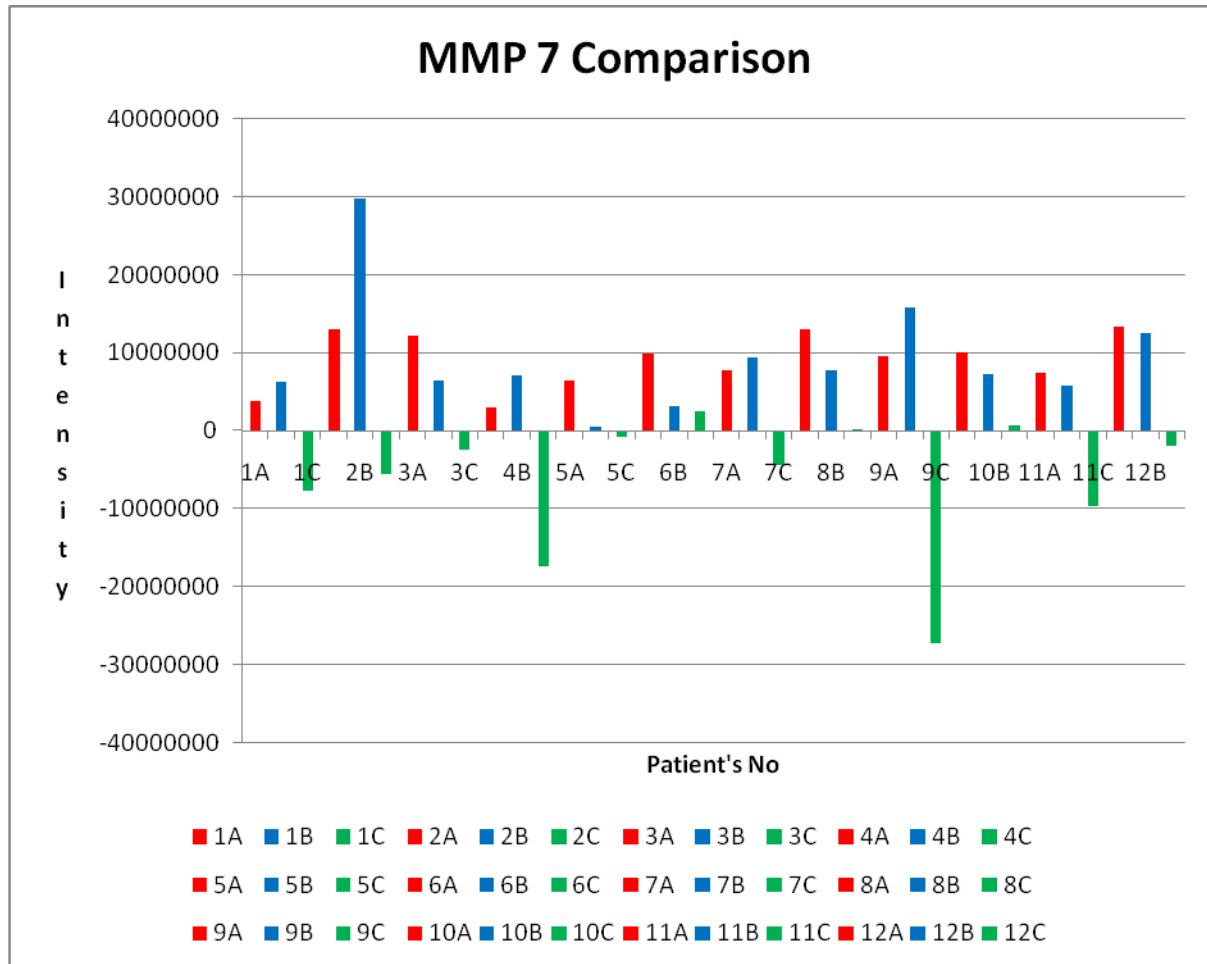**6.3.11 Study of Cathepsin L Protease Assay Data**
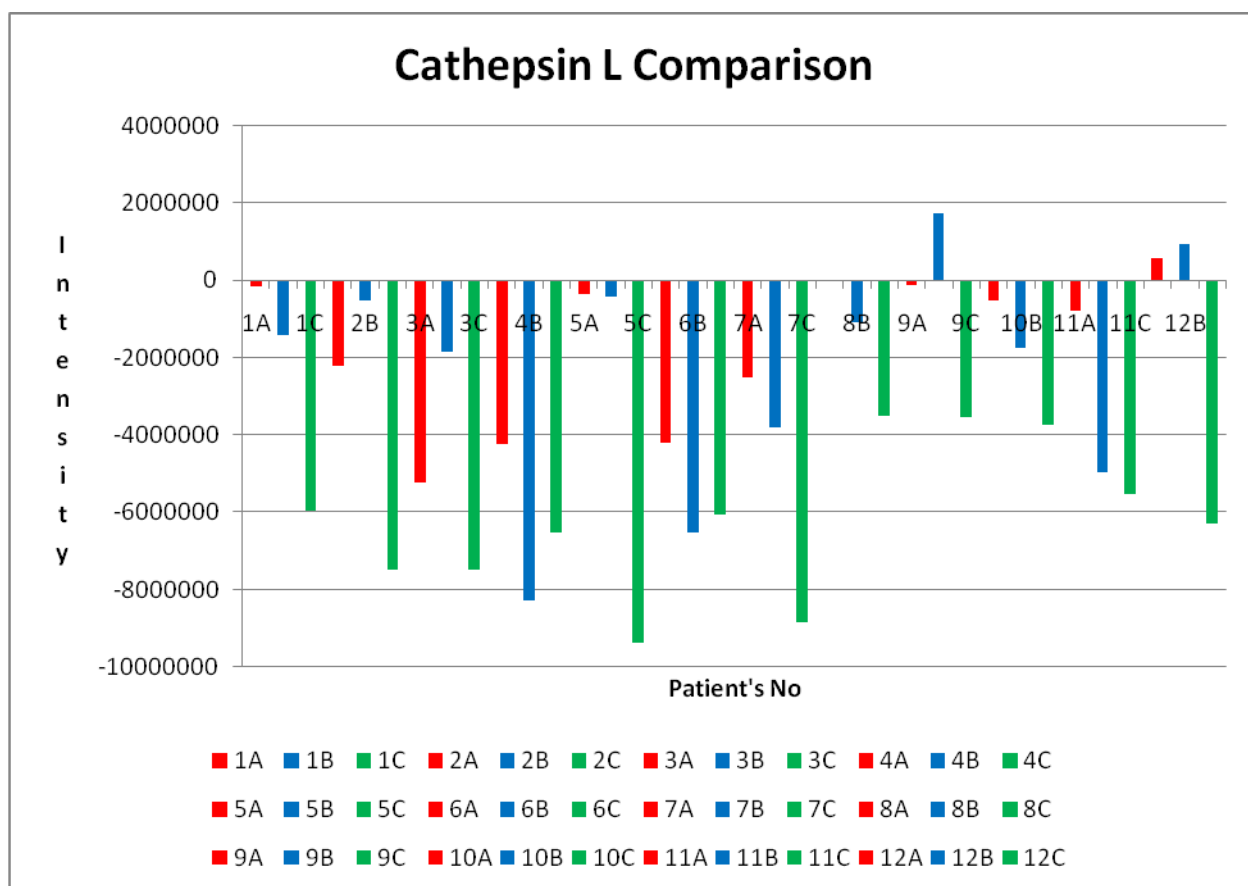
Figure 6.14: Integrated Fluorescence of the Tissue Samples for Cathepsin L Assay

In Figure 6.14 the integrated fluorescence data for all the tissue samples is shown. Cathepsin L is not significantly expressed in the investigated samples, with two exceptions, where the protease expression in the cancer boundary was higher than in the core.

**6.3.12 Study of Urokinase Plasminogen Activator (uPA) Assay Data**
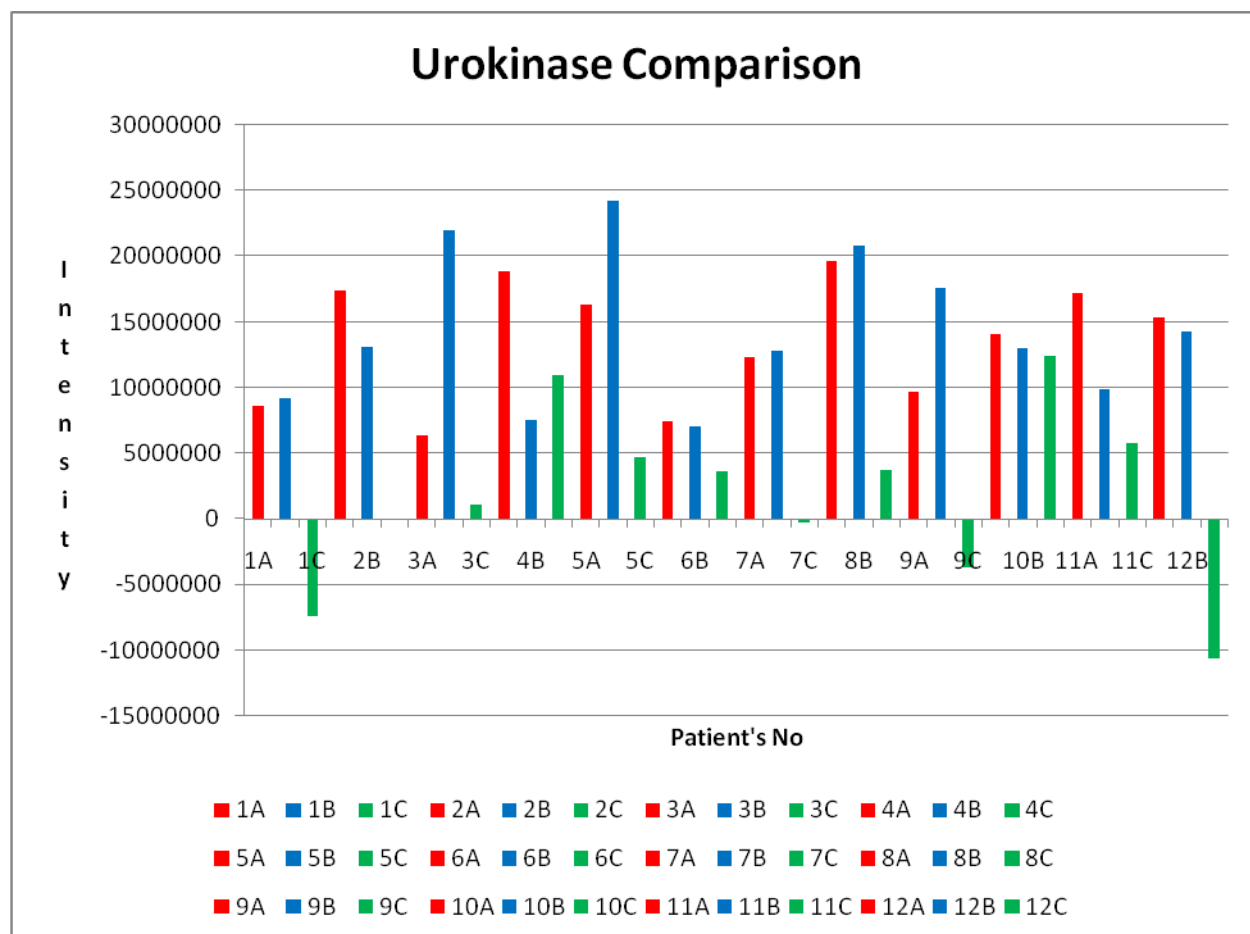
Figure 6.15: Integrated Fluorescence of the Tissue Samples for Urokinase Assay

In Figure 6.15 the integrated fluorescence data for all the tissue samples is shown. Urokinase plasminogen activator has been identified as biomarker for inflammation in breast cancer[3]. It has been also established that inflammation promotes the cancer progression. As summarized in Figure 6.15, uPA is overexpressed in the core and boundary regions of the tumors of all 12 patients. In six tumors, the cores showed highest uPA activity, whereas in the other six patients, the uPA activity in the boundary regions was higher. Furthermore, uPA was significantly expressed in the adjacent tissue regions of six patients. It has been already demonstrated in chapters 4 and 5 that uPA is of a principal diagnostic value in breast cancer. The study described here is clearly reaffirming our earlier findings.

6.4 References

[1] Cowburn, A. S.; Condliffe, A. M.; Farahi, N.; Summers, C.; Chilvers, E. R. Advances in neutrophil biology: clinical implications, *Chest,* **2008**, *134*, 606-612.

[2] Brömme, D.; Lecaille, F. Cathepsin K inhibitors for osteoporosis and potential off-target effects, *Expert Opin. Investig. Drugs*, **2009**, *18*, 585-600.

[3] Duffy, M. J. Proteases as Prognostic Markers in Cancer, *Clin. Cancer Res.* **1996**, *2*, 613-618.

Chapter 7 - IVIS Approach for the Protease Assays

7.1 Background

All the analyses I have discussed in chapters 4, 5 and 6 are based on steady state fluorescence measurements. To get in to statistically relevant conclusions based on our results, we need to analyze a large number of samples from each type. Also if we need to use the protease assay technique in tumor screening work, we have to analyze a lot samples at the same time. When we need to analyze hundreds and thousands of samples, the current method we use is too time consuming.

There are several reasons for this work being time consuming. First, there is only one cuvette holder in the spectrofluorometer (fluoromax2) that we are using. Second, we run two scans per each sample and we do three replicates per each sample. Third, we set the assay for several samples at the same time, do the incubation and get the fluorescence done. In order to finish the fluorescence measurements for nine samples, it takes about two hours. This includes the time that it takes in between transfer of the cuvettes from one to the other. At that point, the time factor will also have an effect on our data.

As an option if we can use a fluorescence plate reader that would cut off most of the drawbacks that I mentioned in the previous paragraph. There are 96 or 384 wells in one plate and we can read the fluorescence of 96/384 samples at the same time. The sample volume we need is clearly less than 100 μL. But we need to use a higher concentration of the sample compared to fluoromax 2, because the optical path is different.

Depending on the availabilities of the machines in the laboratory and with our collaborators, I tried the "IVIS approach" of the protease assays as the final version of the sequence of protease assays I worked with.

7.2 In Vivo Imaging System (IVIS)

      Currently, especially with cancer diagnostics, imaging has become a very handy tool. There are several categories of imaging methods. The classification depends on several factors. They are the energy type that has been used, the spatial resolution, and the type of information obtained.[1]

      Among them, optical tomography (IVIS system) is a versatile method that can be used in several applications, such as life science research and drug discovery. Evaluation of structure and function of a living subject is the major function done by IVIS. There are several advantages of IVIS compared to other diagnostic methods. Major advantages are higher sensitivity, requirement of the less amount of cells, low noise level and non radioactivity.[2]

      Figure 3.1 shows the apparatus of the IVIS.[3]
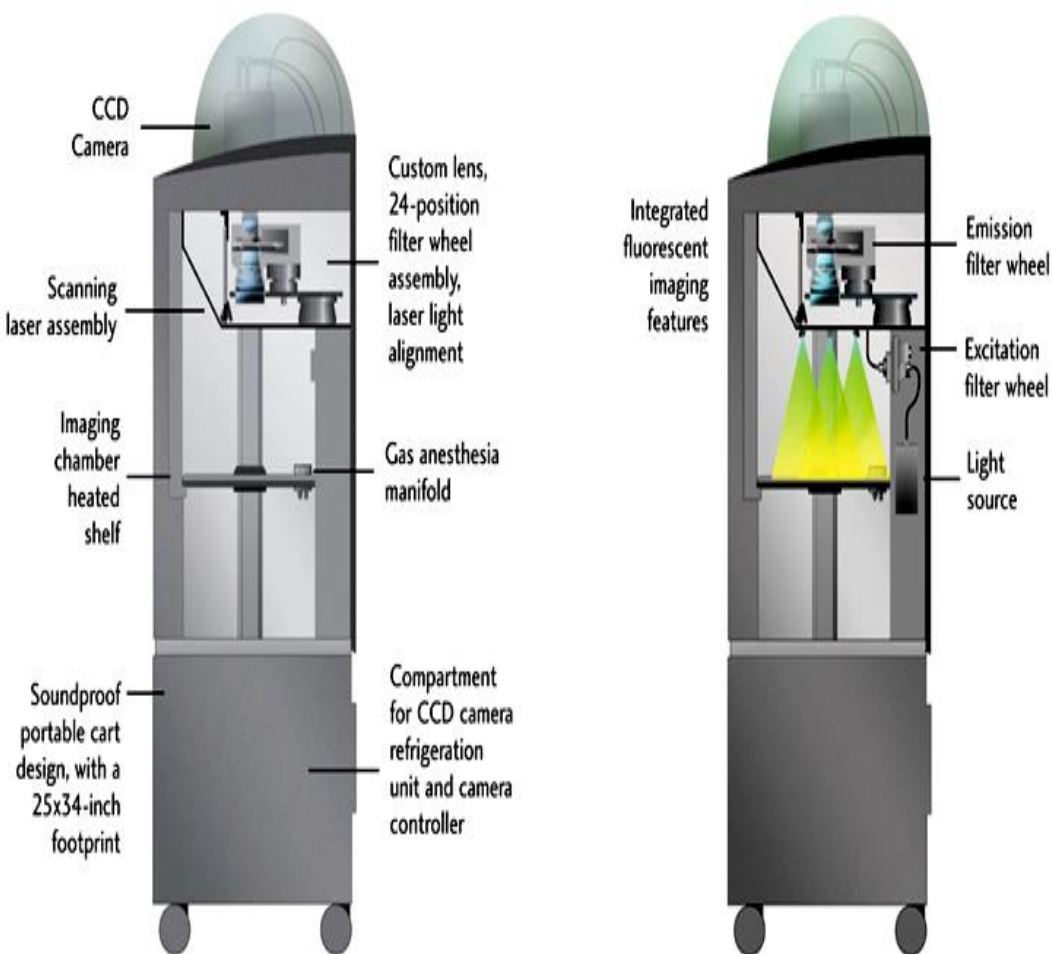
Figure 7.1: IVIS Apparatus (Image Provided by Caliper Lifesciences)

7.3 Analysis of Canine Blood Serum Samples

Five canine blood serum samples were randomly selected form the set of 36 canine blood serum samples we have received from Prof. Dr. Mary Higginbotham, MD, Kansas State Veterinary Hospital. The in-vitro protease assay was performed using the IVIS. The assay was carried out in transparent 96-well plates.

100 μL of the 1x PBS (containing dextran in 10 mg in 1 mL concentration) mixture was pipetted in the well. To the next well 100ul of the MMP 11 nanoplatform was pipetted. Then 50 uL of the canine serum sample was pipetted in to the same well, mixed. Likewise all the samples were pipetted in to the wells. control experiments were also carried out. Then the fluorescence detection was conducted by IVIS apparatus.

Images were obtained by imaging the plate at exposure time 5 min., 10 min., 15min., up to 90 min., in 5 minutes intervals. Quantitative analysis was achieved by analyzing the correlation between the concentration of the protease and the intensity of the fluorescence. The contents of the well and well number are shown in table 7.1 and the image is shown in Fig. 7.2.

Table 7.1: Description of the Plate

Well Number	Contents
A1	150 uL of 1x PBS (with dextran)
A2	100 uL of MMP 11 nanoplatform + 50 uL of 1x PBS (with dextran)
A3	50 uL of Sample 1 + 100 uL of 1x PBS (with dextran)
A4	50 uL of Sample 1 + 100 uL of MMP 11 nanoplatform
A5	50 uL of Sample 2 + 100 uL of 1x PBS (with dextran)
A6	50 uL of Sample 2 + 100 uL of MMP 11 nanoplatform
A7	50 uL of Sample 3 + 100 uL of 1x PBS (with dextran)
A8	50 uL of Sample 3 + 100 uL of MMP 11 nanoplatform
A9	50 uL of Sample 4 + 100 uL of 1x PBS (with dextran)
A10	50 uL of Sample 4 + 100 uL of MMP 11 nanoplatform
A11	50 uL of Sample 5 + 100 uL of 1x PBS (with dextran)
A12	50 uL of Sample 5 + 100 uL of MMP 11 nanoplatform
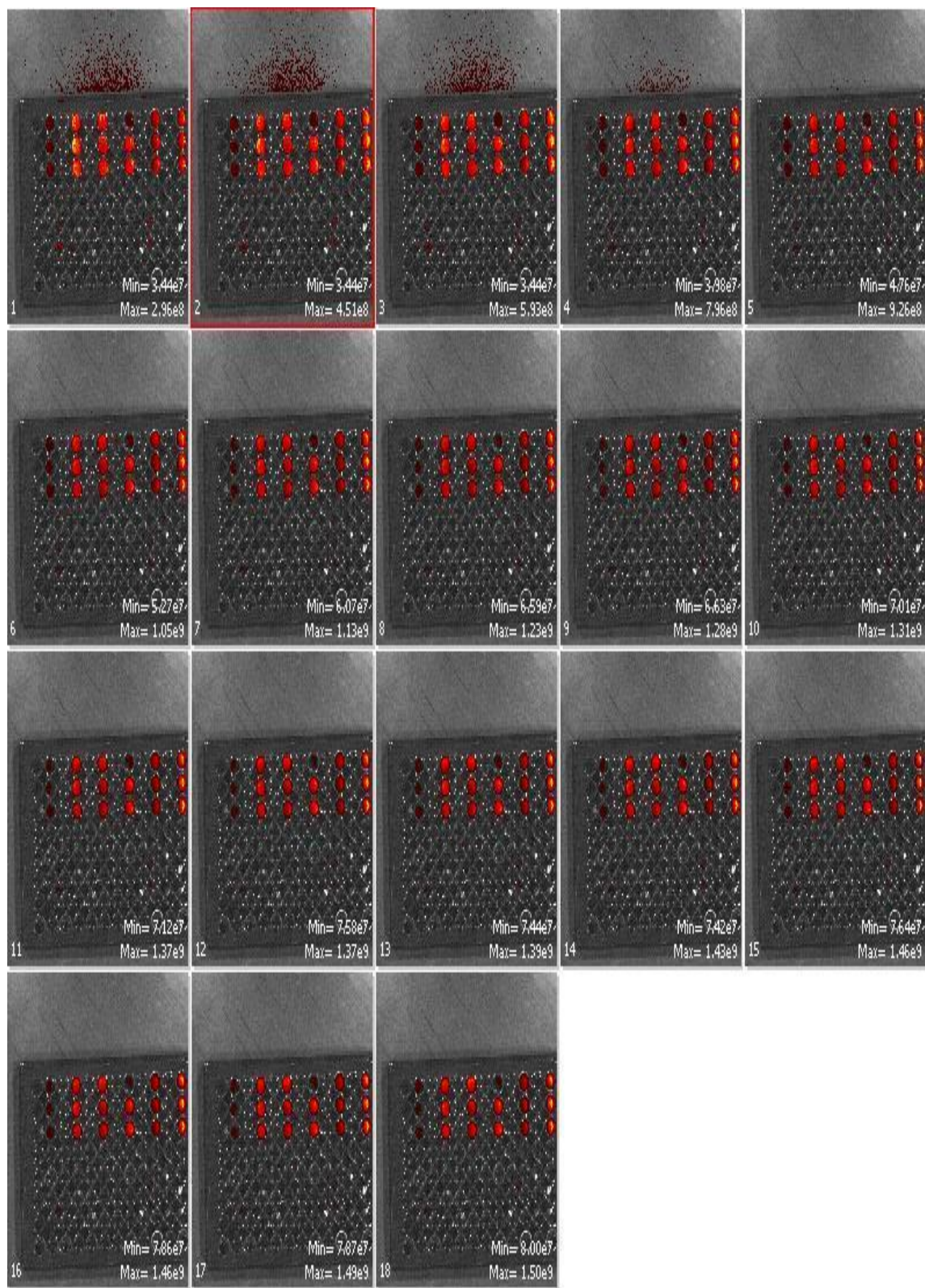
Figure 7.2: IVIS imaging of the Canine Serum Samples
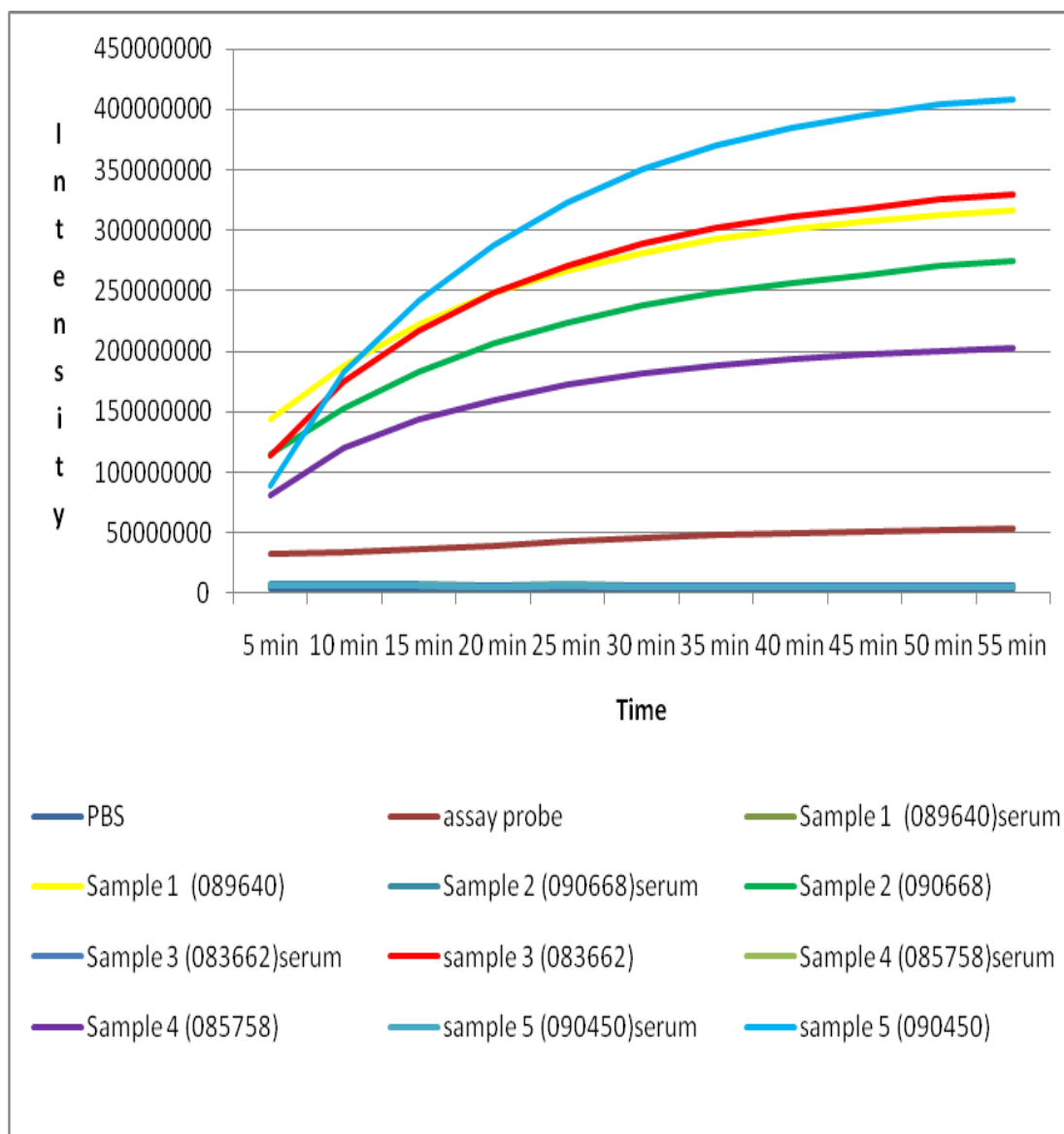
Figure 7.3: Increment in Fluorescence in IVIS

There is no significant increment in fluorescence with serum control samples and assay control sample, which is a good indication that this technique can be used for detection of protease activity. Consequently we can explain that the increment in fluorescence we see arises only due to the activity of MMP 11 protease in blood serum. Here the order of the samples depending on the fluorescence increment is as follows:

Sample 5 (090450) > Sample 3 (083662) > Sample 1 (089640) > Sample 2 (090668) > Sample 4 (085758)

Then I carried out the fluoromax experiments to the same set of canine serum samples.
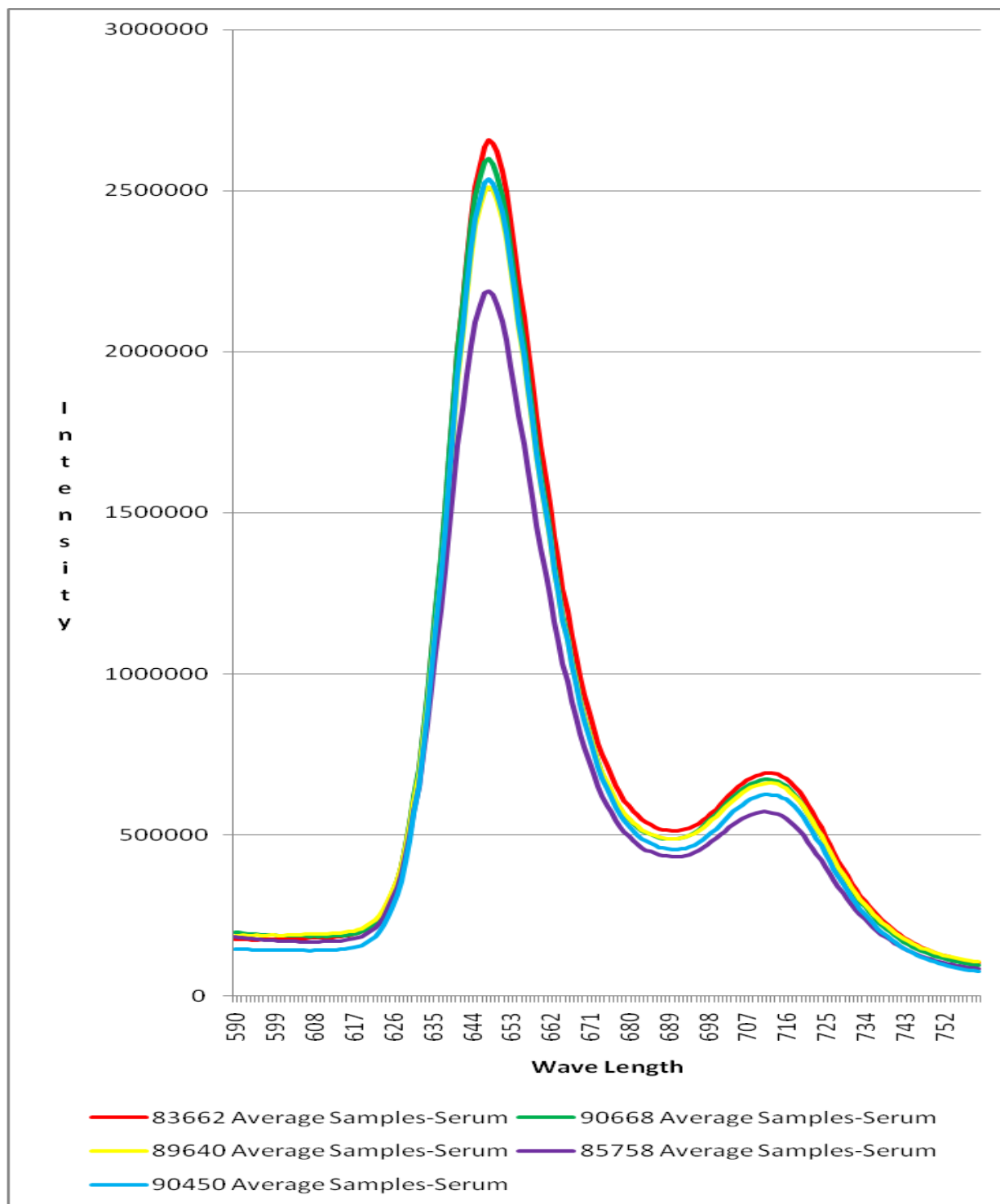
Figure 7.4: Increment in Fluorescence using the Fluoromax

Here the order of the samples depending on the fluorescence increment is as follows. Sample 3 (083662) > Sample 2 (090668) > Sample 1 (089640) > Sample 5 (090450) > Sample 4 (085758).

The next step was to compare the fluorescence increments of the five canine serum samples using both techniques (see Figure 7.5)

Table 7.2: Comparison of Integrated Fluorescence of IVIS and Fluoromax

Sample No	Fluoromax	IVIS
5 (090450)	2478153	408800000
3 (083662)	2637583	329850000
1 (089640)	2547387	316333333
2 (090668)	2588300	274166666
4 (085758)	2146760	202933333
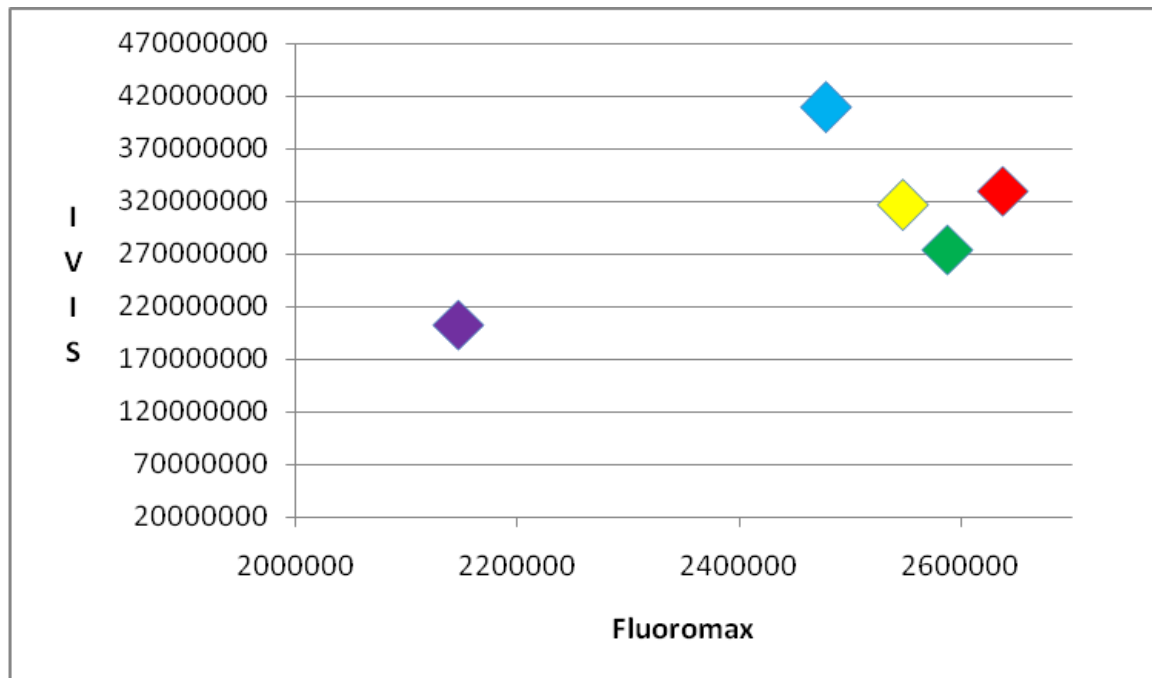
Figure 7.5: Comparison of Integrated Fluorescence of IVIS
5 (090450), 4 (085758), 3 (083662), 2 (090668), 1 (08964)

130

The proof-of-principle experiments described in this chapter clearly demonstrate that fluorescence plate readers can be used to determine the activity of (cancer-related) proteases. The IVIS equipment proved to be sufficiently sensitive to measure protease activity in 96-well plates. Considering that classic fluorescence plate readers are approx. 10 times more sensitive than the IVIS[4], which is configured for optical tomography on small animals, it is my prediction that they will be ideal for measuring protease signatures of (cancer) patients in hospitals. It is of importance for the implementation of the technology that has been developed in my thesis that the equipment required for clinical use already exists and is already in use in many clinical laboratories. However, due to the differences in optical path length and irradiation geometry, the experimental conditions for measuring protease activities will have to be optimized when using fluorescence plate readers.

7.4 References

[1] Condeelis, J.; Weissleder, R.   In vivo imaging in cancer. *Cold Spring Harb.Perspect. Biol.* **2010**.

[2] Zheng, J. F.; Xu, L. F.; Zhou, H. F.; Zhang, W. F.; Chen, Z. Quantitative analysis of cell tracing by in vivo imaging system, *J. Huazhong Univ. Sci. Technolog. Med. Sci.* **2010**, *30*, 541-545.

[3] http://oicf.bsd.uchicago.edu/common/equipment.html

[4] http://www.biotek.com/products/microplate_detection/flx800_fluorescence_microplate_reader.html

Chapter 8 - Surface Properties of the Protease Assay Components

8.1 Introduction

The validation of the protease assay, which is described in chapter 3, has been performed using commercially available proteases in PBS. The analysis, which are described in chapters 4, 5 and 6, have been performed using proteases from biospecimens in PBS. Due to the presence of thousands of proteins in these biospecimens the two situations are different from each other. Therefore, it would be surprising if the photophysical conditions would not be influenced by the presence of (thousands of) proteins. This reasoning made me to look in to the aggregation of the components of the protease assay.

8.1.1 Dynamic Light Scattering

"DLS measurements involve the analysis of the time autocorrelation function of scattered light as performed by a digital correlator."[1] The method is described in detail in reference 1. The hydrodynamic diameters of the nanoplatforms and nanoplatform aggregates were measured using a ZetaPALS Zeta Potential Analyzer (Brookhaven Instruments Corporation) by hydrodynamic light scattering. This instrument is capable of performing routine experiments, which do not require elaborate calculations to obtain hydrodynamic diameters.

8.2 Dynamic Light Scattering Data

DLS measurements have been performed for the assay probes, assay probes with enzymes, assay probes with blood serum, and assay probes with human tissue extracts. DLS data were obtained for urokinase, cathepsin D and MMP 7 assay systems, which served as model enzymes: one member from each protease family has been chosen.

8.2.1 DLS for Cathepsin D

First, DLS measurements were performed using the nanoplatform for cathepsin D. The concentration of the assay probe is 0.10 mg/mL in PBS. The samples were allowed to reach an equilibrium for 24 h and measurements were recorded. In all the measurements shown in Figure 8.1, the final volume in the cuvette was 3 mL.
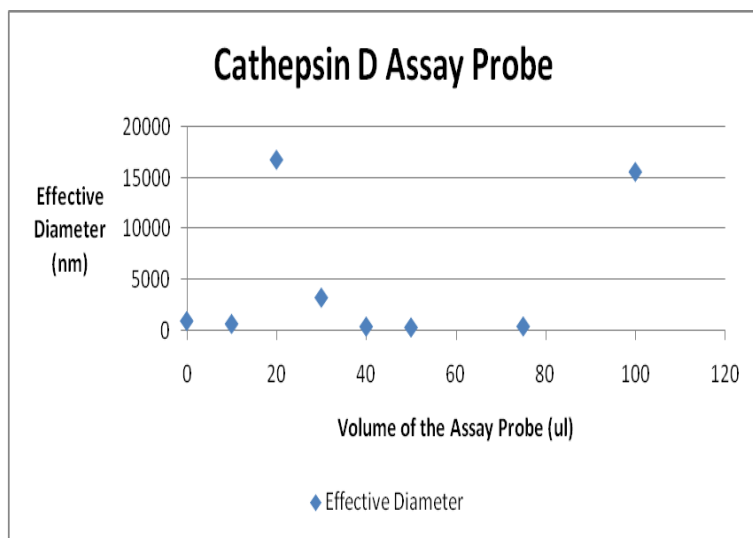
Figure 8.1: DLS of Cathepsin D Assay Probe without Dextran

The data summarized in Figure 8.1 clearly indicate that clustering occurs at each investigated concentration. The clustering is not really concentration dependent, which may be caused by the used algorithms, which were optimized for polymers and not for metal nanoparticles. In order to disperse the nanoplatforms in PBS, dextran (10 mg/mL) was used. Dextran caused a significant decrease in the effective diameters. Furthermore, the hydrodynamic diameters were now dependent on the nanoparticle concentration, which is acceptable, because it is indicating dynamic behavior.
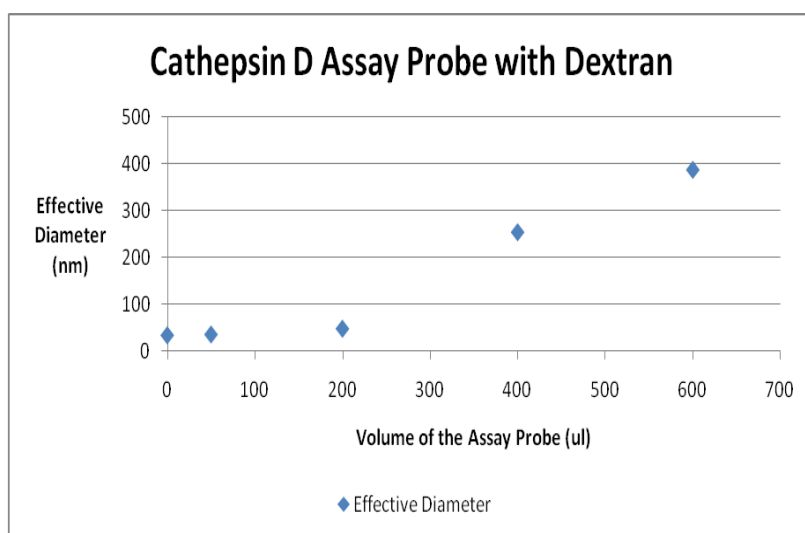
Figure 8.2: DLS of Cathepsin D Assay Probe with Dextran

After demonstrating the anticoagulant effect of dextran, I investigated the influence of three model proteases, blood serum and tissue extracts on the hydrodynamic diameters. First the DLS measurements were taken using only for the commercially available enzymes, blood serum and tissue extracts in order to obtain reference data.
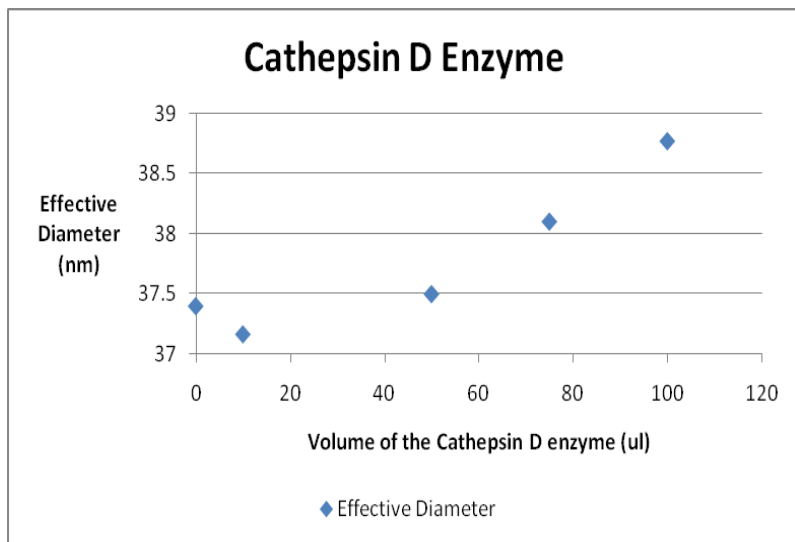
Figure 8.3: DLS of Cathepsin D Enzyme (concentration of 1×10^{-9} mol dm^{-3})

As shown in Figure 8.3, cathepsin D forms modest clusters with itself, which are only mildly concentration-dependent.
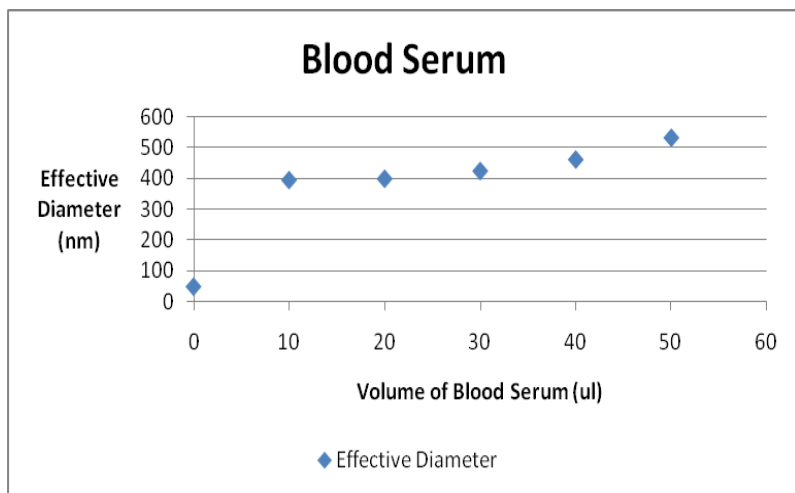
Figure 8.4: DLS for Canine Blood Serum

(sample 070001, obtained from the Kansas State Veterinary Clinic, Dr. Mary Higginbotham, DVM)

Figure 8.4 clearly shows that extensive clustering occurs in PBS-diluted blood serum. The resulting clusters have a hydrodynamic diameter from 400-520nm, depending on the concentration of blood serum in PBS.

Tissue extract 003773 A (tumor core), B (tumor boundary) and C (presumably healthy tissue) types were used.
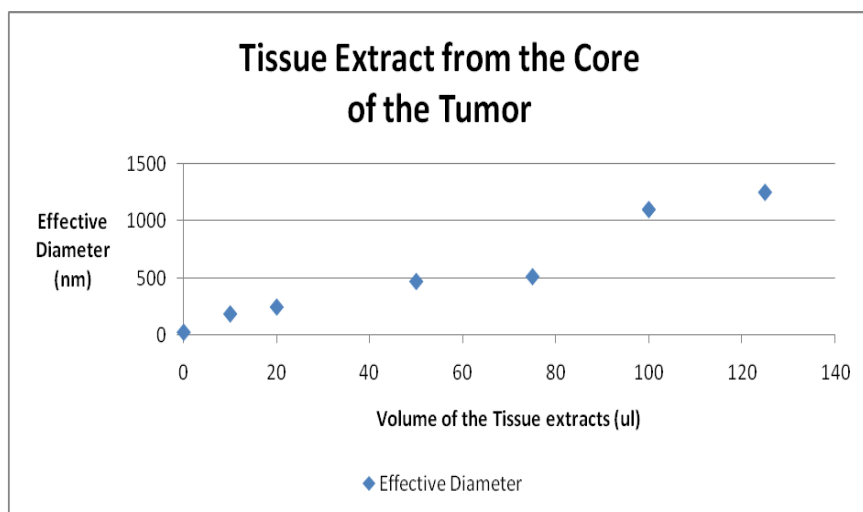
Figure 8.5: DLS for Tissue Extracts from the Core of the Tumor (Tissue extract 003773 A)
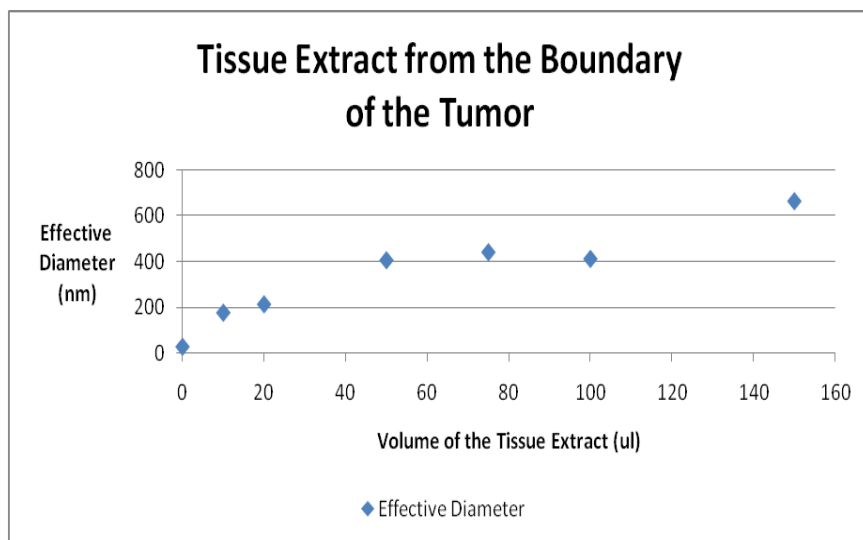
Figure 8.6: DLS for Tissue Extracts from the Boundary of the Tumor (Tissue extract 003773 B)

136
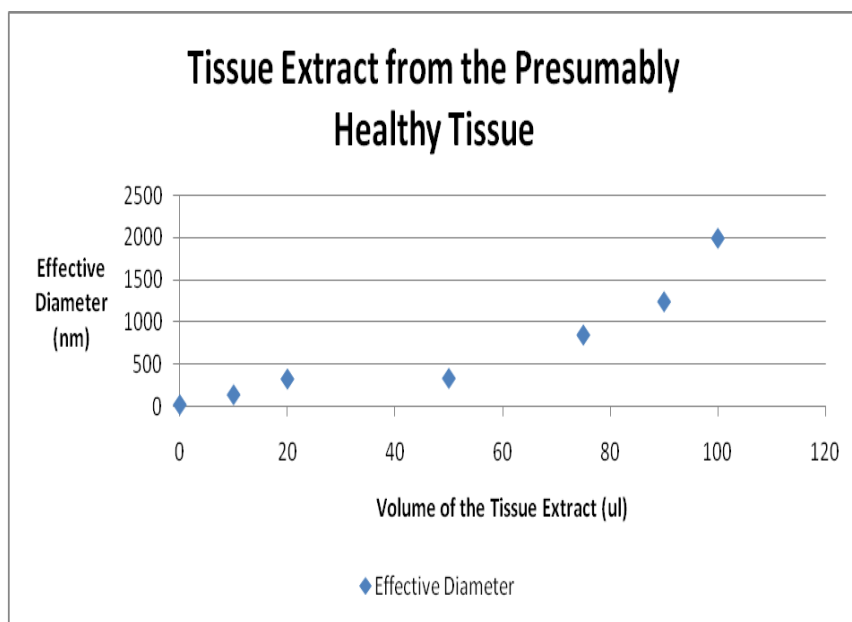
Figure 8.7: DLS for Tissue Extracts from the Presumably Healthy Tissue (Tissue extract 003773 C)

It is noteworthy that the concentration dependences of the dynamic light scattering of tissue extracts from the tumor core, boundary region and adjacent tissue in 1X PBS were remarkably different. At least for patient 003773, the biospecimens from tumor core, boundary region and adjacent tissue permit a clear differentiation. This led to the conclusion that there are differences in protein identity and, possibly, concentration in all three samples. However, since thousands of different proteins are present in all three samples, more detailed conclusions are impossible. However, it is important to remember that all three environments are clearly different from 1X PBS containing dextran. Therefore, a straightforward comparison of the calibration/validation results described in chapter 3 and the results obtained using biospecimens cannot be drawn. Therefore, in chapter 6, we have compared the relative intensities of all three samples with the probe control.

Then DLS measurements were performed for the Cathepsin D assay probe.
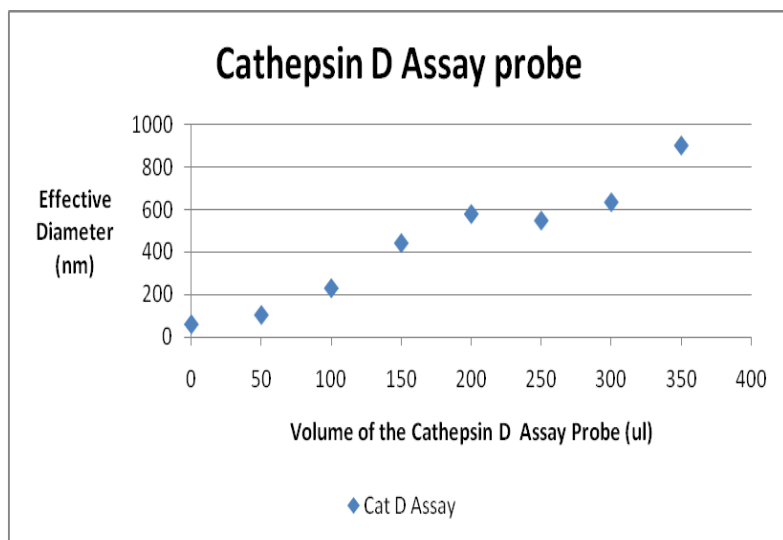
Figure 8.8: DLS for Cathepsin D Assay Probe

The lowest effective diameter was obtained with 50 μLof the assay probe (nanoplatform for cathepsin D) from the concentration of 1 mg/mL, 10 times diluted, in 1X PBS. It was selected for the next experiments. With increasing concentration, extensive clustering of the nanoplatform occurs in 1X PBS.

Then to 50 μL of the cathepsin D assay probe in 3mL of 1X PBS, the enzyme cathepsin D was added to observe the effect of the enzyme on the clustering of the nanoplatform.
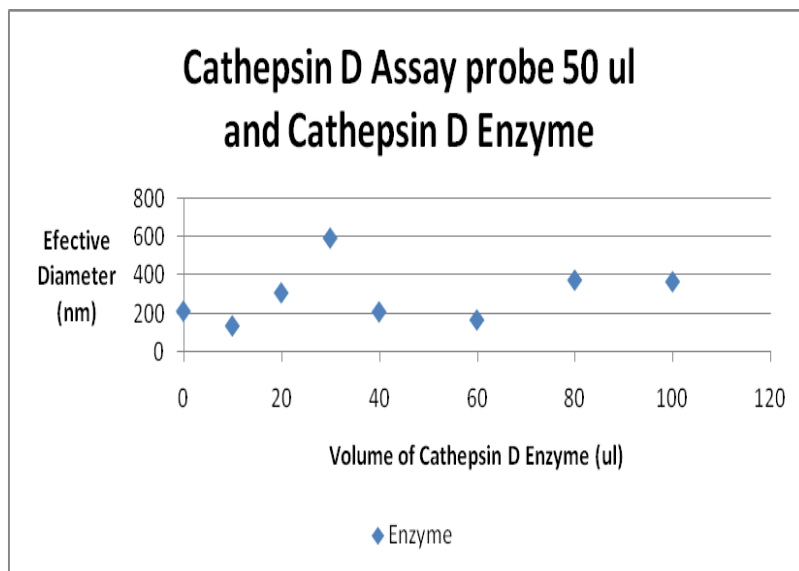
Figure 8.9: DLS for Cathepsin D Assay Probe 50 uL and Cathepsin D Enzyme

138

As it can be seen from Figure 8.9, the presence of cathepsin D increases the hydrodynamic diameter of the nanoplatforms for cathepsin D in PBS. Therefore, we assume that aggregates between the enzymes and the nanoplatform occur. At higher concentration, the consensus sequence for cathepsin D is cleaved faster, which leads to a partial deaggregation.

Then in to 50 uL of the cathepsin D assay probe blood serum was added.
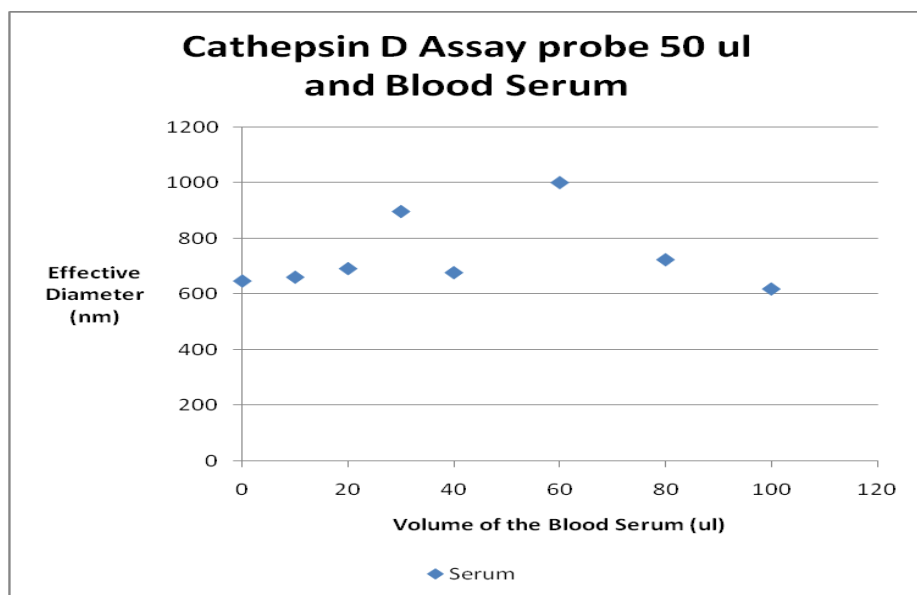
Figure 8.10: DLS for Cathepsin D Assay Probe 50 uL and Blood Serum (091330)

It is apparent that the clustering observed for the blood serum sample alone (see Figure 8.4) can be seen here as well. It is safe to assume that the numerous proteins in blood serum define the environment that is present when the nanoassay is active.

Then in to 50 uL of the cathepsin D assay probe tissue extract was added.
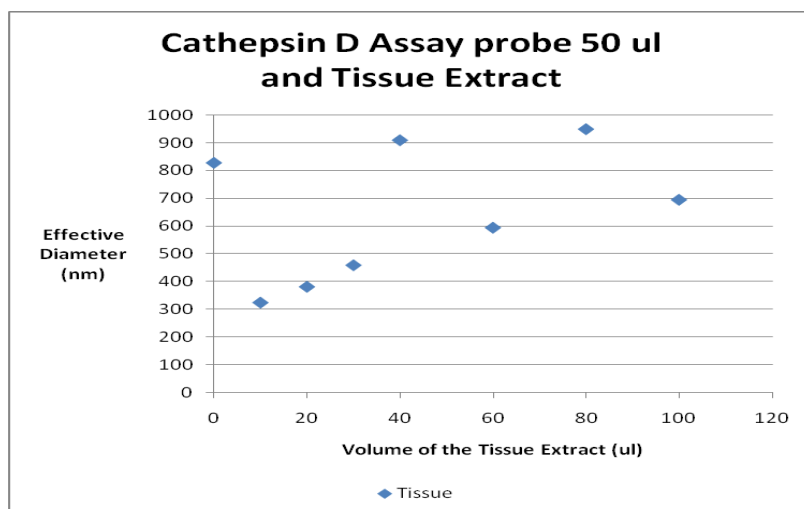
Figure 8.11: DLS for Cathepsin D Assay Probe 50 uL and Tissue Extract (003267B)

Although the data summarized in Figure 8.11 show oscillation of the hydrodynamic diameters, it can, nevertheless, be concluded that the proteins from the tissue extract define the environment that is present during the nanoassay.

8.2.2 DLS for Urokinase

Second, DLS measurements were performed using the urokinase assay probe. Concentration of the assay probe is 1 mg/mL, 10 times diluted with 1X PBS. Measurements were taken 24 h after the preparation. In all the measurements the final volume in the cuvette is 3 ml.

First of all, the DLS measurements were carried out using only the urokinase enzyme.
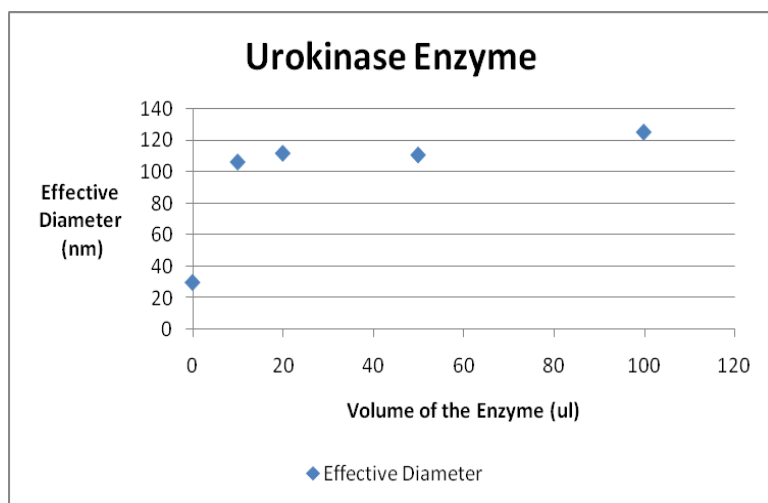
Figure 8.12: DLS of Urokinase Enzyme

Urokinase plasminogen activator with the concentration of 1×10^{-6} mol dm^{-3} was used. It showed a modest tendency to form clusters at higher concentrations.
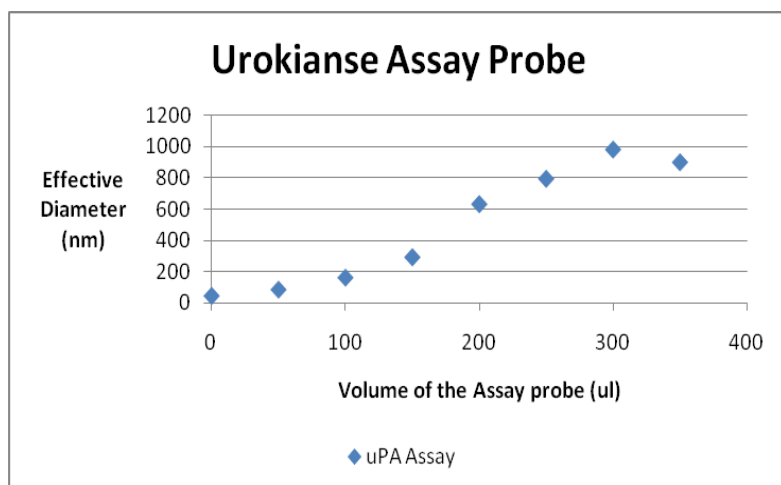
Figure 8.13: DLS for Urokinase Assay Probe

As it shows lowest effective diameter with 50 µL of the assay probe from the concentration of 1 mg/mL 10 times diluted, it was selected for the next experiments. It is noteworthy that the nanoplatform for urokinase detection shows strong clustering, which reaches a plateau after 300 uL.

Then to 50 µL of the urokinase assay probe, urokinase plasimogen activator was added in increasing the volume of it.
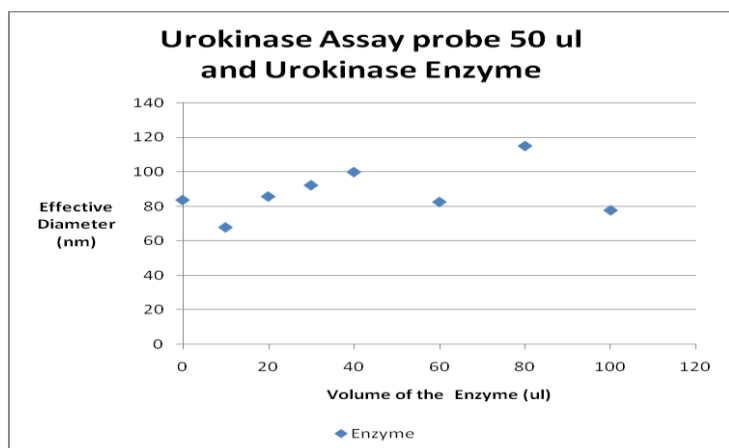
Figure 8.14: DLS for Urokinase Assay Probe 50 uL and Urokinase Enzyme

It is remarkable that the presence of urokinase plasminogen activator is able to suppress the aggregation of the nanoplatform designed for measuring this protease.

Then in to 50 uL of the urokinase assay probe blood serum was added.
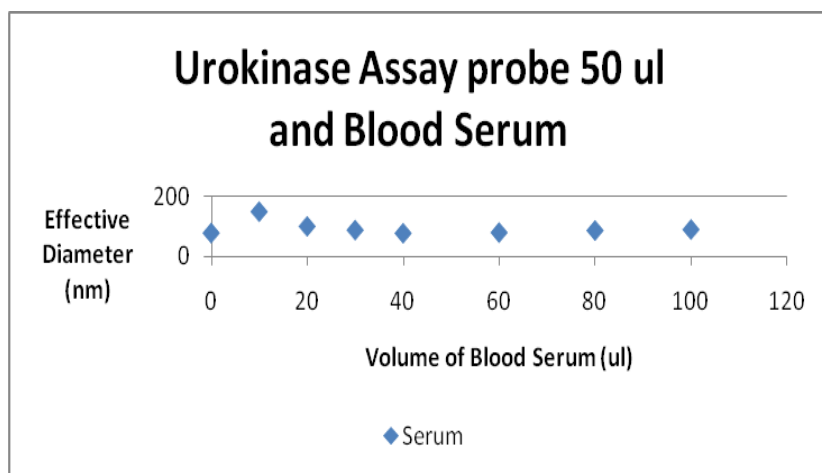
Figure 8.15: DLS for Urokinase Assay Probe 50 ul and Blood Serum (091330)

142

Then to 50 uL of the urokinase assay probe, tissue extract was added in increasing the volume of it.
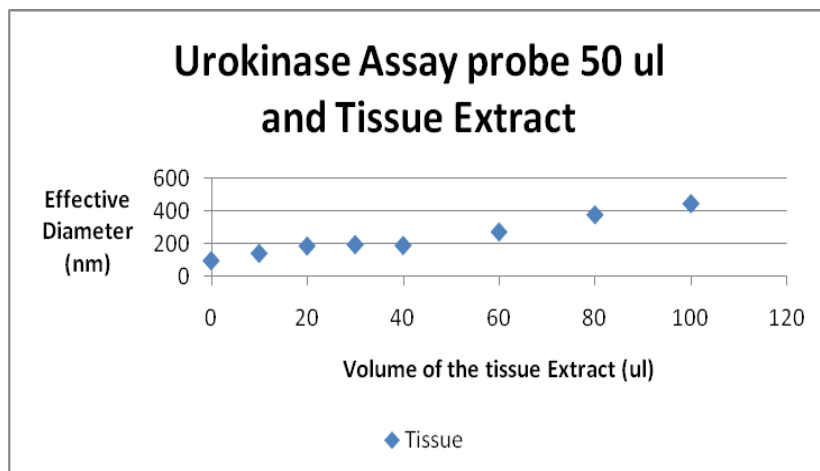
Figure 8.16: DLS for Urokinase Assay Probe 50 uL and Tissue Extract (003780B)

It is noteworthy that the mixture of the nanoplatform for urokinase detection and tissue extract showed different hydrodynamic diameters as function of tissue extract concentration than the system consisting of the nanoplatform for cathepsin D detection and tissue extract. This finding reaffirms our earlier paradigm that each system has different biophysical properties, and that comparisons should be made between biospecimens of the same kind (e.g. tissue samples from core, boundary region and adjacent tissue).

8.2.3 DLS for MMP 7

Third, DLS measurements were performed using the MMP 7 assay probe. Concentration of the assay probe is 1 mg/mL, 10 times diluted with 1X PBS. Measurements were taken after 24 hours after the preparation. With all the measurements the final volume in the cuvette is 3 mL.

First of all, the DLS measurements were carried out using only the MMP 7 enzyme.
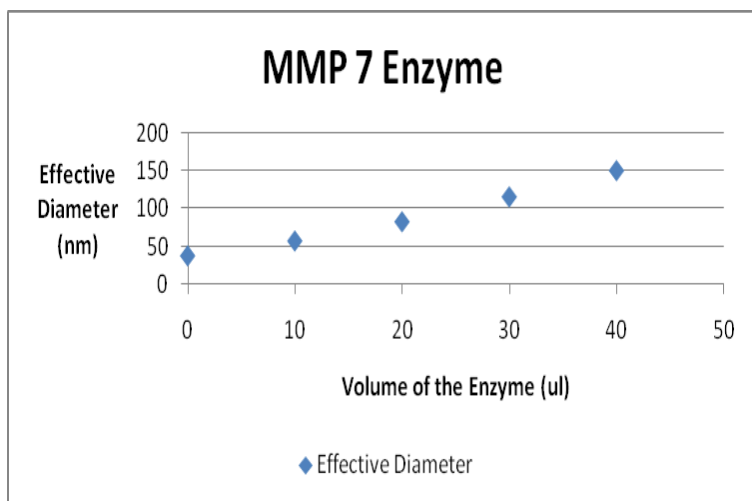
Figure 8.17: DLS of MMP 7 Enzyme - Note that the Light Scattering at 0 uL MMP7 added arises from dextran.

MMP 7 enzyme with the concentration of 1×10^{-9} mol dm^{-3} was used. It shows, like the other two studied proteases, a modest tendency towards clustering at increasing concentration.
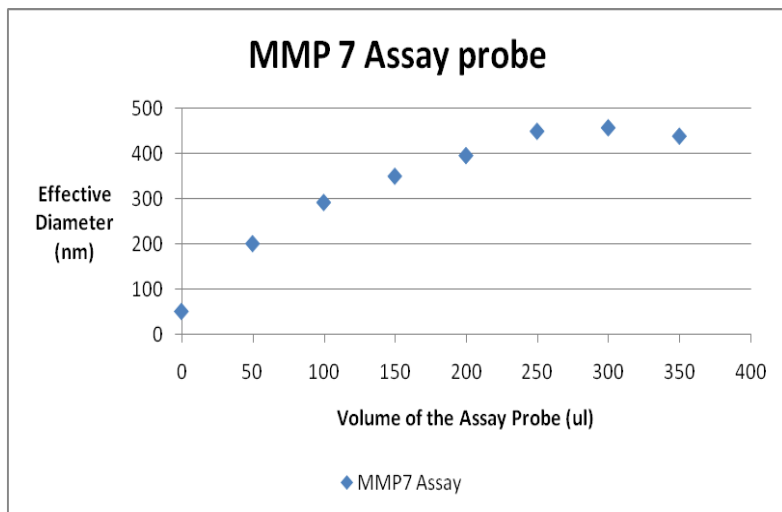
Figure 8.18: DLS for MMP 7 Assay Probe

The nanoplatform for MMP 7 detection shows strong clustering. The formation of aggregates increased with increasing concentration until a plateau region at 250 µL was reached. As it shows lowest effective diameter with 25 µL of the assay probe from the concentration of 1 mg/ mL 10 time diluted. It was selected for the next experiments.

Then to 25 µL of the MMP 7 assay probe, the MMP 7 enzyme was added.

144
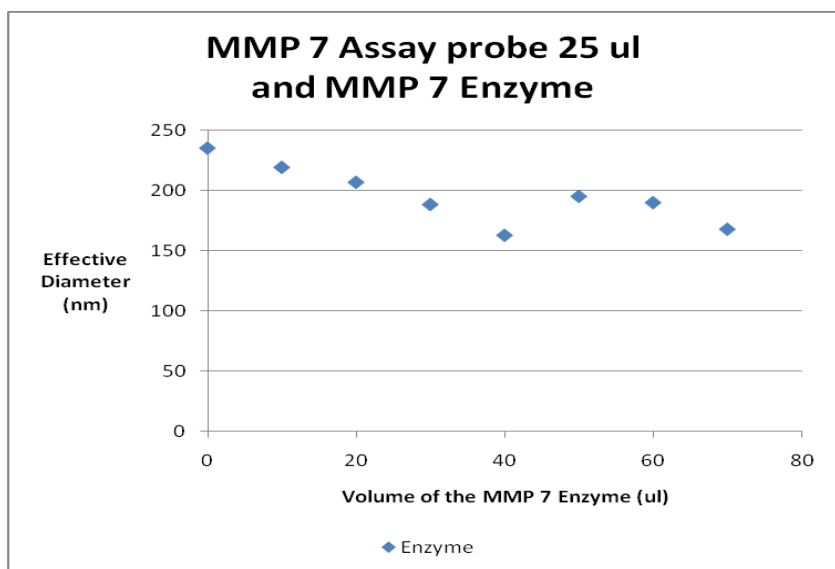
Figure 8.19: DLS for MMP 7 Assay Probe 25 uL and MMP 7 Enzyme

There is a significant decrease in hydrodynamic diameter when MMP 7 is present, compared to the aggregation behavior of the nanoplatform for MMP 7 in 1X PBS in the absence of the enzyme. Then to 25 μL of the MMP 7 assay probe blood serum was added.
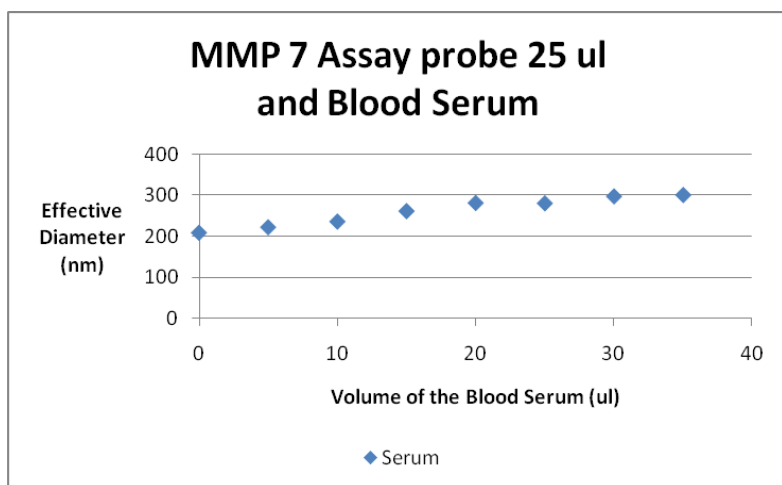
Figure 8.20: DLS for MMP 7 Assay Probe 25 uL and Blood Serum (090668)

Interestingly, there is only a slight increase in the observed hydrodynamic diameter, which is again remarkably different from the observed experimental data in the case of blood serum with the nanoplatforms for cathepsin D and urokinase plasminogen activator. Then to 25 uL of the MMP 7 assay probe tissue extract was added.

145
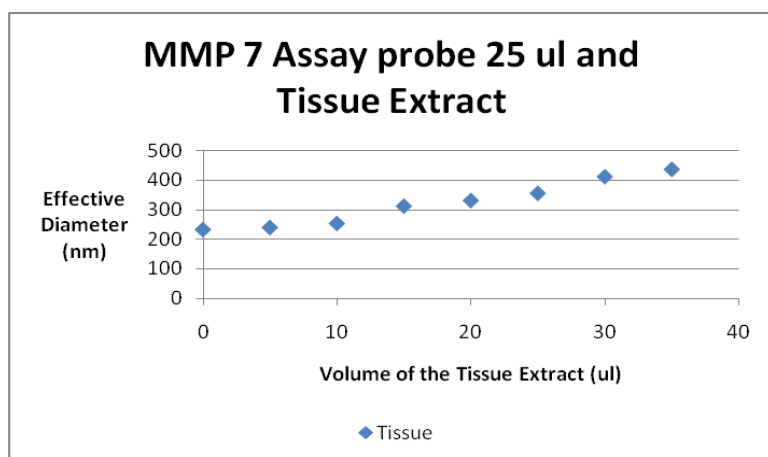
Figure 8.21: DLS for MMP 7 Assay Probe 25 uL and Tissue Extract (003267B)

The hydrodynamic diameters in this system were somewhat similar to earlier systems, in which tissue extract was present. Our conclusion is that the biophysical properties in this very complex mixture are less affected by the presence of the nanoplatform than in "simpler" systems.

8.4 Discussion

I have studied the main hydrodynamic diameters in a series of systems (A: proteases (cathepsin D, urokinase plasminogen activator and MMP7); B: nanoplatforms for protease detection (cathepsin D, urokinase plasminogen activator, MMP7); C: biospecimens (blood serum and tissue extracts), as well as combinations thereof. All measurements have been performed at defined concentrations and temperature (298 K) in 1X PBS (sterilized and filtered).

A: All three enzymes showed, to various degrees, concentration dependent clustering.

B: All three nanoplatforms showed strong clustering. The resulting supramolecular structures feature hydrodynamic diameters in the range of 500 to 1000nm. Adding the respective enzymes led to partial dispersion of the supramolecular structures. These conditions are very similar to those during the calibration and validation of the nanoplatform. It is of importance that each nanoplatform shows a different tendency towards the formation of clusters in PBS and that each mixture of nanoplatform and respective enzyme behaves differently.

C: Both investigated biospecimens in 1X PBS showed large hydrodynamic diameters, due to the presence of thousands of peptides in these mixtures. The light scattering properties of blood serum in 1X PBS were strongly, but again differently, affected by the presence of nanoplatforms for protease detection. Tissue extracts were less affected by the presence of nanoplatforms, but tissue extracts from different positions (tumor core, boundary region and presumably healthy tissue adjacent to the tumor) were quite different with respect to each other.

Based on my dynamic light scattering experiments, we have arrived at the conclusion that kinetic measurements for the determination of protease activity can only be compared if the medium, in which the measurements have been performed, is the same.

8.5 References

[1] Frisken. B. J., Revisiting the method of cumulants for the analysis of dynamic light scattering data, *Applied Optics*, **2001**, *40*, 4087-4091.

Chapter 9 - Conclusion

Cancer related proteases including Matrix Metalloproteinases (MMPs), Tissue Serine Proteases (uPA), and Cathepsins (CTS's) have the potential to become reliable biomarkers for the detection of solid tumors in early stages. We have successfully designed and developed a magnetic-nanoparticle (Fe/Fe$_3$O$_4$) - based Nanoplatforms (Light - Switch) for highly sensitive fluorescence detection of cancer-related proteases. Monitoring the protease signature of the patient provides the basic concept for early cancer detection. The nanoplatform consist of dopamine-coated Fe/Fe$_3$O$_4$ core/shell nanoparticles to which the fluorescent dye TCPP (Tetrakis(4-carboxyphenyl)porphyrin) and the FRET-acceptor (Förster Resonance Energy Transfer) cyanine 5.5 are co-attached. The consensus sequences between TCPP and the central nanoparticle are hydrolytically cleaved by their respective proteases, which are highly selective.

Due to the very small experimental error, the detection of protease concentrations down to 1 x 10^{-16} mol L^{-1} is achieved for MMP1, MMP2, MMP3, MMP7, MMP9, MMP11, MMP13, uPA, CTS B, CTS D, CTS L, and CTS K after 1h of incubation. These nanoplatforms are sensitive enough for future use in routine clinical diagnostics for the early detection of solid tumours and enable the recording of "protease signatures", which may be patient- or tumor-specific.

Based on our calibration results, we have found three principal groups for the protease activities. The group of proteases that causes the fastest increase of fluorescence intensity upon enzyme activation of their respective nanoplatforms is comprised of MMP7, MMP11, MMP13, and cathepsin L. The nanoplatforms for measuring MMP1, MMP2, MMP3, cathepsin B and cathepsin D show less pronounced fluorescence increases. The group comprising the nanoplatforms designed for measuring uPA, MMP9 and cathepsin K interestingly shows a decrease and not an increase.

We identified several protease combinations, which can be used to detect different stages of the breast and lung cancer as different from the control conditions. With breast cancer, stage IV can be detected using a panel consisting of Cathepsin B, Cathepsin L, MMP 1, MMP 9 and urokinase proteases. Stage III can be detected with a panel consisting of Cathepsin B, MMP 1, MMP 9 and urokinase proteases. Stage II can be detected with MMP 7 and urokinase proteases. With lung cancer, Stage III can be detected using Cathepsin B, Cathepsin L, MMP 1, MMP 7

and MMP 9 proteases. Stage II can be detected using Cathepsin B, Cathepsin L, MMP 1 and MMP 9 proteases. Stage I can be detected using MMP 1, MMP 7 and MMP 9 proteases.

We recognized some other protease combinations, which have the ability to detect triple negative breast cancer (TNBC). MMP 11 is potentially of high diagnostic value for detecting TNBC. There is a significant overexpression of MMP 13 with TNBC. Cathepsin B was elevated with TNBC. MMP 9 overexpression is apparently a hallmark of all breast cancers. There can be several sub-groups of TNBC's feature different protease signatures. We require a higher number of blood serum samples from TNBC patients to arrive at a statistically significant conclusion. To date, we have established that cathepsin B, together with MMP1 and MMP9 is a reliable late-stage marker for breast cancer.

Regarding the data we obtained from breast cancer tissue analysis, MMP 1 does not seem to be implicated in aggressive tissue invasion. MMP 2 and MMP 3 were not identified as a significant cancer marker. MMP 7 overexpression in tumor cores and boundaries seems to be universal in all types of breast cancer at stage 2. High MMP 9 levels in the boundary region and adjacent tissue will be a prognosticator of low survival probability. MMP 13 may be a good biomarker for mapping early breast tumors and to observe the transition between benign and cancerous lesions.

From the data of hydrodynamic parameters that we obtained several conclusions can be made. Enzymes show, to various degrees, concentration dependent clustering. Nanoplatforms show strong clustering. Biospecimens in 1X PBS show large hydrodynamic diameters, due to the presence of thousands of peptides in these mixtures. Therefore, kinetic measurements for the determination of protease activity can only be compared if the medium, in which the measurements have been performed, is the same.

Appendix A - NMR
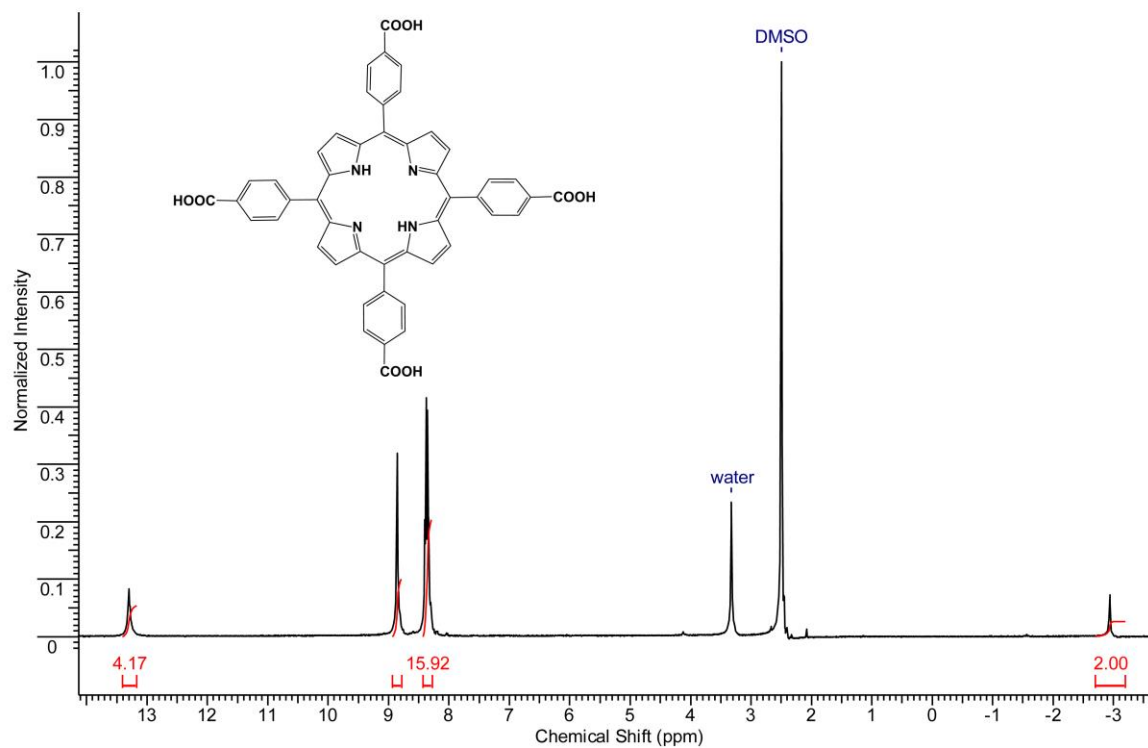
Figure 9.1: ^{1}H-NMR of (4-carboxyphenyl)porphyrin (TCPP) (Varian, 400 MHz)
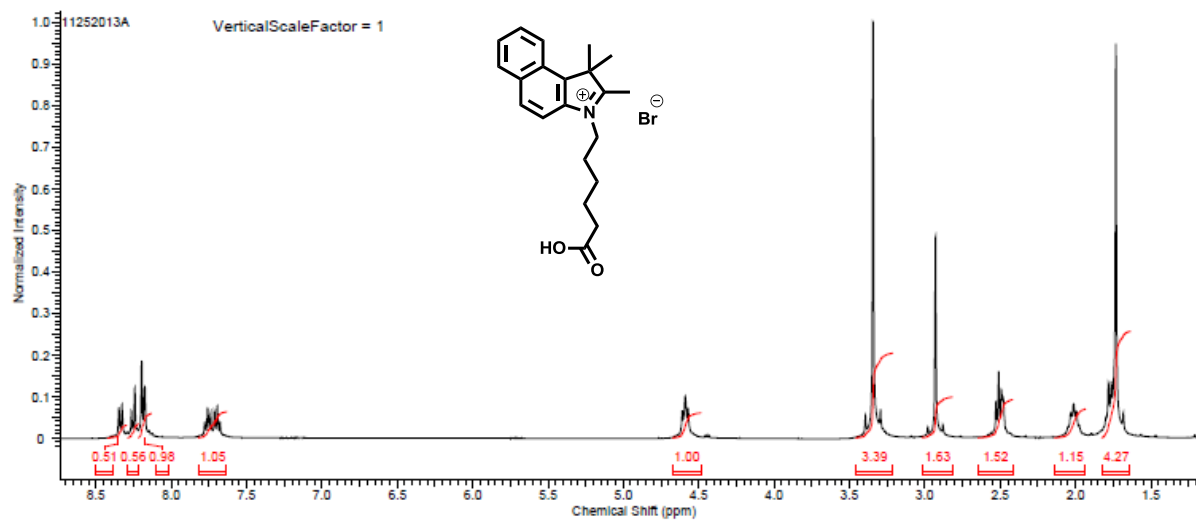
Figure 9.2: [^1]H-NMR of 3-(5-carboxypentyl)-1,1,2-trimethyl-1H-benzo[e]indol-3-ium (Varian, 400 MHz)
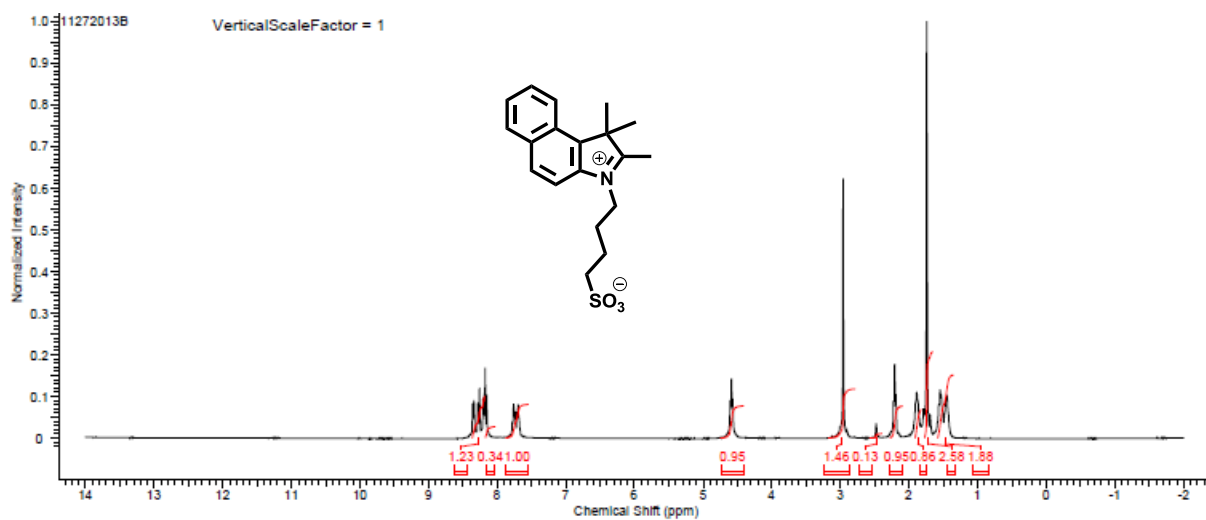
Figure 9.3: ¹H-NMR of 4-(1,1,2-trimethyl-1H-benzo[e]indol-3-ium-3-yl)butane-1-sulfonate (Varian, 400 MHz)
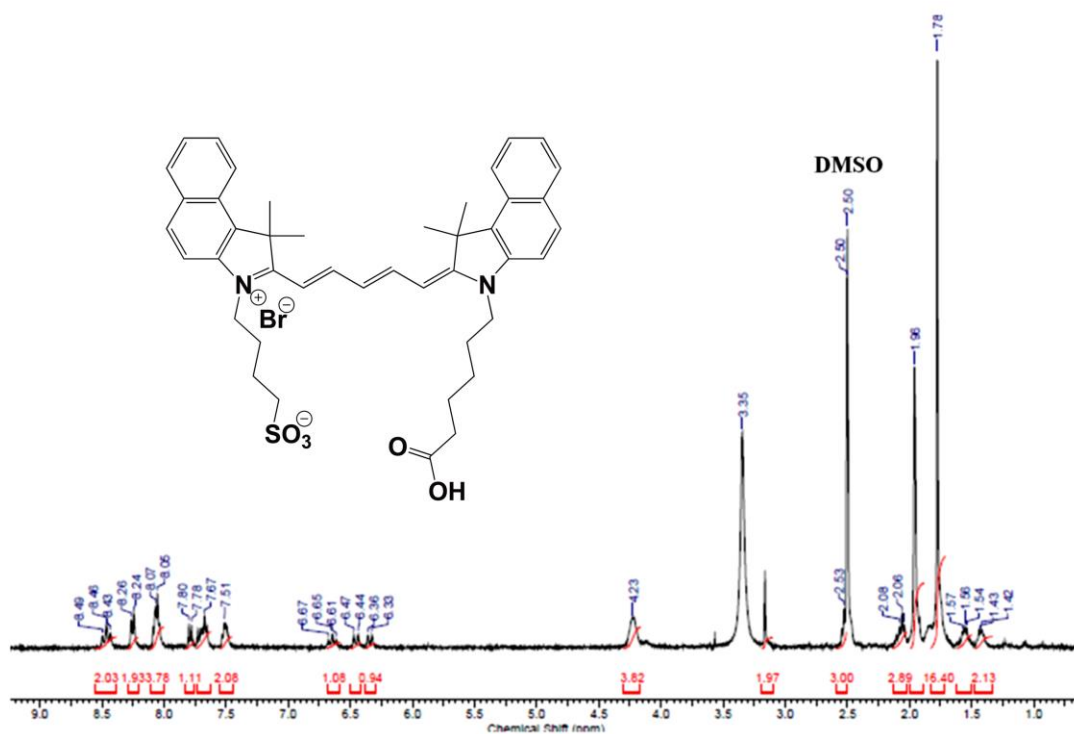
Figure 9.4: ^{1}H-NMR spectrum of Cyanine 5.5 (Varian, 400 MHz)

Appendix B - Mass Spectra
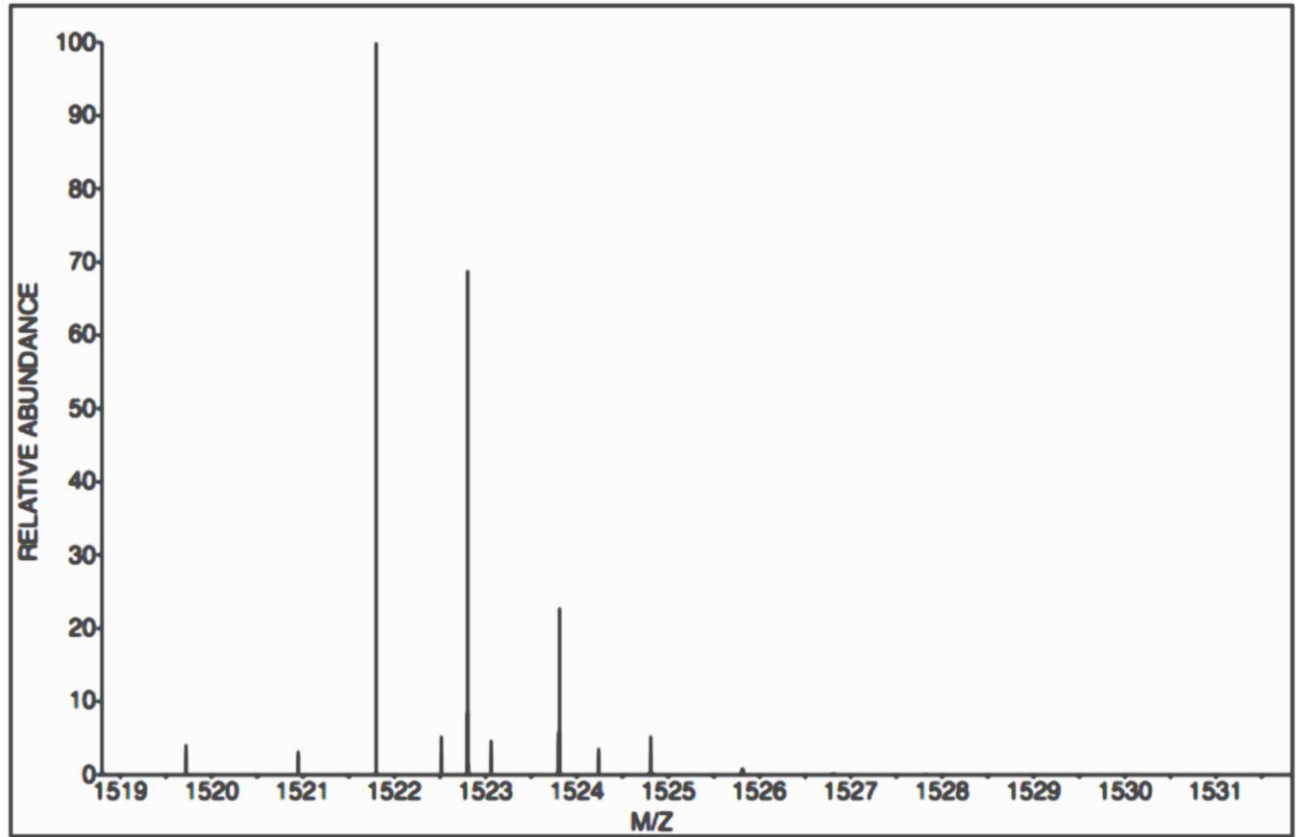
Figure 9.5 : Mass Spectrum (MALDI-TOF) of consensus sequence for MMP 13 (GAGGPQGLAGQRGIVGAG). Calculated mass for MMP 13 s 1522.67.
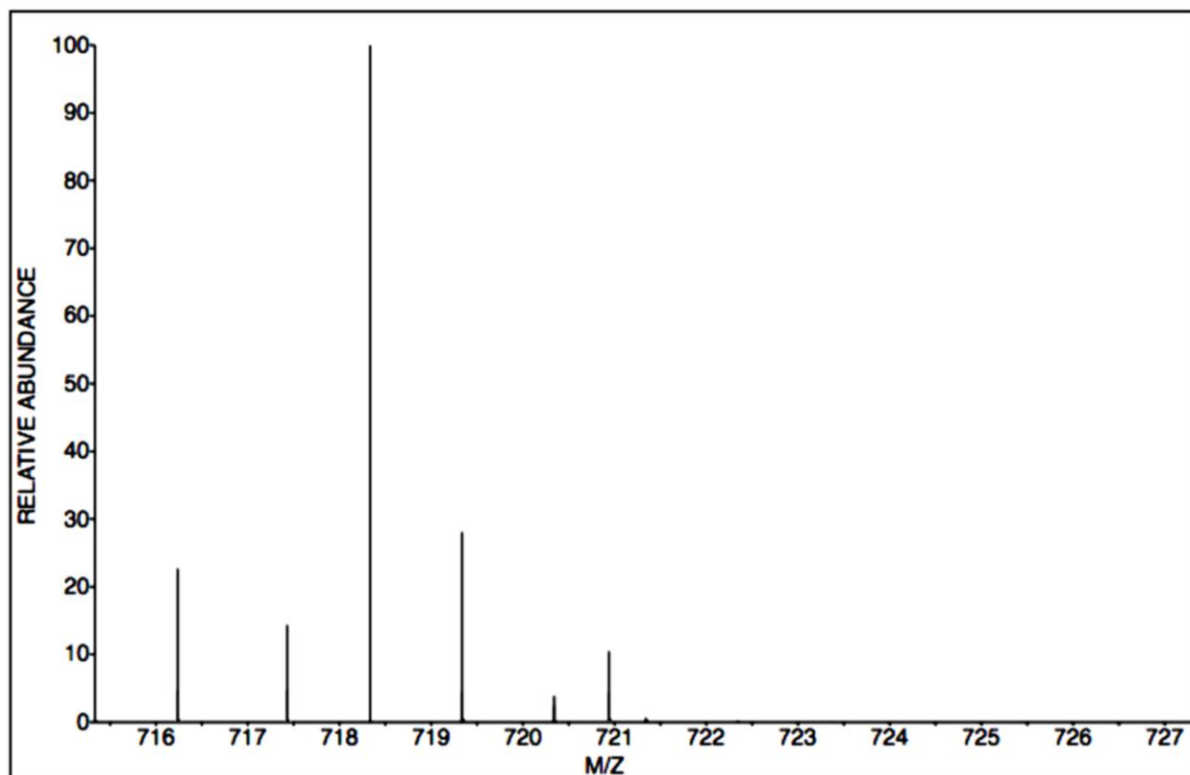
Figure 9.6 : Mass Spectrum (MALDI-TOF) of consensus sequence for uPA (GAGSGRSAG). Calculated mass for uPA is 718.72.
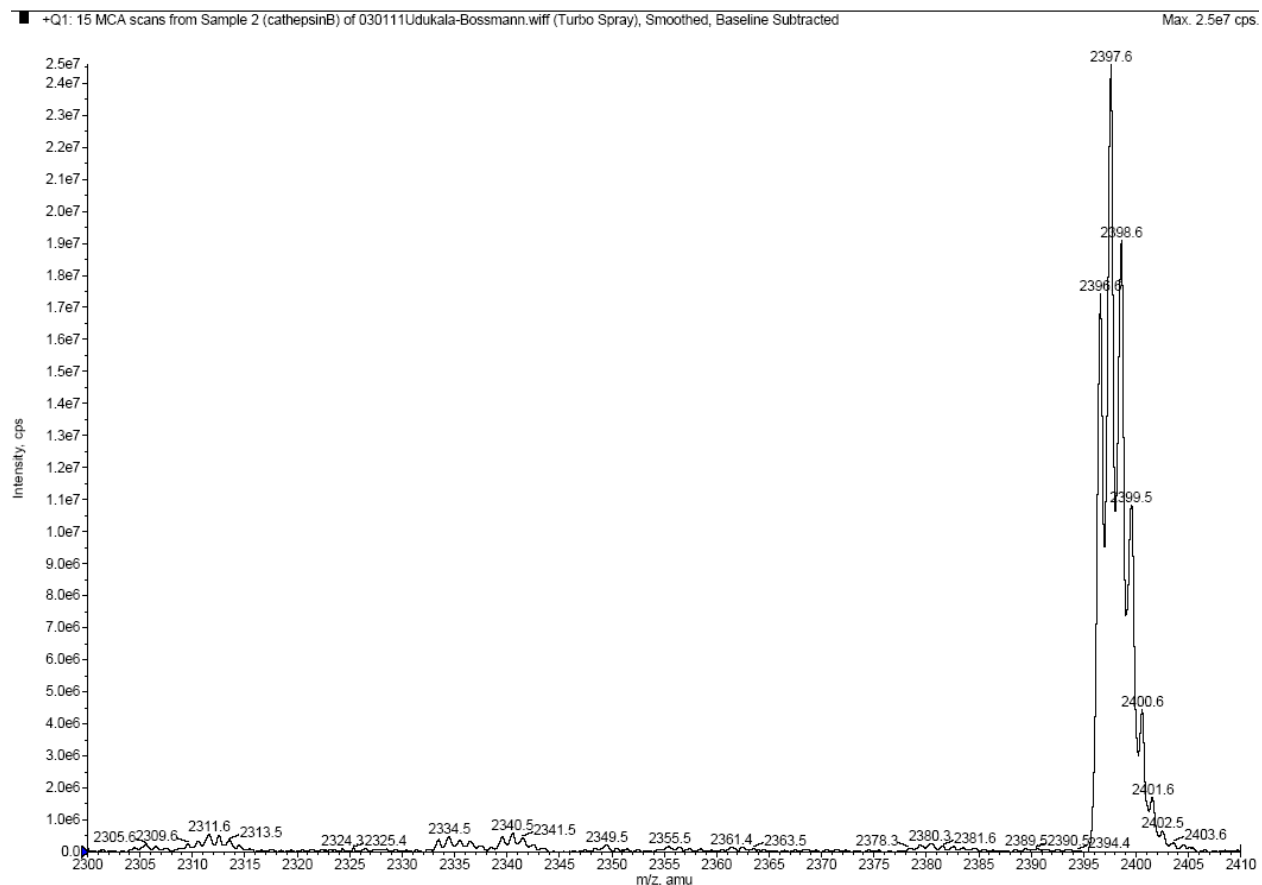
Figure 9.7: Mass Spectrum (electrospray) of TCPP-labeled consensus sequence for cathepsin B (TCCP-SLLKSRMVPNFN) - Calculated mass for $C_{112}H_{135}Cl_3N_{22}Na_4O_{24}S$ = 2,400.84.
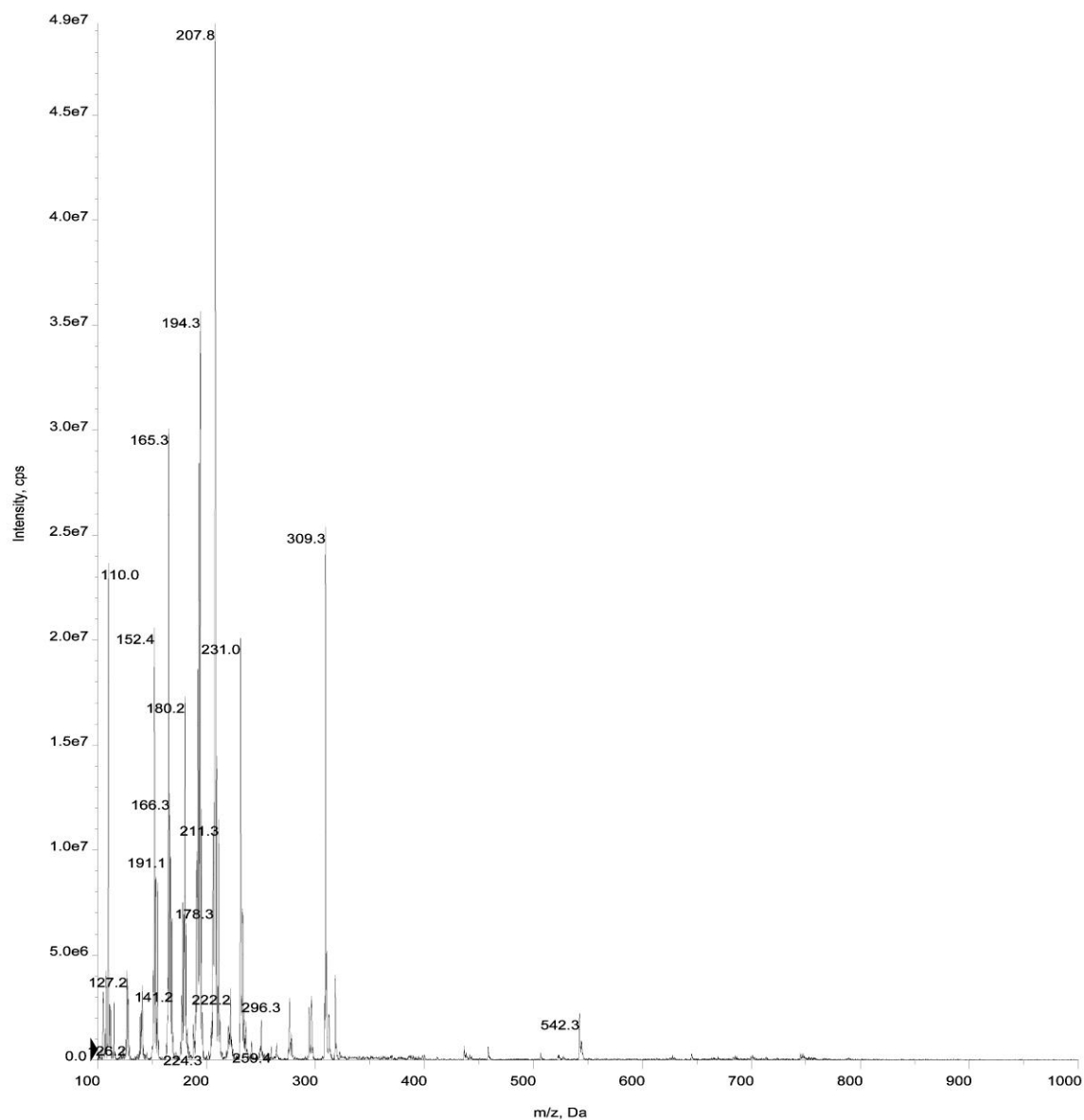
Figure 9.8 : Mass Spectrum (electrospray) of 3-(5-carboxypentyl)-1,1,2-trimethyl-1H-benzo[e]indol-3-ium. Calculated mass for 3-(5-carboxypentyl)-1,1,2-trimethyl-1H-benzo[e]indol-3-ium is 309.1.
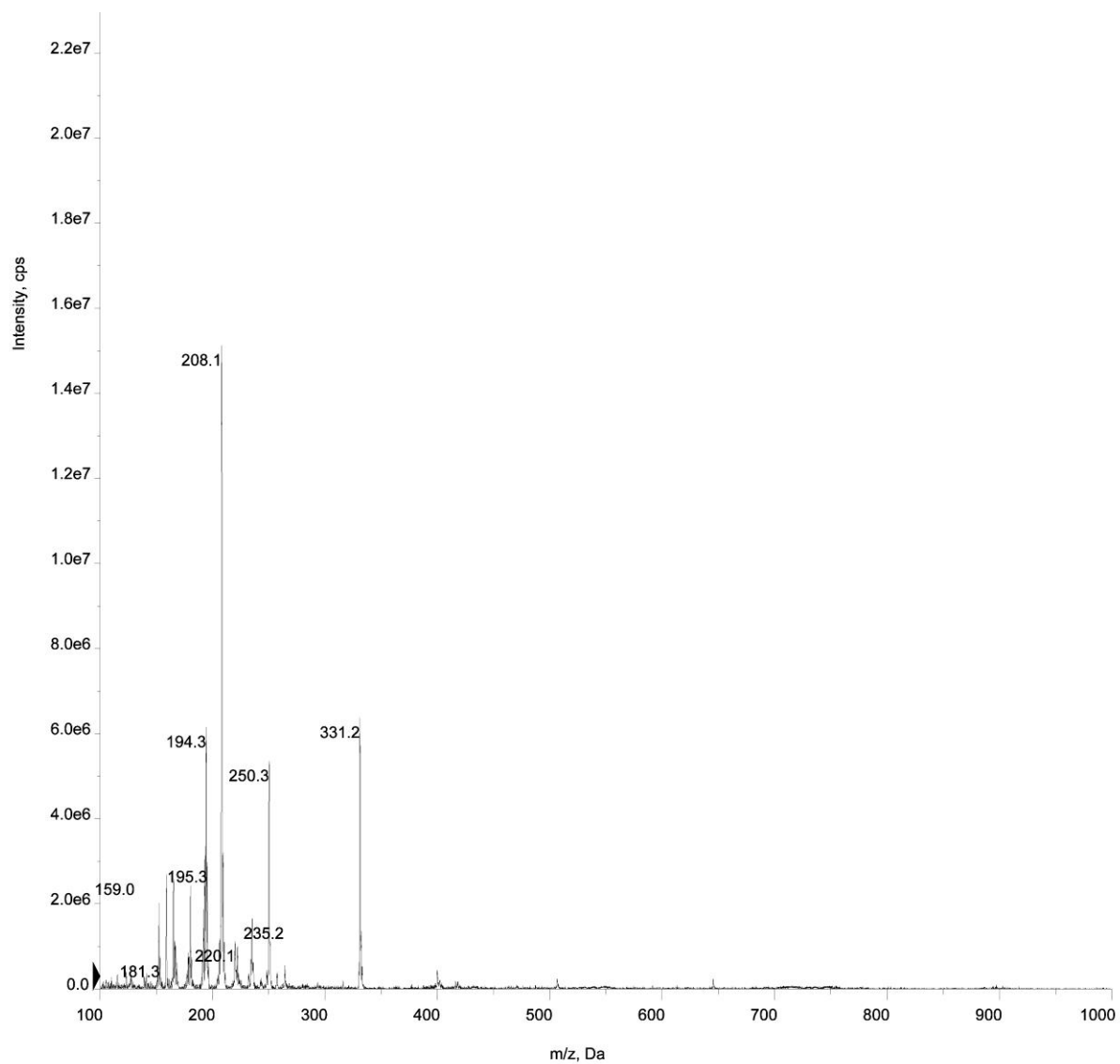
Figure 9.9 : Mass Spectrum (electrospray) of 4-(1,1,2-trimethyl-1H-benzo[e]indol-3-ium-3-yl)butane-1-sulfonate. Calculated mass for 4-(1,1,2-trimethyl-1H-benzo[e]indol-3-ium-3-yl)butane-1-sulfonate is 331.12.
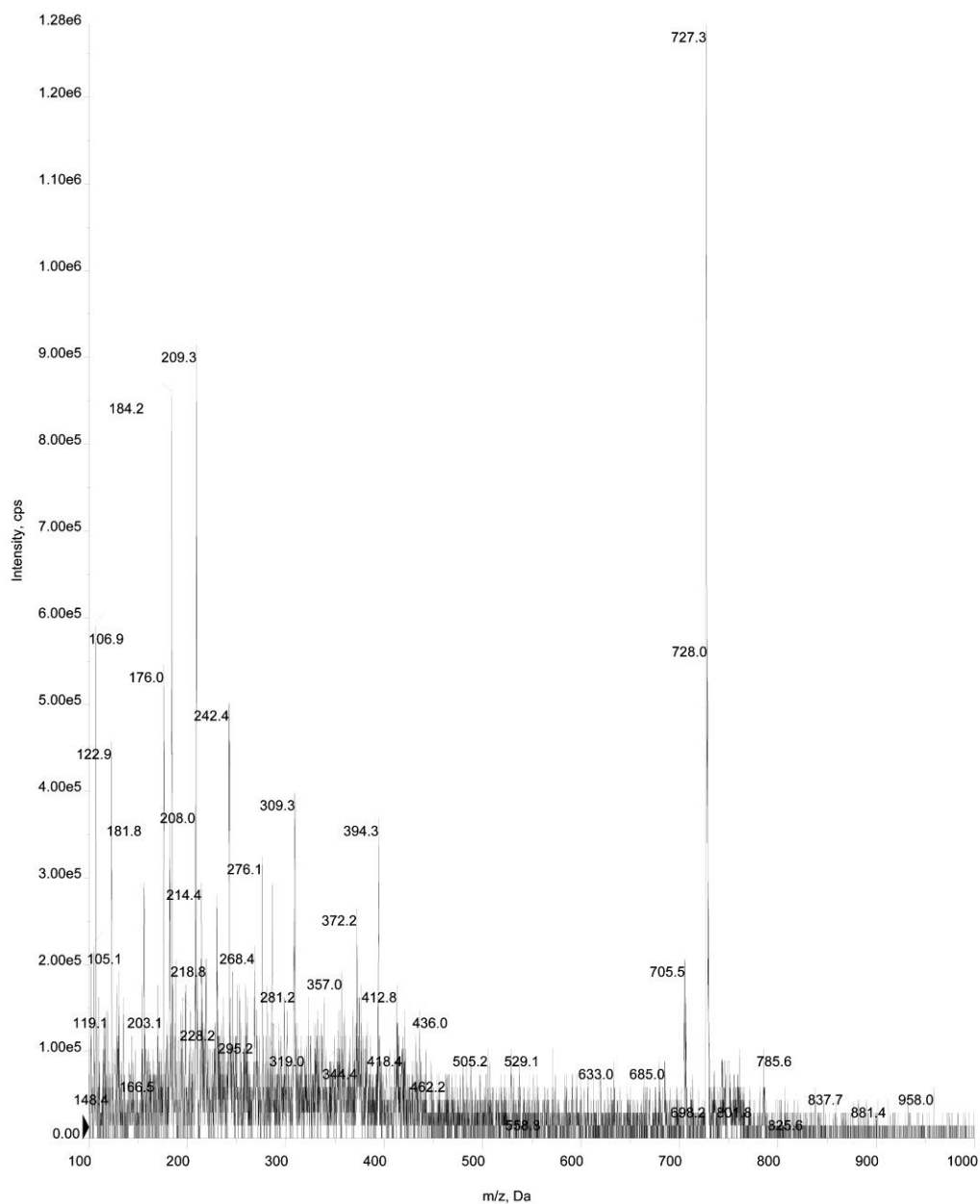
Figure 9.10 : Mass Spectrum (electrospray) of Cyanine 5.5. Calculated mass for Cyanine 5.5 is 704.3.
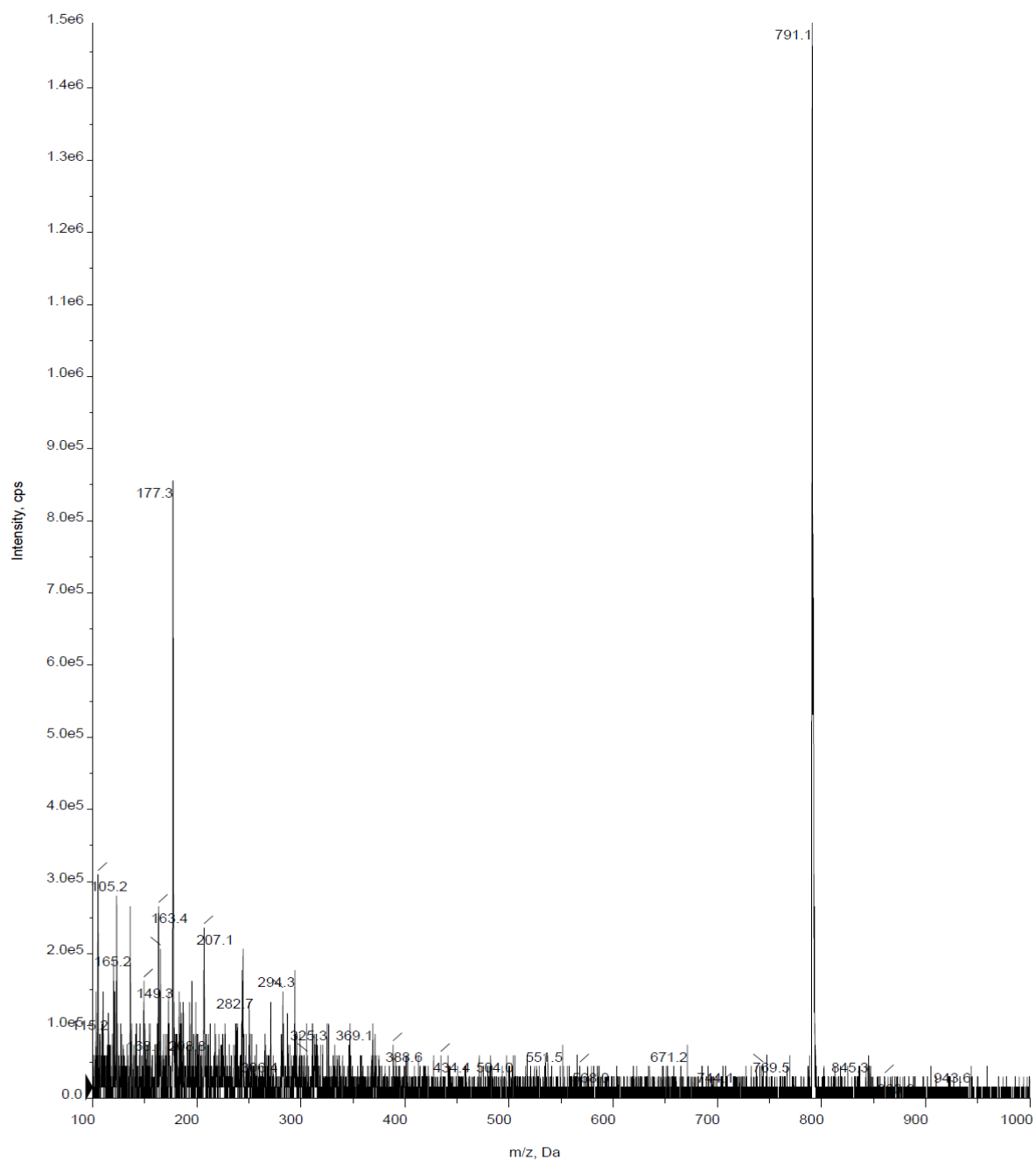
Figure 9.11 : Mass Spectrum (electrospray) of (4-carboxyphenyl)porphyrin (TCPP). Calculated mass for (4-carboxyphenyl)porphyrin (TCPP) is 790.2.

Appendix C - Statistical Analysis Report

Analysis of Data for the Project: Protease-based Cancer Diagnostics

0. Summary of Results

Tables 0.BC and 0.LC summarize findings in the analysis of the data for the KBA project. Table 0.BC summarizes results that compare the stage of disease in breast cancer (BC) patients with the control condition. There were five stages of disease present in BC patients. Table 0.LC summarizes results that compare the stage of disease in non-small lung cancer (LC) patients with the control condition. There were three stages of disease present in LC patients.

An "N" indicates that no statistical difference was seen between that stage of disease and the control condition. An "H" means that a difference was seen and that the mean value of the outcome variable was higher in the disease stage than the control stage. An "L" means that a difference was seen and that the mean value of the outcome variable was lower in the disease stage than the control stage. Statistical differences were determined using 95% confidence intervals with a Bonferroni adjustment within each separate analysis. Thus, five comparisons were made in each analysis of BC data and three comparisons in each analysis of LC data.

Table 0.BC: Summary of results comparing stage of disease in BC patients with the control condition. "N" indicates no statistical difference, "H" indicates that the outcome was estimated to be higher in the disease stage versus control, and "L" indicates that the outcome was estimated to be lower in the disease stage versus control.

Outcome	Stage 0	Stage I	Stage II	Stage III	Stage IV
Cath B	N	N	N	H	H
Cath L	N	N	N	N	H
MMP1	N	N	N	H	H
MMP2	N	N	N	N	N
MMP3	N	N	N	N	N
MMP7	N	N	H	N	N
MMP9	N	N	N	H	H
MMP13	N	N	N	N	N
uPA	N	N	L	L	L

Table 0.LC: Similar to Table 0.BC except for the analysis of LC data versus controls.

Outcome	Stage I	Stage II	Stage III
Cath B	N	H	H
Cath L	N	H	H
MMP1	H	H	H
MMP2	N	N	N
MMP3	N	N	N
MMP7	H	N	H
MMP9	L	L	L
MMP13	N	N	N
uPA	N	N	N

1. Overview of Data and Approach to Analyses

Data for 20 breast cancer (BC) patients, 12 non small lung cancer (LC) patients, and 12 control patients were analyzed. The 20 BC patients were categorized into five stages: stage 0 (2 patients), stage I (2 patients), stage II (3 patients), stage III (6 patients), and stage IV (7 patients).

The LC patients were categorized into three stages: stage I (1 patient), stage II (6 patients), and stage III (5 patients). There were no stage 0 or stage IV LC patients.

A covariate, Age, was also recorded. The BC patients tended to be older than the control patients. The age of BC patients ranged from 36 to 81 years of age with an average age of 57.4 years. The control patients ranged in age from 26 to 62 years with an average age of 42.9 years. LC patients had a similar age distribution with control patients. The age of LC patients ranged from 27 to 63 years with a mean of 46.2 years.

For each patient, 9 primary outcome variables were measured: Cath B, Cath L, MMP1, MMP2, MMP3, MMP7, MMP9, MMP13, and uPA. A sample was obtained from each patient and the measurement process for the outcome variables was carried out independently three times. There were two BC patients with the same label, B6. These patients were subject codes NS2011-013B and NS2011-014B. The latter was given the label B6a. This particular labeling code will be used as a "Patient" variable in a repeated measures analysis.

Each outcome variable will be modeled separately. In each model, the outcome variable (or a transformation of it) will be the response and explanatory variables will be Age (if significant) Stage of disease (including control), and Patient as a random effect. A test for an Age – Stage interaction will also be considered. BC and LC patients will be analyzed separately along with the control patients. Of primary interest is a contrast comparing stage of disease versus control. Approximate t-distribution based (with Satterthwaite degrees of freedom) interval estimates of contrasts along with P-values for a test of significance will be reported. Interval estimates will have 95% confidence and include a separate Bonferroni adjustment for each analysis (i.e., 5 contrasts for BC data and 3 for LC data). All analyses were conducted using R (www.r-project.org) and SAS (The SAS Institute, Cary, NC). These data are observational and samples are relatively small. Whether results that follow extend to a larger population will depend on how representative these patients are of a broader target population.

2. Analysis of Cath B (cathepsin B)

2A) BC patients versus Control

There were three measurements that were detected as outliers and removed from the analysis. These were the third measurement for patient NS2011-010C, and the first and second measurements for patient NS2011-006B. Thus there were a total of 93 Cath B observations that were analyzed in a repeated measures model. Diagnostics suggested transforming the Cath B measurements by natural logarithm transformation. After outlier removal and transformation, diagnostic plots on both residuals and random effects looked reasonable to proceed with analyses. The age of patient was not significant (P=0.75) and, so, was not considered further.

Results of Cath B for BC patients:

Table 1 shows estimated contrasts on the log-scale. Each contrast compares a stage of the disease to the control condition. Confidence intervals not covering zero are considered showing a "statistically significant" difference between that stage of disease and the controls. Table 2 shows estimates of contrasts on the original scale of measurement. These are then estimates of multiplicative effects of a disease stage versus controls. A confidence interval not covering 1 is considered statistically significant.

Table 1: Estimates of contrasts. The Label column states the comparison being tested. The other columns are, respectively, the estimate of the contrast, a P-value for a two-tailed test of the contrast equaling zero, and the lower and upper 95% confidence interval estimates with Bonferroni adjustment.

Label	Estimate	P-value	Lower	Upper
0 minus C	-0.1492	0.6855	-1.1490	0.8505
I minus C	-0.5757	0.1243	-1.5745	0.4231
II minus C	0.1970	0.5273	-0.6472	1.0412
III minus C	0.9487	0.0004	0.2948	1.6026
IV minus C	1.2644	<.0001	0.6424	1.8864

Table 2: Similar to Table 1 but on the original scale of measurement. Only estimates are shown.

Label	Estimate	Lower	Upper
0 minus C	0.8614	0.3168	2.3418
I minus C	0.5623	0.2071	1.5269
II minus C	1.2177	0.5235	2.8327
III minus C	2.5823	1.3427	4.9660
IV minus C	3.5410	1.9010	6.5958

Discussion of Cath B BC analysis:

Tables 1 and 2 suggest that stage III can be detected as different from the control condition using the cathepsin B measurements. Table 2, in particular, estimates that the mean cathepsin B value to be approximately 2.58 times greater in stage III patients versus control patients. This value could be as small as 1.34 times or as large as 4.97 times at 95 % confidence (adjusted for simultaneous estimates). These values are larger when comparing stage IV patients with controls.

2B) LC patients versus Control

The outlying third measurement for control patient NS2011-010C was removed as for the BC analysis. Thus there were a total of 71 cathepsin observations that were analyzed. Diagnostics again suggested transforming the cathepsin measurements by natural logarithm transformation. After outlier removal and transformation, diagnostic plots on both residuals and random effects showed a possible influential observation due to patient NS2011-019L. This stage II cancer patient had cathepsin B values considerably lower than the values for other stage II patients. Analyses were first conducted using the data that included this patient and then using data that omitted this patient. As before, age was not significant in the model and not considered further.

Results of Cath B for LC patients:

Using all of the data except the third measurement for control patient NS2011-010C, there were no significant differences detected among the stages of disease and the control condition. An overall test of significance of staging in the model gave an approximate P-value equal to 0.28. As a secondary analysis, data for patient NS2011-019L were omitted from analyses resulting in a total of 68 observations for analysis. Age remained not significant with this change. Results similar to those described for Table 1 are shown below for the lung cancer data in Table 3. Table 4 shows interval estimates on the original scale and are results analogous to those in Table 2 for the BC data.

Table 3: Estimates of contrasts comparing stage of disease and controls. Column descriptions are those as described for Table 1.

Label	Estimate	P-value	Lower	Upper
I minus C	-0.9971	0.0249	-2.0698	0.0755

II minus C	0.6024	0.0094	0.0538	1.1510
III minus C	0.6515	0.0055	0.1029	1.2000

Table 4: Estimates of contrasts on original scale. Effects are thus multiplicative.

Label	Estimate	Lower	Upper
I minus C	0.3689	0.1262	1.0789
II minus C	1.8265	1.0551	3.1620
III minus C	1.9183	1.1081	3.3209

Discussion of Cath B LC analysis:

Results suggest some significant differences between the control group and stage II and III cancer patients, after a multiple testing adjustment is applied. For example, Table 4 estimates that stage II patients, on average, will have approximately 1.86 times higher cathepsin B values versus controls. The uncertainty in this value ranges from 1.06 to 3.16. Again, these results hinge on omitting the data representing the stage II patient, NS2011-019L. Including this patient in the analyses eliminates any statistical significance due to the unusually low values of cathepsin B in this patient versus the other five stage II patients in the data set.

3. Analysis of Cath L Data

3A) BC patients versus Control

Control patient NS2011-016C was an extreme outlier in all models considered and was dropped from the analysis. The measurements for Cath L were not unusual, but two measurements for this patient were high and the other much lower. Thus all three residuals for this patient were extreme. Thus 93 measurements were analyzed. A natural logarithm of Cath L was used as the outcome variable. Age was only marginally significant (P=0.084) and, thus, not used in the model.

Results of Cath L for BC Patients

Table 5 shows estimated contrasts on the log-scale. Each contrast compares a stage of the disease to the control condition. Confidence intervals not covering zero are considered showing a "statistically significant" difference between that stage of disease and the controls. Table 6 shows estimates of contrasts on the original scale of measurement. These are then estimates of multiplicative effects of a disease stage versus controls. A confidence interval not covering 1 is considered statistically significant.

Table 5: Estimates of contrasts comparing stage of disease and controls. Column descriptions are those as described for Table 1.

Label	Estimate	P-value	Lower	Upper
0 minus C	0.2230	0.4496	-0.5761	1.0222
I minus C	0.7882	0.0110	-0.0110	1.5874
II minus C	0.2035	0.4158	-0.4736	0.8807
III minus C	0.4269	0.0338	-0.1007	0.9546
IV minus C	0.6472	0.0013	0.1446	1.1499

Table 6: Similar to Table 5 but on the original scale of measurement.

Label	Estimate	Lower	Upper
0 minus C	1.2499	0.5621	2.7793
I minus C	2.1994	0.9891	4.8907
II minus C	1.2257	0.6228	2.4125
III minus C	1.5326	0.9042	2.5975
IV minus C	1.9102	1.1556	3.1578

Discussion of Cath L BC analysis:

Tables 5 and 6 suggest that stage IV can be detected as different from the control condition using the Cath L measurements. Table 6, in particular, estimates that the mean Cath L value to be approximately 1.91 times greater in stage IV patients versus control patients. This value could be as small as 1.16 times or as large as 3.16 times at 95 % confidence (adjusted for simultaneous estimates).

3B) LC Patients versus Control

Control patient NS2011-016C was again removed from the data to be analyzed. Thus 69 measurements were analyzed. A natural logarithm of Cath L was used as the outcome variable. Age was not significant (P=0.671) and, thus, not used in the model.

Results of Cath L for LC Patients

Results on the log-scale are given in Table 7 and results on the original scale are given in Table 8. Only three contrasts were estimated since data for only three LC stages were available.

Table 7: Estimates of contrasts for Cath L LC patients. Confidence intervals are 95% with Bonferroni adjustment. Columns are as given in Table 1.

Label	Estimate	P-value	Lower	Upper
I minus C	0.4823	0.2650	-0.6073	1.5719
II minus C	0.6590	0.0039	0.1296	1.1885
III minus C	0.8412	0.0008	0.2786	1.4039

Table 8: Similar to Table 7 but on the original scale.

Label	Estimate	Lower	Upper
I minus C	1.6198	0.5447	4.8175
II minus C	1.9329	1.1382	3.2826
III minus C	2.3192	1.3210	4.0717

Discussion of Cath L LC analysis:

Tables 7 and 8 suggest that stage II and III can be detected as different from the control condition using the Cath L measurements for LC patients. Table 8, for example, estimates that the mean Cath L value to be approximately 2.31 times greater in stage III patients versus control patients. This value could be as small as 1.32 times or as large as 4.07 times at 95 % confidence (adjusted for simultaneous estimates).

4. Analysis of MMP1 Data

4A) BC Patients versus Control:

There were no unusual observations and no transformation was indicated necessary. Thus 96 measurements were analyzed. Age was not significant (P=0.646) and, thus, not used in the model. The largest residuals in the final model were attributed to two of the measurements for control patient NS2011-012C, but they were not extreme enough to warrant any removal or modification of these measurements. So all measurement for NS2011-012C were used.

Results of MMP1 for BC Patients

Table 9 shows estimated contrasts on the original scale (i.e., no transformation was used for this analysis). Each contrast compares a stage of the disease to the control condition. Confidence intervals not covering zero are considered showing a "statistically significant" difference between that stage of disease and the controls.

Table 9: Estimates of contrasts for MMP1 BC patients. Confidence intervals are 95% with Bonferroni adjustment and reported on the original scale of measurement. Columns are as given in Table 1.

Label	Estimate	P-value	Lower	Upper
0 minus C	-0.0878	0.4816	-0.4255	0.2499
I minus C	0.3094	0.0174	-0.0284	0.6471
II minus C	0.2624	0.0170	-0.0230	0.5479
III minus C	0.3481	0.0001	0.1270	0.5692
IV minus C	0.2945	0.0006	0.0842	0.5048

Discussion of MMP1 BC analysis:

Table 9 suggests that stage III and IV can be detected as different from the control condition using the MMP1 measurements. Note, though, that the P-value is significant at a nominal 0.05 level in a comparison of stage I condition versus the control condition. So one could argue that the MMP1 measurement is sensitive to a stage I versus control with some marginal statistical significance; however, the P-value does not attain the threshold of significance after a Bonferroni adjustment for 5 simultaneous tests (this threshold is 0.01).

4B) LC Patients versus Control

Age was not significant (P=0.946) and, thus, not used in the model. There were some marginal outliers but these were not removed from the analysis. Data provided some indication that a logarithm transformation might be necessary. Analyses were done with and without this transformation and yielded the same results in terms of statistical significance. Thus, no transformation was done to be consistent with the MMP1 analysis for the BC data in section 4A.

Results of MMP1 for LC Patients

Results are given in Table 10 and are on the original scale. Only three contrasts were estimated since data for only three LC stages were available.

Table 10: Estimates and tests of contrasts on the original scale. Interval estimates are with 95% confidence after Bonferroni adjustment for three intervals.

Label	Estimate	P-value	Lower	Upper
I minus C	0.5993	0.0004	0.2266	0.9719
II minus C	0.4202	<.0001	0.2411	0.5992
III minus C	0.4889	<.0001	0.2983	0.6795

Discussion of MMP1 LC analysis:

Table 10 suggests that stages I, II, and III in the LC data can be detected as different from the control condition using the MMP1 measurements. For example, the mean stage I level of MMP1 is estimated to be about 0.6 units higher in LC patients versus control.

5. Analysis of MMP2 Data

5A) BC Patients versus Control

The third measurement for subject NS2011-023B was an outlier and removed from the data set. Diagnostics provided some evidence of a need for transformation, though it was not

170

strong. On the original scale of measurement, however, there was some evidence of a significant Age-Staging interaction though Age by itself was not significant. A natural logarithm transformation improved the looks of diagnostic plots and removed the significance of the Age-Staging interaction. Age itself was also not significant on the log scale (P=0.342) and, so, was not used in the model. A total of 95 observations were analyzed.

Results and Discussion of MMP2 for BC Patients:

Results are given in Table 11 for the log-scale and Table 12 for the original scale. Confidence intervals not covering zero in Table 11 are significant and intervals not covering one in Table 12 are significant after the Bonferroni adjustment. As can be seen, the MMP2 measurement does not detect any of the stages as different from control. The marginal significance seen in some P-values is likely to be due to random chance. A P-value equal to 0.0476 is not significant after adjustment for multiple testing.

Table 11: Estimates of contrasts comparing stage of disease and controls. Column descriptions are those as described for Table 1.

Label	Estimate	P-value	Lower	Upper
0 minus C	-0.2887	0.0558	-0.6871	0.1097
I minus C	0.2997	0.0476	-0.0987	0.6981
II minus C	0.1997	0.1143	-0.1371	0.5365
III minus C	0.0742	0.4416	-0.1866	0.3350
IV minus C	0.1404	0.1311	-0.1077	0.3885

Table 12: Similar to Table 11 but on the original scale. Only interval estimates are given. Estimates are on a multiplicative scale.

Label	Estimate	Lower	Upper
0 minus C	0.7492	0.5030	1.1159
I minus C	1.3494	0.9060	2.0099
II minus C	1.2210	0.8718	1.7100
III minus C	1.0770	0.8298	1.3980
IV minus C	1.1507	0.8979	1.4747

5B) LC Patients versus Control

There were no outliers detected in these data, so a total of 72 observations were analyzed. Diagnostics did not suggest a transformation; however, a natural logarithm did not alter diagnostic plots to any large extent. So it was decided to use a natural logarithm transformation

on the MMP2 outcome variable to remain consistent with the above MMP2 analysis for BC patients. Age was not significant in the model (P = 0.154).

Results and Discussion of MMP2 for LC Patients:

Results are reported in Table 13 for the log-scale and in Table 14 for the original scale. The data do not detect any significant differences between stage of disease and control.

Table 13: Estimates of contrasts comparing stage of disease and controls on the log-scale. Column descriptions are those as described for Table 1.

Label	Estimate	P-value	Lower	Upper
I minus C	0.4058	0.0660	-0.1363	0.9479
II minus C	0.0083	0.9359	-0.2522	0.2686
III minus C	0.1389	0.2097	-0.1383	0.4161

Table 14: Similar to Table 13 but on the original scale. Only interval estimates are given. Estimates are on a multiplicative scale.

Label	Estimate	Lower	Upper
I minus C	1.5005	0.8725	2.5806
II minus C	1.0083	0.7770	1.3083
III minus C	1.1490	0.8707	1.5162

6. Analysis of MMP3 Data

6A) BC Patients versus Control

There did not seem to be any required transformation of the MMP3 outcome variable for this analysis. The third measurement for subject NS2011-001B (Stage 0 BC patient) and the third measurement for subject NS2011-004C (control patient) were identified as outliers and removed from the analysis. Age was not significant (P = 0.225) in the model. A total of 94 observations were analyzed.

Results and Discussion of MMP3 for BC Patients:

Results are reported in Table 15 for the original scale of data since no transformations were required before analysis. The data do not detect any significant differences between stage of disease and control. All P-values are large and all intervals cover zero.

Table 15: Estimates of contrasts comparing stage of disease and controls on the original scale. Column descriptions are those as described for Table 1.

Label	Estimate	P-value	Lower	Upper

172

Label	Estimate	P-value	Lower	Upper
0 minus C	0.0789	0.8397	-0.9806	1.1384
I minus C	0.2550	0.5145	-0.8042	1.3142
II minus C	0.0737	0.8232	-0.8215	0.9688
III minus C	-0.1481	0.5628	-0.8415	0.5453
IV minus C	0.1746	0.4737	-0.4850	0.8342

6B) LC Patients versus Control

Again, there did not seem to be any required transformation of the MMP3 outcome variable for this analysis. The third measurement for subject NS2011-004C (control patient) was again removed from analysis as an outlier as it was for the BC data. Age was not significant (P = 0.466) in the model. Data for stage II LC patient NS2011-019L seemed to produce slight outlying residuals in the fitted model, but it was decided that the data for this patient be left in the analysis. A total of 71 observations were analyzed.

Results and Discussion of MMP3 for LC Patients:

Results are reported in Table 16 for the original scale of data since no transformations were required before analysis. The data do not detect any significant differences between stage of disease and control for LC patients. All P-values are large and all intervals cover zero.

Table 16: Estimates of contrasts comparing stage of disease and controls on the original scale. Column descriptions are those as described for Table 1.

Label	Estimate	P-value	Lower	Upper
I minus C	-0.1268	0.8600	-1.9561	1.7025
II minus C	0.0492	0.8867	-0.8296	0.9280
III minus C	0.3210	0.3862	-0.6146	1.2565

7. Analysis of MMP7 Data

7A) BC Patients versus Control

Diagnostics suggested a natural logarithm transformation of the MMP7 measurements. The third measurement for subject NS2011-027B (Stage III BC patient) and the third measurement for subject NS2011-010C (control patient) were identified as outliers and removed from the analysis. Age was not significant (P = 0.621) in the model. A total of 94 observations were analyzed.

Results and Discussion of MMP7 for BC Patients:

Results are reported in Table 17 on the log-scale and Table 18 for the original scale of data. Estimates in Table 17 are estimates of multiplicative effects. Confidence intervals in Table

16 show significance if they do not cover zero after the Bonerroni adjustment for five simultaneous estimates. There is some evidence that mean log-MMP7 for stage II is different from control. The fact that P-values remain small for comparisons of stage III and IV with the controls suggest that the MMP7 measurements do distinguish between a stage of disease and control for BC patients. The lack of significance could be due to the smaller sample sizes and the fact that this particular measurement seemed to contain more noise than others. Interval estimates on the original scale are shown in Table 18. Intervals not covering 1 are showing significance.

Table 17: Estimates of contrasts comparing stage of disease and controls on the log-scale. Column descriptions are those as described for Table 1.

Label	Estimate	P-value	Lower	Upper
0 minus C	-0.1059	0.6226	-0.6896	0.4777
I minus C	0.3818	0.0827	-0.2018	0.9655
II minus C	0.5076	0.0082	0.0144	1.0009
III minus C	0.2797	0.0535	-0.1024	0.6618
IV minus C	0.2880	0.0375	-0.0754	0.6515

Table 18: Similar to Table 17 but on the original scale. Only interval estimates are given. Estimates are on a multiplicative scale.

Label	Estimate	Lower	Upper
0 minus C	0.8995	0.5018	1.6124
I minus C	1.4650	0.8172	2.6261
II minus C	1.6613	1.0145	2.7207
III minus C	1.3228	0.9027	1.9383
IV minus C	1.3338	0.9274	1.9184

7B) LC Patients versus Control

A natural logarithm transformation of the MMP7 measurements was again used here. The third measurement for subject NS2011-010C (control patient) was an outlier as before and removed from the analysis. Stage II LC subject NS2011-019L produced some outlying residuals in the model, but they were not deemed extreme enough to warrant removal of those observations from the analysis. Age was not significant (P = 0.963) in the model. A total of 71 observations were analyzed.

Results and Discussion of MMP7 for LC Patients:

Results are reported in Table 19 for the log-scale and in Table 20 for the original scale. The data show some evidence of significant differences between stage of disease and control for LC

patients. In particular, levels of MMP7 appear to be elevated in LC patients versus controls. Table 20 shows that estimated average levels of MMP7 in LC patients is 1.7 times larger than controls in stage I, 1.1 times larger than controls in stage II, and 1.4 times larger than controls in stage III. The inconsistency of statistical significance across the three stages could be due to the small sample size. A larger sample size may help to resolve whether the inconsistency is real or an artifact of low power.

Table 19: Estimates of contrasts comparing stage of disease and controls on the log-scale. Column descriptions are those as described for Table 1.

Label	Estimate	P-value	Lower	Upper
I minus C	0.5294	0.0068	0.0698	0.9891
II minus C	0.1087	0.2175	-0.1121	0.3295
III minus C	0.3089	0.0025	0.0739	0.5440

Table 20: Similar to Table 19 but on the original scale. Only interval estimates are given. Estimates are on a multiplicative scale.

Label	Estimate	Lower	Upper
I minus C	1.6979	1.0721	2.6891
II minus C	1.1148	0.8939	1.3904
III minus C	1.3620	1.0766	1.7230

8. Analysis of MMP9 Data

8A) BC Patients versus Control

Measurements of MMP9 were very large in scale. To make them more manageable numerically, they were divided by 100,000. The resulting range for MMP9 values after this scaling was 40.17 to 166.79. No transformation was indicated and no outliers were seen in diagnostic plots of residuals. It was noted that all measurements for subjects NS2011-003B (stage IV BC patient) and NS2011-011B (stage III BC patient) were unusually small compared to other measurements for these stages of disease. These patients were left in the analysis. Another note was that MMP9 measurements for BC patients seemed to systematically increase from the first patient in the data set to the 20th BC patient. In particular, a change was seen after the 7th patient in the data set. Some of the increases in MMP9 values after this patient were due to later stages in disease tending to occur more frequently in the observations 8 to 20 versus observations 1 to 7. But it is not clear that this was the only reason that these increases were

seen. If these measurements were carried out in sequence, it might suggest some condition in the laboratory process that is creating dependence in measurements. If this is the case, the validity of results that follow could be questionable. Age was not significant in the model (P = 0.456).

Results and Discussion of MMP9 for BC Patients:

Results are reported in Table 21 for the original scale of data after division by 100,000. No nonlinear logarithmic transformation was needed. The data suggest significant differences between stage III and IV of disease versus control. There is some evidence that the mean MMP9 values in BC patients begin to depart significantly from the control condition beginning at stage II. For example, the mean MMP9 level for a stage II BC patient is estimated to be 45.8 units higher than control. To return to the original scale of the MMP9 values, all estimates in Table 21 would need to be multiplied by 100,000.

Table 21: Estimates of contrasts comparing stage of disease and controls on the original scale but after division by 100,000. Column descriptions are those as described for Table 1.

Label	Estimate	P-value	Lower	Upper
0 minus C	-6.2123	0.7752	-65.2869	52.8624
I minus C	5.5644	0.7981	-53.5103	64.6390
II minus C	45.7877	0.0173	-4.1395	95.7149
III minus C	72.0707	<.0001	33.3973	110.740
IV minus C	69.2386	<.0001	32.4528	106.020

8B) LC Patients versus Control

This set of data was different from others in that MMP9 measurements for LC patients were of a scale lower than control patients. Summary measures of location for MMP9 measurements in control patients were 5.6 to 9 times larger than those of LC patients. The standard deviation of MMP9 measurements was 3.5 times large in control patients than LC patients. Outlying observations were noted and due to the larger variance in MMP9 values in control patients, but there was no single observation that stood out, so all data were left in the analysis. As in the BC measurements it was noted that measures of MMP9 in LC patients seemed to be systematically higher in the observations appearing later in the data set versus those that appeared earlier. Again, if measurements of MMP9 for LC patients were taken in sequence, it is possible some dependence was introduced in the laboratory process of obtaining measurements. The substantial gap in MMP9 measurements between control and LC patients, as well as the increased variance of measurements in controls made it difficult to transform data so

176

that model diagnostics looked adequate for linear modeling. Nevertheless, a natural logarithm transformation was applied to MMP9 values and used as the response variable. Age was not significant (P = 0.703). A total 72 observations were analyzed.

Results and Discussion of MMP9 for LC Patients:

Results are reported in Table 22 for the log-scale and Table 23 for the original scale of data. The data suggest very significant differences between stage of disease and control for LC patients. All P-values are small and all intervals fall below zero in Table 22 and below 1 in Table 23. This indicates that mean levels of MMP9 are smaller in LC patients versus controls for all three stages available in the data (stages I, II, and III). As illustration of Table 23, mean MMP9 values in both stage II and III LC patients is estimated to be about 15% of the mean value in control patients. With 95% confidence, this percentage could be as small as about 10% and as large as 22%.

Table 22: Estimates of contrasts comparing stage of disease and controls on the log-scale. Column descriptions are those as described for Table 1.

Label	Estimate	P-value	Lower	Upper
I minus C	-2.7396	<.0001	-3.4769	-2.0023
II minus C	-1.8566	<.0001	-2.2108	-1.5024
III minus C	-1.8862	<.0001	-2.2633	-1.5091

Table 23: Similar to Table 22 but on the original scale. Only interval estimates are given. Estimates are on a multiplicative scale.

Label	Estimate	Lower	Upper
I minus C	0.0646	0.0309	0.1351
II minus C	0.1562	0.1096	0.2226
III minus C	0.1516	0.1040	0.2211

9. Analysis of MMP 13 Data

9A) BC Patients versus Control

A natural logarithm transformation was suggested for the MMP 13 outcome variable. Age was not significant in the model and no outlying residuals were noted. It was noted that the predicted subject effects for BC patients NS2011-011B (stage III) and NS2011-020B (stage IV) were unusually large due to unusually large measurements of MMP 13 for these two subjects. Since the residuals for these observations were not unusual, these observations were left in the

following analyses. However, a second analysis was conducted for comparison purposes that omitted the three measurements for these two subjects. A total 96 observations were analyzed in results that follow.

Results and Discussion of MMP 13 for BC Patients:

Table 24 shows results on the log-scale and Table 25 shows results on the original scale. There were no significant differences seen for any stage in BC patients versus controls. As a second check, the two BC patients mentioned above were omitted from another analysis. A difference between stage I versus control was seen, but this difference was not apparent in any other stage versus the control condition.

Table 24: Estimates of contrasts comparing stage of disease and controls on the log-scale. Column descriptions are those as described for Table 1.

Label	Estimate	P-value	Lower	Upper
0 minus C	-0.2574	0.4612	-1.2027	0.6878
I minus C	0.6003	0.0916	-0.3450	1.5455
II minus C	-0.2223	0.4516	-1.0212	0.5765
III minus C	0.0402	0.8599	-0.5786	0.6590
IV minus C	-0.1093	0.6145	-0.6979	0.4793

Table 25: Similar to Table 24 but on the original scale. Only interval estimates are given. Estimates are on a multiplicative scale.

Label	Estimate	Lower	Upper
0 minus C	0.7730	0.3004	1.9893
I minus C	1.8226	0.7083	4.6902
II minus C	0.8007	0.3602	1.7798
III minus C	1.0410	0.5607	1.9328
IV minus C	0.8964	0.4976	1.6149

9B) LC Patients versus Control

A natural logarithm transformation was done for the MMP 13 response variable. Subject code NS2011-019L (LC Stage III, patient L4) had unusually large values of MMP13. After transformation, the predicted subject effect for this patient was large but not extreme. Moreover, this observation did not produce outliers in residuals from the model. So data for this patient was left in the analyses that follow. Age was not significant in the model (P = 0.878).

Results and Discussion of MMP 13 for LC Patients:

Table 26 shows results on the log-scale and Table 27 shows results on the original scale. There were no significant differences seen for any stage in LC patients versus controls.

Table 26: Estimates of contrasts comparing stage of disease and controls on the log-scale. Column descriptions are those as described for Table 1.

Label	Estimate	P-value	Lower	Upper
I minus C	0.1063	0.7434	-0.7195	0.9320
II minus C	-0.1142	0.4661	-0.5109	0.2825
III minus C	-0.0778	0.6399	-0.5001	0.3440

Table 27: Similar to Table 26 but on the original scale. Only interval estimates are given. Estimates are on a multiplicative scale.

Label	Estimate	Lower	Upper
I minus C	1.1121	0.4869	2.5403
II minus C	0.8921	0.5999	1.3266
III minus C	0.9252	0.6064	1.4115

10. Analysis of uPA Data

10A) BC Patients versus Control

A natural logarithm of uPA was suggested by diagnostic plots. The first measurement for subject NS2011-008C (control subject) was an outlier and removed from the analysis. There were measurements for subject NS2011-037B (stage III BC patient) that were boarder line outliers, but these observations were left in the analyses that follow. Age was marginally significant (P = 0.027) and, so, was included as a covariate in this model. An Age-Staging interaction term was not significant. A total of 95 observations were analyzed.

Results and Discussion of uPA for BC Patients:

Table 28 shows results on the log-scale and Table 29 shows results on the original scale. Mean uPA levels are estimated to be significantly lower in stage II, III, and IV versus control patients. Table 29 indicates that for stage II BC patients, the mean uPA level is estimated to be about 14% that of the control condition. The uncertainty in this value ranges from about 3% to 63% at 95% confidence. The uncertainty range is wide due, most likely, to small sample sizes. The effect of Age in the model indicated that older patients tended to have slightly higher levels of uPA.

Table 28: Estimates of contrasts comparing stage of disease and controls on the log-scale for uPA measurements in BC patients. Column descriptions are those as described for Table 1.

Label	Estimate	P-value	Lower	Upper
0 minus C	0.5279	0.4133	-1.2159	2.2717
I minus C	-1.2101	0.0991	-3.1610	0.7407
II minus C	-1.9529	0.0011	-3.4443	-0.4614
III minus C	-1.5402	0.0020	-2.7944	-0.2860
IV minus C	-1.5160	0.0017	-2.7277	-0.3042

Table 29: Estimates of contrasts comparing stage of disease and controls on the original scale for uPA measurements in BC patients on the original scale. Estimated effects are multiplicative.

Label	Estimate	Lower	Upper
0 minus C	1.6953	0.2964	9.6969
I minus C	0.2982	0.0424	2.0978
II minus C	0.1419	0.0319	0.6304
III minus C	0.2143	0.0611	0.7513
IV minus C	0.2196	0.0654	0.7378

10B) LC Patients versus Control

A natural logarithm of uPA was again used as the response variable, and the first observation for subject NS2011-008C (control subject) was an outlier and removed from the analysis as it was for the analysis of data for BC subjects. Residuals from the model were slightly heavy tailed even after the logarithm transformation. This is not likely to influence overall conclusions. A larger sample size would help determine an optimal model to use for this analysis. There was no one patient that contributed to the heavy tailed distribution of residuals. Age was not significant in this model (P = 0.645) and was not used as a covariate.

Results and Discussion of uPA for LC Patients:

Table 30 shows results on the log-scale and Table 31 shows results on the original scale. There were no significant differences seen for any stage in LC patients versus controls.

Table 30: Estimates of contrasts comparing stage of disease and controls on the log-scale for uPA for LC patients. Column descriptions are those as described for Table 1.

Label	Estimate	P-value	Lower	Upper
I minus C	-0.6060	0.5285	-3.0432	1.8313
II minus C	-0.6915	0.1417	-1.8624	0.4793
III minus C	-0.9500	0.0616	-2.1964	0.2964

Table 31: Estimates of contrasts comparing stage of disease and controls on the original scale for uPA measurements in LC patients on the original scale. Estimated effects are multiplicative.

Label	Estimate	Lower	Upper
I minus C	0.5455	0.0476	6.2475
II minus C	0.5008	0.1552	1.6156
III minus C	0.3867	0.1111	1.3457